TRANSIENT RESPONSES OF PHOSPHORIC ACID FUEL CELL POWER PLANT SYSTEM

Cheng-yi Lu

M.S. (CH.E.) University of Cincinnati 1980

B.S. (CH.E.) Tunghai University 1976

Submitted in partial fulfillment of requirements for the degree

DOCTOR OF ENGINEERING

at

THE CLEVELAND STATE UNIVERSITY

November, 1983

This thesis has been approved

for the Department of Mechanical Engineering

and the College of Graduate Studies by

K. A. Alhassan

Thesis Adviser MECH. ENGINEERING DEC. 12, 1983

(Department/Date)

12/12/83

~~Term College of Engr.~~

(Department/Date)

12/12/83

Mechanical Engineering

(Department/Date)

Mech. Eng. 12/12/83

(Department/Date)

ACKNOWLEDGEMENT

I would like to express my deep gratitude and appreciation to my advisor, Professor Kalil Alkasab. His support and encouragement were invaluable to me during the course of this investigation.

I thank Professors George C. Chang, Vincent H. Larson, and Rama S.R. Gorla for serving on my dissertation committee.

This thesis is based on a research project sponsored by the U. S. Department of Energy through a cooporative agreement between Cleveland State University and the NASA Lewis Research Center Fuel Cell Project Office. The author expresses sincere appreciation for the support of Dr. A. F. Presler, the NASA Technical Officer.

Finally, for love, faith, and encouragement, I shall be eternally indebted to my family.

ABSTRACT

An analytical and computerized study of the steady state and transient response of a phosphoric acid fuel cell (PAFC) system was completed. Parametric studies and sensitivity analyses of the PAFC system's operation were accomplished.

Four non-linear dynamic models of the fuel cell stack, reformer, shift converters, and heat exchangers were developed based on nonhomogeneous non-linear partial differential equations, which include the material, component, energy balance, and electrochemical kinetic features. Due to a lack of experimental data for the dynamic response of the components, only the steady state results were compared with data from other sources, indicating reasonably good agreement.

A steady state simulation of the entire system was developed using nonlinear ordinary differential equations. The finite difference method and trial-and-error procedures were used to obtain a solution.

Using the model, a PAFC system, that was developed under NASA Grant NCC 3-17, was improved through the optimization of the heat exchanger network.

Three types of cooling configurations for cell plates were evaluated to obtain the best current density and temperature

distributions.

The steady state solutions were used as the initial conditions in the dynamic model. The transient response of a simplified PAFC system, which included all of the major components, subjected to a load change was obtained.

Due to the length of the computation time for the transient response calculations, analysis on a real-time computer was not possible. A simulation of the real-time calculations was developed on a batch type computer. The transient response characteristics are needed for the optimization of the design and control of the whole PAFC system.

All of the models, procedures, and simulations were programmed in Fortran and run on IBM 370 computers at Cleveland State University and the NASA Lewis Research Center.

TABLE OF CONTENTS

LIST OF TABLES

LIST OF FIGURES

CHAPTER 1

INTRODUCTION

A primary objective of the energy conservation efforts is to reduce the consumption of premium fuels such as oil and natural gas. This can be realized by displacing the premium fuels with noncritical fuels such as coal, or by developing energy conversion systems that can siginificantly increase the utilization efficiency of fossil fuels. Fuel cells can achieve both objectives by efficiently using a variety of fossil fuels, from which hydrogen can be derived, in applications where electric power and process heat are simultaneously in demand. In addition to their efficiency and fuel flexibility, fuel cells are potentially attractive because of modularity, environmental acceptability, and adaptability to both utility and on-site integrated energy systems. Thus, fuel cell system analysis efforts which are essential for design optimization to improve system performance and cost effectiveness have acquired significant practical importance.

For a device that was invented in 1839 by Sir William Grove, the fuel cell has taken a long time to come into its own. It did furnish power for the Gemini and Apollo spacecraft and the space shuttle, but that was an exotic and expensive application. Now the fuel cell, vastly improved over the spacecraft versions and in assemblies 1,000 times larger than the ones carried by the spacecraft, appears to have reached

a stage where it can make a significant contribution to a nation's supply of electricity.

1.1 Definition of Fuel Cells

"A fuel cell is an electrochemical cell which can continuously change the chemical energy of a fuel and oxidant to electrical energy by a process involving an essentially invariant electrode-electrolyte system" (Ref. 1).

A fuel cell consists of two electrodes, a positive electrode (the cathode) and a negative one (the anode), separated by an electrolyte, which transmits ions but not electrons. A fuel, typically hydrogen, is supplied to the anode and oxygen (in air) is supplied to the cathode. A catalyst on the porous anode causes hydrogen molecules (H_2) to dissociate into hydrogen ions (H+) and electrons. The hydrogen ions migrate through electrolyte to the cathode, where they react with electrons (supplied through the external-circuit load) and oxygen to form water (H_2O). This electrochemical transformation is isothermal; that is, the fuel cell directly uses the available free energy in the fuel at its operating temperature. Thus, it is not Carnot-cycle limited and can yield a high fuel to DC power conversion efficiency. Unlike a battery, a fuel cell does not run down or require recharging, it will operate as long as both fuel and oxidant are supplied to the electrodes.

1.2 Fuel Cell Efficiency

The main attraction of fuel cells is efficiency: A fuel cell can convert chemical energy directly into electricity and heat. Therefore, it is important to mention the theoretical efficiency of fuel cells here. The following includes a comparison of maximum fuel cell efficiency with maximum theoretical efficiency of conventional power generation techniques to illustrate the basic attractiveness of fuel cells.

The process of galvanic oxidation that produces electricity in a fuel cell resembles that of a conventional storage battery. However, the fuel cell does not store electrical energy; instead, it combines electrochemical oxidation (a property of the storage battery) with continuous feeding of sufficient fuel (a feature of the mechanical engine) to maintain a desired output.

The efficiency, ϵ, of steam or internal combustion engines, which are two of the most widely used conventional methods of generating electricity, is limited by the temperatures at which heat is supplied (T2C) and rejected (T1C), according to the Carnot cycle-

$$\epsilon = \frac{T2C-T1C}{T2C} \qquad (1-1)$$

The maximum practical theoretical efficiency for heat engines is 40% to 50%. Fuel cells convert energy isothermally (not Carnot-cycle limited), and most of the chemical energy of the fuel may be converted to electricity.

In a H_2/O_2 fuel cell, the following reactions occur:

Anode Reaction $H_2 = 2H^+ + 2e^-$ (1-2)

Cathode Reaction $2e^- + 1/2\ O_2 + 2H^+ = H_2O(g)$ (1-3)

Overall Reaction $H_2 + 1/2\ O_2 = H_2O(g)$ (1-4)

The overall reaction occured at 177 °C, based on the lower heating values (LHV),

$G = -52.9$ kcal/g-mol

$H = -58.2$ kcal/g-mol

The maximum amount of heat energy that can be produced isothermally and isostatically by the overall reaction is the enthalpy change, ΔH, but the fuel cell can only convert to electricity an amount equivalent to the Gibbs free energy, ΔG. The difference, $T\Delta S = \Delta H - \Delta G$, is the minimum amount of heat that is produced in fully reversible processes both on cathode and anode sides. Therefore, the maximum efficiency of a H2/O2 fuel cell at 177 °C is

$$\varepsilon_{max} = \left(\frac{\Delta G}{H}\right)_{(100)} = \left(\frac{-52.9}{-58.2}\right)_{(100)} = 91.0\ \% \qquad (1\text{-}5)$$

The standard potential of a fuel cell, E°, is directly related to the Gibbs free-energy change for the overall reaction, according to the expression

$$\Delta G = -nFE^\circ \qquad (1\text{-}6)$$

where n is the number of electrons transferred, or g-equiv/g-mol, and F is the Faraday constant, which is equal to 23.06 kcal/V-g-equiv.

In a fuel cell, all of the free energy, ΔG, of the reaction is available as cell electromotive force (emf) and a large fraction of the

$T\Delta S$ heat can be recovered in a bottoming cycle or cogeneration scheme. In contrast, in any heat engine a smaller fraction of the ΔH of the combustion reaction is available for useful work as a result of the Carnot efficiency limitation.

Nevertheless, there are inefficiencies in a fuel cell, for example, the irreversibility which will be discussed in Section 2.2.1, fuel utilization, and electronic and ionic conduction resistance through components and at contact points. Deviation from ideal behavior caused by irreversibility is illustrated in Figure 1-1. Therefore, under realistic operating conditions the efficiency of fuel cell is between 40 to 45 percent (Ref. 2).

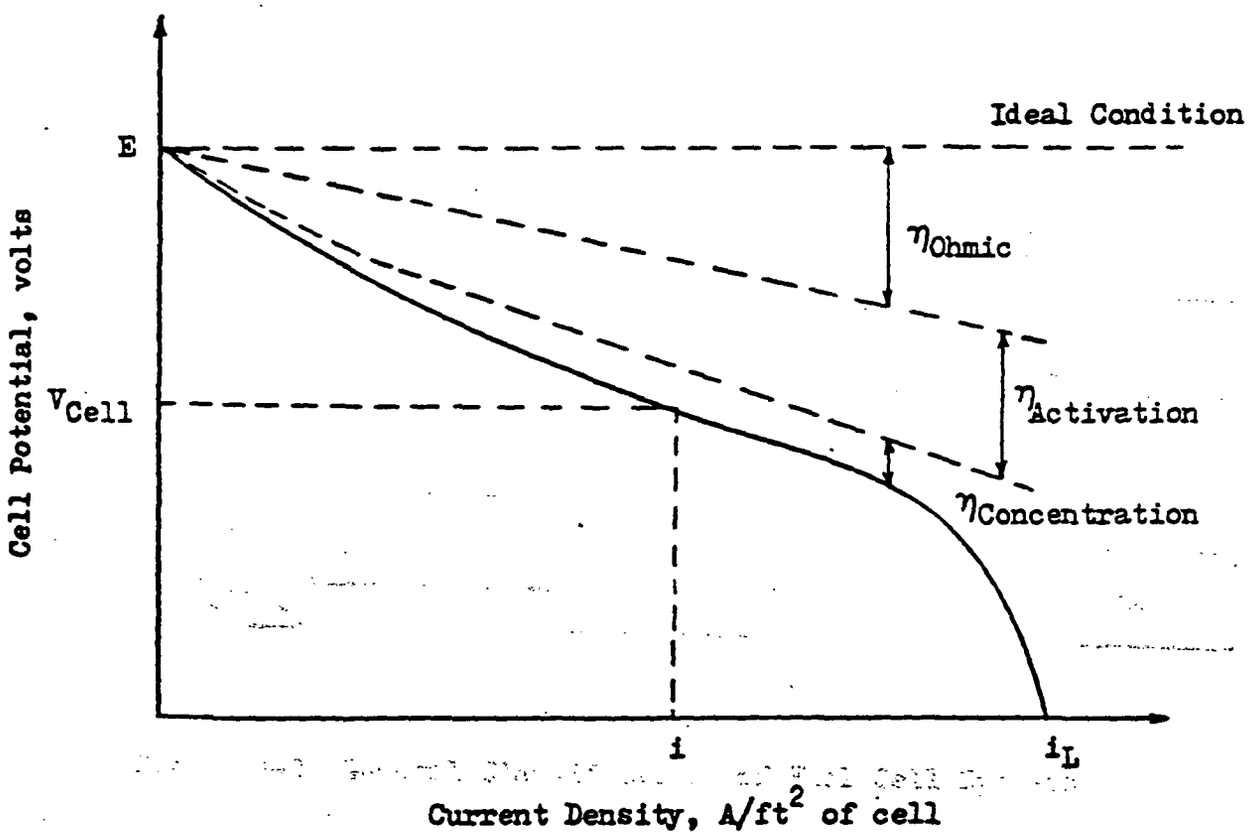

Figure 1-1 Schematic Fuel Cell Polarization Curve

1.3 Types of Fuel Cells

Fuel cells are usually classified according to the type of electrolyte and the operating temperature, as shown in Figure 1-2. A brief introduction to the four fuel cell types follows.

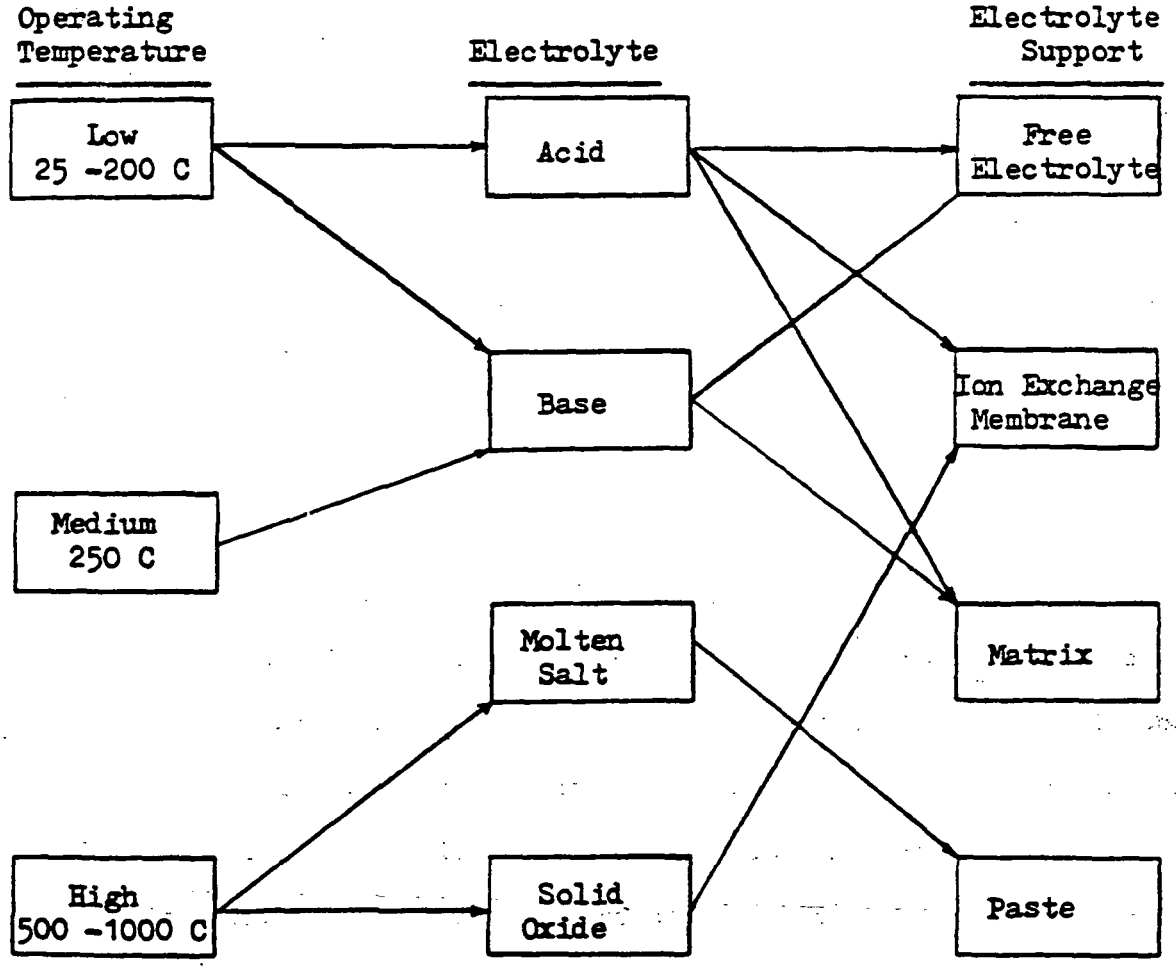

Figure 1-2 General Classification of Fuel Cell Systems

(1) Solid Oxide Fuel Cells. Fuel cells with solid oxide electrolytes operate at temperatures between 700 °C to 1000 °C using non-noble metal electrodes. The electrolyte is usually yttria or calcia stabilized zirconia (ZrO2) (Ref. 7), which conducts oxygen ions at the operating temperature. Solid oxide fuel cells are intended to offer the advantage of burning electrochemically conventional carbonaceous fuels with air, without posing any particular electrocatalytical problem. This technology is still at the research stage.

(2) Molten Salt Fuel Cells. This type of cell operates at temperatures of 600 °C to 700 °C, using impure hydrogen and air, non-noble metal electrodes, and an electrolyte of molten alkali-metal carbonates in a porous ceramic carrier. As with solid oxide cells, high-quality waste heat is available for use in cogeneration to increase the overall system efficiency. Molten salt fuel cells are entering the pilot plant technology stage.

(3) Basic Fuel Cells. Aqueous KOH electrolyte fuel cells operate at lower temperatures (50 to 150 °C) or medium temperatures (210 to 235 °C). The latter is called a Bacon cell which was used as the foreruner of the Apollo fuel cell system. The alkaline electrolyte used in these fuel cells cannot tolerate oxides of carbon in either the fuel or the oxidant, therefore, their nonspace use is limited by the cost of producing reactants that are free of carbon oxides.

(4) Acid Fuel Cells. Many acid electrolytes have been considered for use in fuel cells because acids are tolerant to carbon dioxide, which allows the use of impure hydrogen and air. Phosphoric acid fuel cells are the most advanced of all the fuel cell technologies: Pilot plants up

to 4.8-MW have been successfully operated (Ref. 8) both in New York city and Tokyo. Meanwhile, UTC (United Technology Corporation) is developing an 11-MW plant and Westinghouse Electric Corporation is working on a 7.5-MW design, also using phosphoric acid. Because of these facts, This research concentrates on this particular system which is called the phosphoric acid fuel cell (PAFC) power plant system.

1.4 PAFC System

Figure 1-3 is a block diagram of a phosphoric acid fuel cell (PAFC) power plant with three principle modules: fuel processor, fuel cell power section, and DC power conditioner.

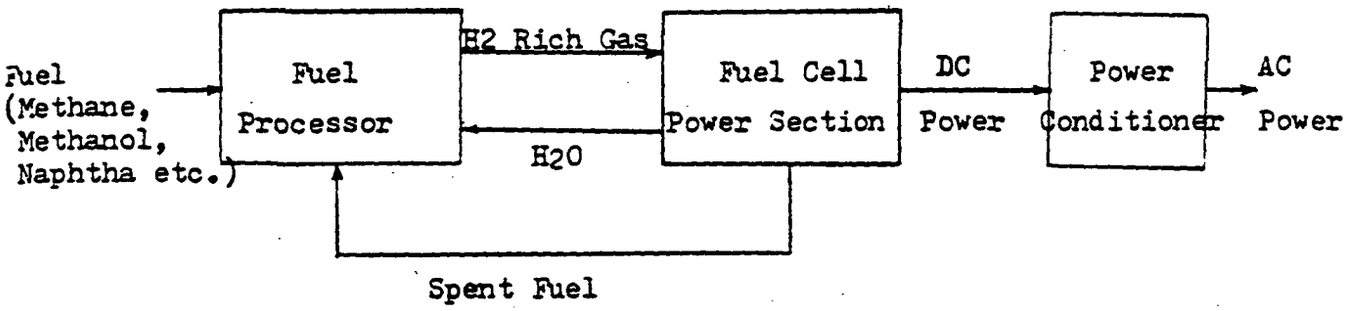

Figure 1-3 Fuel Cell Power Plant Modules

Natural gas, methanol, and naphtha are principly considered for fuel cell use, so these three fuels are the fuel options treated in the present model. Production of hydrogen, thich is the major function of fuel processor , occurs by reaction of the fuel with steam. The overall reactions are:

$$C_n H_m + 2n\ H_2O = nCO_2 + \left(2n + \frac{m}{2}\right) H \qquad (1\text{-}7)$$

for naphtha and methane, and

$$CH_3OH + H_2O = CO_2 + 3H_2 \qquad (1\text{-}8)$$

for methanol.

flow diagram is shown in Figure 1-4.

The major components in the fuel processor subsystem are; the

reformer, two shift converters, and several heat exchangers. The reformer is basically a nonadiabatic, nonisothermal catalytic reactor which can operate as high as 1200 °C and 10 atm. The shift converters are simulated as adiabatic packed bed catalytic reactors which produce hydrogen through a water shift reaction:

$$H_2O + CO = H_2 + CO_2 \qquad (1\text{-}9)$$

The heat exchangers are modeled as shell and tube type heat exchangers.

Within the fuel cell stack subsystem (Power Section), hydrogen and oxygen react to continuously produce DC electricity, waste heat, and steam (as a reaction product). The reacting oxygen is obtained from air and the waste heat produced can be removed by passing a coolant through the fuel cell stack. For the present simulation, air is used as the coolant.

The reaction which take place at the anode and the cathode, respectively, are;

$$H_2 = 2H^+ + 2e^- \qquad (1\text{-}2)$$

$$1/2\ O_2 + 2H^+ + 2e^- = H_2O \qquad (1\text{-}3)$$

and the overall reaction is

$$H_2 + 1/2\ O_2 = H_2O + \text{energy} \qquad (1\text{-}4)$$

The electrical power production in the fuel cell stack is accompanied by approximately equal amounts of heat generation which should be removed to avoid overheating of the stack. A more detailed system flow diagram is shown in Figure 1-4.

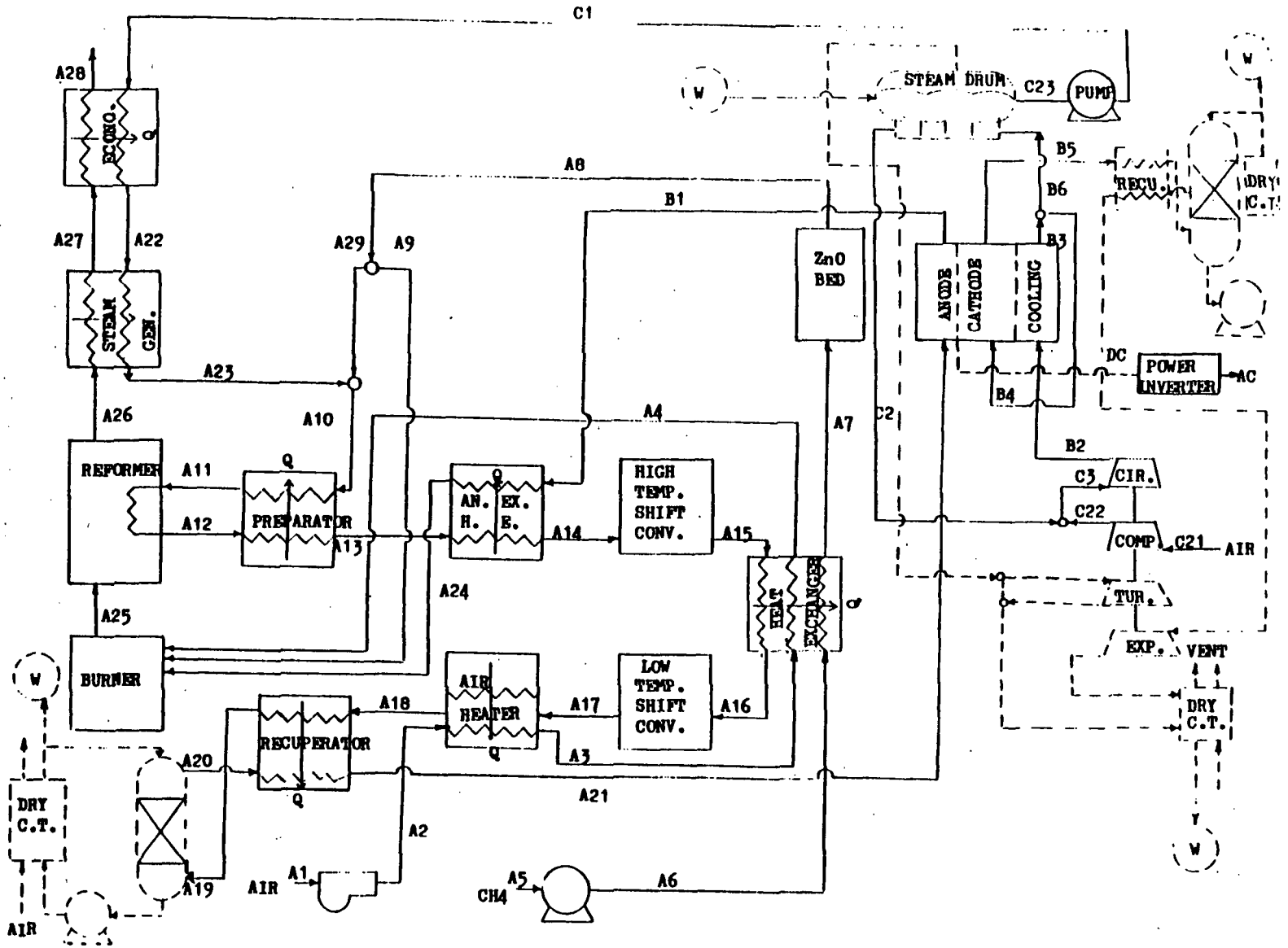

Figure 1-4 Flow Diagram of Phosphoric Acid Fuel Cell Power Plant System

Page Intentionally Left Blank

Page Intentionally Left Blank

the catalyst/electrolyte interface, it is electrochemically oxidized according to Equation (1-2). The electrons are transported through the external circuit, and the hydrogen ions are conducted to the cathode through the 96% phosphoric acid electrolyte held in place by and inert inorganic or polymeric matrix.

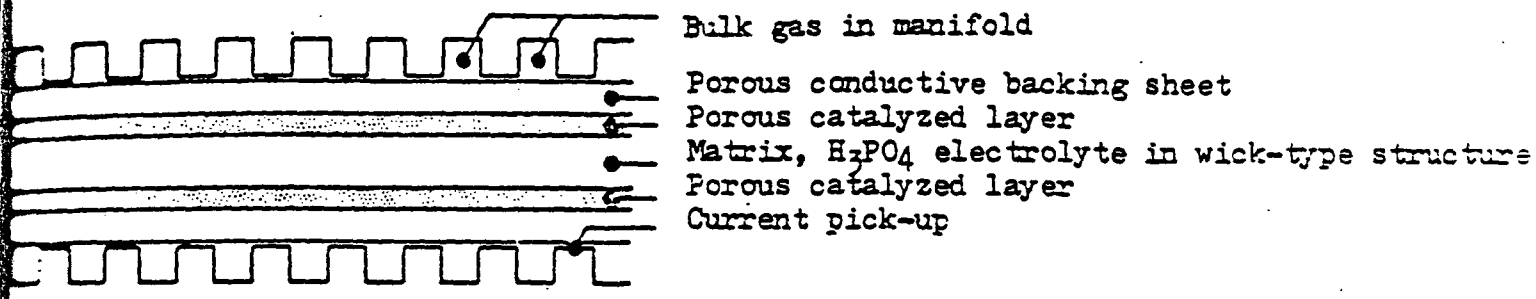

Figure 1-5 Elemental Phosphoric Acid Fuel Cell Schematic

The basic cathode structure and materials are the same as the anode's (the cathode is not doped) although the physical parameters (pore size, thickness, etc.) may be different to achieve the desired mass transfer characteristics. When the hydrogen ions arrive at the cathode reaction sites, they react with the oxygen, which has diffused through the pores of the cathode's Teflon region. The reaction is Equation (1-3).

Single cell assemblies are stacked in a series-connected bipolar mode. The directions of flow channels for air and hydrogen fuel are perpendicular to each other. In addition to the DC power generated, heat is produced as a result of the reaction. This heat is removed from the cell stack by cooling air passing through channels in cooling plates

located approximately every fifth cell so as to maintain the cells at the desired temperature. Figure 2-17 is one of the symmetric parts in the stack. The heat carried away by the cooling air is used to generate low pressure steam to drive a steam turbine. The cooling air is then recirculated back to the fuel cell system.

The effluent fuel from anode side goes to the burner after mixing with air from the air compressor. The cathode exhaust is first allowed to pass through an expander to recover some power. It is then cooled to condense out water in the stream. The condensed water is separated from the gas stream and sent to storage so that it can be used for the fuel processor or steam turbine.

1.4.3 Power Conditioning Subsystem

The primary functions of power conditioning subsystem are to control the magintude of the direct current DC generated in the fuel cell stack and to combine and convert the DC to alternating current (AC). Secondary functions are to povide appropriate fault protection, reduce harmonic distoration, and to provide power factor correction capability. The DC power source will be connected in various series/parallel arrangements to deliver the power at the required voltage and current.

CHAPTER 2

DESIGN OF PAFC SYSTEM

A primary objective of the energy conservation efforts is to reduce the consumption of premium fuels such as oil and natural gas. This can be realized by displacing the premium fuels with less critical fuels such as coal, or by developing energy conversion systems that can significantly increase the utilization efficiency of fossil fuels. Fuel cells can achieve both alternatives by more efficiently using a variety of fossil fuels, from which hydrogen can be derived, in applications where electric power and process heat are simultaneously in demand. However, while the potential conservation of fuel is important, the ability of fuel cell to penetrate the marketplace is essential in order to succesfully achieve that potential. Thus, fuel cell system analysis efforts, which are essential for design optimization to improve system performance and cost effectiveness have acquired significant practical importance.

The purpose of this chapter is to utilize mass and energy balance techniques with electrochemical and chemical kinetic disciplines to develop mathematical models and the associated digital computer simulations. The purpose of the computer simulation is to develop a simple but sufficiently accurate model of a PAFC system to allow for careful engineering evaluation of the system. The temperature,

pressure, and material balance at various locations in the systen and the sensitivity of operating conditions in major components are determined using the computer code. In addition, alternative design configurations in the reformer and fuel cell stack will also be examined for the optimal design of the system. The philosophy of the computer simulation is not to develop a highly accurate, rigorous mathematical analysis in microscopic detail but rather a workable but sufficiently accurate approach to a practical engineering problem.

In this chapter we consider two kinds of mathematical models for the components. One is the lumped model and the other is the distributed model. The lumped or "single-staged" model calculates the material and energy balances and the physical and chemical properties of the streams at one operating condition, such as the mean temperature and pressure. On the contrary, the distributed or "multi-staged" model, which usually is solved by the finite-differences method, handles the balances and properties at different sections. In the reformer and both shift converters, the lumped model utilizes the approach differential temperature (ADT)*, however, chemical kinetic will be considered in the distributed model.

There are two schemes of PAFC system which will be simulated in this chapter for steady state performance. One is the design developed

*: The approach differential temperature is the temperature difference between the exit temperature and the assumed operating temperature at which equilibrium occurs.

with this research which will be referred to as the CSU design, the other is the Westinghouse conceptual design (Ref. 12) which was described in Chapter 1. The CSU design scheme can be described as follows:

As shown in Figure 2-1, methane which is circulated by compressor (C) is preheated by heat exchanger E-1 prior to mixing it with the super heated steam which receives its heat by passing through heat exchanger E-9. Before entering the reformer, the methane steam mixture is heated via heat exchangers E-2 and E-3. Inside the reformer, methane is catalytically reformed by reaction with excess steam to produce carbon monoxide, carbon dioxide, and the desired product, hydrogen. The effluent from the reformer is cooled by flowing through heat exchanger E-2 before it enters the high temperature shift converter S-1. The function of the high temperature shift converter is to increase the hydrogen concentration and to reduce the carbon monoxide concentration of the reformer gas effluent. The temperature of the effluent from the shift converter S-1 is then reduced by passing through heat exchangers E-1, E-9, and E-6 before entering the low temperature shift converter S-2. The low temperature shift converter further increases the hydrogen concentration by promoting the shift reaction at a lower operating temperature. The effluent from the low temperature shift converter then enters the fuel cell containing H_2, CO, CH_4, CO_2 and H_2O. The fuel cell converts inputs of hydrogen and oxygen to DC power, water and heat. Oxygen is delivered to the fuel cell by air compressor A which also provides air to the reformer burner. The spent fuel from the fuel cell anode goes to the burner after mixing with air supplied by compressor A.

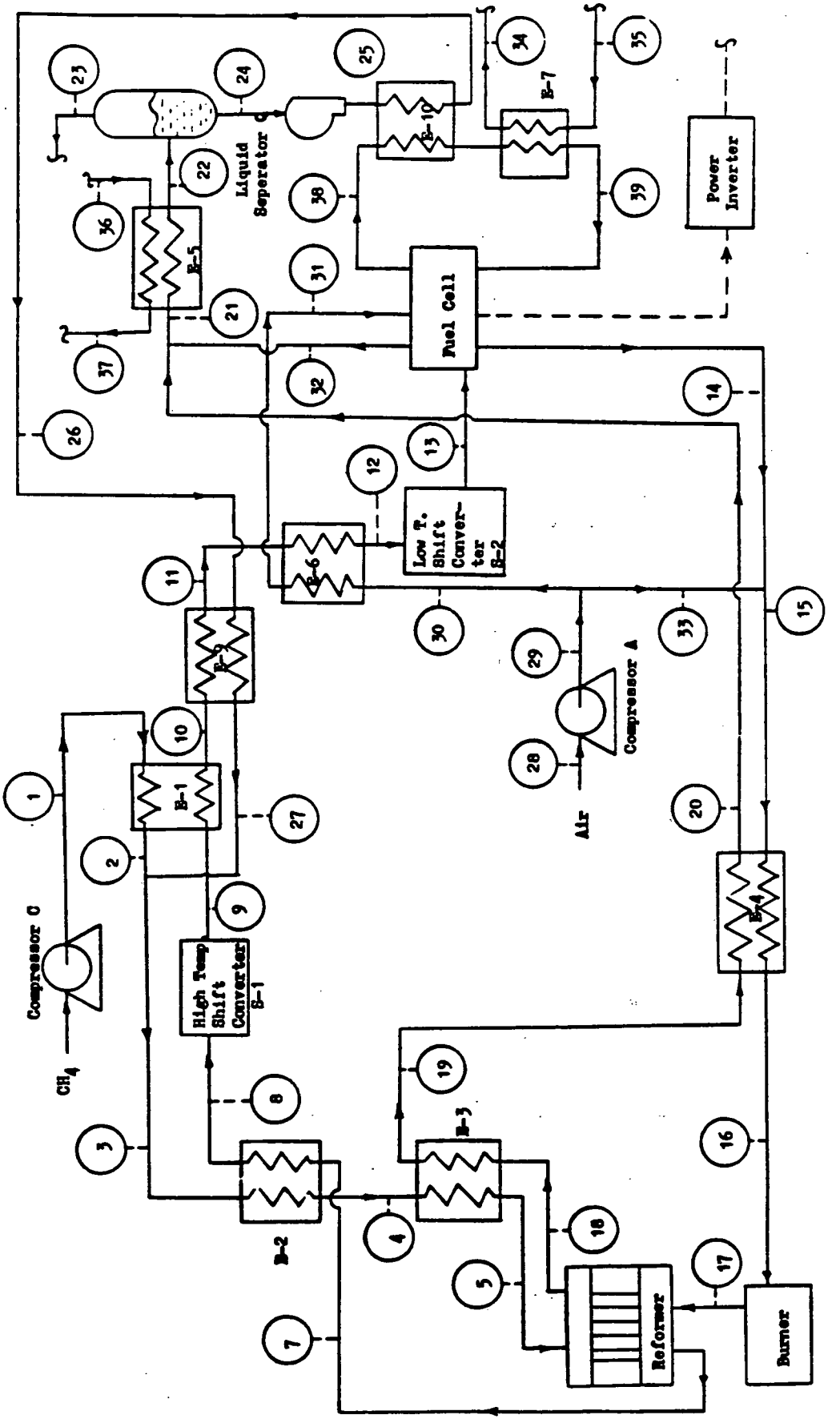

Figure 2-1 Flow diagram of CSU designed PAFC system

Before entering the burner, the mixture is preheated by the burner effluent via heat exchanger E-4. The spent fuel is then burned with whatever additional methane is needed to provide the thermal energy necessary for the reformer reaction.

Heat generated in the fuel cell is removed by heat exchangers E-7 and E-10. Heat from heat exchanger E-7 can then be utilized in industrial heat processing or space heating and cooling, while exchanger E-10 is used to preheat the water supplied by liquid separator Q to provide the necessary steam needed for the reforming process. The effluents from the burner and fuel cell cathode will have their water removed and separated by condenser E-5 and liquid separator Q before allowing them to be exhausted to the atmosphere.

This chapter will begin by modeling the components in the fuel processing subsystem and fuel cell subsystem, then the system steady state performance will be presented.

2.1 Modeling of Fuel Processing Subsystem

Production of hydrogen, which is the major function of the fuel processing subsystem, occurs by reaction of the fuel with steam. The major components in this subsystem are the reformer, the high temperature shift converter, the low temperature shift converter, and several heat exchangers.

2.1.1 Heat Exchanger

A zero capacitance sensible heat exchanger is modeled in the double-pipe counter mode.

Lumped Model

For the counter mode, given the hot and cold side inlet temperatures and flow rates, the effectiveness is calculated for a given fixed value of the overall heat transfer coefficient. The mathematical description which follows is covered in detail in Ref. 20.

$$T_{ho} = T_{hi} - E\left(\frac{C_{min}}{C_h}\right)(T_{hi} - T_{ci})$$

$$T_{co} = E\left(\frac{C_{min}}{C_c}\right)(T_{hi} - T_{ci}) + T_{ci}$$

$$Q_T = EC_{min}(T_{hi} - T_{ci})$$

and

$$E = \frac{1-e^{-\frac{UA}{C_{min}}(1-C_{min}/C_{max})}}{1-(C_{min}/C_{max})e^{-\frac{UA}{C_{min}}(1-C_{min}/C_{max})}}$$

where Cc: capacity rate of fluid on cold side, $\dot{M}_c C_{pc}$, J/s-K

Ch: capacity rate of fluid on hot side, $\dot{M}_h C_{pc}$, J/s-K

Cmax: maximum capacity rate, J/s-K

Cmin: minimum capacity rate, J/s-K

Cpc: specific heat of cold side fluid, J/g-K

Cph: specific heat of hot side fluid, J/g-K

E: heat exchanger effectiveness

$\dot{M}_c$: fluid mass flow rate on cold side, g/s

$\dot{M}_h$: fluid mass flow rate on hot side, g/s

Q_T: total heat transfer rate across heat exchanger, J/s

Tci: cold side inlet temperature, K

Tco: cold side outlet temperature, K

Thi: hot side inlet temperature, K

Tho: hot side outlet temperature, K

UA: overall heat transfer coefficient of exchanger, J/m²-s-K

Distributed Model

From the first law of thermodynamics, the energy balances for tubeside gas, shellside gas, and tubewall can be written as,

Tubeside: $h_i \pi d_i (T_w - t) = \frac{\rho_i v_i \pi (d_i)^2 C_{pi}}{4} \frac{dt}{dz}$

Shellside: $h_o d_o (T - T_w) = -\rho_o A_o C_{po} V_o \frac{dT}{dz}$

Tubewall: $h_o d_o (T - T_w) - h_i d_i (T_w - t) = 0$

where h: composite heat transfer coefficient, J/sec-m²-K

ρ: density, g-mole/m³

Cp: heat capacity, J/g-mole-K

t: temperature of tubeside gas, K

T: temperature of shellside gas, K

Tw: temperature of tubewall, K

V: velocity, m/sec

d: diameter, m

subscript i: tubeside

o: shellside

w: tubewall

Boundary conditions

z=0 t=t inlet

z=L T=T inlet

These simultaneous ordinary differential equations were solved by finite-difference method. The diagram of one section is shown in Figure 2-2.

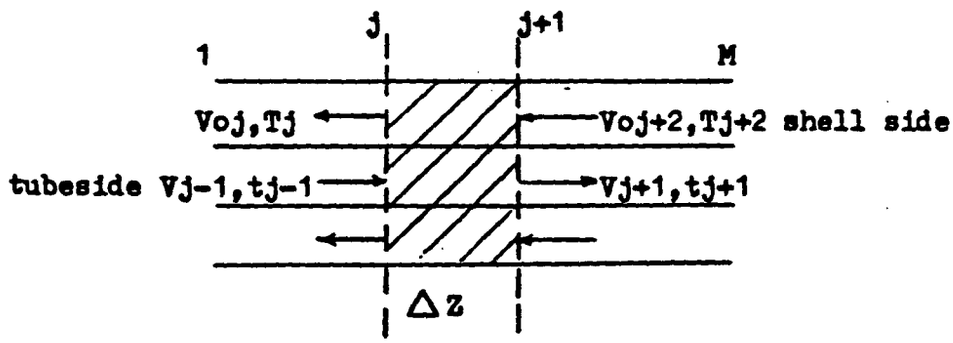

Figure 2-2 Section j of heat exchanger

Results

Distributed model was used to estimate the dimensions of the heat exchangers in Figure 1-3. Table 2-1 shows the results where the known inlet and outlet temperatures are from the Westinghouse conceptual

design (Ref. 12). These results will be used as input data for the system steady state and transient state simulations.

2.1.2 Shift Converters

The function of both types of shift converters (high temperature and low temperature) is to further increase the hydrogen concentration and to reduce the carbon monoxide concentration of the reformer gas effluent. The equation,

$CO + H_2O = H_2 + CO_2$ (water shift reaction),

dominates the material changes in the shift converters. The methanol input fuel does not need to pass through shift converters because the carbon monoxide level is low.

Lumped Model

In this model, the water shift reaction is assumed to be at equilibrium and utlizes an approach differential temperature (ADT) ranging from 15 to 25 °F. The material balance is

$$K_2 = \frac{P_{CO_2} P_{H_2}}{P_{CO} P_{H_2O}} = \frac{(F_{CO_2}+x)\ (F_{H_2}+x)}{(F_{CO}-x)\ (F_{H_2O}-x)} \qquad (2\text{-}1\text{-}1)$$

where K_2: equilibrium constant of shift reaction at ADT

P : partial pressure of component, atm

F : inlet molar flow rate of component, g-mole/s

x : reacted amount rate, g-mole/s

Equation 2-1-1 can be solved for x. Newton's method was used in the computer program.

Air Heater

Inlet :

Flow Rate / Flow No.	CH4	CO	CO2	H2O	H2	N2	O2	T	P
A2	0	0	0	5.0	0	389.9	103.7	80	1.36
A17	11.8	10.9	134.3	113.3	561.7	7.6	0	495	4.26

Outlet :

Resource / T	A3	A18
Westinghouse Simulation	192	401
Our Results *	155	428

*

NO. of tubes	80	
ID of tube	0.25	ft
OD of tube	0.28	ft
OD of shell	0.36	ft
Length of exchanger	7.5	ft

Anode Exhaust Heat Exchanger

Inlet :

Flow Rate / Flow No.	CH4	CO	CO2	H2O	H2	N2	O2	T	P
B1	11.8	10.5	134.3	60.7	112	7.8	0	376	3.4
A13	11.8	100.1	44.6	203.7	473	7.6	0	899	5.1

Outlet :

Resource / T	A24	A19
Westinghouse Simulation	761	720
Our Results *	765.7	720.1

*

NO. of tubes	220
ID of tube	0.1485 ft (1.782 in)
OD of tube	0.1667 ft (2 in)
OD of shell	0.24 ft (2.88 in)
Length of exchanger	14 ft

Table 2-1 Estimation of dimensions of heat exchangers in Westinghouse PAFC system

Heat Exchanger

Inlet:

Flow Rate / Flow No.	CH4	CO	CO2	H20	H2	N2	O2	T	P
A3	0	0	0	5.0	0	389.9	103.7	192	1.56
A6	161	0	0	0	0	8	0	180	6.8
A15	11.8	48.7	96.6	151.1	523.1	7.6	0	840	4.76

Units : Flow Rate : lb-mole/hr.
Temperature: F
Pressure : atm

Outlet:

Resource / T	A4	A7	A16
Westinghouse Simulation	700	700	397
Our Results *	699.4	698.0	381.6

* A double pipe heat exchanger model is considered with these conceptual design parameters :

NO. of tubes for A3	402
NO. of tubes for A6	178
ID of tube	0.0652 ft (0.782 in)
OD of tube	0.0833 ft (1 in)
OD of shell	0.1215 ft (1.458 in)
Length of exchanger	19 ft

Preparator

Inlet :

Flow Rate / Flow No.	CH4	CO	CO2	H20	H2	N2	O2	T	P
A10	156.3	0	0	392.4	0	7.8	0	556	6.8
A12	11.8	100.1	44.6	203.7	473.0	7.6	0	1100	5.1

Outlet :

Resource / T	A11	A13
Westinghouse Simulation	800	899
Our Results *	790	889

*

NO. of tubes	177
ID of tube	0.1485 ft
OD of tube	0.1667 ft
OD of shell	0.24 ft
Length of exchanger	9 ft

Table 2-1 continued

The energy balance equation for the gases in the shift converter includes the reaction and sensible enthalpies. For adiabatic the process in the shift converter

$$\sum_{PS} nj\ (\Delta h^{\circ} f)j - \sum_{RS} ni\ (\Delta h^{\circ} f)i + \sum_{PS} nj \int_{298}^{Tf} (Cp)j\ dT - \sum_{RS} ni \int_{298}^{Ti} (Cp)i\ dT = 0 \qquad (2\text{-}1\text{-}2)$$

where the subscripts PS, RS correspond to the products and reactants in the shift converter, respectively. Tf, Ti are the final and initial temperatures of the gases, respectively. The only unknown in the equation ,Tf, is determined iteratively.

The Ergun equation, which estimates pressure drop caused by the flow of gas through dry packings, is used to determine the pressure drop in shift converter and reformer. The equation is (Ref. 22)

$$\Delta P = 1878 \cdot \frac{1-\epsilon}{\epsilon^3}\ \frac{G}{dp\ g_c \rho}\left(\frac{150(1-\epsilon)\mu}{dp\ G} + 1.75\right) \cdot h \qquad (2\text{-}1\text{-}3)$$

where ϵ : void fraction in bed

μ : viscosity, Kg/m-s

dp: effective diameter of packing particle, m

G : superficial gas mass velocity, Kg/s-m

h : packed height, m

ρ : density, Kg/m^3

ΔP: pressure drop, atm

Distributed Model

In the distributed model simulation, the shift converter is simulated as an adiabatic packed bed catalytic reactor which produces

hydrogen through the water shift reaction.

The general assumptions made for simulation of a packed bed reactor (like the reformer and shift converter) are discussed here;

(1) Axial dispersion and radial gradient are negligible - plug flow condition. Generally if the ratio of the length of the reactor to the catalyst's diameter is greater than 100, the axial dispersion effect is negligible.

(2) A uniform temperature exists throughout each catalyst particle, and this temperature is the same as the gas temperature in that section of catalyst bed.

(3) The kinetic expression represents a global rate, and therefore neglects reactivity differences found between the inside and outside of the catalyst particles.

(4) Entrance effects are negligible.

(5) Heat transfer by radiation is negligible.

(6) A single reactor tube is analyzed. Thus, all the tubes in the reformer or shift converters behave independently of one another.

(7) Ideal gas behavior is assumed.

(8) The outside shell wall is adiabatic.

A more detailed discussion of assumptions (2) and (3) is provided in Appendix 2 by examination of the "internal" and "external" effectiveness factors of commercial catalysts used in reformer and shift converters.

Mass Balance

From the general continuity and assumptions, the kinetic mass balance for the shift converter is

$$V \frac{dC}{dz} = \frac{-r_a' e_B}{\epsilon} \qquad (2\text{-}1\text{-}4)$$

where V : average velocity of fluid through the bed, m/s

C : g-mole of CO per m^3 fluid

ra': reaction rate, g-mole of CO/s-Kg catalyst

e_B: density of catalyst, Kg/m^3 bed

Reaction Rate

From Ref. 24 the rate expression for a high temperature shift converter with a catalyst composed of Fe_2O_3 and Cr_2O_3 is (Ref. 23)

$$r = \frac{k(P_{H_2O} P_{CO} - K_2^{-1} P_{CO_2} P_{H_2})}{A P_{H_2O} + P_{CO_2}} \qquad (2\text{-}1\text{-}5)$$

where r : reaction rate, m^3CO @ STP/m^3 bed-s

k : rate constant

A : constant

for a low temperature shift converter with a catalyst composed of ZnO, Cr_2O_3, and CuO, the first order rate and Arrhenius expression is

$$-r = Ko\, e^{-EA/RT} P_{CO} \qquad (2\text{-}1\text{-}6)$$

where r in g-mole of CO/s-kg cat.

Ko: Arrhenius frequency factor, g-mol/s-kg cat.-atm

EA: activation energy, J/g-mol

R : gas constant

T : temperature, K

The [illegible] will be used as [illegible] the [illegible] transient response simul[illegible]

Energy Balance

The energy balance for the reacting gas is

$$Cp\, \rho\, V \frac{dt}{dz} = (-\Delta H) \frac{r_a' e_B}{\epsilon} \qquad (2\text{-}1\text{-}7)$$

where Cp: heat capacity of fluid, J/g-mole-K

ρ: fluid density, g-mol/m^3

$-\Delta H$: heat of reaction, J/g-mol of CO

t : temperature of reacting gas

These two oridinary differential equations were solved by the finite-difference method. A diagram of one section is shown in Figure 2-3.

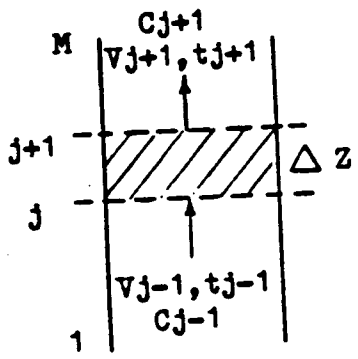

Figure 2-3 Section j of shift converter

Results

The distributed model was used to estimate the dimensions of the high temperature and low temperature shift converters in Figure 1-3. The results are shown in Table 2-2, where the known inlet and outlet compositions and temperatures are from Ref. 12. These results will be used as input data for the steady state and transient response simulations of the system.

High Temperature Shift Converter

Inlet:

Flow Rate / Flow No.	CH4	CO	CO2	H2O	H2	N2	O2	T	P
A14	11.78	100.16	44.6	203.66	472.96	7.57	0	720	5.1

Units: Flow Rate: lb-mole/hr
Temperature: F
Pressure: atm

Outlet:

Flow Rate / Resource	CH4	CO	CO2	H2O	H2	N2	O2	T	P
Westinghouse Simulation	11.78	48.2	96.56	151.7	524.92	7.57	0	840	4.8
Our Results*	11.78	49.8	95.0	153.3	523.4	7.57	0	864	5.0

* A single Pipe reactor is considered with these conceptual design parameters:

NO. of reactor tubes	92
ID of reactor tube	0.3 ft
Height of reactor tube	6 ft

Low Temperature Shift Converter

Inlet:

Flow Rate / Flow No.	CH4	CO	CO2	H2O	H2	N2	O2	T	P
A16	11.78	48.2	96.56	151.7	524.92	7.57	0	397	4.42

Outlet:

Flow Rate / Resource	CH4	CO	CO2	H2O	H2	N2	O2	T	P
Westinghouse Simulation	11.78	10.8	133.96	114.3	562.3	7.57	0	495	4.42
Our Results*	11.78	10.9	133.8	114.4	562.2	7.57	0	502.2	4.36

* NO. of reactor tubes 92
ID of reactor tube 0.25 ft
Height of reactor tube 2 ft

Table 2-2 Estimation of dimensions of shift converters in Westinghouse PAFC system

2.1.3 Reformer

The key component in the fuel processing subsystem is the reformer which catalytically reforms methane (methanol or naphtha) by reaction with excess steam to produce carbon monoxide, carbon dioxide, and the desired product, hydrogen. Methane will be the only input fuel in the following discussion.

Two reactions are assumed to be the principle reforming reactions in the model, they are

$CH_4 + H_2O = CO + 3H_2$ (demethanation reaction)

$CO + H_2O = CO_2 + H_2$ (water shift reaction).

Appendix 1 lists all of the possible reactions and discusses the minimum steam to carbon ratio (S/C) required to avoid carbon formation.

Lumped Model

In the lumped model both of the reactions, demethanation and shift reaction, were assumed to be at equilibrium by utilizing the respective ADT's of each. The equilibrium constants were determined from the temperature. The equilibrium expression are

$$K_1 = \frac{P_{CO_2} P^3_{H_2}}{P_{CH_4} P_{H_2O}} = \frac{Y_{CO_2} Y^3_{H_2}}{Y_{CH_4} Y_{H_2O}}$$ (demethanation)

$$K_2 = \frac{P_{CO_2} P_{H_2}}{P_{CO} P_{H_2O}} = \frac{Y_{CO_2} Y_{H_2}}{Y_{CO} Y_{H_2O}}$$ (water shift),

where K1 and K2 are the equilibrium constants of demethanation and water shift reaction, respectively. Expressing the mole fractions as the individual molar flows divided by the total molar flows yields:

$$K_1 = \frac{(F_{CO} - x + y)\,(F_{H_2} + x + 3y)^3\,P^2}{(F_{CH_4} - y)\,(F_{H_2O} - x - y)\,(F_T + 2y)^2} \qquad (2\text{-}1\text{-}8)$$

and

$$K_2 = \frac{(F_{CO_2} + x)\,(F_{H_2} + x + 3y)}{(F_{CO} - x + y)\,(F_{H_2O} - x - y)} \qquad (2\text{-}1\text{-}9)$$

where y is the conversion amount rate in the demethanation reaction and F is the total inlet flow rate. Equations (2-1-8) and (2-1-9) can be solved for x and y. Newton's method was used in the computer program. Figure 2-4 and 2-5 show the equilibrium conversion of methane at different S/C ratios, temperatures, and pressures. It can be observed that greater pressures and greater S/C ratios will favor the conversion, but over the temperature ranges, temperature seems to be the major factor.

The quantities involved in the energy balance will be the sensible enthalpies of the gases, the reaction enthalpies of the gases, and the heat transferred from the combustion gases to the reformer gases, $Q_{B\text{-}R}$. The value of $Q_{B\text{-}R}$ can be determined from

$$Q_{B\text{-}R} = UA\,\Delta T_m = Hout - Hin \qquad (2\text{-}1\text{-}10)$$

where, ΔT_m is the log mean temperature defined as

$$\Delta T_m = \frac{(T_{fC} - T_{iR}) - (T_a - T_{fR})}{\ln \dfrac{T_{fC} - T_{iR}}{T_a - T_{fR}}} \qquad (2\text{-}1\text{-}11)$$

where, T_{fC} is the temperature of the combustion gases after leaving the reformer; T_{iR} and T_{fR} are the temperatures of the reformer gases before entering and after leaving the reformer; A is the heat transfer area; and U is a modified form of a heat transfer coefficient.

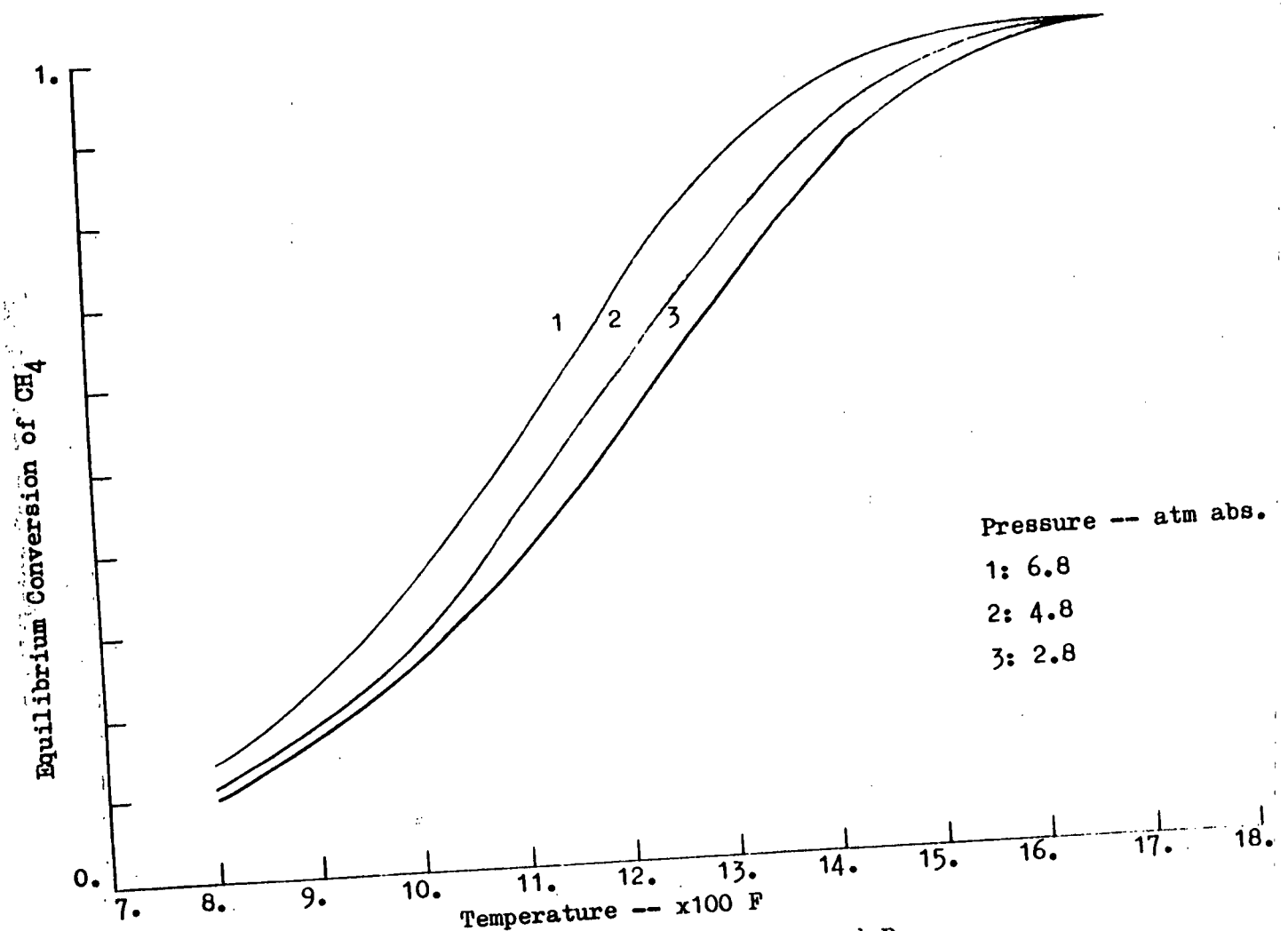

Figure 2-4 Equilibrium conversion of CH_4 with T and P

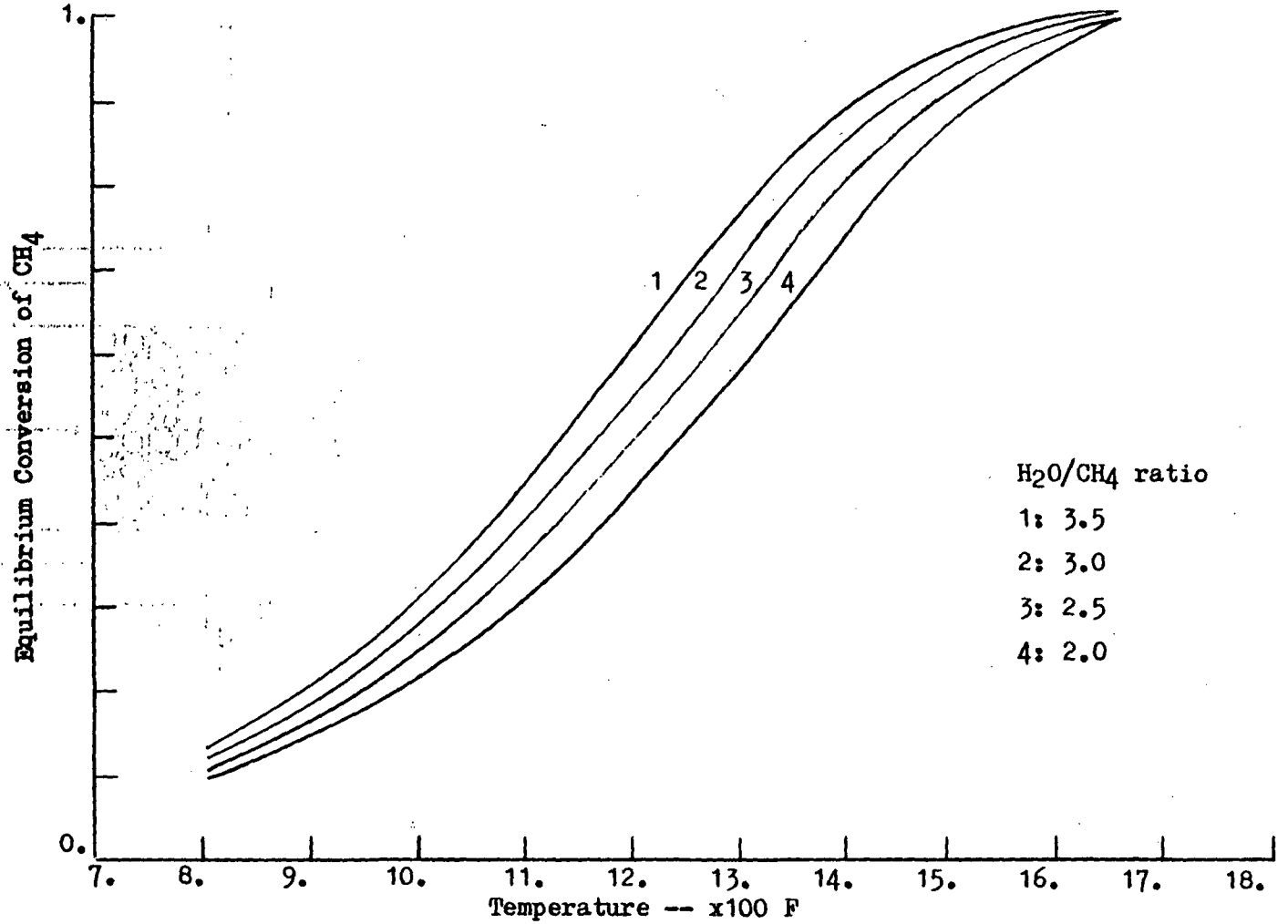

Figure 2-5 Equilibrium conversion of CH_4 with T and H_2O-CH_4 ratio

Thus, from the first law of thermodynamics and equation (2-1-11), the energy balance for the reformer gases can be written as,

$$UA\Delta T_m = \sum_{PR} m_j \, (\Delta h_f^\circ)_j - \sum_{PR} m_i \, (\Delta h_f^\circ)_i + \sum_{PR} m_j \int_{298}^{T_{fR}} (C_p)_j \, dT$$

$$- \sum_{rR} m_K \int_{298}^{T_{iR}} (C_p)_i \, dT, \ldots \qquad (2\text{-}1\text{-}12)$$

where the subscripts PR and rR stand for products and reactants in the reformer, respectively.

Distributed Model

Kinetical analysis was used for simulation of the performance of the reformer. The reformer is basically a nonadiabatic, nonisothermal catalytic reactor, that is heated on the shell side by combustion gases from burner. Figure 2-6 shows its simplified scheme.

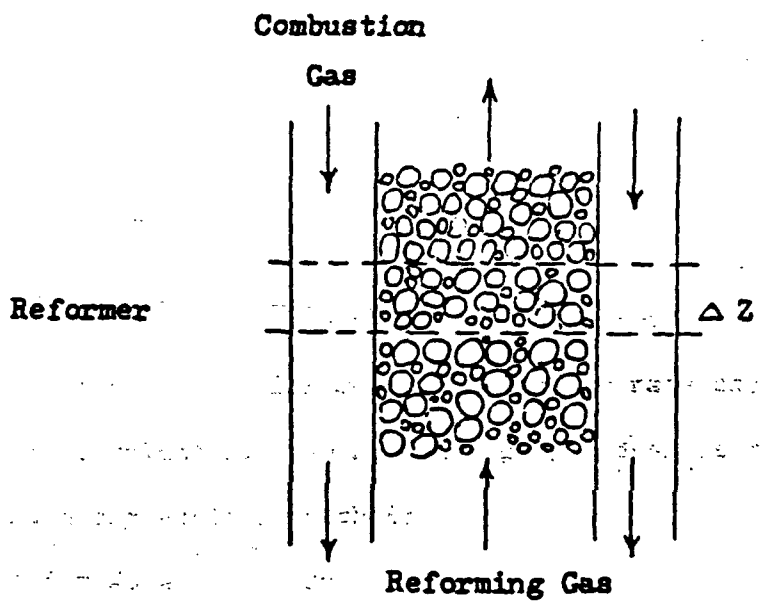

Figure 2-6 Simplified reformer diagram

The demethanation reaction is assumed to be kinetically controlled and, hence, occurs at a finite rate, while the water gas shift reaction is assumed to be equilibrium controlled. The modeling assumptions discussed in Section 2.1.2 are also applied here. The demethanation reaction used in this model is slightly modified with linear combinations of the original demethanation reaction and shift reaction, which results in

$$CH_4 + 2H_2O = CO_2 + 4H_2 \qquad (2\text{-}1\text{-}13)$$

In the equilibrium calculations, the demethanation reaction choice causes no changes in the final results. However, the kinetic consideration will cause the final results to vary slightly with the reaction choice.

Mass Balance

From the generalized continuity and the assumptions, the kinetic mass balance is

$$V\frac{dC}{dz} = -\frac{r_a' \rho_B}{\epsilon}, \qquad (2\text{-}1\text{-}14)$$

this is the same as Equ. 2-1-4 except that the basis is changed to methane.

Various kinetic expressions for the reforming of methane with steam have been proposed which could provide the rate equation (Ref. 24, 25, 26). The simplest form among the proposed expressions is the first order rate expression, which is

$$-r_a' = K_o e^{-EA/RT} P_{CH_4} \qquad (2\text{-}1\text{-}15)$$

in Arrhenius form (the same definitions as Equ. 2-1-6). Unfortunately,

little agreement can be found for the values of the kinetic parameters, some values may be three orders of magnitude different from others. The data from Ref. 26 using a commercial catalyst (Gindler G-56B) is used in this model.

The water gas shift reaction is assumed to be at equilibrium. The conversion quantity is based upon the carbon dioxide mass balance. Thus, when coupled with the demethanation reaction, the water gas shift reaction proceeds in reverses, therefore, the shift conversion is always negative. Using these two reaction schemes, all of the molar flows anywhere in the reformer can be written in terms of the feed quantities and the conversions of the two reactions.

Energy Balance

Two energy balances are required for the system: one for the reformer gases and one for the combustion gases. The reformer gas balance includes its own sensible heat change, reaction enthalpies, and heat transfer from the hotter combustion gases. The combustion gas balance involves sensible heat change and heat transfer. This translates quantitatively into Equation (2-1-16) and (2-1-17).

$$\rho\, Ai V\, Cp \frac{dt}{dz} = (-\Delta H_1)\frac{dY}{dz} + (-\Delta H_2)\frac{dx}{dz} + hi\,\pi\, di\,(Tw-t) \qquad (2\text{-}1\text{-}16)$$

$$\rho_o\, Vo\, Ao\, Cpo \frac{dT}{dz} = -ho\,\pi\, do\,(T-Tw) \qquad (2\text{-}1\text{-}17)$$

where ΔH_1: demethanation reaction enthalpy, J/g-mol CH_4

ΔH_2: water shift reaction enthalpy, J/g-mol CO

Ai : inner tube cross area, m^2

hi : wall heat transfer coefficient of tube side, $J/s\text{-}m^2\text{-}K$

Tw : wall temperature,K

di : inner tube diameter, m

T : combustion gas temperature, K

do : outer tube diameter, m

subscript o refers to the combustion gas side

There is greater uncertainty in estimating the heat transfer coefficient at the wall of tube than the rate expression. The scatter in experimental data is very high (Ref. 22, 24, 25). The situation will be even more complicated by considering the unequal stoichimetric reaction (Ref. 28). Due to Beek's recommendation (Ref.29) the modified Thoenes-Kramers (Ref. 30) correlation should be used for sphere-like particles near the wall, which are used in the model.

$$hi(dp/k_f) = 2.58(Re)^{1/3}(Pr)^{1/3} + .094(Re)^{0.8}(Pr)^{0.4} \qquad (2\text{-}1\text{-}18)$$

where dp: equivalent particle diameter, m

k_f: thermal conductivity, J/s-m-K

Pr: Prandtl number

Re: partical Reynolds number

Differential equations, (2-1-1), (2-1-14), (2-1-16), and (2-1-17) were solved simultaneously with the inlet conditions as the boundary conditions. The Ergun equation (Equation 2-1-3) is used to evaluate the pressure drop. The Computer code which was developed to simulate the performance used the finite-difference method to solve these simultaneous ordinary differential equations. Figure 2-7 shows one section of the reformer, and the program flowchart for the model is given in Figure 2-8.

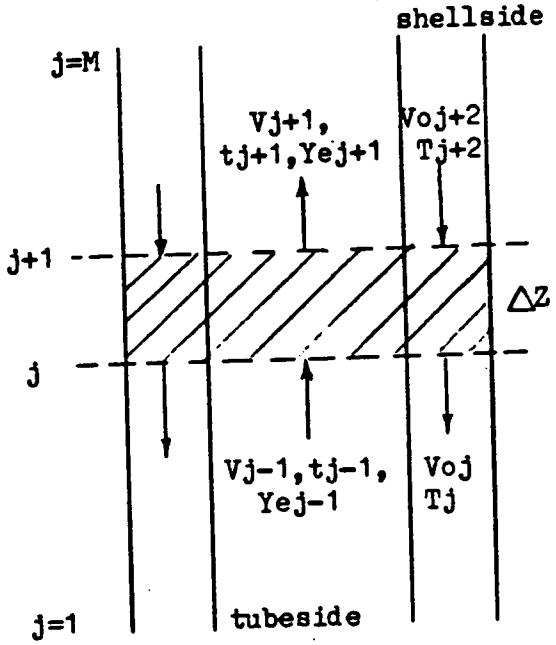

Figure 2-7 Section j of reformer

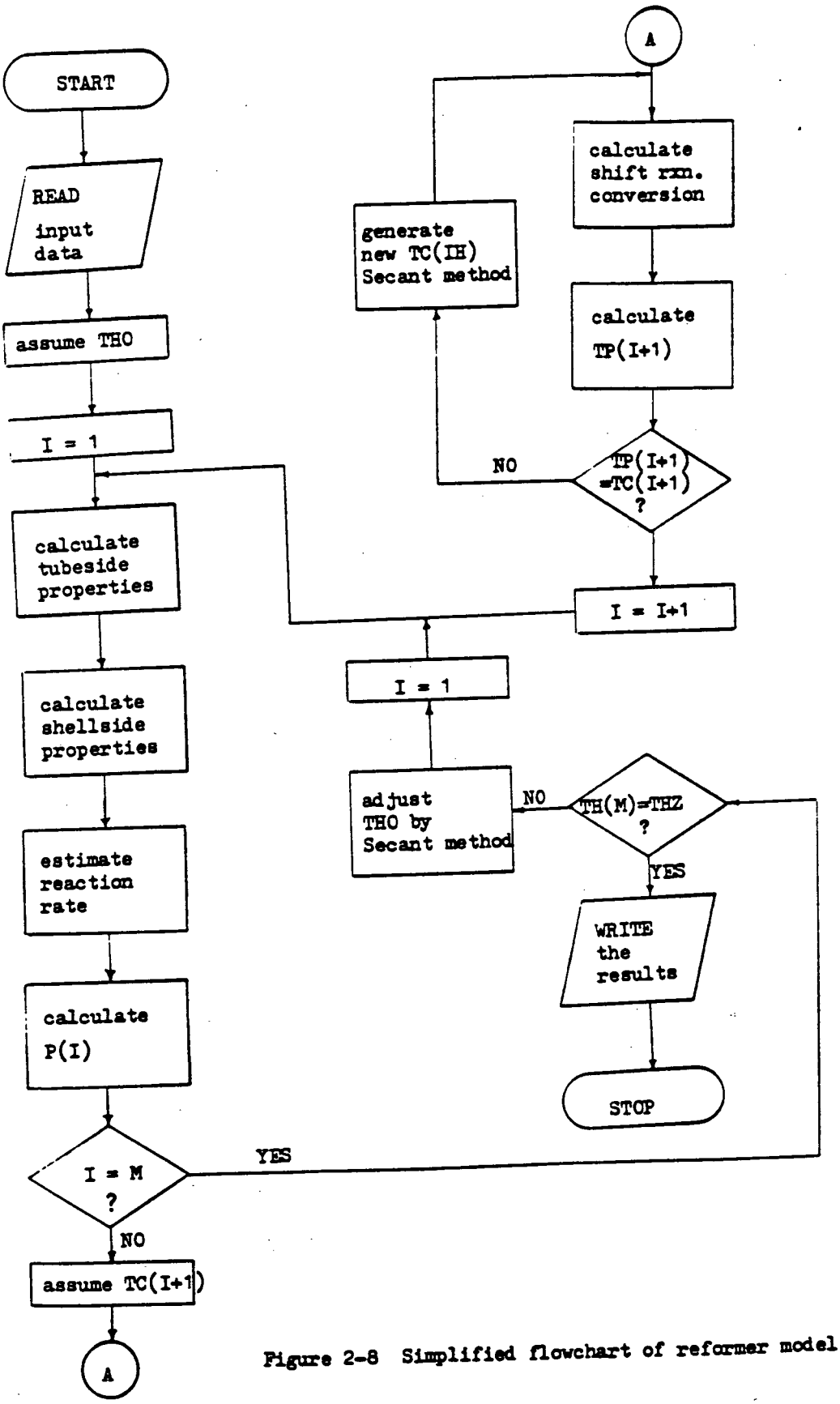

Figure 2-8 Simplified flowchart of reformer model

Results and Comparison

The model results were compared to the Phillips Petroleum reformer data (Ref. 25). The reformer described in Ref. 25 is used in the refinery industry, so the tube is electrically heated to maintain a vertical temperature profile. The model discussed in this section were modified to fit this special condition. Figure 2-9 gives the temperature, pressure, and conversion profiles along the reformer tube. Table 2-3 shows the comparison together with Westinghouse BOLTAR simulation results (Ref. 11). As the results indicate, the model corresponds to the given data very well. Pressure drop considerations, different rate expressions, and different heat transfer coefficient estimation enable the CSU model to better simulate the Phillips Petroleum reformer in comparison to BOLTAR.

The CSU model can also be modified to simulate the "regenerative" reformer which will be discussed in Section 2.2.3. Because the reformer's performance greatly depends on the temperature level, the uncertainty in the rate expression and heat transfer coefficient will limit the simulation model accuracy.

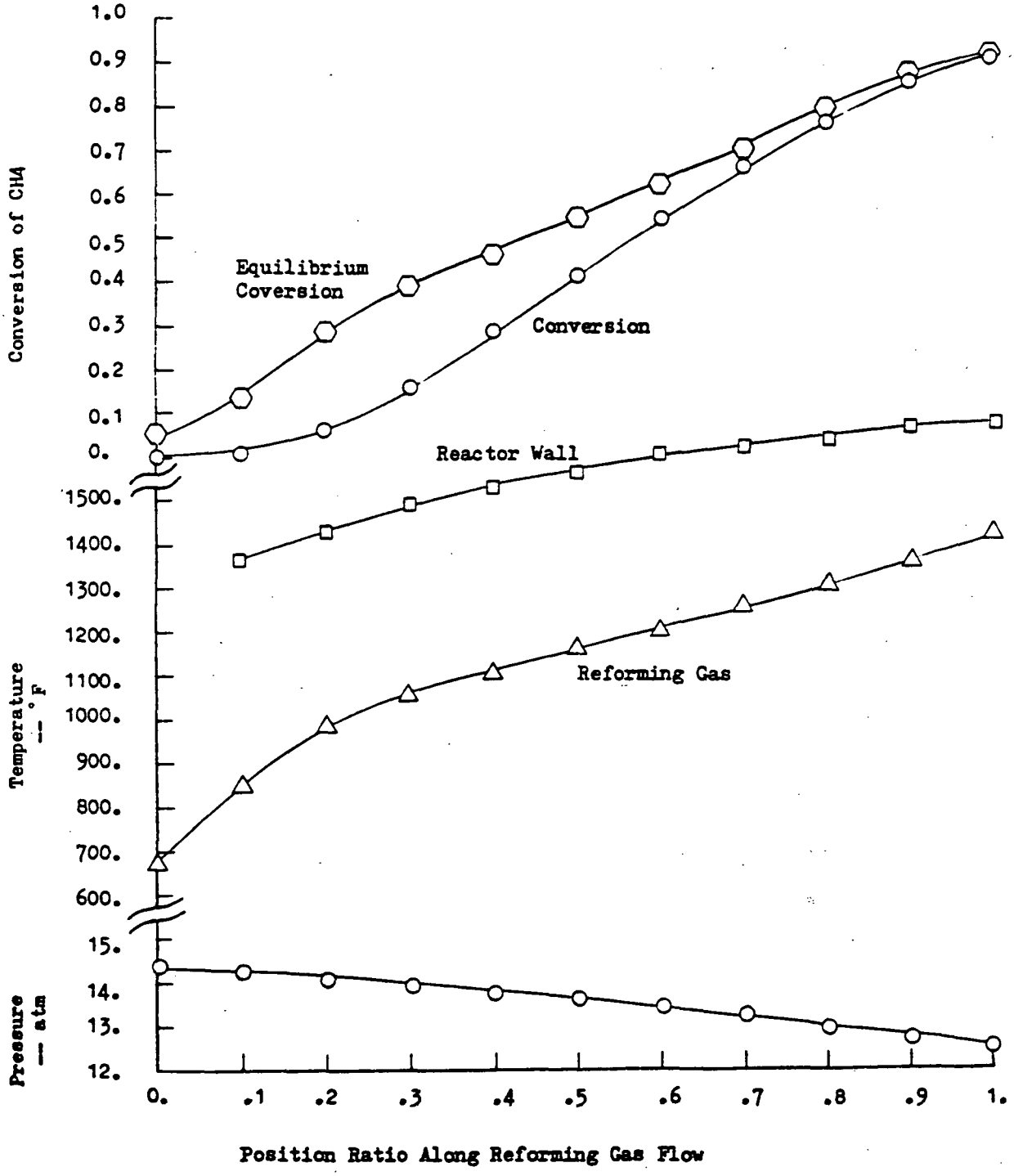

Figure 2-9 The reforming tube profile obtained for the distributed model

Reformer Results Comparison

Input Data	Phillips Petroleum Reformer Data (Ref. 25).	BOLTAR(Ref. 13)	CSU
Height, m	12.2	12.2	12.2
Tube ID, cm	13.	D2=13.	D2=13.
Tube wall thickness,cm	1.35	1.3	1.35
Catalyst part. size, cm	1.59x1.19x.48 rings	1.27 spheres	1.27 spheres
Mass flow rate (superficial)	26700 $kg/hr-m^2$	FO=19.1 kg-mole/hr	FO=19.1 kg-mole/hr
Steam/methane ratio	7:1	7:1	7:1
Gas inlet temp., °C	364.	364.	364.
Tube wall temp., °C	$704+31xz-1.2xz^2$ (z in m)	same	same
Inlet pressure, MPa a.	14.3	13.2 throughout	14.3
Output Results	**Given**	**BOLTAR**	**CSU**
Outlet pressure, MPa a.	12.2	13.2	12.7
Outlet temp., °C	793.	823	776
Conversion, %	91.7	86.1	91.9

Table 2-3 Comparison of CSU model with experimental data and BOLTAR

2.2 Modeling of Fuel Cell Stack Subsystem

In the fuel cell power section, air, in excess of the stoichiometric mixture, enters the cathode side of the cell, and effluents from the low temperature shift converter enter at the anode. The anode input contains CH_4, H_2O, H_2, CO and CO_2. In this analysis, it is assumed that a fixed percentage of hydrogen is consumed at the anode, and the H_2O being formed exits the fuel cell, with the depleted air, through the cathode exit. The overall reaction in the fuel cell power section is,

$$H_2 + 1/2\ O_2 = H_2O \qquad (2\text{-}2\text{-}1)$$

This section presents the two distinct mathematical models of fuel cells that were developed and computer programs that were written to perform the necessary calculations.

The simplified lumped model is an "input-output" model developed for the system trade-off studies.

The detailed distributed model is a finite -difference model of the operation of the fuel cell which was used to calculate the effects of the cell and module design on performance. It calculates the current density distribution in the cells as a function of the local reactant compositions, local temperatures, catalyst utilization factors, etc. Since these are interdependent (e.g. the local temperature depends on the local current density), the computations are highly iterative and require considerably more computer capacity and time than the lumped model. An associated computer program will be used to compare an

alternative design of cooling scheme in the stack.

2.2.1 Lumped Model and Voltage-Current Characteristics

The simplified lumped model provides a rapid (in terms of computer time) means of calculating the fuel cell module output characteristics (voltage, current, and heat generation rate) in terms of the inputs from the fuel processing subsystem and the gross fuel cell design parameters such as catalyst loading.

The mass balances of hydrogen, oxygen and water are as follows:

$$NX_{H_2} = NI_{H_2} - (Imean \cdot A)/(n \cdot \mathcal{F}) \qquad (2\text{-}2\text{-}2)$$

$$NX_{O_2} = NI_{O_2} - (Imean \cdot A)/(2n \cdot \mathcal{F}) \qquad (2\text{-}2\text{-}3)$$

$$NX_{H_2O} = NI_{H_2O} + (Imean \cdot A)/(n \cdot \mathcal{F}) \qquad (2\text{-}2\text{-}4)$$

where NX: exit flow rate of hydrogen, oxygen, or steam, g-mole/sec

NI: inlet flow rate of hydrogen, oxygen, or steam, g-mole/sec

Imean: mean current density, A/cm²

A: effective area of cell plate, cm²

n: number of Faraday equivalents transfered

$\mathcal{F}$: Faraday constant

The energy balance for the fuel cell is,

$$-(Q + W_e) = \sum_{PF} n_j (\Delta h_f^\circ)_j - \sum_{rF} n_i (\Delta h_f^\circ)_i \qquad (2\text{-}2\text{-}5)$$

$$+ \sum_{PF} n_j \int_{298}^{T_{fF}} (C_p)_j \, dT - \sum_{rF} n_i \int_{T_{iF}}^{298} (C_p)_i \, dT$$

where the subscripts PF, rF represent the products and reactants in the fuel cell, respectively. TfF is the final temperature of the products

and TiF is the initial temperature of the reactants in the fuel cell. The nj and ni are the species flow rates of the products and reactants, respectively. The terms Q and W are the rates of heat and the electrical energy generation by the fuel cell, respectively. Q is proportional to the specific heat generation Q_F where:

$$Q = Np \cdot Xn \cdot Yn \cdot Q_F \qquad (2\text{-}2\text{-}6)$$

and $$Q_F = \left(\frac{\Delta H_r}{n\mathcal{F}} - V\right) I \qquad (2\text{-}2\text{-}7)$$

where Q : total heat generated, J/sec.

Q_F : heat generated per unit area of cell, J/sec.cm²

Np : number of cells

Xn : width of cell plate

Yn : length of cell plate

I : fuel cell current density, A/cm²

ΔH_r : heat of reaction, J/g-mole of H_2

Voltage-Current Characteristics

Because of the irreversibility, the voltage V for a working fuel cell is the difference between the open circuit voltage and the cell polarization terms:

$$V = E - \eta \qquad (2\text{-}2\text{-}8)$$

where E: Nernst potential (reversible open circurt E.M.F.)

η: overpotential or polarization

The reversible cell potential, E is given by the Nernst equation

$$E_0 = E(T) + \frac{RT}{ZF} \ln\left(\frac{Y_{H_2}\sqrt{P_t Y_{O_2}}}{Y_{H_2O}}\right) \qquad (2\text{-}2\text{-}9)$$

with Pt: total pressure, atm

$E_o(T)$: standard E.M.F. of cell at temperature T, volts

$E_o(T)$= 1.261-0.00025 T, T, K (Ref. 10)

YH_2: mean mole fraction of hydrogen at anode

YO_2: mean mole fraction of oxygen at cathode

YH_2O: mean mole fraction of water vapor at cathode

The polarization term η consists of four components,

$$\eta = \eta a + \eta r + \eta d + \eta co \qquad (2\text{-}2\text{-}10)$$

where ηa: activiation poparization at cathode, volts

ηr: resistance polarization, volts

ηd: diffusion polarization, volts

ηco: activiation polarization at anode due to co poisoning of catalyst, volts

and

$$\eta a = \frac{RT}{\alpha_o ZF} \ln \frac{i}{(io)(SA)(CL)(CU)} \qquad (2\text{-}2\text{-}11)$$

with αo: transfer coefficient

i : current density, mA/cm^2

io: exchange current density of cathode, mA/cm^2

SA: specific catalyst surface area, cm^2/g

CL: catalyst loading on cathode, g/cm^2

CU: catalyst utilization factor.

The exchange current is a function of the acid concentration, temperature, and partial pressure of the oxygen. The acid concentration is a function of the water vapor partial pressure which permits correlation of io as a function of YO2, YH2O, and T. An empirical fit is

$$io = 232.7\ (PtYO2)^{0.8} \cdot (PtYH2O)^{0.4377}\ \exp(-6652/T) \qquad (2\text{-}2\text{-}12)$$

The resistance polarization is

$$\eta r = ir$$

where r: specific cell resistance, ohm-cm² .

The expression of η co was chosen to have strong temperature dependence, be directly proportional to Yco, and have a logarithmic dependence on i, iao and catalyst effective area. The resulting expression (Ref. 10) is

$$\eta co = 0.0782 PtYco \exp\left[9190\left(\frac{1}{T} - \frac{1}{450}\right)\right] \ln\left(\frac{i}{CLa\ SA\ CU\ iao}\right) \qquad (2\text{-}2\text{-}13)$$

where CLa: anode catalyst loading, mg

iao: anode exchange current, mA/cm²

Diffusion polarization has been neglected here because it is significant only at very high current densities.

In the associated computer program, Subroutine VI, calculates cell voltage as a function of the current density or alternatively solves the nonlinear equation to evaluate current density as a function of the cell voltage.

It is difficult to compare the predictions of a cell voltage equation with experimental data because of the generally incomplete electrode or other cell specifications. Figure 2-10 illustrates the effect of electrode performance on cell potential. Each of the six curves was developed for different catalyst utilization factors, using

Figure 2-10 V-C.D. characteristic chart with different CU

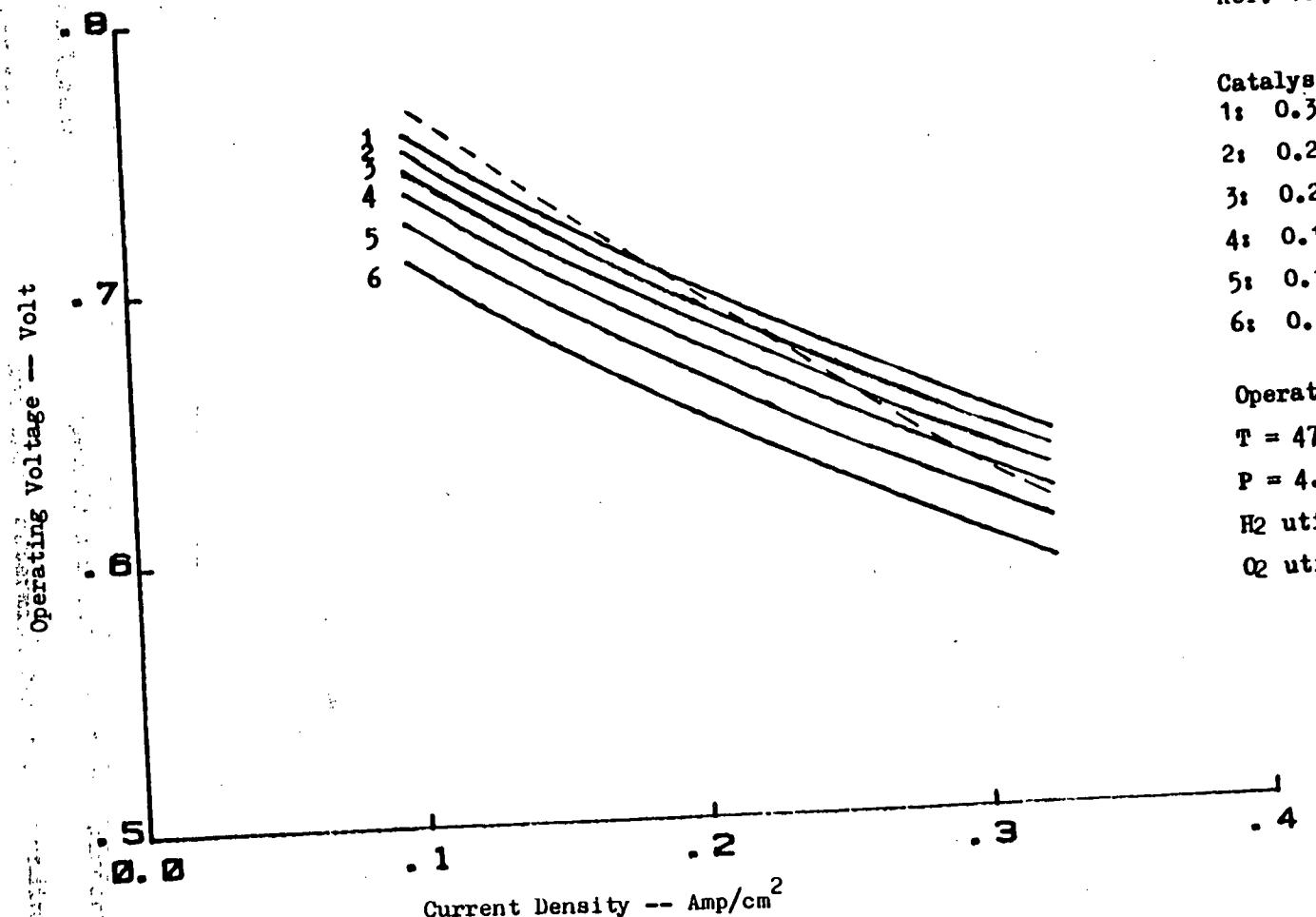

- - - - -
Ref. 10

Catalyst Utilization
1: 0.30
2: 0.26
3: 0.22
4: 0.18
5: 0.14
6: 0.10

Operating Conditions
T = 473 K
P = 4.70 atm abs.
H_2 utilization = 80 %
O_2 utilization = 50 %

Equation 2-2-8. The curves are compared with the prediction of the design relations from Ref. 10 . The latter are in the nature of off-design corrections to a baseline fuel cell operating on pure hydrogen and oxygen, 1 atm, pressure, 175°C, and low utilization.

2.2.2 Current Density Distribution

In the fuel cell module, the combined modeling of temperature and current distribution is an absolute condition for reliable scaling-up of the results obtained with small cells, and for predictive models starting from elementary porous-electrode representations.

This subsection describes the calculation of the current density distribution over a cell plate on which the air and fuel flows are at right angles. The procedure divides a cell plate into "grids" which are small enough so that variations in fuel and oxidant composition and temperature are negligible. Then by means of calculation of the boundary conditions for each "grid" and iteration, a solution will be obtained that satisfies the input specifications (e.g. average current density, fuel and air utilization, and reactant flow rates). A diagram of the "grid" is shown in Figure 2-11 .

The overall method is to first specify a desired average current density i for the whole plate and then determine the corresponding voltage V for the plate. This voltage will be determined such that it produces unique local current densities over the plate whose average value approximates i within a specified tolerance. A trial-and-error

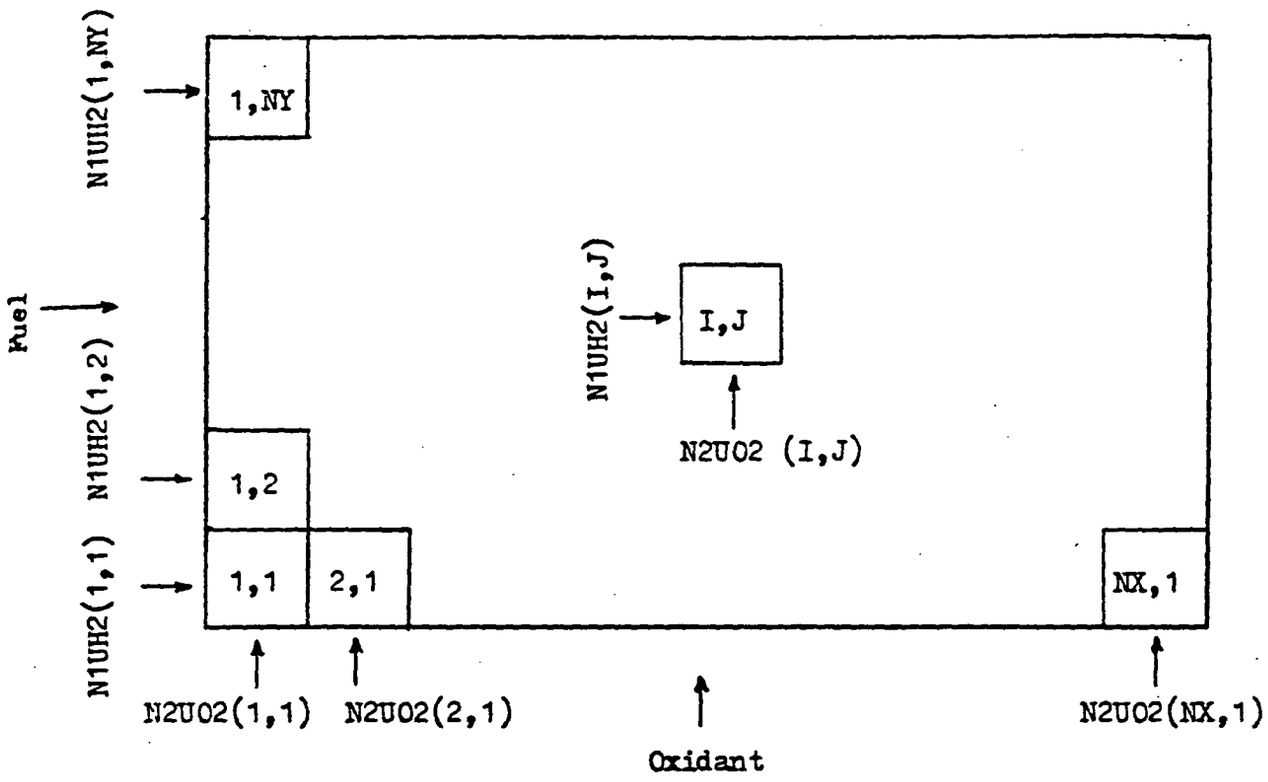

Figure 2-11 Finite Difference Model Definition of Current Density Distribution on Cell Plate

procedure is used to estimate the local current density and overall voltage. The model basically applies the same voltage-current equation used in the lumped model (described in Section 2.2.1) to each grid section of the cell.

Mathematical Formulation

Exit flow of hydrogen from grid (i,j)

$$NX_{H_2}(i,j) = NI_{H_2}(i,j) - (I(i,j)\ A)/(n \cdot F) \qquad (2\text{-}2\text{-}14)$$

Exit flow of oxygen from grid (i,j)

$$NX_{O_2}(i,j) = NI_{O_2}(i,j) - (I(i,j)\ A)/(2 \cdot n \cdot F) \qquad (2\text{-}2\text{-}15)$$

Exit flow of water from grid (i,j)

$$NX_{H_2O}(i,j) = NI_{H_2O}(i,j) + (I(i,j)\ A)/(n \cdot F) \qquad (2\text{-}2\text{-}16)$$

where $NX_{H_2,\ O_2,\ H_2O}$ (i,j) : hydrogen (oxygen or water) portion flow rate at exit of grid (i,j), g-mole/sec.

$NI_{H_2,\ O_2,\ H_2O}$ (i,j) : hydrogen (oxygen or water) portion flow rate at inlet side of grid (i,j) g-mole/sec.

I (i,j) : current density of grid (i,j), A/cm²

A : area of grid, cm²

The flow chart of executive program for calculating current density distribution is shown in Figure 2-12 .

Results

A current density distribution over an isothermal cell plate whose dimensions are 0.30 m x 0.43 m and whose average operating temperature

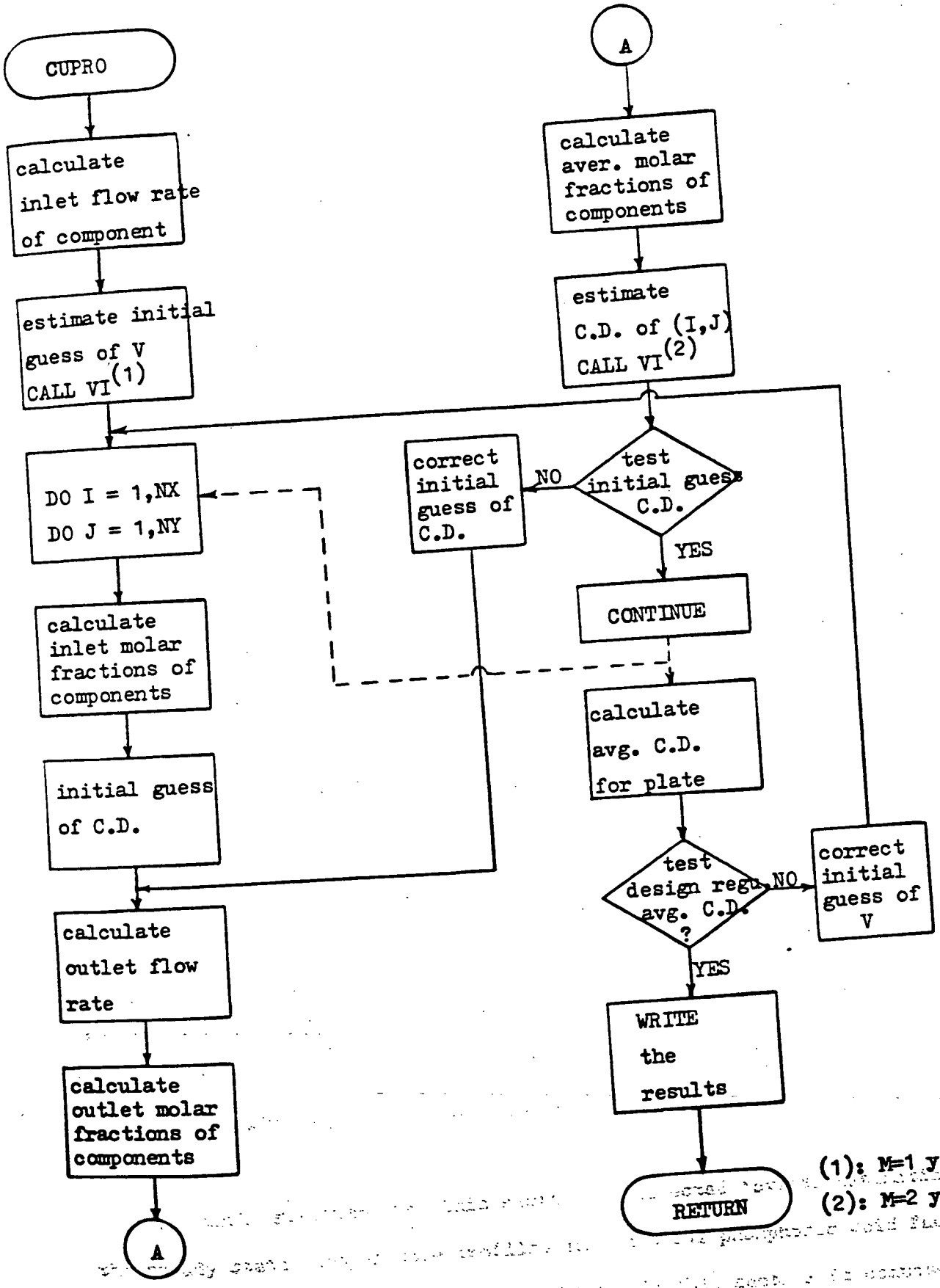

Figure 2-12 Flow Chart of Current Density Distribution on Cell Plate

is 450°K has been determined from the computer program. This distribution is presented in Figure 2-13 as a field plot of lines of constant current density. The fuel and process air conditions are given in the figure: where η_F, η_o represent utilization of fuel and oxygen respectively. The maximum current density occurs at the corner of the plate common to the two inlet streams and is 30% above the average current density, however the minimum current density occurs in the opposite corner and is 20% below the average. Since there is no satisfactory experimental method of measuring the local current density (Ref. 11), confirmation of the predicted current density must be inferred from temperature measurement.

The computer program can be modified to simulate different types of cell plates - i.e. Zee plate (Ref. 11) and hexagonal type plates. The operating conditions and results for these two alternatives are shown in Figure 2-14 and Figure 2-15 .

2.2.3 Thermal Analysis and Temperature Distribution

The electrical energy production in phosphoric acid fuel cells is accompanied by approximately equal amounts of heat energy generation. Removal of this heat can be accomplished by a suitable flow of input gases or by using separate cooling plates.

The work reported in this section is directed towards estimating the steady state temperautre profiles in practical phosphoric acid fuel cell stacks. The fuel cell stack considered in this section is composed

Figure 2-13 Current density distribution on a cell plate

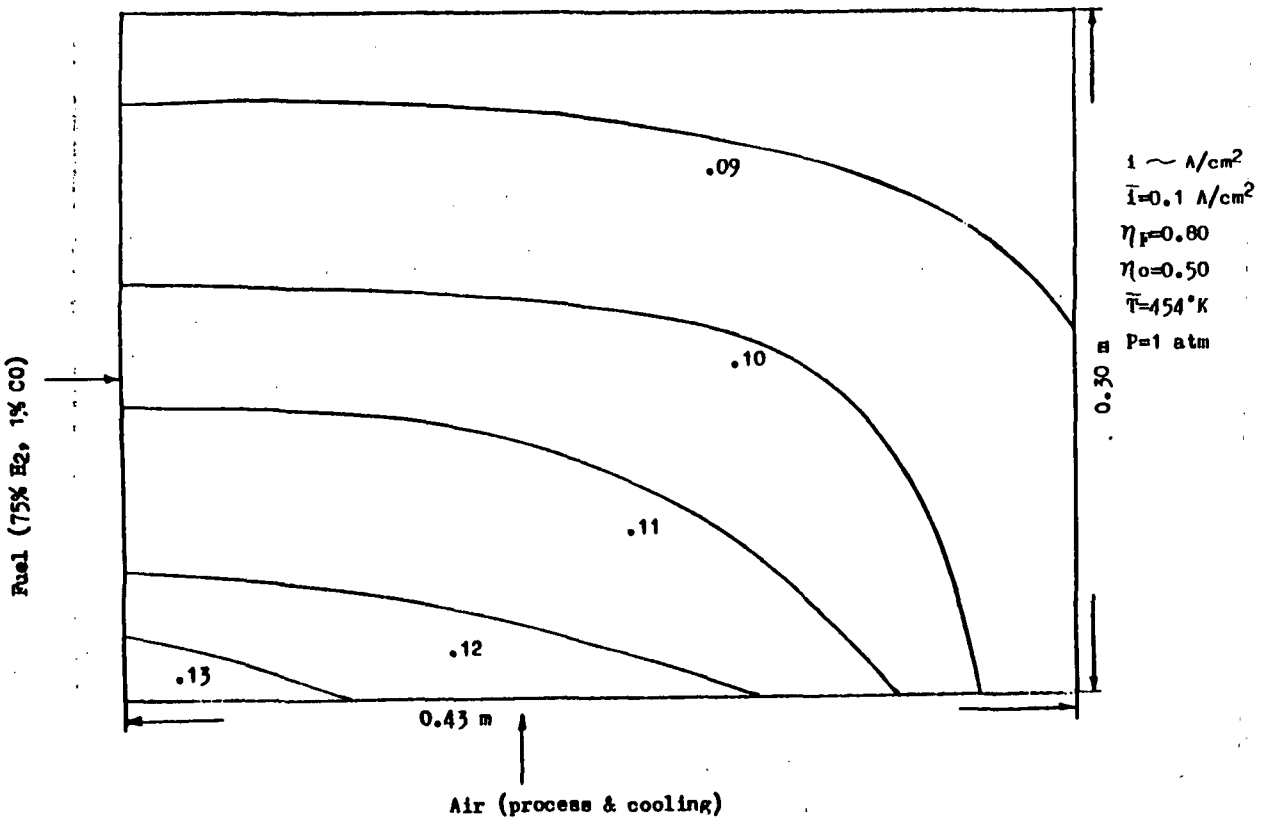

Figure 2-14 Current density profile (180.5°C, 1 atm) — Zee plate

Figure 2-15 Current density profile (180.5°C, 1 atm)

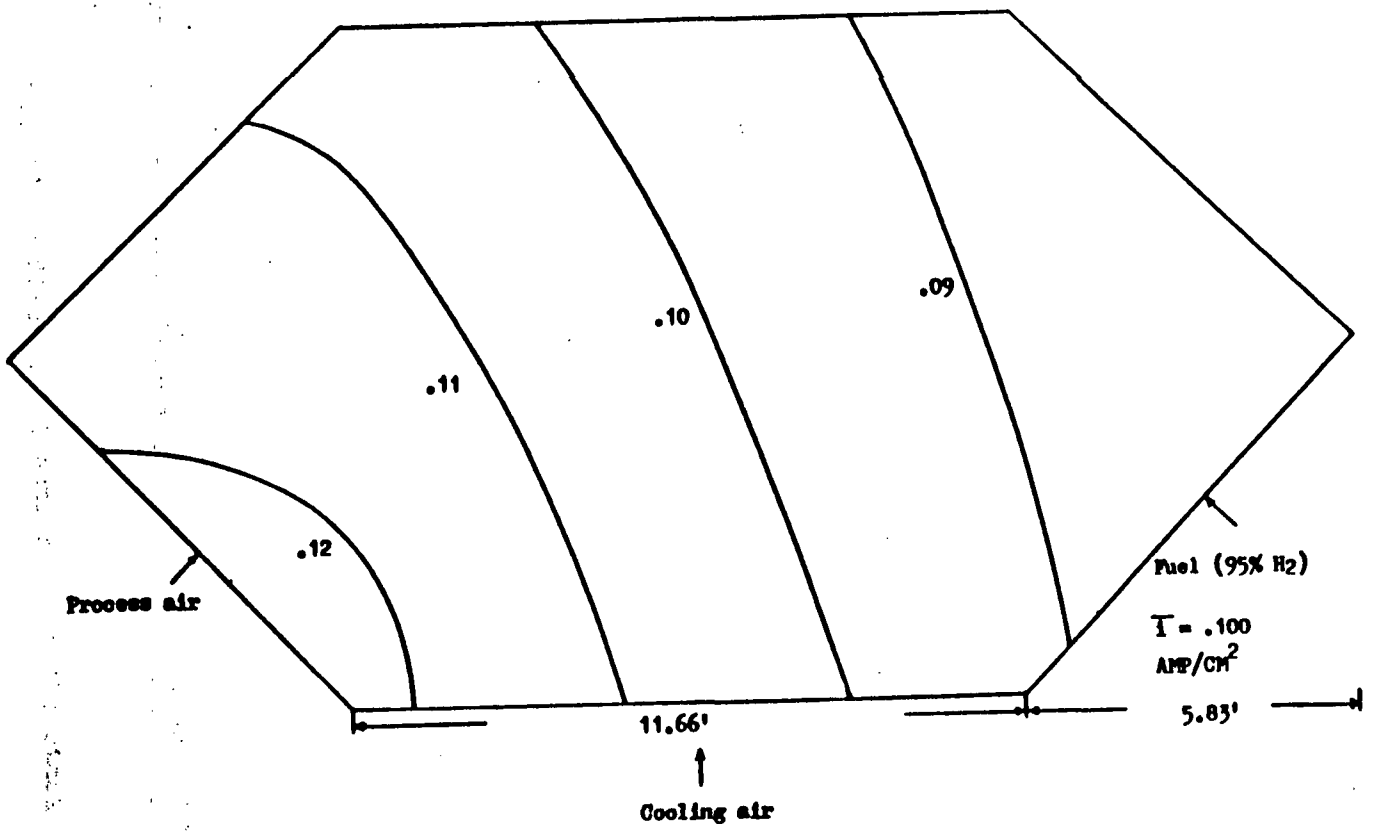

of cell plates on which the air (oxygen) and fuel (hydrogen) flows are at right angles. A cooling plate is placed between individual groups of cells at a regular interval. Symmetry in the stacking direction occurs at the middle of a cooling plate and midway between cooling plates.

2.2.3.1 Previous Work

Estimation of the temperature profiles in an operating cell is important for the estimation of the power density distribution, thermal stability, and cooling requirements. Only a limited amount of information on this subject has been reported in the past. Baker and co-workers recognized this need and have performed a comprehensive study of steady state heat transfer in electrochemical systems (Ref. 6,14,15). They studied various cases involving one dimensional analysis of a single adiabatic fuel cell and a three dimensional analysis of a multicell stack.

A single fuel cell with no lateral heat transfer and no conduction of heat through the cell in the direction perpendicular to the gas flow was considered (Ref. 14). Heat transfer by conduction in the direction of the gas flow was considered negligible in comparison to the heat transfer by convection, and analytical expressions for the electrolyte, fuel, and air temperature profiles were derived.

For the three dimensional analysis of the stack, it was assumed that all of the walls except for the wall from which the air enters were maintained at a constant temperature. The rate of heat generation per unit volume of the stack was assumed constant. An analytical solution

for the temperature profile was developed, assuming that the electrolyte and gas temperatures were not very different.

Another paper (Ref. 15) considered various limiting and special cases to determine the maximum temperature of a stack. Two dimensional heat transfer analysis was carried out in the case of a thick stack where heat transfer in the direction of stacking was neglected. In the case of thin stacks, three-dimensional heat transfer was considered with each wall at a different temperature. Infinite series solutions were developed for both thick and thin stacks. The authors estimated the maximum stack temperature for the constant wall temperature case. An approximate formula to predict the effect of conductivities, size, and current density on the maximum stack temperature was developed. A generalized analysis, which can incorporate the effect of finite resistance to heat transfer at the wall, the effect of cold or hot feeds, or nonuniform heat generation, was also carried out using the method of Green's function.

2.2.3.2 Temperature Distribution

The temperature distribution for the module was developed from the temperature distributions within representative slices or strips within a set of cell and cooling plate cells. The analysis includes conduction within bipolar plates, conduction between plates, the separate cooling effects of the process air and the coolant (basically air is considered as the coolant), and the temperature change of air flows along their respective channels. The distribution of the heat generation is determined from the current density distribution.

The model assumes that (1) the temperature gradients in the direction of the fuel flow are small. This assumption is justified since the major temperature gradients are in the air flow direction and since the heat capacity of the fuel stream is only a few percent of the heat capacity of the air stream. (2) The edge of the cell is operating adiabatically. (3) A half set of cell plates between cooling plates is analyzed, which includes one half cooling plate and two and a half cell plates. Thus because of the symmetry all of the stack behaves similarly. The geometry of a representative slice (Lx X Ly X Lz) through the stack is shown in Figure 2-17.

Mathematical Formulation

The material balances of the fuel and the oxident have been presented in section 2.2.2. There are four energy balance equations for the cell plate, cooling plate, process air, and coolant.

cell on process air side in air flow direction

$$t\,Ky\frac{\partial^2 T}{\partial y^2} + Kx\frac{\partial T}{\partial x}\bigg|_{x+t} - Kx\frac{\partial T}{\partial x}\bigg|_{x} - \frac{C_p\,\dot{m}_p}{Pp}\frac{\partial Tp}{\partial y} = -(V^* - V)\,I \qquad (2\text{-}2\text{-}17)$$

cooling plate in coolant direction

$$t'\,Ky\frac{\partial^2 T}{\partial y^2} + 2Kx\frac{\partial T}{\partial x}\bigg|_{x+t'/2} - \frac{Cc\,\dot{m}_c}{Pc}\frac{\partial Tc}{\partial y} = 0 \qquad (2\text{-}2\text{-}18)$$

process air side

$$\frac{d\,Tp}{d\,y} = \frac{hp\,Sp}{mp\,Cp}\,(T - Tp) \qquad (2\text{-}2\text{-}19)$$

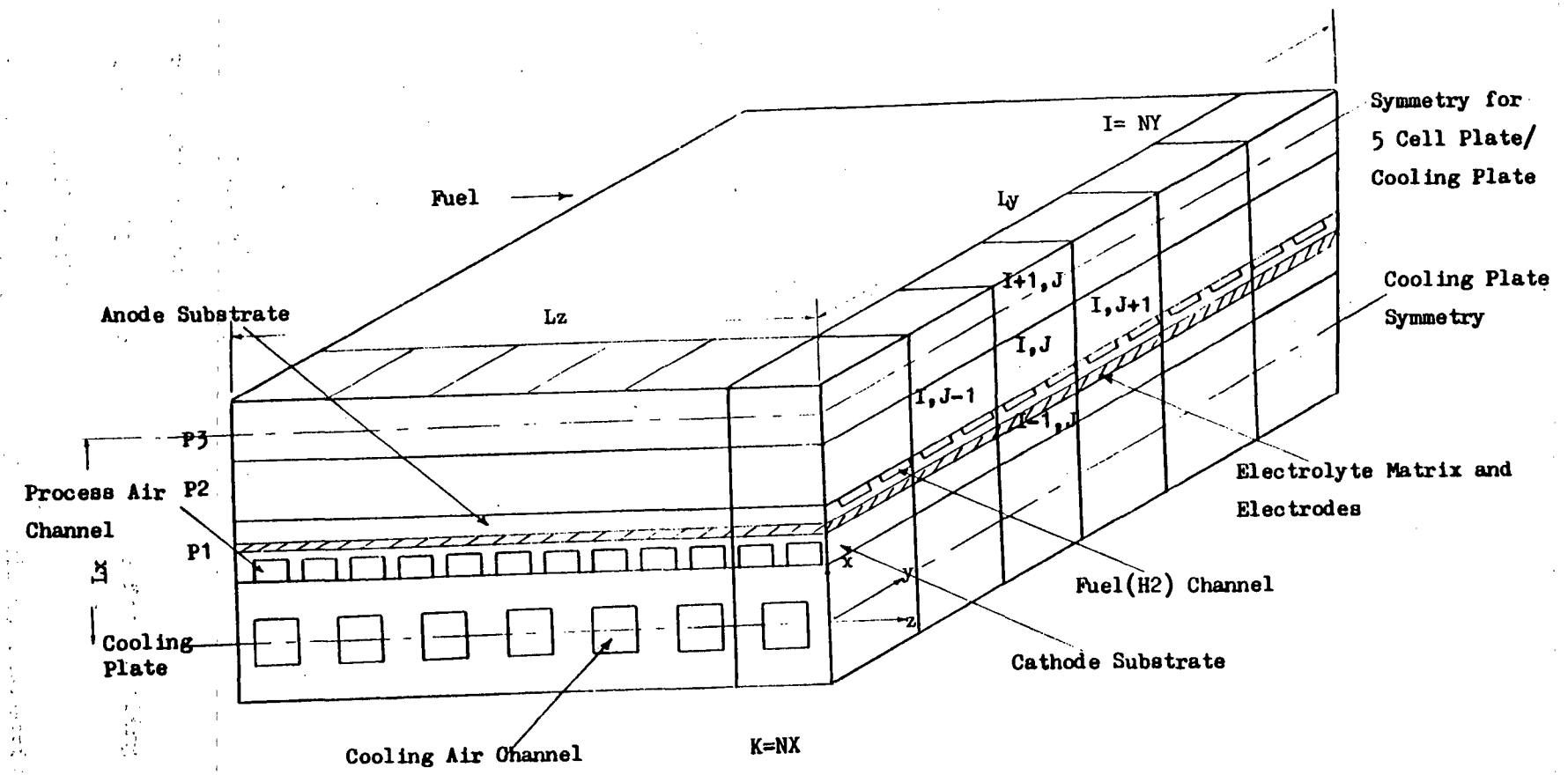

Figure 2-17 Geometry of a Strip of Element for the Thermal Analysis Model

coolant side

$$\frac{d\ Tc}{d\ y} = \frac{hc\ Sc}{mc\ Cc}\ (\ T-Tc\ ) \qquad (2\text{-}2\text{-}20)$$

Boundary conditions

x = 0	∂T/∂x = 0	symmetric condition
y = 0	∂T/∂y = 0	adiabatic assumption
x = Lx	∂T/∂x = 0	symmetric condition
y = Ly	∂T/∂y = 0	adiabatic assumption
y = 0	Tp = Tp, inlet	
y = 0	Tc = Tc, inlet	

where

m = mass flow rate, Kg/hr-channel

c = heat capacity, J/Kg-K

Ky = effective thermal conductivity of cell in flow direction, J/hr-m-K

Kx = effective thermal conductivity of cell on stacking direction, J/hr-m-K

t = thickness of cell including fuel and air channel, m

x1 = effective conduction distance from plate to upper cell plate, m

x2 = effective conduction distance from plate to lower cell plate, m

p = pitch of channel, m

x1' = effective conduction distance from cooling plate to upper cell plate, m

Lx,Ly = height and length of one slice, respectively, m

V* = $-\Delta H/ZF$, V

t' = thickness of cooling plate, m

h = heat transfer coefficient, J/hr-m^2-K

S = perimeter of the channel, m

Subscription

p = process air

c = cooling air

These simultaneous ordinary differential equations and corresponding boundary conditions were solved by the finite-difference method. The final difference equations are in next subsection.

Finite-Difference Model

The energy balance on an internal element j ($2 \le j \le N-1$) for bipolar plate i ($2 \le i \le N1$) can now be written as (see Figure 2-17)

$$-\left(\frac{Ky \cdot t}{\Delta Y^2}\right) Ti,j-1 + \left(2\frac{Ky \cdot t}{\Delta Y^2} + \frac{Kx}{X1} + \frac{Kx}{X2}\right) Ti,j$$
$$-\left(\frac{KY \cdot t}{\Delta Y^2}\right) Ti,j+1 - \left(\frac{Kx}{X1}\right) Ti-1,j - \left(\frac{Kx}{X2}\right) Ti+1,j \qquad (2\text{-}2\text{-}21)$$
$$+\left(\frac{Mp \cdot Cp}{Pp \cdot \Delta Y}\right) (Tpi,j - Tpi,j-1) = (V^* - V)\, Ii,j$$

The energy balance on an internal element j ($2 \le j \le N-1$) of the cooling plate i=1 can be written as

$$-\left(\frac{Ky \cdot t'}{\Delta Y^2}\right) T1,j-1 + \left(2\frac{Ky \cdot t'}{\Delta Y^2} + 2\frac{Kx}{X1'}\right) T1,j$$
$$-\left(\frac{Ky \cdot t'}{\Delta Y^2}\right) T1,j+1 - \left(2\frac{Kx}{X1}\right) T2,j \qquad (2\text{-}2\text{-}22)$$
$$+\left(\frac{Mc \cdot Cp}{Pc \cdot \Delta Y}\right) (TCj - TCj-1) = 0$$

The energy balance on interior element j ($2 \leq j \leq N-1$) of the symmetric plate i=N1 is

$$-\left(\frac{Ky \cdot t}{\Delta Y^2}\right) T_{N1,j-1} + \left(2\frac{Ky \cdot t}{\Delta Y^2} + \frac{\delta\, Kx}{X2}\right) T_{N1,j}$$

$$-\left(\frac{Ky \cdot t}{\Delta Y^2}\right) T_{N1,j+1} - \left(\frac{\delta\, Kx}{X2}\right) T_{N1-1,j} \qquad (2\text{-}2\text{-}23)$$

$$+\left(\frac{Mp \cdot CP}{Pp \cdot \Delta Y}\right) \left(Tp_{N1,j} - Tp_{N1,j-1}\right) = \left(V^* - V_{N1}\right) I_{N1,j}$$

where $\delta = 2$ for odd values of NK

$\delta = 1$ for even values of NK

NK: the number of cell plates between two adjacent cooling plates

N1: 1 + NK/2 for even NK

1 + (NK+1)/2 for odd NK

The energy balance on elements j=1 are obtained as above except for: the values of Ti,0 are replaced by Ti,1; the values of Tpi,0 are replaced by TPO, which is the inlet process air temperature; and TCo is replaced by TCO, the inlet cooling air temperature. The energy balances on elements j=N are obtained from the above with Ti,j+1 replaced by Ti,N.

For the process air flow, one can set up N1xN equations of the form

$$TPi,j = TPi,j-1 + (Ti,j - TPi,j)\left(1 - e^{-\phi_{pi,j}}\right) \qquad (2\text{-}2\text{-}24)$$

where

$$\phi_{pi,j} = \frac{h_{i,j}\, Sp}{Mp\ Cp} \Delta Y \qquad (2\text{-}2\text{-}25)$$

For the cooling air flow, one obtains N equations of the form

$$TCj = TCj-1 + (Ti,j - TCj-1)\ (1-e^{-\phi_{cj}}) \qquad (2\text{-}2\text{-}26)$$

where

$$\phi_{cj} = \frac{h_{cj}\ Sc}{Mc\ Cc}\ \Delta Y \qquad (2\text{-}2\text{-}27)$$

Thus the total number of temperature equations matches the number of unknown temperatures and the set can be solved using the Gaussian elimination method with calculated or input values of cell voltages, current densities, mass flow, heat generation and heat transfer coefficients. Each resulting temperature distribution is used to recalculate the current density distribution until convergence is reached. The relationship between voltage and current and the calculation of heat generation have been presented in Section 2.2.1.

Heat Transfer Coefficients

An empirical equation (Ref. 18) for the Nusselt number for fully developed laminar flow in a rectangular channels is:

$$Nuf = 3.61 + 4.63\ (1-\alpha)^{3.2} \qquad (2\text{-}2\text{-}28)$$

where $\alpha = a/b$; a is the smaller side of rectangular channel and b is the larger side of the channel.

Near the inlet of a channel, the heat transfer coefficient is larger than the fully developed value due to development of the laminar boundary layer. If R is the ratio of the average Nusselt number for the region 0 to x to the fully developed Nusselt number, then (Ref. 19)

$$R = 1 + \frac{0.0183\ Gz}{1 + 0.04\ Gz^{2/3}} \qquad (2\text{-}2\text{-}29)$$

where GZ: Graetz number = Re Pr (D_H/x)

Re: Reynolds number based on D_H

Pr: Prandtl number of gas

D_H: Hydraulic diameter, m

For turbulent flow, the average Nusselt number over the region 0 to x is described as (Ref. 22)

$$Nu_t = 0.116\ [Re^{2/3} - 125]\ Pr^{1/3}\ [1 + (D/x)^{2/3}\ ]. \qquad (2\text{-}2\text{-}30)$$

The flow chart of the executive program for calculating the temperature distribution in the stack is shown in Figure 2-18.

Results

A temperature distribution in the fuel cell stack with 0.30 m x 0.43 m cell plate has been determined using the computer program. This distribution is presented in Figure 2-19 as a field plot of lines of constant temperature on the second cell plate. The operating conditions are shown in the figure where Kx, Ky represent thermal conductivity along stacking direction and on the cell plate respectively. The maximum temperature occurs at the corner of fuel inlet and air outlet and the minimum occurs at the opposite corner. The stacking direction temperature profile will be discussed in the next section.

Comparison with Experimental Data

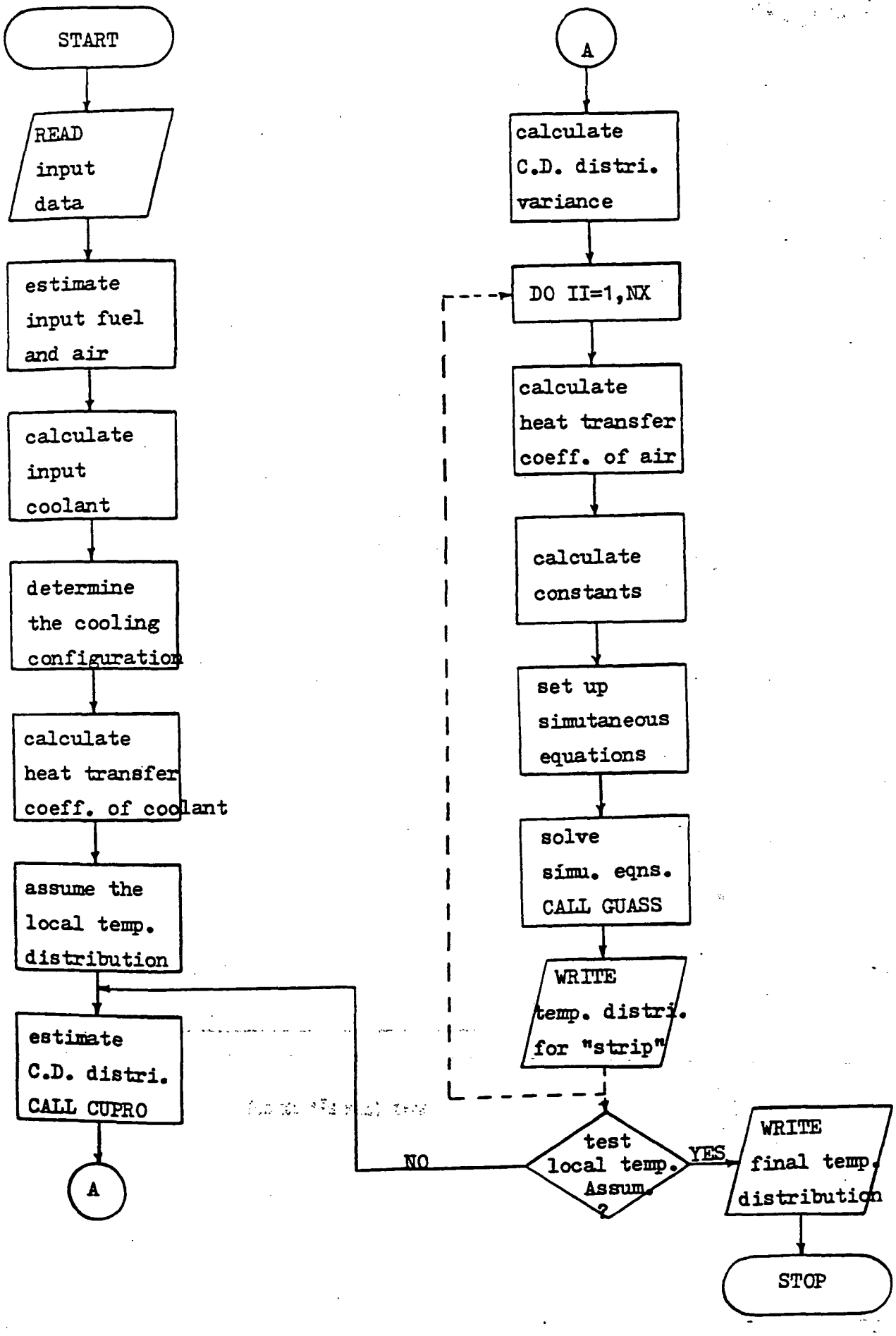

Figure 2-18 Flow Chart for the Temperature Distribution in Cell Stack

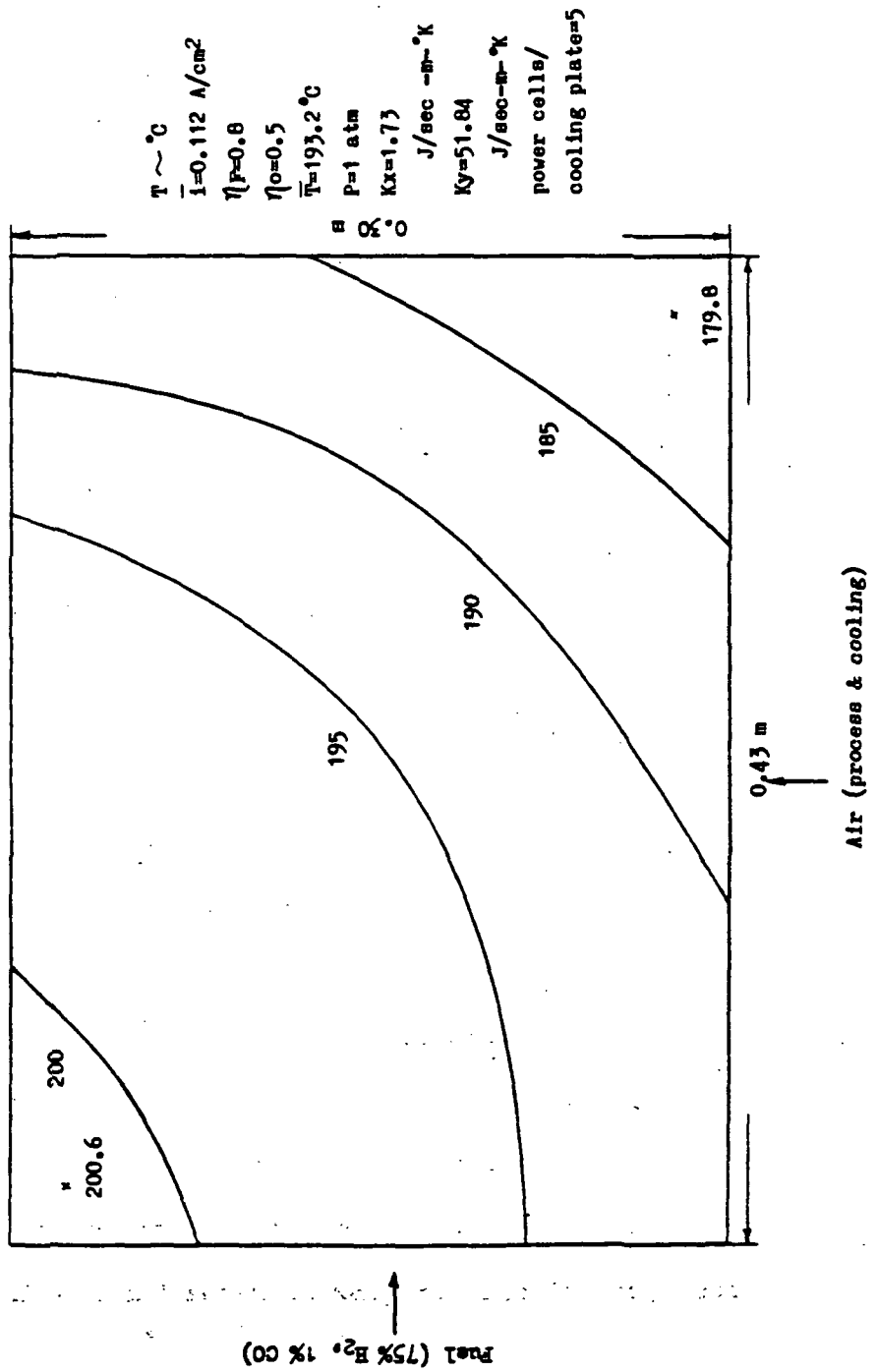

Figure 2-19 Temperature distribution on cell plate

A comparison of the temperature profile on the cell plate as predicted by the developed model was made with the Westinghouse measured data (Ref. 11). Figure 2-20 shows the Westinghouse measured temperature distribution with a "branch" cooling configuration which will be discussed in detail in the next section. Figure 2-21 shows the calculated results. The significant difference between the operating temperature and the anode inlet temperature in the experimental work conflict with the assumption which neglects the anode flow effect (Section 2.2.3.2). Therefore, the computer peogram was modified to include a fuel flow cooling effect and the results are shown in Figure 2-22 with the parameters listed on the figure. The "hot spot" shifted to right with the addition of the add anode flow effect (compare Figure 2-21 with Figure 2-22).

The temperature contour lines are very sensitive to many parameters which will be discussed in next section. For example, Figure 2-23 shows the contour lines for the same parameters as Figure 2-22 except the temperature of the process air (TKA) (not the cooling air) was decreased by 10°C. Therefore, considering the complex interaction among temperature levels, reaction rates, reactant depletions, current densities, heat generation rates and reactant distributions and that only temperatures can be measured directly; the agreement between calculated and measured temperatures is very good.

2.2.3.3 Parametric Sensitivity and Cooling Scheme

The plate temperature is a function of the current density, the

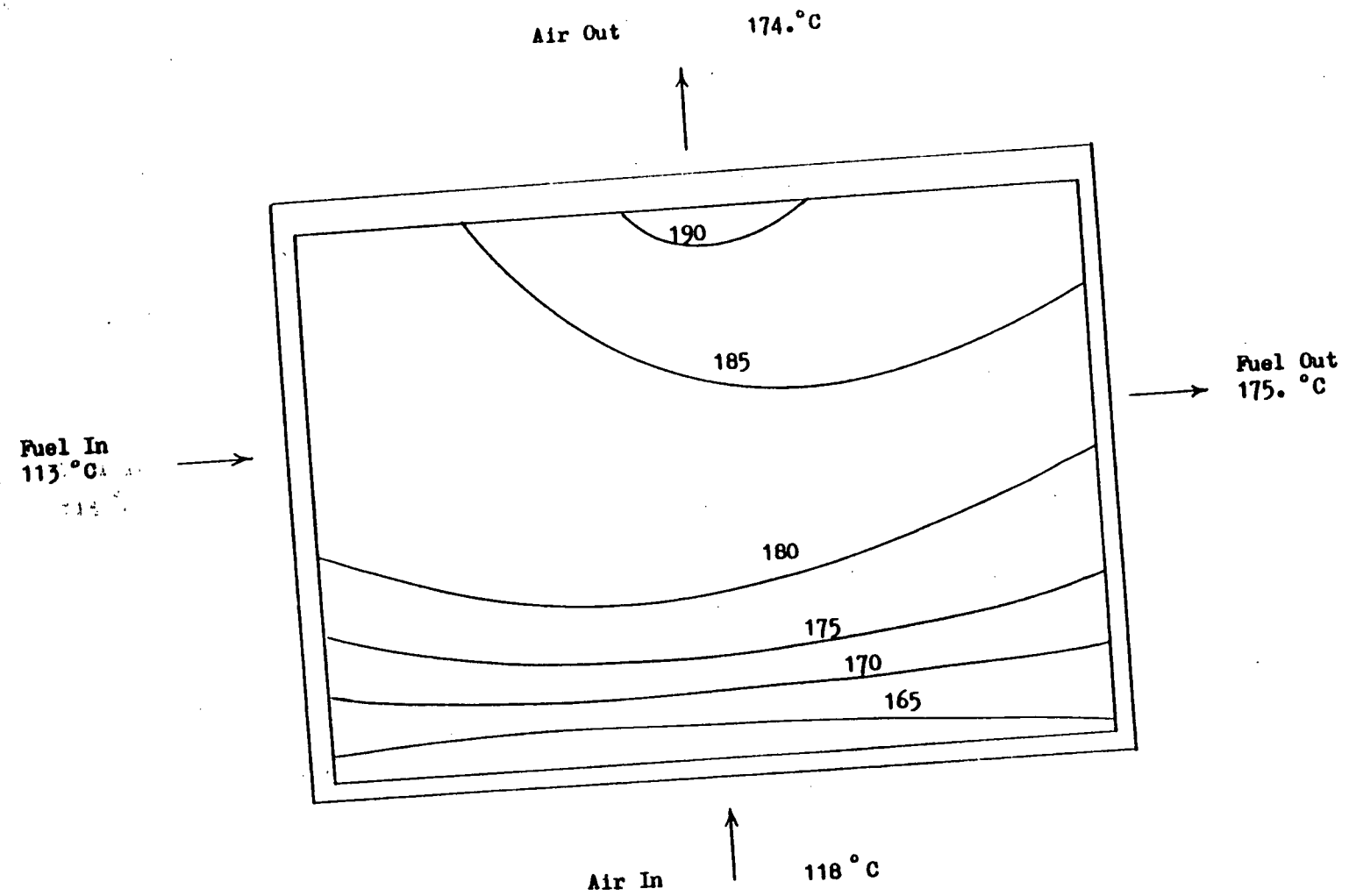

Figure 2-20 Westinghouse experimental work on temperature distribution in stack 561 (Ref. 11)

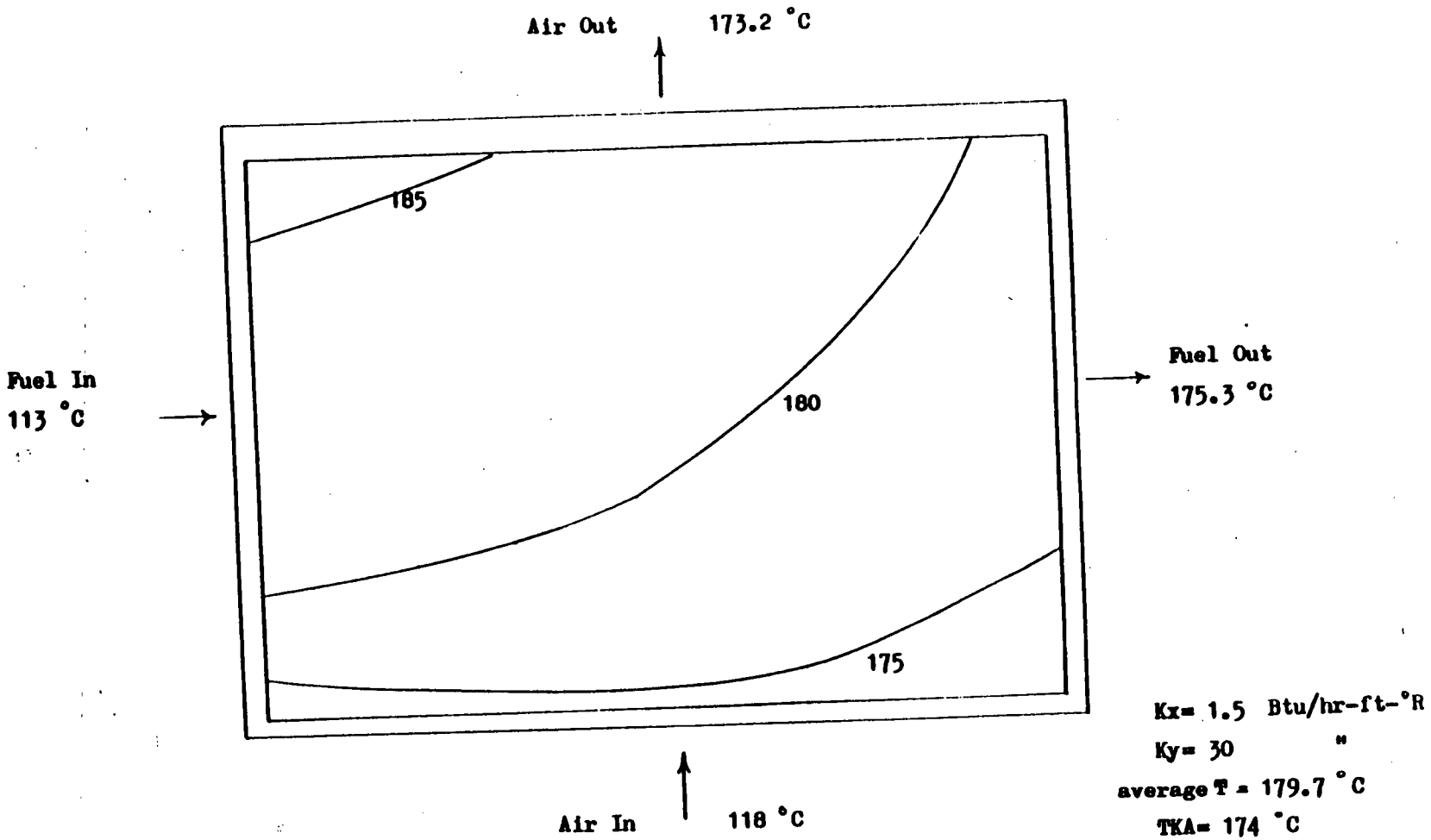

Figure 2-21 Calculated temperature distribution - H2 not considered

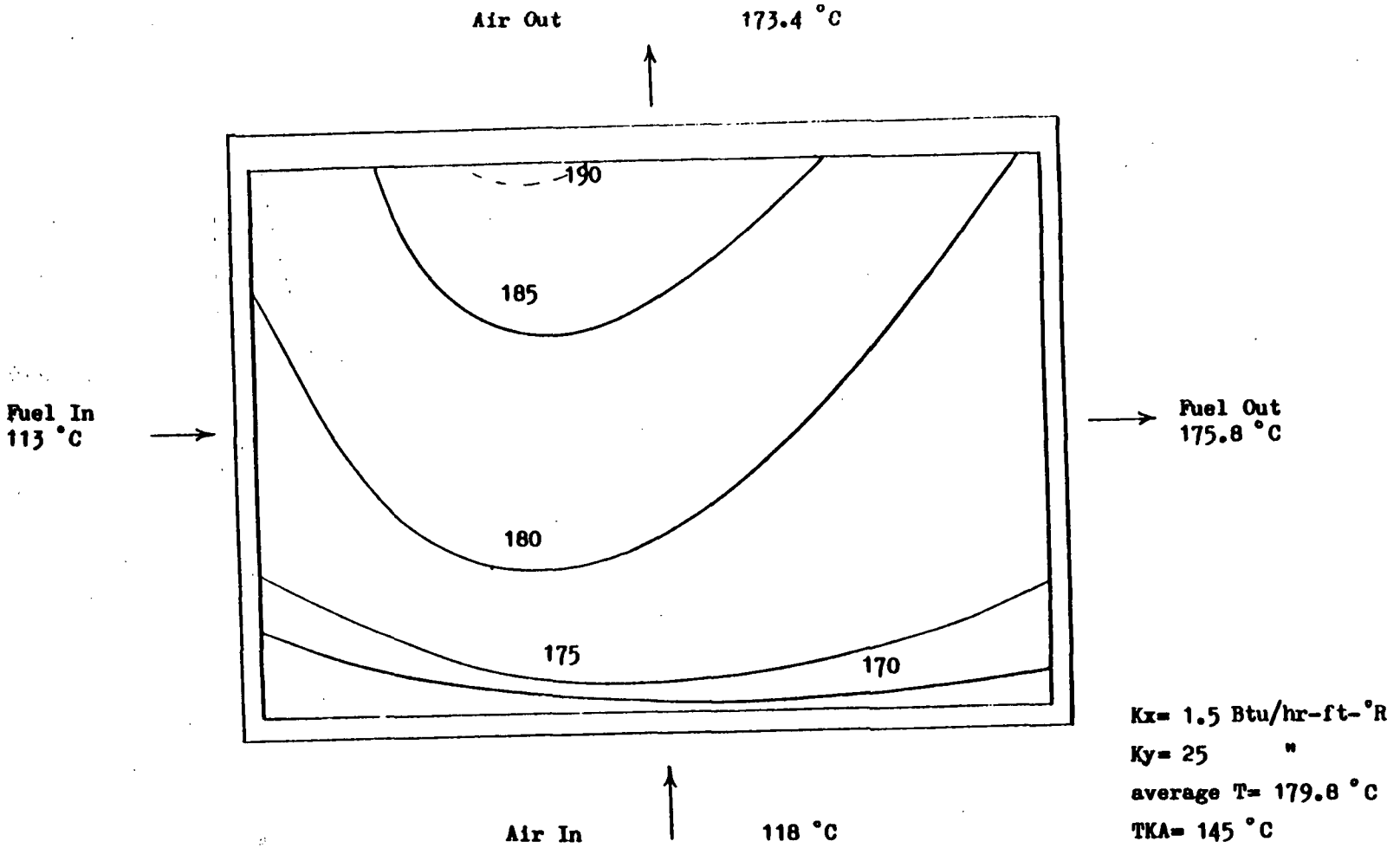

Figure 2-22 Calculated temperature distribution for comparison with the Westinghouse experimental work

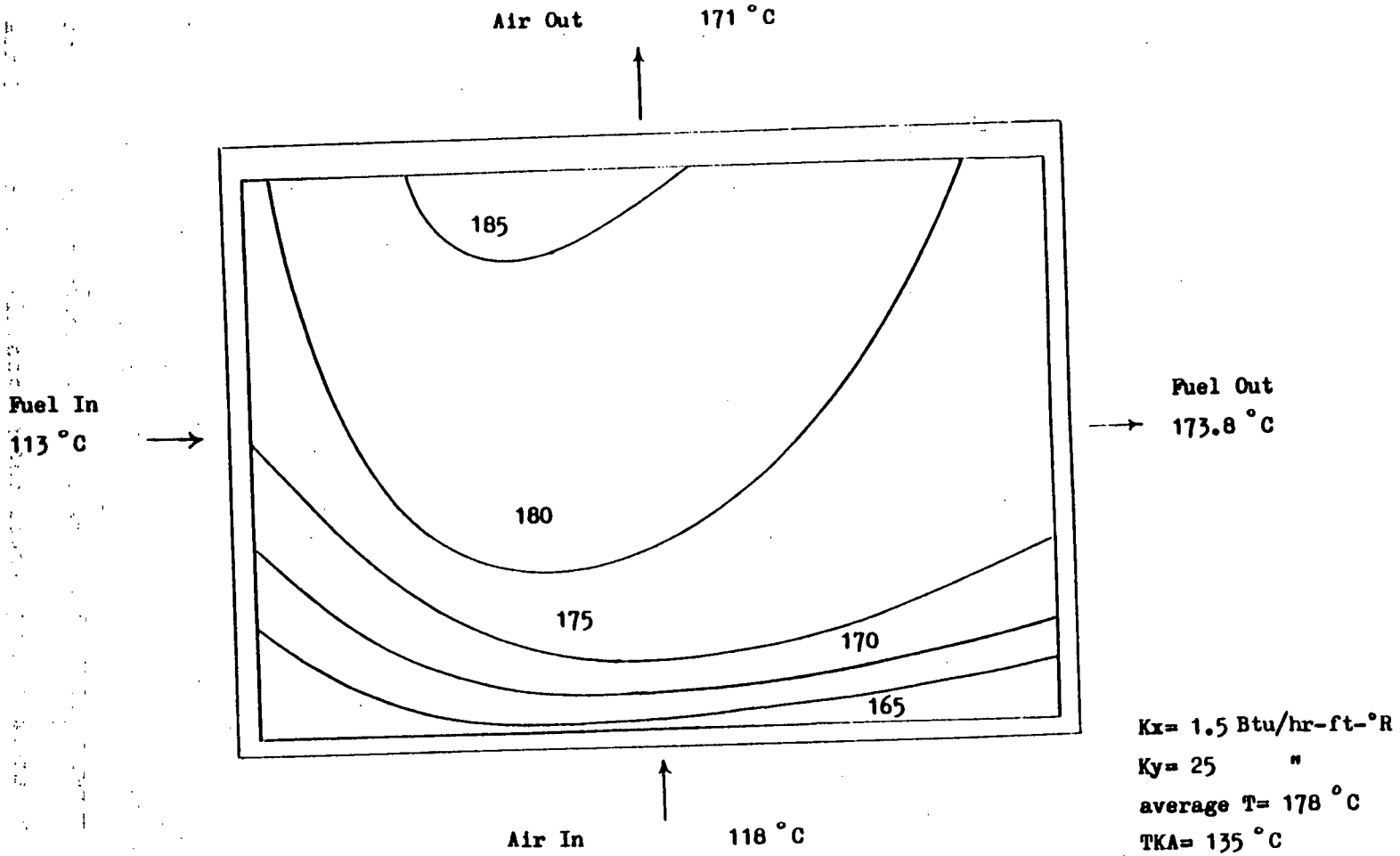

Figure 2-23 Calculated temperature distribution with TKA = 135°C

concentrations of hydrogen and oxygen, and the cooling effectiveness. In order to achieve the optimum design with respect to the temperature distribution, more studies of the parameters involved and the cooling scheme are necessary. Here the computer program discussed in the previous section is used to examine and compare these design parameters.

Thermal Conductivity in Stacking Direction

The temperature profile for four different values of thermal conductivity are shown in Figure 2-24 . It can be observed that the temperature gradient in the direction of stacking increases with a decrease in Kx. The temperature drop across a cell is 2°C (mean value) for Kx = 1 Btu/hr-ft-R (1.73 J/sec-m-K) whereas it is 0.5°C for Kx = 2.5 Btu/hr-ft-R.

Dimension of The Cell Plate

The temperature distribution for two different sets of dimensions of cell plates were simulated and compared with, and the results were shown in Figure 2-19. All of the operating conditions were the same as in Figure 2-19 except for the plate dimensions (width and length). The first one (Figure 2-25) with the reversed width and length of Figure 2-19 and the second (Figure 2-26) with square dimensions. The results show that the rectangluar shape with a fuel flow length longer than the air flow length will obtain the lowest peak temperature and have a good average temperature. Lower peak temperatures mean a more uniform temperature distribution and a lower average temperature means that less auxiliary power will be required to pump the coolant.

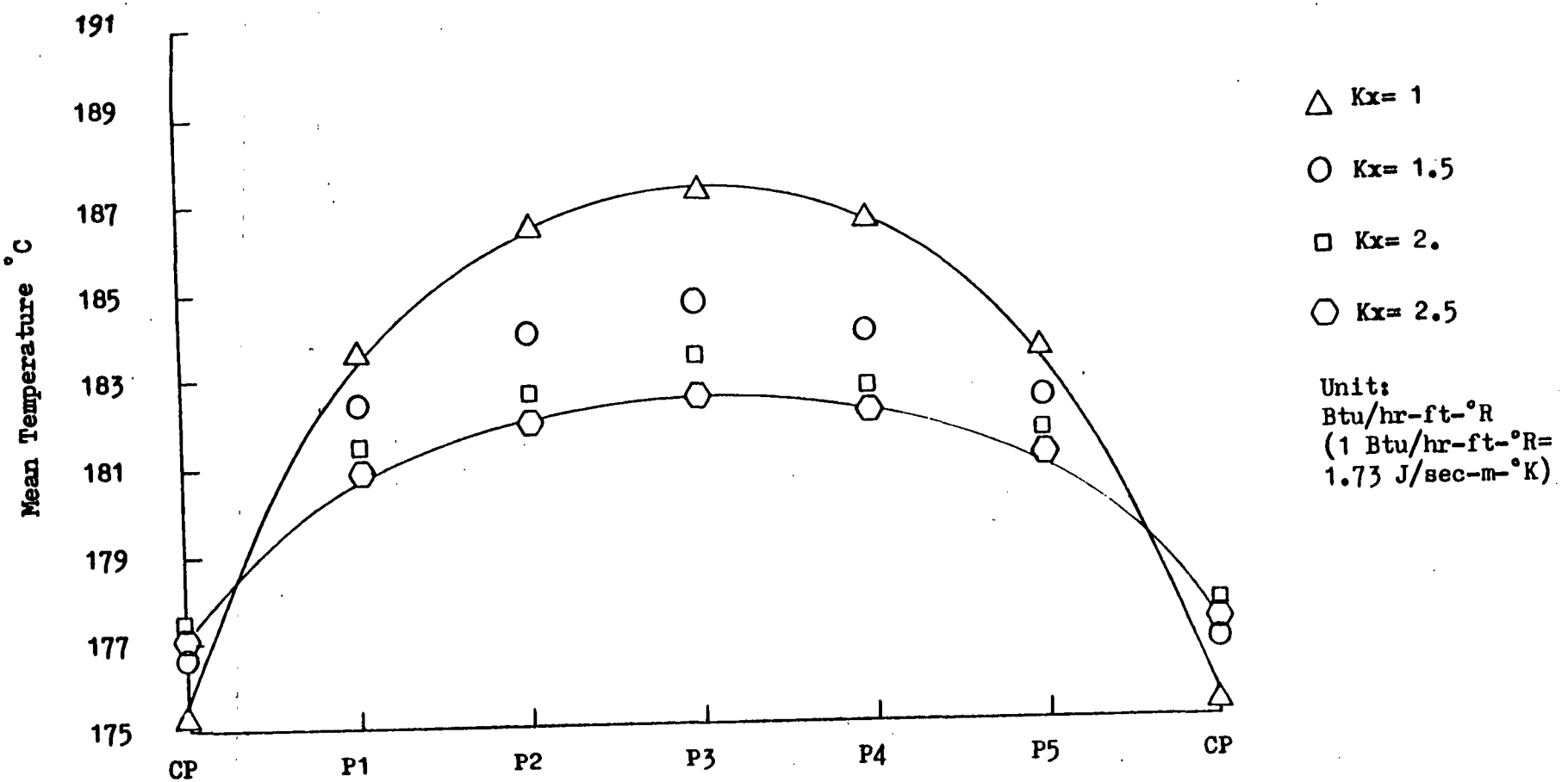

Figure 2-24 Comparison of mean temperature for cell plates and cooling plates with different thermal conductivities in the stack direction

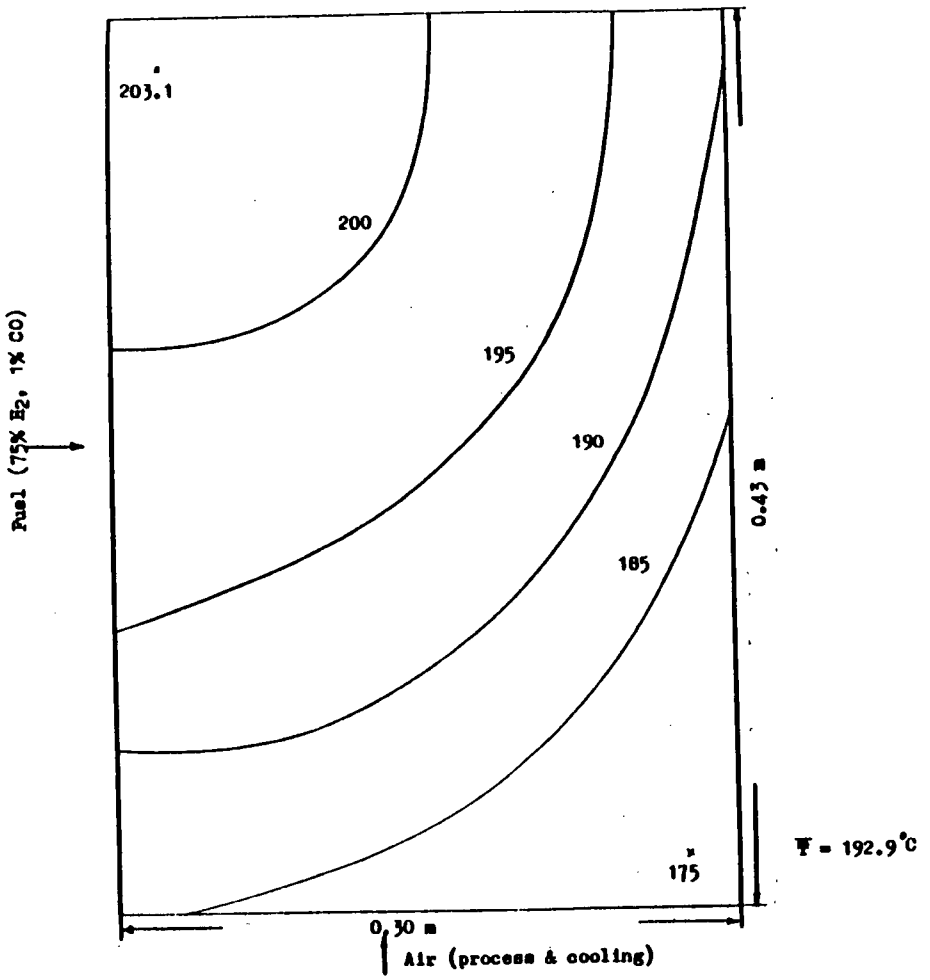

Figure 2-25 Temperature distribution with different dimensions (compared to Figure 2-19)

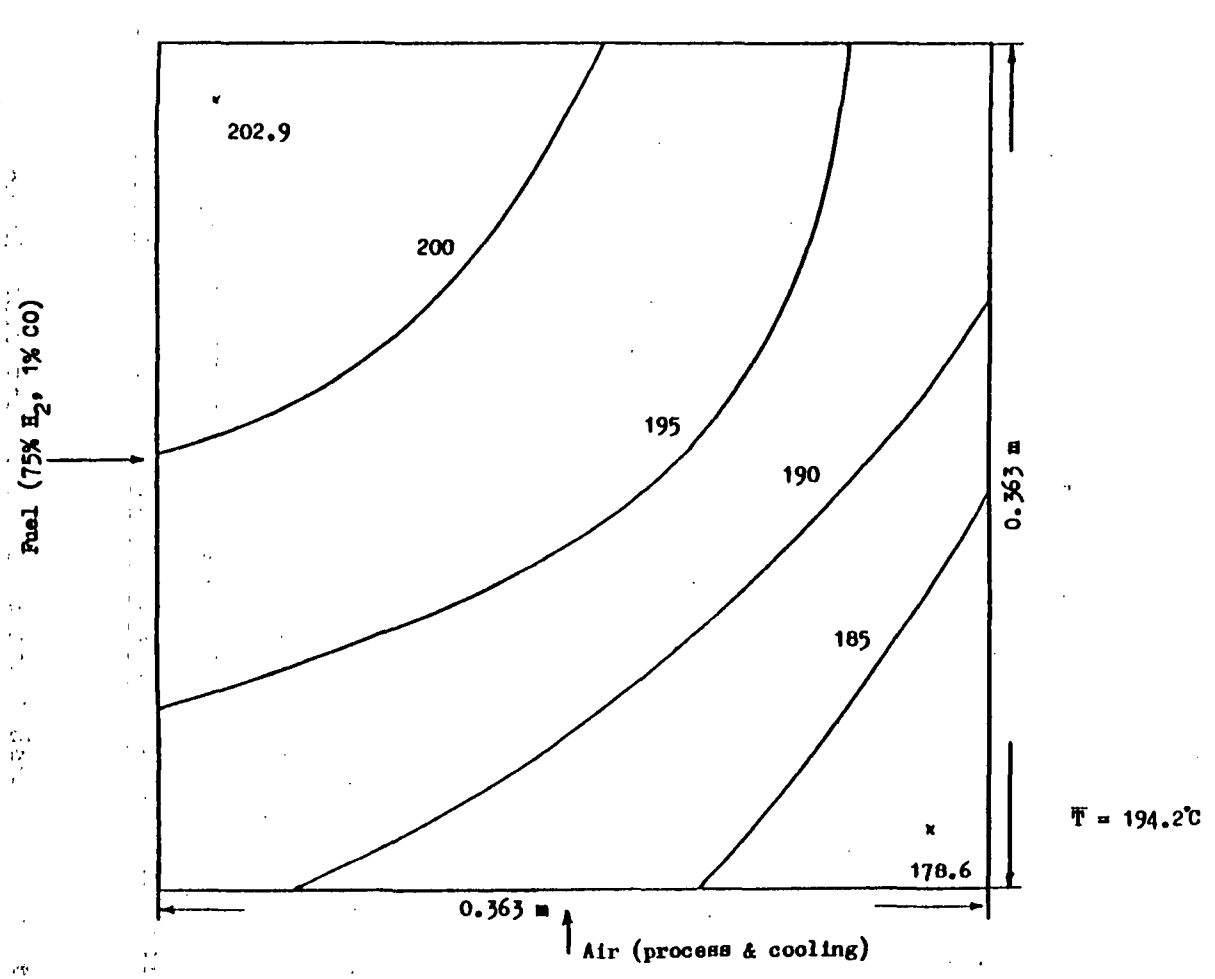

Figure 2-26 Temperature distribution with square dimensions(compared to Figure 2-19)

Size

The computer analysis was done for a sequence of cell plate sizes under the same operating conditions. The various sizes are 2" x 2" (5.08 cm x 5.08 cm), 6" x 4" (15.24 cm x 10.16 cm), 10" x 7" (25.4 cm x 17.8 cm), and 12" x 10' (30.48 cm x 25.4 cm). The normalized current densities and temperatures along the plate diagonals, are given in Table 2-4 . The table shows that for a relatively small cell, both current density and temperature vary almost linearly from the reactants inlet corner to the exhaust corner. As cell size increases, both distributions become somewhat parabolic along the "A" diagonal, while on The "B" diagonal, the temperature extremes are accentuated for the larger plate sizes.

The smallest plate shows the most uniform temperature distribution but the worst current density distribution. The greater change of hydrogen or oxygen concentration in the small plate results in a varying current density.

The indicated trend in temperature extremes as plate size increases (while average temperature stays constant) can create a potential problem for very large plates. Some portions of the plates could possibly exceed the boiling point temperature of the electrolyte.

It is noted that the average current density and the average temperature are the same along the "A" and "B" diagonals (and the plate) for all of the plates sizes. This result indicates a convenience of the

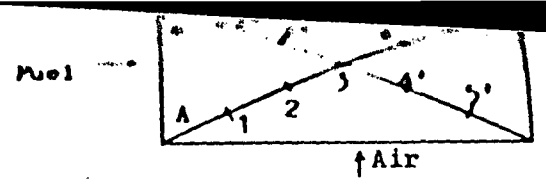

Diagonal Coordinate X/L	Node Number	Current Densities on "A" Diagonal (A/sq.cm.) 2" x 2"	4" x 6"	7" x 10"	10" x 12"	Current Densities on "B" Diagonal (A/sq.cm.) 2" x 2"	4" x 6"	7" x 10"	10" x 12"
.1	1	.3416	.3379	.3192	.2923	.2665	.2744	.2806	.2972
.3	2	.3194	.3248	.3146	.3031	.2834	.2837	.2970	.3091
.5	3	.3006	.3025	.3070	.3100	.3006	.3025	.3070	.3100
.7	4	.2811	.2778	.2904	.3052	.3158	.3157	.3060	.2989
.9	5	.2602	.2603	.2667	.2870	.3265	.3089	.2937	.2807
Avg. Current Density		.2997	.2998	.2994	.2992	.2997	.2998	.2994	.2992

Diagonal Coordiante X/L	Node Number	Temperature Distribution on "A" Diagonal (C) 2" x 2"	4" x 6"	7" x 10"	10" x 12"	Temperature Distribution on "B" Diagonal (C) 2" x 2"	4" x 6"	7" x 10"	10" x 12"
.1	1	202.6	203.7	197.5	187.8	203.3	206.7	211.4	213.3
.3	2	201.9	203.0	201.2	195.5	202.2	205.0	208.4	209.4
.5	3	201.7	202.9	204.2	202.9	201.7	202.9	204.2	202.9
.7	4	200.7	200.9	204.2	207.9	200.3	199.0	197.2	194.1
.9	5	197.9	195.2	199.8	208.5	193.6	192.2	186.5	183.9
Avg. Temperature		200.95	201.6	201.9	200.6	200.95	201.6	201.9	200.6

Table 2-4 Effect of size on fuel cell performance

diagonal analysis method.

Average Current Density

When the output power requirement of a PAFC system are determined, the average current density is also decided due to its relationship with voltage. The typical relationship between power and current density is shown in Figure 2-27 for a fixed plate area. In addition, examination of the effect of current density on the temperature distribution will decide the size or the number of plates needed.

The computer program was run with four different values of the average current density which are 0.1, 0.2, 0.3, and 0.4 A/cm^2 . The diagonal analysis of "A" type diagonal (see Table 2-4) on a 25.4 cm x 17.8 cm plate is shown in Figure 2-28 and Figure 2-29 . It can be observed that the smaller average current density the more uniform the temperauture distribution. Another important result is that the current density distribution corresponded to the temperature profile for the larger average current density. This is contrary to the isothermal current density distribution which has a minimum value at the right side corner (Figure 2-13).

Coolant Flow Rate

A majority of the heat energy removal is accomplished by the flow of coolant through the cooling plate. For example, 2 times the stoichiometrically required amount (2 stoich) of cathode gas is passed through individual cells and a 30 stoich cathode gas is going through

Figure 2-27 DC power with different current density

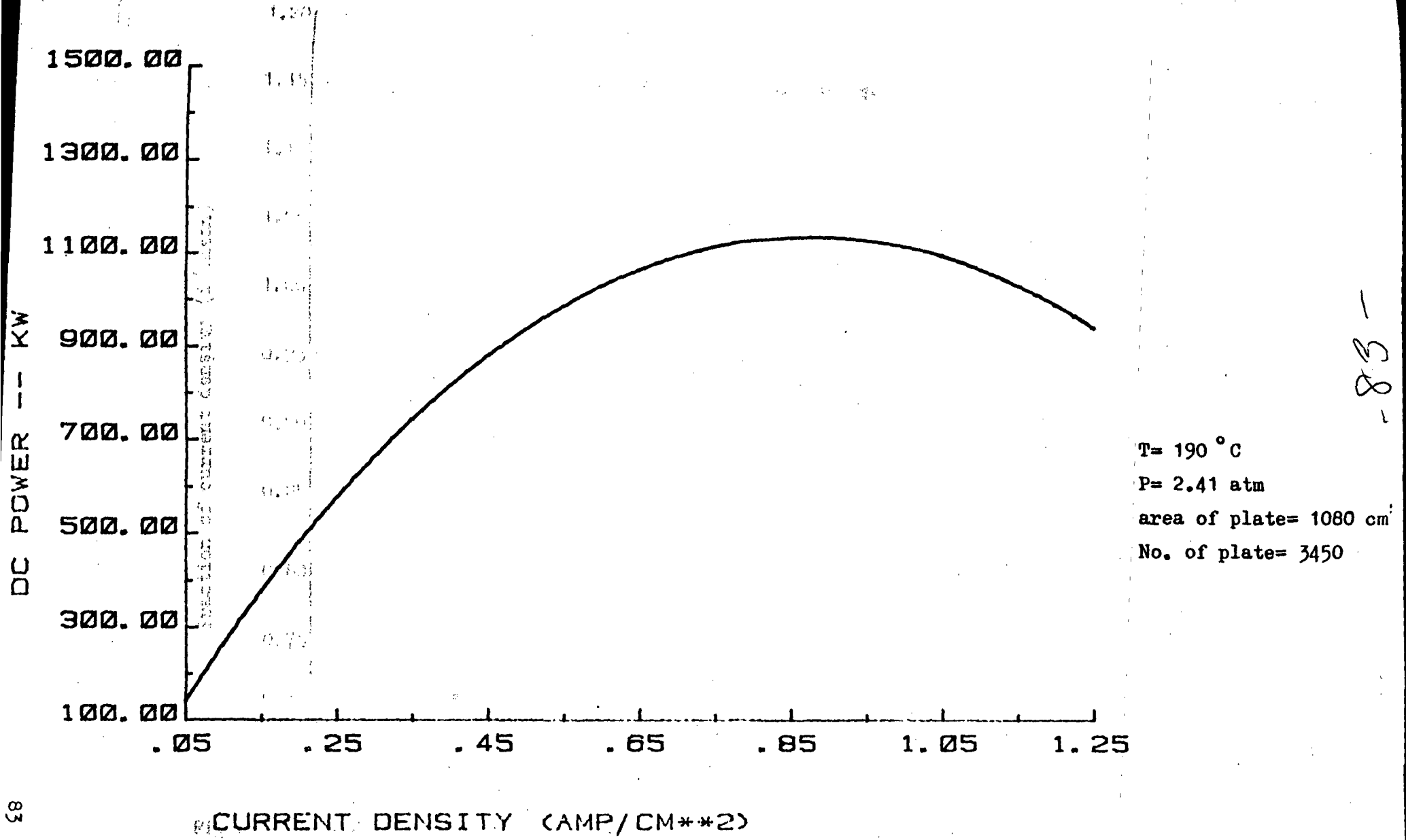

T= 190 °C

P= 2.41 atm

area of plate= 1080 cm²

No. of plate= 3450

-85-

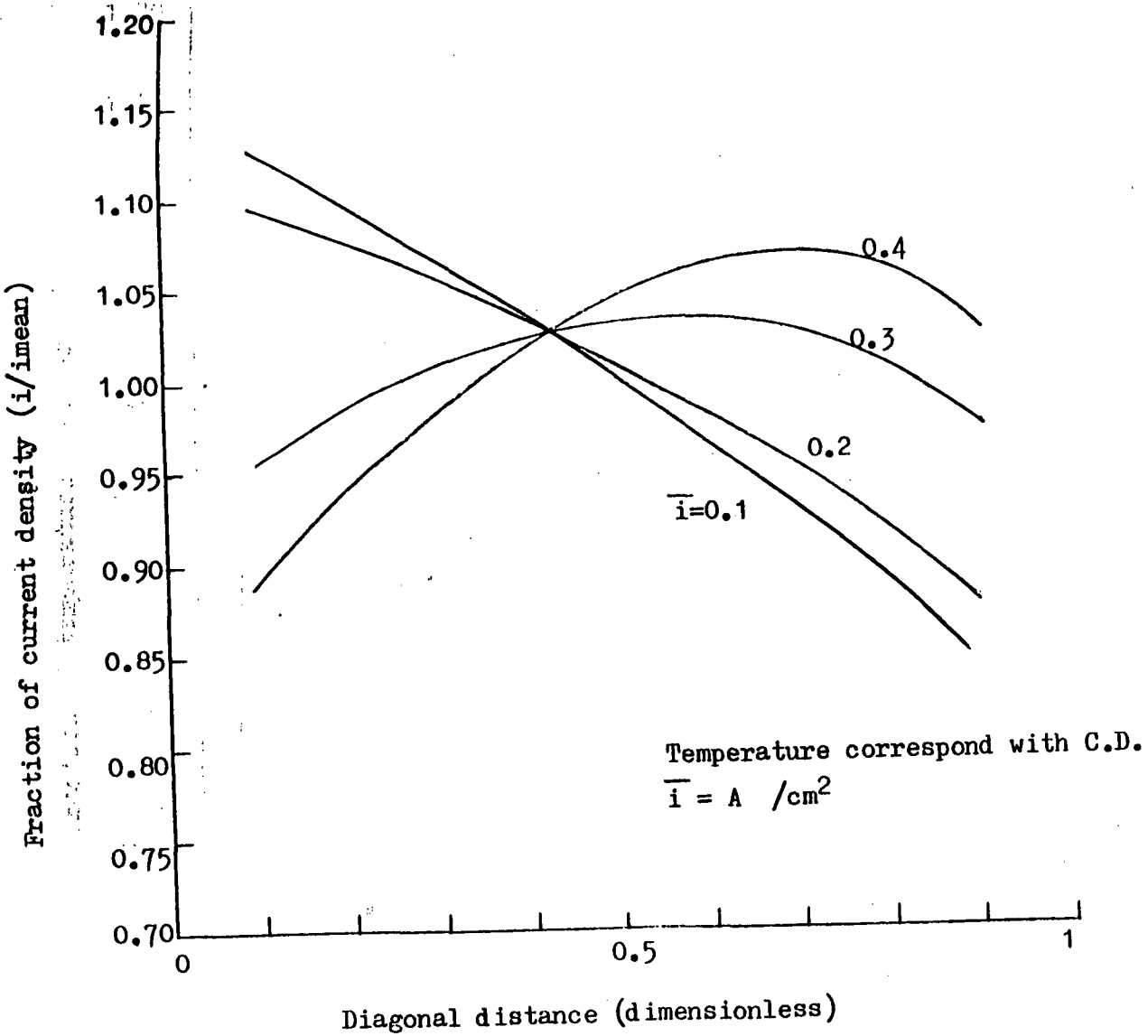

Figure 2-28 Effect of the mean C.D. on the diagonal C.D. distribution

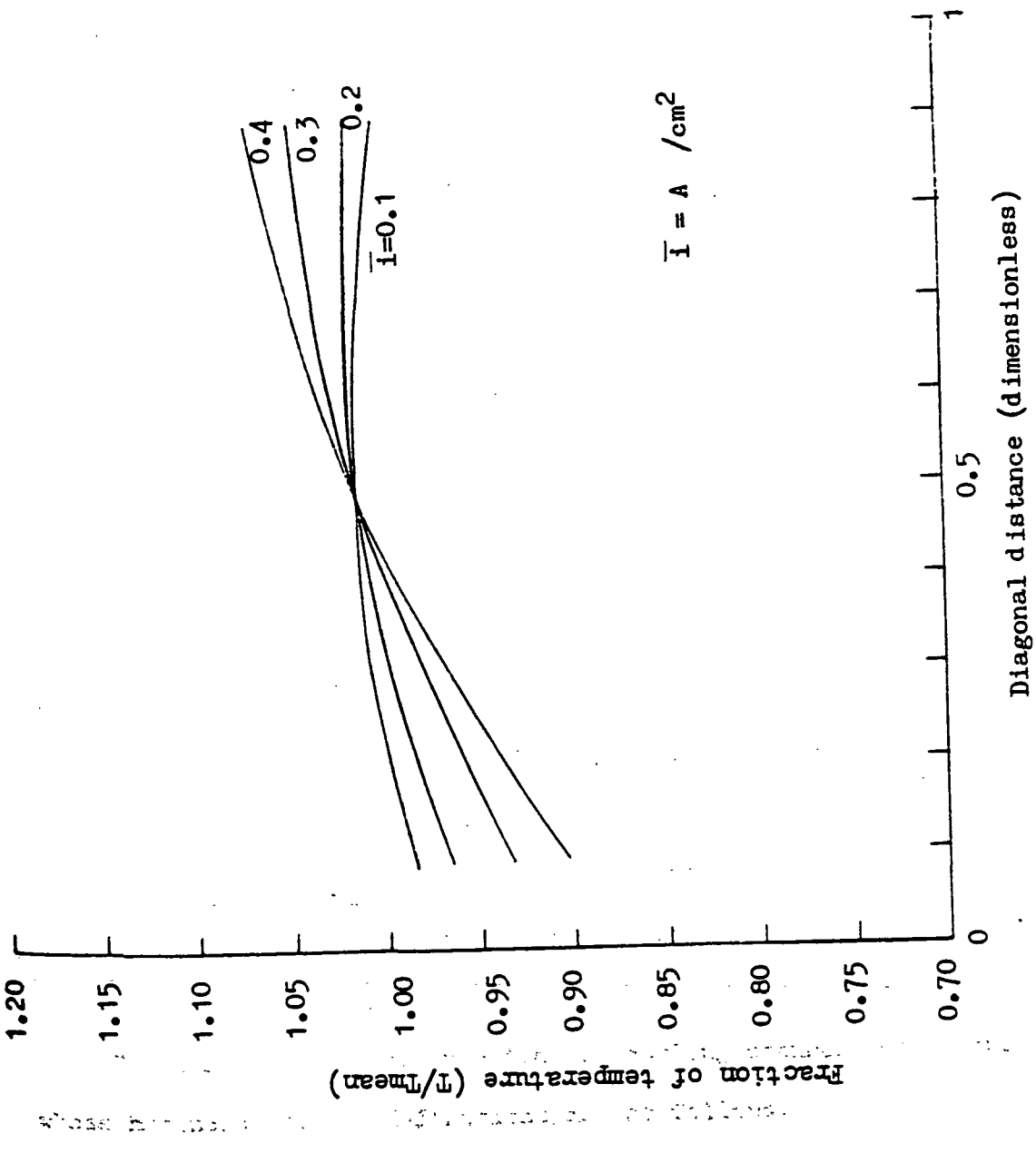

Figure 2-29 Effect of the mean C.D. on the diagonal temperature distribution

cooling plate. From a cost view point, the greater the flow rate of coolant the greater the auxiliary power needed to recycle the coolant. Moreover, the flow rate of coolant will also affect the temperature profile. Figure 2-30 shows an example for the stacking direction temperature profile with two different stoich values of coolant. The more coolant that is used, the lower the mean temperature will be, but the greater the temperature difference between plates will be.

The thermal conductivity in flow direction and inlet temperature of both fuel and process air also affect the temperature distribution. This will be discussed after we compare different cooling schemes.

Cooling Scheme

The cooling factor is conceived to be a function of the heat transfer characteristics, plate size, and stack construction. The latter will primarily specify the number of power plates between a pair of cooling plates. The heat transfer characteristics will be a function of the type of coolant (gas or liquid), cooling plate design, and the thermal conductivities of the plate material. Some of these factors have been examined in the previous subsection. This subsection will concentrate on the design of the cooling channel.

There are three configurations of cooling channels considered here, whose nomenclature and definitions are as follows,

1. Straight: the dimensions of cooling channel are fixed.
2. Branch: the cooling channel is branched along the coolant flow direction, one example is in Figure 2-31 .

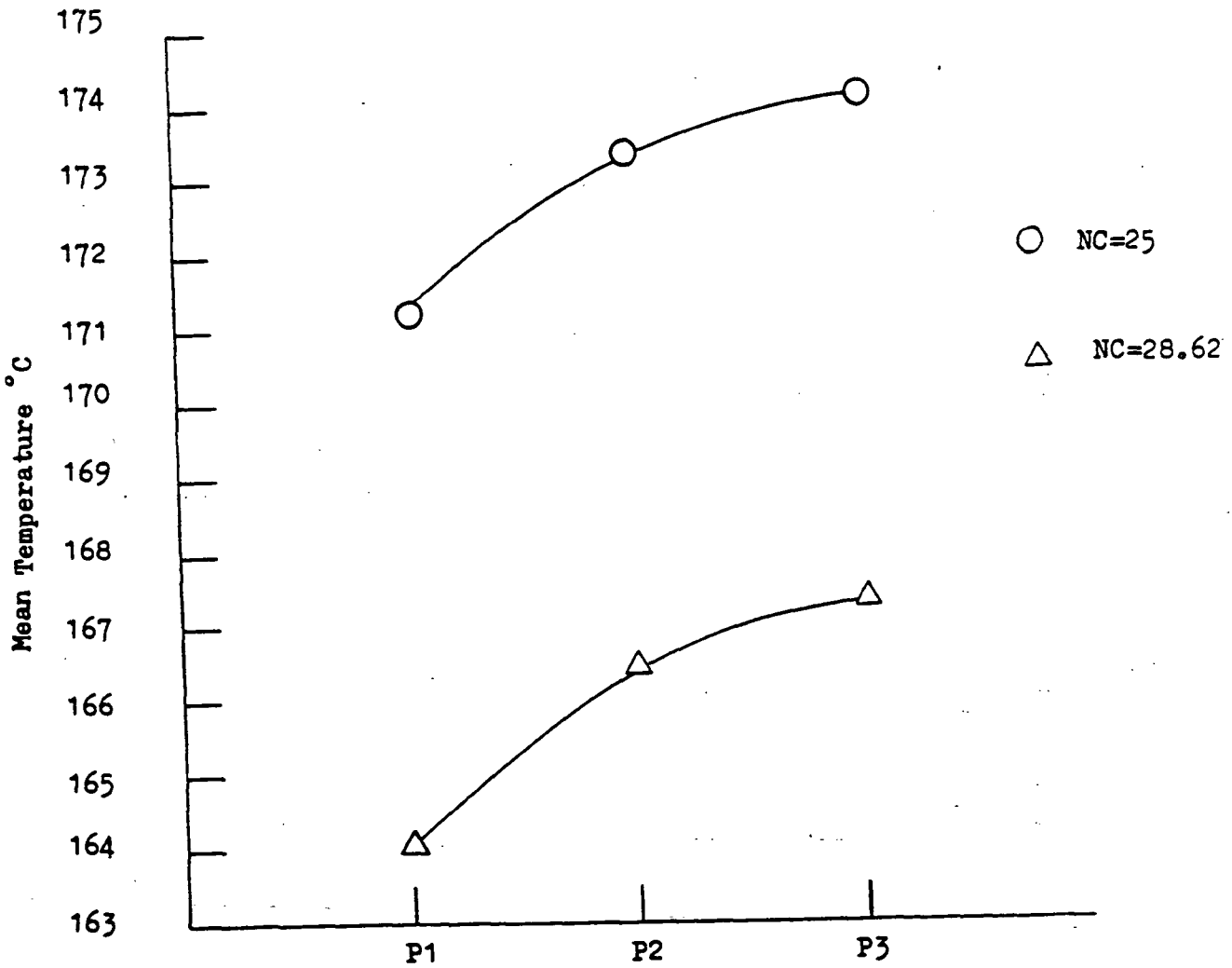

Figure 2-30 Comparison of the effect of the coolant flowrate on the mean temperature for plates in the stack direction

Width ratio W1:W2:W3 = 1:0.5:0.25

Section length L1:L2:L3 = 5:3:2 ratio

Figure 2-31 One "Branch" cooling channel

3. Varying width: the width of cooling channel is different along the fuel flow direction.

After the cooling stream has become fully developed the heat transfer coefficient drop dramatically (see Subsection 2.2.3.2). The "branch" configuration was designed to prevent the formation of fully developed flow and to increase the flow rate (as the total crossectional area is decreased). The "varying width" configuration will put more coolant on the larger heat generation side, but the heat transfer coefficient does not change.

In the "branch" configuration, a study was done to optimize the arrangement of different sections. The number of sections and the width of each section were hold fixed. The computer code developed in the previous section was modified to meet this configuration. Table 2-5 presents the results for various length ratios (dimensionless) with comparison to the "straight" configuration. The estimated standard deviation of the temperature and the peak temperature provide an indication of the uniformity of the thermal distribution. The average temperature can be used to estimate the cooling effect. Both of these results are not quite concordant. For example, Figure 2-32 plots the results for different length ratios of the first section, which include the "straight" configuration. It can be observed that the most uniform distribution occurs at higher (around 7) ratios, whereas, the best cooling effect occurs at lower (around 2) ratios. The results of the comparison among different section length arrangements are shown in Figure 2-33 in which the temperature profiles along the coolant

Length Ratio / Plate No.		[illegible]	[illegible]	[illegible]	[illegible]	[illegible]	[illegible]	[illegible]	[illegible]
C.D.	1	0.0208	0.0214	0.0202	0.0192	0.0195	0.0202	0.0217	0.0230	0.0230
Estimated	2	0.0217	0.0184	0.0179	0.0174	0.0173	0.0173	0.0178	0.0183	0.0183
Standard	3	0.0204	0.0183	0.0179	0.0175	0.0173	0.0172	0.0174	0.0176	0.0177
Deviation	M	0.0236	0.0194	0.0187	0.0180	0.0180	0.0183	0.0190	0.0196	0.0196
Temperature	1	170.5	165.5	164.6	163.4	162.8	162.1	161.9	161.6	162.0
(Average)	2	182.7	178.0	177.1	176.1	175.5	174.7	174.7	174.3	174.7
°C	3	186.7	182.2	181.3	180.2	179.7	179.0	178.8	178.5	178.9
	M	180.0	175.2	174.3	173.2	172.7	171.9	171.8	171.5	171.9
Temperature	1	10.5	7.4	7.1	6.8	7.0	7.3	7.7	8.0	8.0
Estimated	2	9,8	7.4	7.1	6.9	7.1	7.2	7.5	7.7	7.7
Standard	3	9.6	7.4	7.1	6.9	7.2	7.2	7.4	7.6	7.6
Deviation	M	10.0	7.4	7.1	6.9	7.1	7.2	7.5	7.8	7.8
Peak	1	17.7	10.8	10.7	11.0	11.7	12.7	13.0	13.7	13.5
Temperature	2	17.0	11.9	11.6	11.5	11.8	12.4	12.7	13.3	13.1
°C	3	16.7	12.2	11.7	11.6	12.0	12.3	12.7	13.1	12.9
	M	17.1	11.6	11.3	11.4	11.8	12.5	12.8	13.4	13.2
Cooling Air output Temperature		136.6	137.8	138.0	138.1	138.1	138.4	138.5	138.5	138.4

Length Ratio / Plate No.		2:2:6	2:6:2	2:3:5	2:5:3	1:2:7	1:7:2
C. D.	1	0.0256	0.0237	0.0240	0.0229	0.0275	0.0239
Estimated	2	0.0193	0.0187	0.0187	0.0183	0.0202	0.0189
Standard	3	0.0182	0.0180	0.0178	0.0177	0.0188	0.0182
Deviation	M	0.0210	0.0201	0.0202	0.0196	0.0222	0.0203
Temperature	1	161.1	162.8	161.3	162.1	161.2	163.4
(Average)	2	173.9	175.5	174.0	174.8	173.9	176.0
°C	3	178.1	179.6	178.1	179.0	178.1	180.2
	M	171.0	172.6	171.1	172.0	171.1	173.2
Temperature	1	8.7	8.2	8.3	8.0	9.2	8.2
Estimated	2	8.2	7.8	7.9	7.7	8.5	7.9
Standard	3	8.1	7.8	7.8	7.6	8.4	7.8
Deviation	M	8.3	7.9	8.0	7.7	8.7	7.9
Peak	1	15.0	12.7	14.5	13.1	15.5	12.5
Temperature	2	14.2	12.8	13.7	12.9	14.7	12.9
°C	3	14.1	13.1	13.6	12.9	14.4	13.0
	M	14.4	12.9	13.9	13.0	14.9	12.8
Cooling Air output Temperature		138.5	138.2	138.5	138.4	138.4	138.1

Table 2-5 Effect of section length in branched cooling scheme

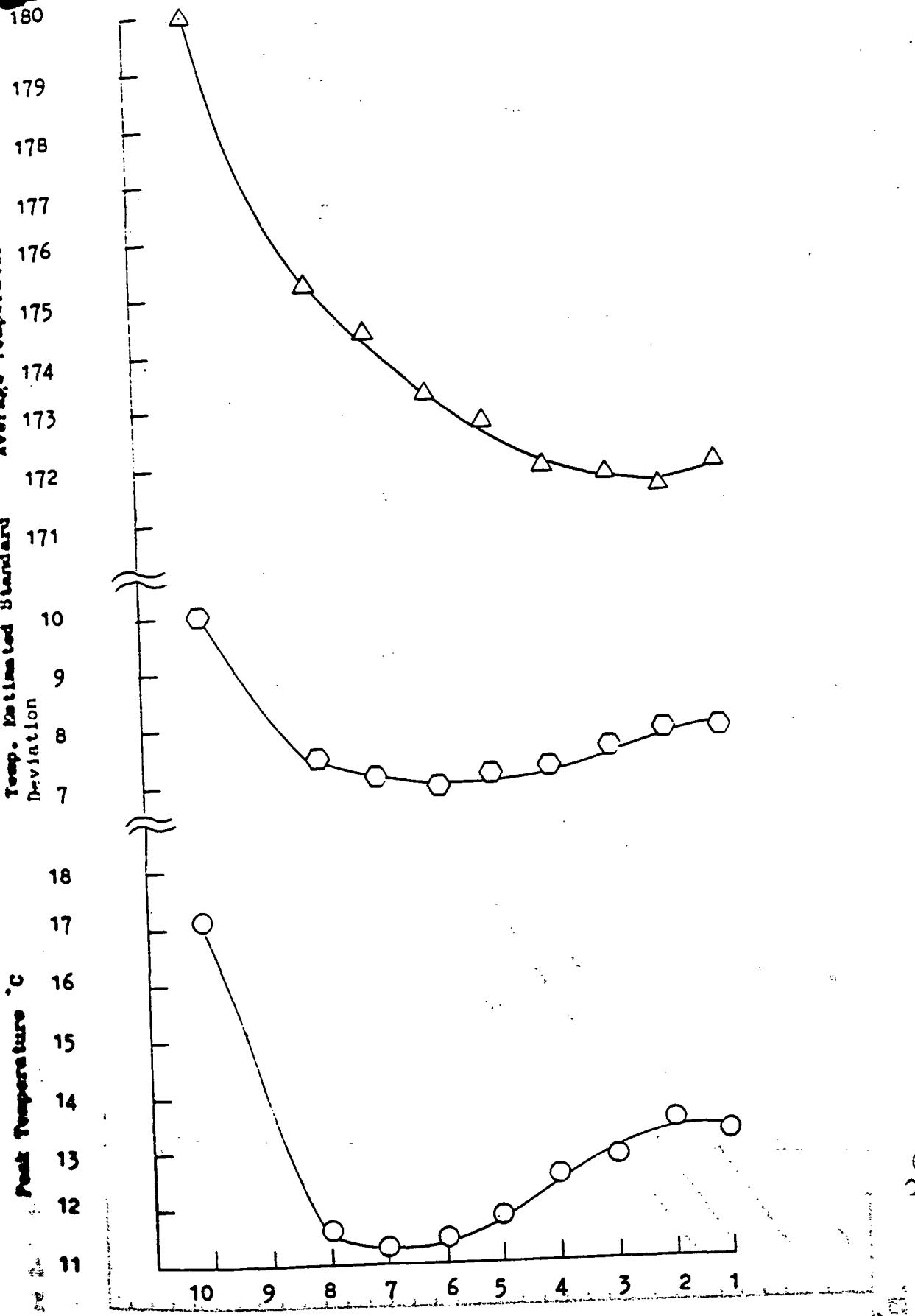

Figure 2-32 Comparison of temperature on the cell plate with different first separating section

Figure 2-33 Temperature profile with different section ratios in branch configuration

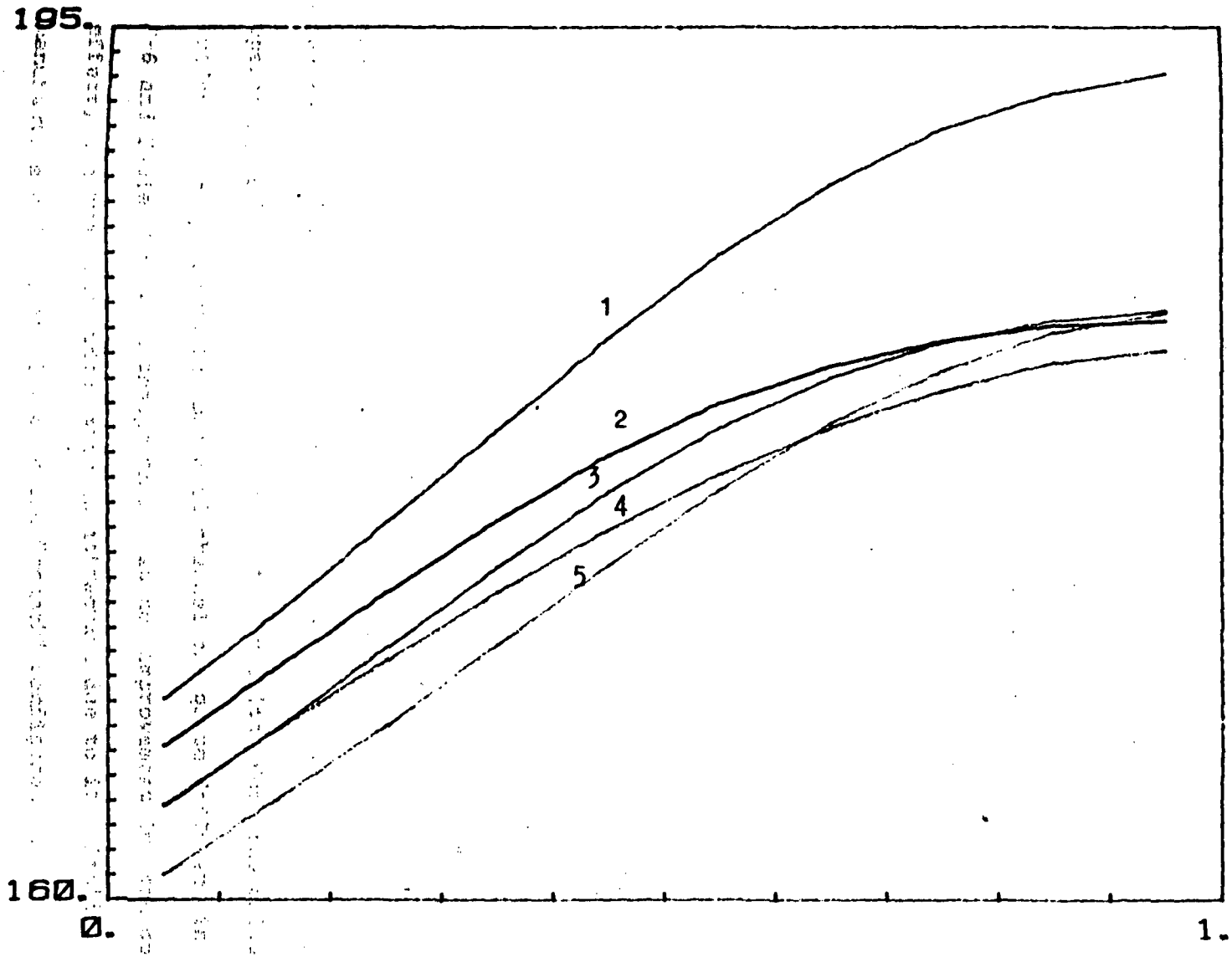

		average T
1: no separ.	182.7	°C
2: 7:2:1	177.1	
3: 1:7:2	176.0	
4: 4:3:3	174.7	
5: 1:2:7	173.9	

direction are drawn. There are five arrangements in this figure, they are the straight configuration, the longest first section (7:2:1), the longest second section (1:7:2), the average length (4:3:3), and the longest third section (1:2:7). The arrangement of average length shows the best cooling effect and good thermal uniformity (the values are listed in Table 2-5). More detailed comparisons among the three configuration are shown in Table 2-6 with a fixed ratio of coolant and Table 2-7 with a fixed operating temperature. The section ratio in "varying width" configuration is the ratio of the number of channels in each section which have different width ratios. The different channel width will result in different coolant flow rates.

It can be observed that: (1) from the uniformity view point, the branched channel is 23% ((10.-7.7)/10.) better than "straight" configuration and 14% ((8.9-7.7)/7.7) better than "varying width" configuration and the peak temperature is much lower (Table 2-6); (2) from the cooling effect view point, the branched channel is 17% ((35-29)/29) better than the other two configurations (Table 2-7).

The "varying width" configuration requires further examination of the effects of the section and width ratios on the uniformity to determine an optimal design. However, there is no optimal ratio for all operating conditions. For example, the results for the calculated uniformity compared to the branched channel are quite different in Table 2-6 and Table 2-7 . Although there is no improvement in the cooling effect, the "varying width" type is attractive due to its simplicity for manufacture and reliability over the "branch" configuration.

	no separation	branched channel (section ratio 2:3:5)	varying width (section ratio 3:2:1) (width ratio 1:0.95:0.9)
C.D. estimated standard deviation	0.0236	0.0202	0.0152
average temperature	180.0	171.1	180.2
peak temperature	17.1	8.0	13.3
temperature estimated standard deviation	10.0	7.7	8.9

unit: temperature: °C
C.D.: Amp/cm^2

general input data:

plate dimension: 12. x 10. in^2
utilization of H_2: 0.75
utilization of O_2: 0.50
input H_2 fraction: 0.75
input cooling air temperature: 375°K
average C.D.: 0.300 Amp/cm^2

Table 2-6 Comparison of different cooling configurations with fixed ratio of cooling air

	no separation	branched channel (section ratio 3:2:1)	varying width (section ratio 3:2:1) (width ratio 1:0.91:0.77)
C.D. estimated standard deviation	0.08172	0.06151	0.05382
average temperature	190.0	190.2	190.8
peak temperature	36.3	24.7	25.6
temperature estimated standard deviation	18.77	13.52	15.62
ratio of cooling air	35	29	35

unit: temperature: °C
C.D.: Amp/cm^2

general input data:

plate dimension: 13.95 x 12. in^2
utilization of H_2: 0.8
utilization of O_2: 0.5
input H_2 ratio: 0.76
input CO ratio: 0.01
input cooling air temperature: 403.3°K
average C.D.: 0.325 Amp/cm^2

Table 2-7 Comparison of different cooling configurations with the same average operating temperature

Thermal Conductivity in The Flow Direction

The temperature profiles along the coolant flow direction are simulated in Figure 2-34 for two different Ky values (thermal conductivity in flow direction) in the "branch" configuration. For the smaller Ky value, the break of the fully developed phenomenon can be observed more apparently which increases the heat transfer coefficient. As was expected, the greater Ky values produces better thermal distribution and a worse cooling effect. The material and construction of cell plate decide the Ky value.

Inlet Temperature of Process Air

Though the cooling effect of the process air is less than 10% of the total cooling, the inlet temperature of process air (TKA), or more precisely the temperature difference (ΔT) between average operating temperature and TKA, is an important factor in thermal analysis. For example, in the "branch" configuration, a small ΔT (183-155=28°C) will obtain more uniform temperature profile than that of higher ΔT (163-118=45 °C). The results are shown in Figure 2-35 and Figure 2-36 . Therefore, it is suggested that both the anode and cathode inlet temperatures should be close to the average stack temperature.

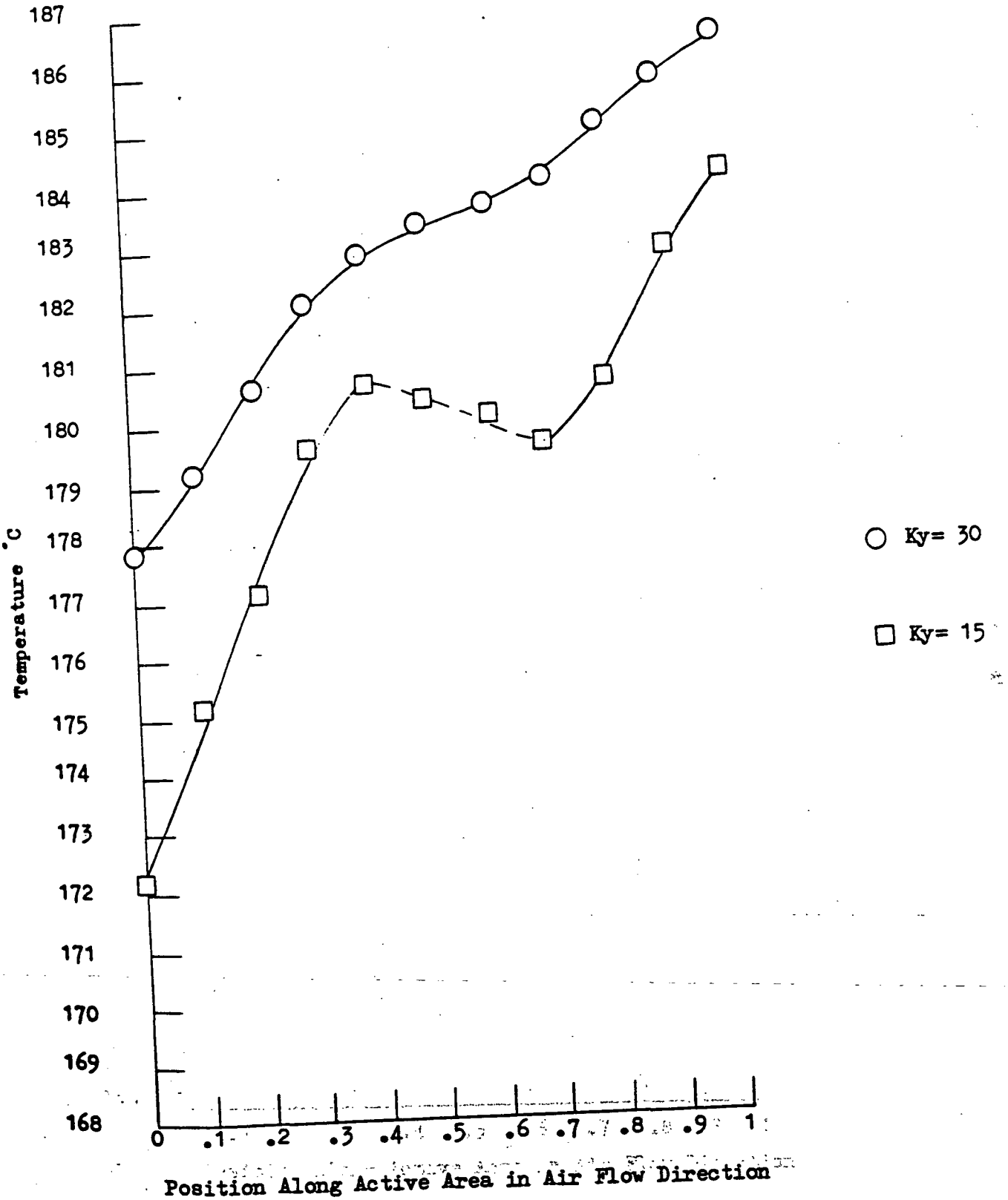

Figure 2-34 Comparison of temperature distribution with different thermal conductivities in the plate direction

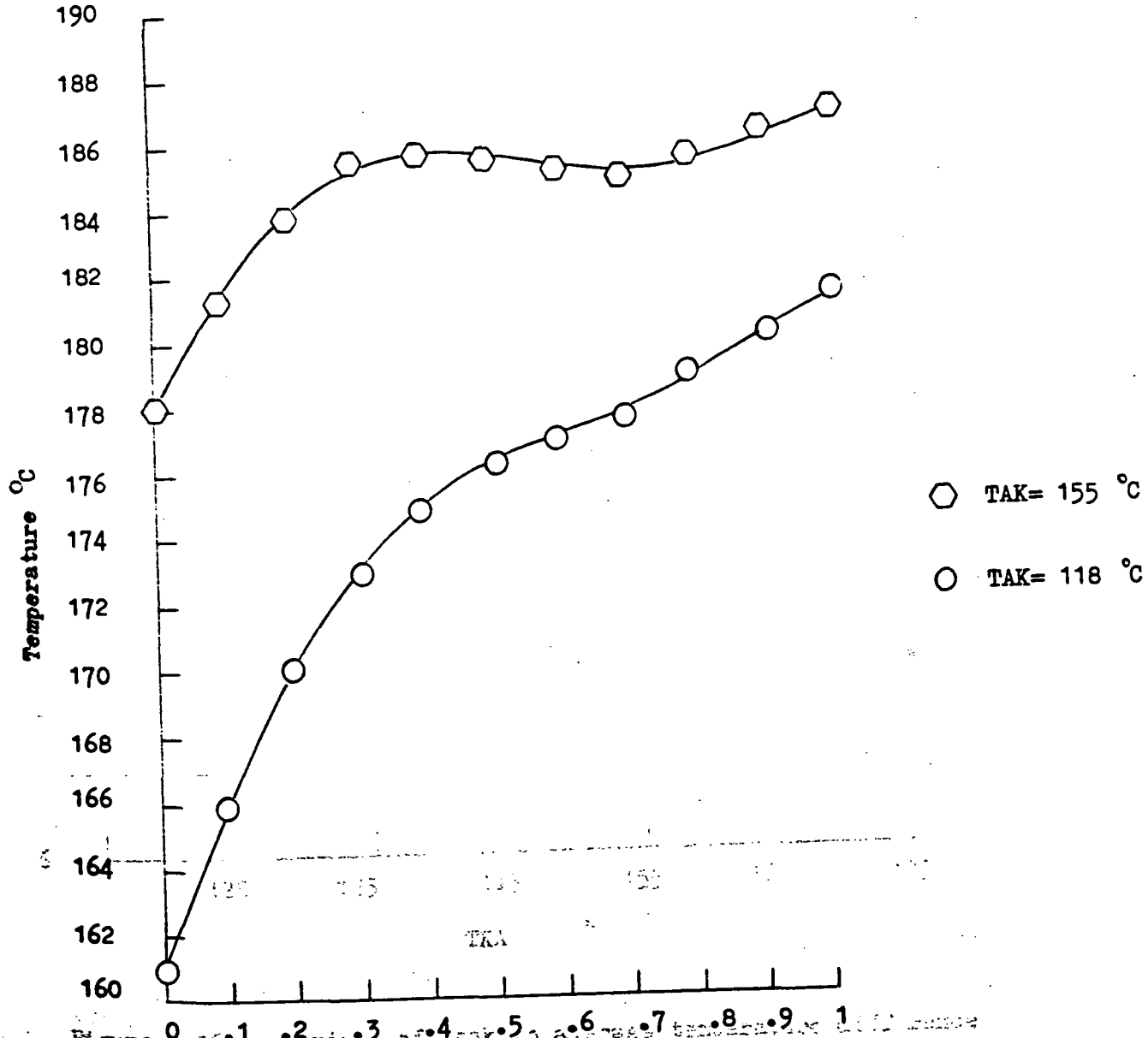

Figure 2-35 Comparison of P3 temperature distribution with different inlet process air temperatures

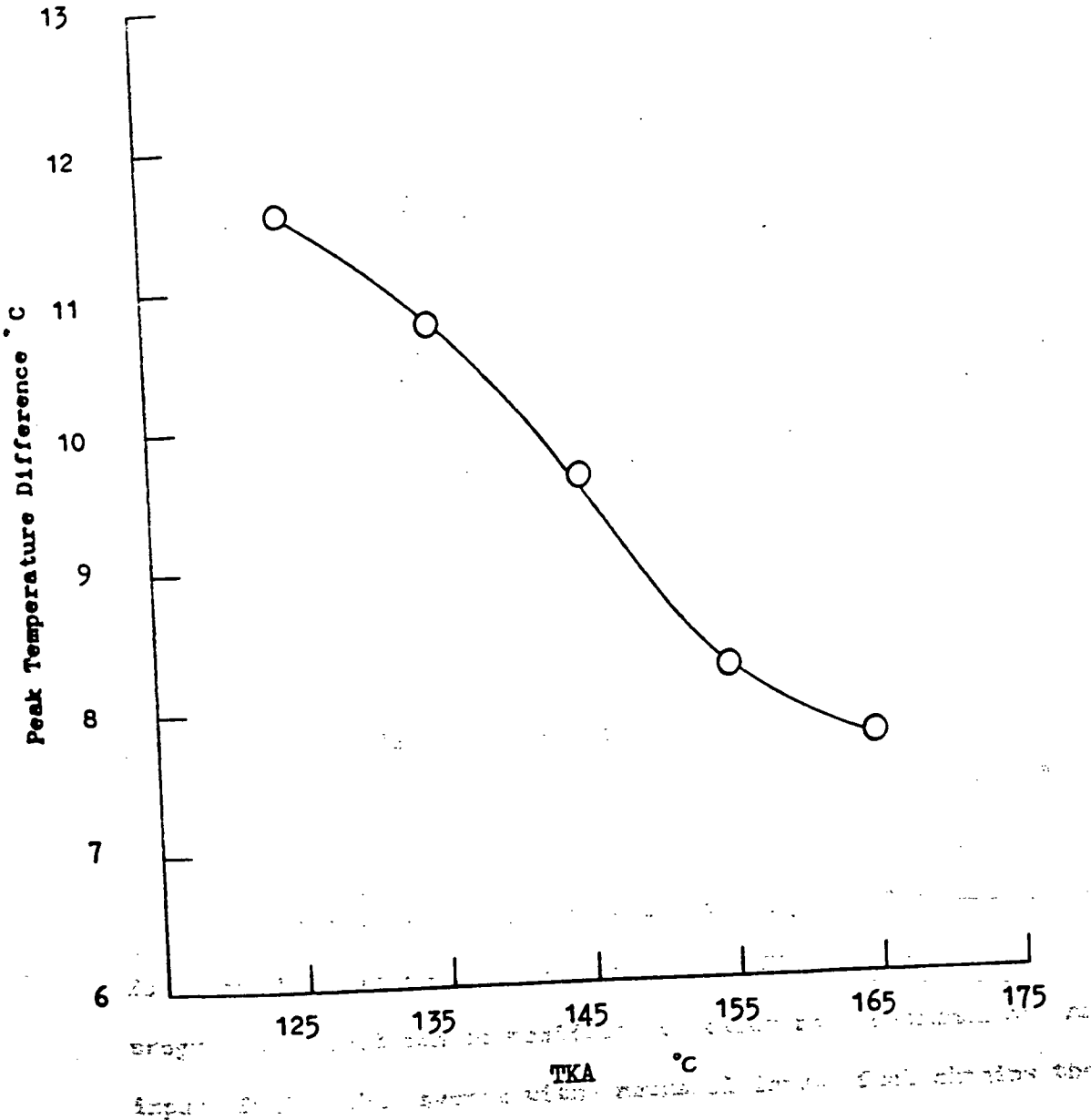

Figure 2-36 Comparison of peak to average temperature difference with different inlet process air temperature

2.3 Steady State Performance of PAFC System

The computer codes developed in previous sections were combined to simulate the PAFC system performance. The main program is the executive which controls the flows, manages and tests the iteration procedures, reads input data, and writes the final results. There are two PAFC systems which will be simulated: The CSU design and the Westinghouse design.

Results for the CSU Design

The lumped model of each component was used to simulate the original CSU design (Figure 2-1) except in the reformer where the distributed model was used. The flowchart of the executive program is shown in Figure 2-37 and the input data definitions and values are listed in Appendix 5. Figure 2-38 provides the final results which are presented as the P-T-V (V as a flow rate) status of each stream numbered on the flow diagram. The calculated electrical and heat generated are 124 Kw DC and 4.78×10^8 J/hr, respectively with a fuel cell efficiency of 37.4%.

There has been much interest in the effect of alternate commercial fuels on the performance and costs of PAFC power plants. The computer program developed can be modified to allow for methanol or naphtha as input fuel. The system with methanol input fuel obtains the highest effeciency (approximately 42% for total the system) among the three fuels. More detailed discussions on this topic are presented in Ref. 16.

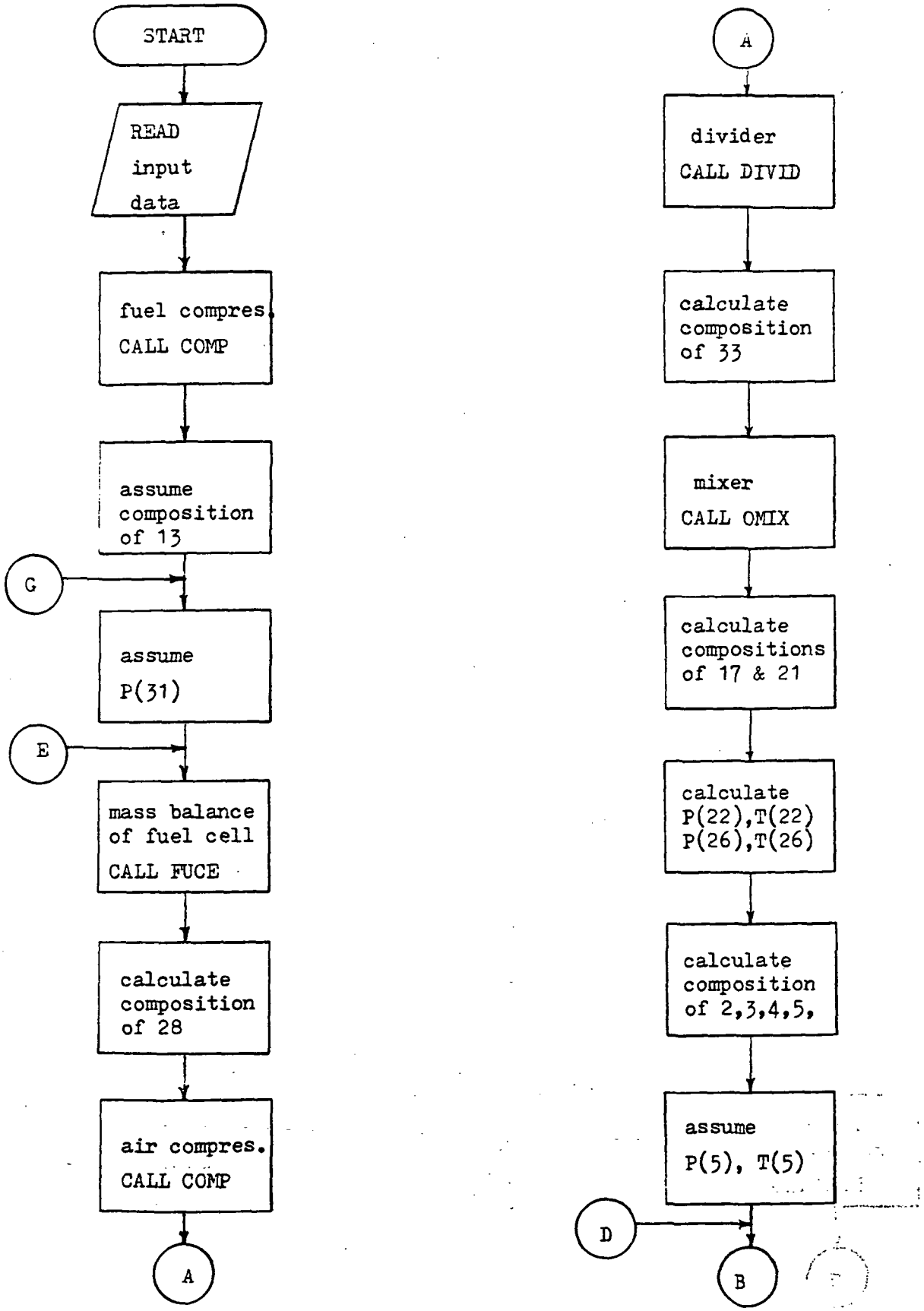

Figure 2-37 Flow chart of executive program for simulating CSU's PAFC system steady state performance

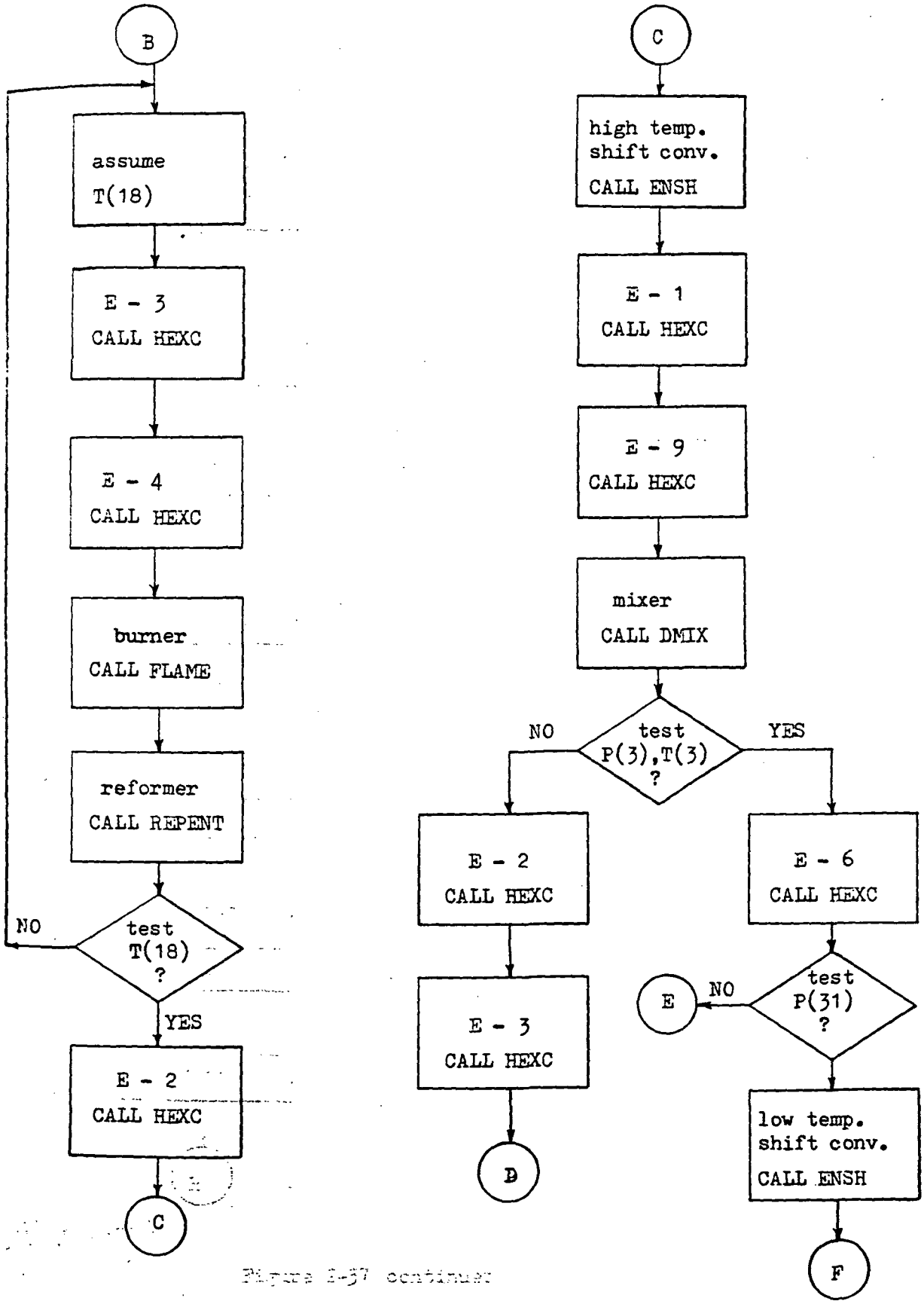

Figure 2-37 continued

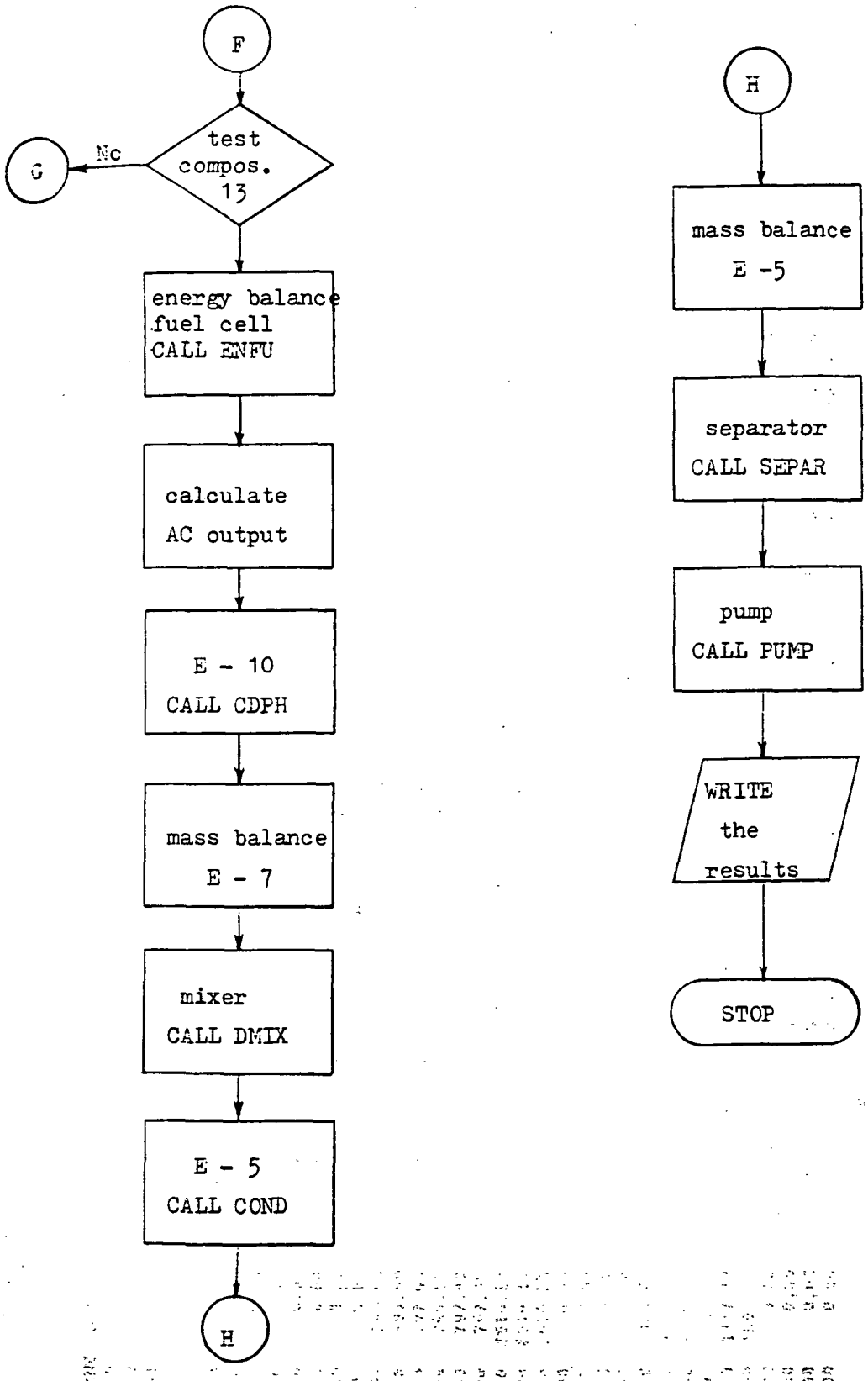

Figure 2-37 continued

STREAM	METHANE	OXYGEN	CAR. MONOXIDE	CAR. DIOXIDE	HYDROGEN	WATER	NITROGEN	FLOW RATE	TEMP.(K)	PRE.(ATM)
1	1216.00	0.00	1.36	21.80	166.00	0.00	0.00	1405.16	298.00	5.1000
2	1216.00	0.00	1.36	21.80	166.00	0.00	0.00	1405.16	696.66	5.0995
3	1216.00	0.00	1.36	21.80	166.00	3648.00	0.00	5053.16	674.15	5.0018
4	1216.00	0.00	1.36	21.80	166.00	3648.00	0.00	5053.16	917.66	5.0010
5	1216.00	0.00	1.36	21.80	166.00	3648.00	0.00	5053.16	1110.88	5.0000
7	182.10	0.00	665.23	391.83	3637.71	2244.08	0.00	7120.94	1089.42	4.7557
8	182.10	0.00	665.23	391.83	3637.71	2244.08	0.00	7120.94	877.93	4.7556
9	182.10	0.00	453.67	603.38	3849.27	2032.52	0.00	7120.95	877.93	4.7556
10	182.10	0.00	453.67	603.38	3849.27	2032.52	0.00	7120.95	777.70	4.7554
11	182.10	0.00	453.67	603.38	3849.27	2032.52	0.00	7120.95	655.97	4.7553
12	182.10	0.00	453.67	603.38	3849.27	2032.52	0.00	7120.95	423.18	4.7553
13	182.10	0.00	3.61	1053.44	4299.32	1582.46	0.00	7120.94	423.18	4.7640
14	182.96	0.00	3.58	1052.25	858.57	1585.42	0.00	3682.78	443.00	4.7640
15	182.96	1593.99	3.58	1052.25	858.57	1767.52	5993.40	11452.27	351.22	4.7232
16	182.96	1593.99	3.58	1052.25	858.57	1767.52	5993.40	11452.27	788.69	4.7217
17	0.00	797.00	0.00	1238.79	0.00	2992.01	5993.40	11021.20	1623.20	4.3954
18	0.00	796.99	0.00	1238.79	0.00	2992.01	5993.40	11021.19	1221.65	4.1756
19	0.00	797.00	0.00	1238.79	0.00	2992.01	5993.40	11021.20	1111.42	4.1747
20	0.00	797.00	0.00	1238.79	0.00	2992.01	5993.40	11021.20	701.91	4.1740
21	0.00	2514.13	0.00	1238.79	0.00	6818.60	18906.22	29477.74	546.04	4.3739
22	0.00	2514.13	0.00	1238.79	0.00	6818.60	18906.22	29477.74	357.11	4.3783
23	0.00	2514.13	0.00	1238.79	0.00	3170.57	18906.22	25829.71	357.11	4.3783
24	0.00	0.00	0.00	0.00	0.00	3648.02	0.00	3648.02	357.11	4.3783
25	0.00	0.00	0.00	0.00	0.00	3648.00	0.00	3648.00	357.11	5.0025
26	0.00	0.00	0.00	0.00	0.00	3648.00	0.00	3648.00	421.65	5.0025
27	0.00	0.00	0.00	0.00	0.00	3648.00	0.00	3648.00	650.00	5.0017
28	0.00	5028.25	0.00	0.00	0.00	574.43	18906.21	24508.89	298.00	1.0000
29	0.00	5028.25	0.00	0.00	0.00	574.43	18906.21	24508.89	298.00	4.7878
30	0.00	3434.26	0.00	0.00	0.00	392.33	12912.82	16739.41	298.00	4.7878
31	0.00	3434.26	0.00	0.00	0.00	392.33	12912.82	16739.41	409.40	4.7640
32	0.00	1717.13	0.00	0.00	0.00	3826.59	12912.82	18456.54	443.00	4.7639
33	0.00	1593.99	0.00	0.00	0.00	182.10	5993.40	7769.49	298.00	4.7878
34	0.00	0.00	0.00	0.00	0.00	201417.44	0.00	201417.44	333.00	1.0000
35	0.00	0.00	0.00	0.00	0.00	201417.44	0.00	201417.44	355.00	1.0000
36	0.00	0.00	0.00	0.00	0.00	111381.38	0.00	111381.38	298.00	1.0000
37	0.00	0.00	0.00	0.00	0.00	111381.38	0.00	111381.38	355.00	1.0000

Figure 2-38 Temperature, pressure, and mass balance of CSU's PAFC system

Comparison with the Westinghouse Conceptual Design

Both the lumped and distributed models were used to simulate the Westinghouse PAFC system (Figure 1-3). The estimated dimensions of the heat exchangers, shift converters, and reformer discussed in previous sections were used as input data for the distributed model simulation. The definitions and values of input data are listed in Appendix 6.

Because the flow diagram of this system differed from the CSU system, the executive program was modified to meet this change. The flowchart of executive program is shown in Figure 2-39 . Results for the mass balance, temperature, and pressure of the gas stream at various locations for Westinghouse PAFC system are given in Table 2-8 . The stream number refers to Figure 1-4 and the gas component values are in mole fractions. There are three values presented for each stream, the first row is the Westinghouse conceptual design (Ref. 12), the second row is the results from the "lumped" simulation, and the third row is the results from the "distributed" simulation. A comparison of results is shown in Table 2-9 . Because the type of reformer in the distributed simulation is "once-through" and the reformer in the Westinghouse conceptual design is "regenerative"*, the outlet temperature of reforming gas is higher (939°K) and the temperature of combustion gas is lower (835°K) in the CSU simulation than that (867°K and 1051°K respectively) in Westinghouse conceptual design. The results in both shift converters are also affected by this temperature difference. One serious problem that arises with the CSU "once-through" reformer is that not enough heat for evaporating water is available from the outlet

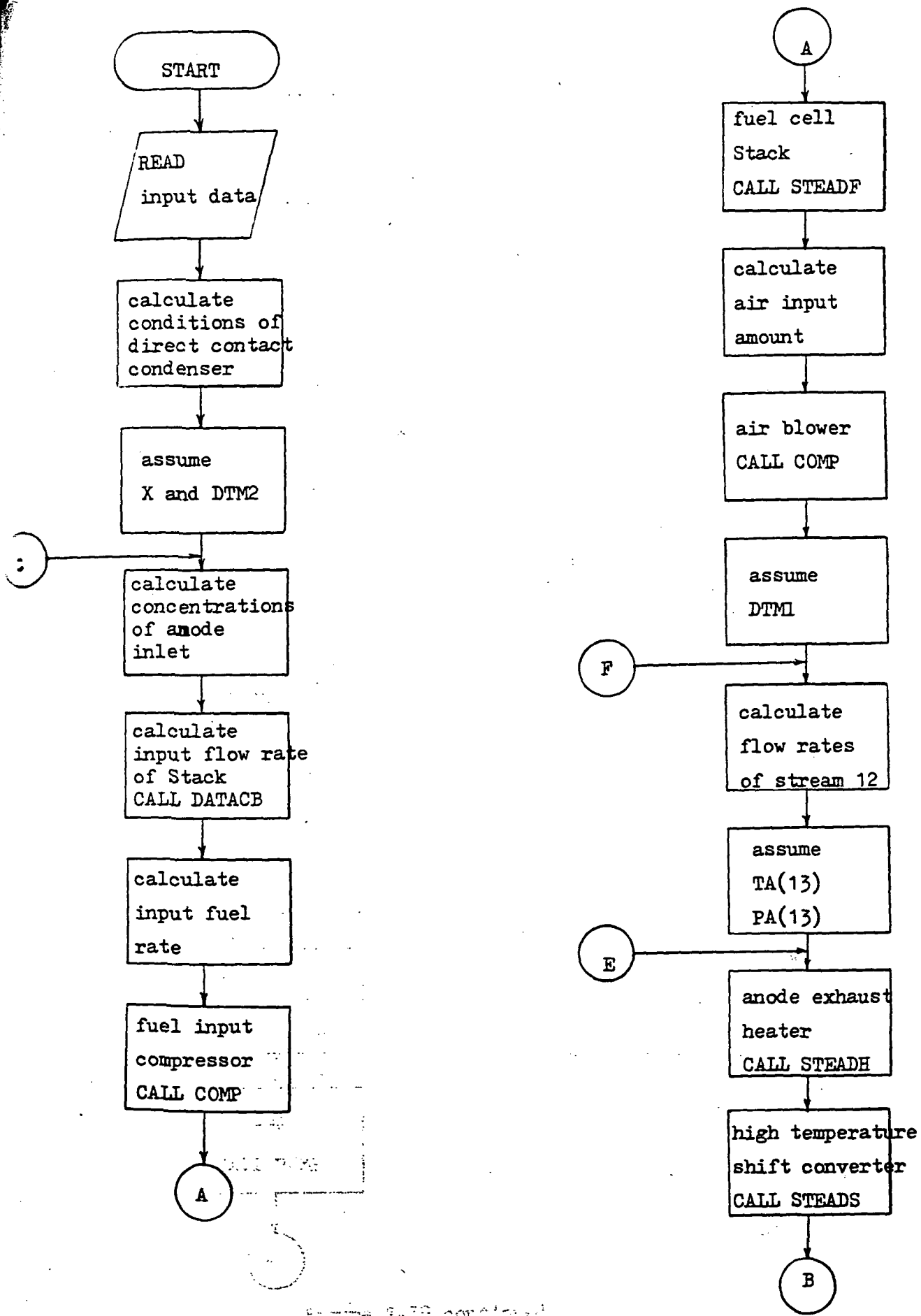

Figure 2-39 continued

Figure 2-39 The flow chart of executive program for steady state simulation of Westinghouse PAFC system

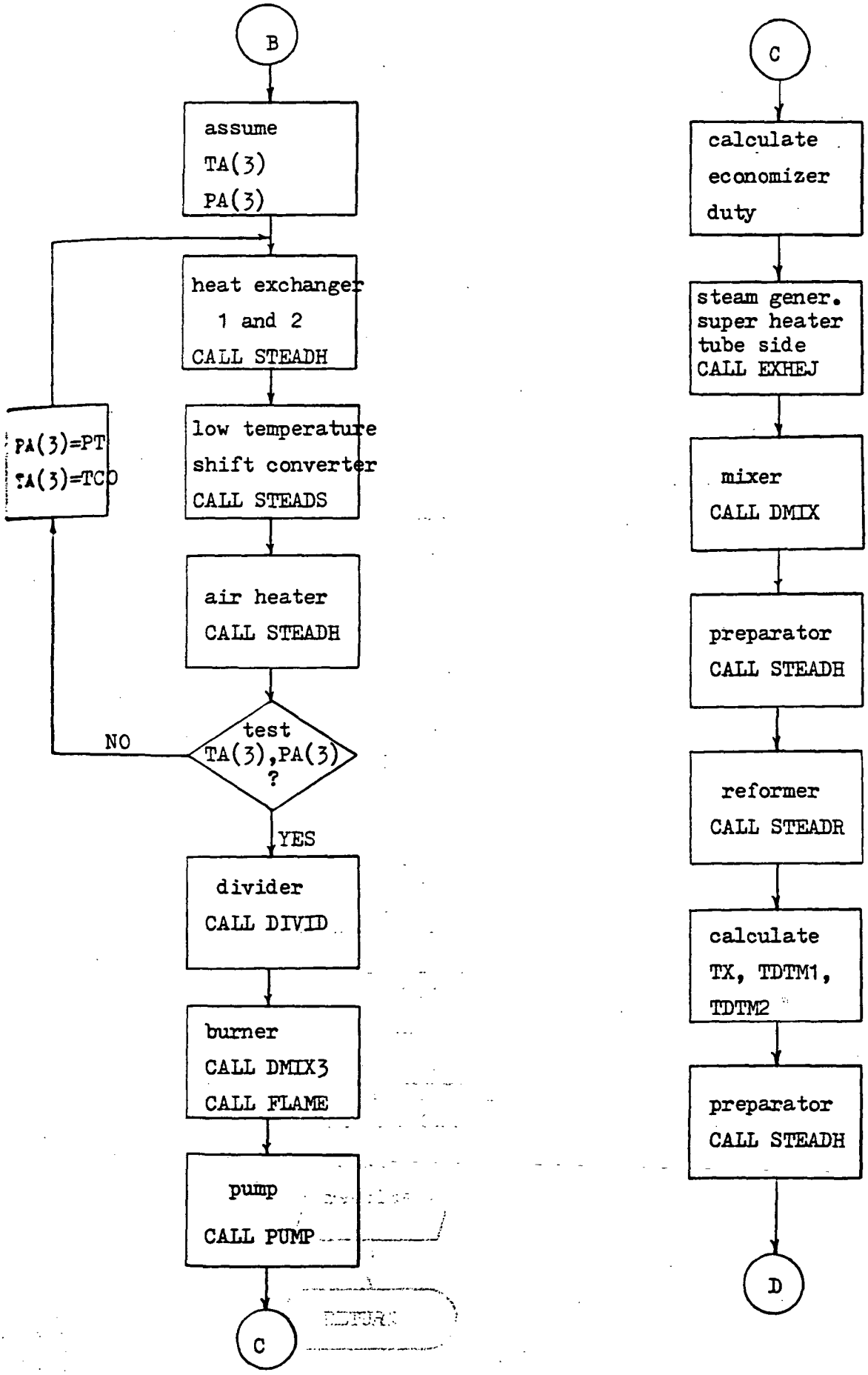

Figure 2-39 continued

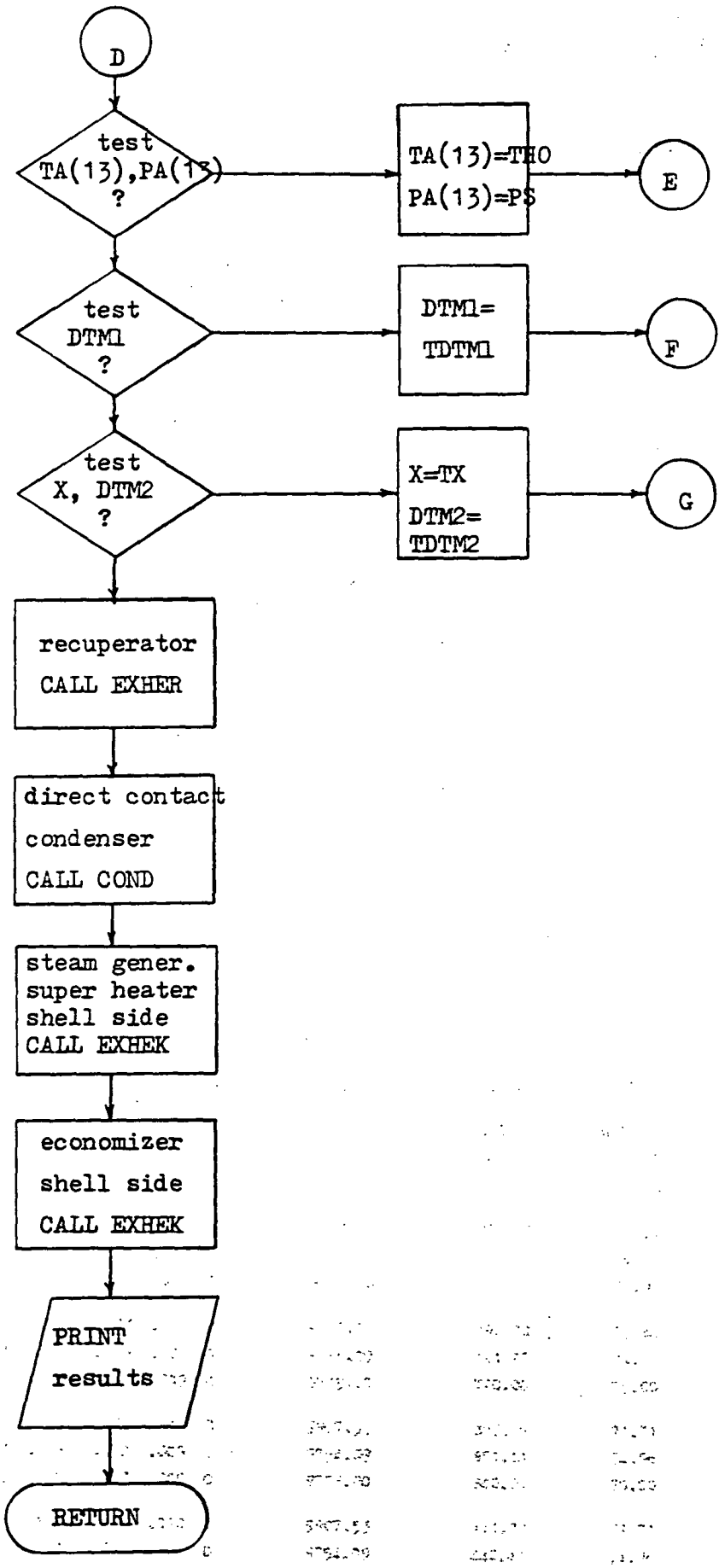

Figure 2-39 continued

STREAM	CH4	CO	CO2	H2O	H2	N2	O2	FLOW RATE(lb/hr)	TEMPERATURE(F)	PRESSURE(psia)
1	0	0	0	.010	0	.782	.208	14084.68	80.00	14.70
	0	0	0	.010	0	.782	.208	14326.57	80.00	14.70
	0	0	0	.010	0	.782	.208	14358.00	77.00	14.70
2	0	0	0	.010	0	.782	.208	14084.68	80.00	19.99
	0	0	0	.010	0	.782	.208	14326.57	137.04	19.99
	0	0	0	.010	0	.782	.208	14358.00	80.00	20.00
3	0	0	0	.010	0	.782	.208	14084.68	214.45	19.97
	0	0	0	.010	0	.782	.208	14326.57	255.03	18.80
	0	0	0	.010	0	.782	.208	14358.00	192.00	20.00
4	0	0	0	.010	0	.782	.208	14084.68	747.61	19.84
	0	0	0	.010	0	.782	.208	14326.57	724.72	18.79
	0	0	0	.010	0	.782	.208	14358.00	700.00	20.00
5	.950	0	0	0	0	.050	0	2853.75	80.00	49.98
	.953	0	0	0	0	.047	0	2800.00	80.00	49.98
	.950	0	0	0	0	.050	0	2797.00	77.00	50.00
6	.950	0	0	0	0	.050	0	2853.75	181.42	98.48
	.953	0	0	0	0	.047	0	2800.00	183.83	99.96
	.950	0	0	0	0	.050	0	2797.00	180.00	100.00
7	.950	0	0	0	0	.050	0	2853.75	735.48	98.48
	.953	0	0	0	0	.047	0	2800.00	724.72	99.95
	.950	0	0	0	0	.050	0	2797.00	700.00	100.00
8	.950	0	0	0	0	.050	0	2853.75	735.48	95.53
	.953	0	0	0	0	.047	0	2800.00	724.72	99.95
	.950	0	0	0	0	.050	0	2797.00	700.00	100.00
9	.950	0	0	0	0	.050	0	82.64	735.48	95.53
	.953	0	0	0	0	.047	0	81.09	724.72	99.95
	.950	0	0	0	0	.050	0	81.00	700.00	100.00
10	.281	0	0	.704	0	.015	0	9907.54	553.36	97.88
	.282	0	0	.704	0	.014	0	9754.09	551.33	102.26
	.271	0	0	.714	0	.014	0	9779.00	556.00	100.00
11	.281	0	0	.704	0	.015	0	9907.54	856.50	97.88
	.282	0	0	.704	0	.014	0	9754.09	798.80	102.26
	.271	0	0	.714	0	.014	0	9779.00	800.00	100.00
12	.014	.101	.070	.222	.583	.010	0	9907.55	1229.84	76.04
	.012	.122	.051	.237	.569	.009	0	9754.09	1100.06	74.97
	.014	.119	.053	.242	.562	.009	0	9779.00	1100.00	75.00
13	.014	.101	.070	.222	.583	.010	0	9907.55	990.57	76.04
	.012	.122	.051	.237	.569	.009	0	9754.09	899.19	74.97
	.014	.119	.053	.242	.562	.009	0	9779.00	899.00	75.00
14	.014	.101	.070	.222	.583	.010	0	9907.54	792.70	75.84
	.012	.122	.051	.237	.569	.009	0	9754.09	721.99	74.96
	.014	.119	.053	.242	.562	.009	0	9779.00	720.00	75.00
15	.014	.063	.108	.184	.621	.010	0	9907.53	887.46	71.71
	.012	.060	.113	.175	.632	.009	0	9754.09	851.44	74.96
	.014	.058	.115	.180	.623	.009	0	9779.00	840.00	70.00
16	.014	.063	.108	.184	.621	.010	0	9907.53	411.87	71.71
	.012	.060	.113	.175	.632	.009	0	9754.09	442.41	74.96
	.014	.058	.115	.180	.623	.009	0	9779.00	397.00	65.00

Table 2-8 Temperature, pressure, and mass balance of Westinghouse PAFC system with three kinds of simulation

17	.014	.002	.169	.123	.683	.010	0	9907.52	557.25	66.03
	.012	.009	.164	.124	.683	.009	0	9754.09	553.63	74.95
	.014	.013	.160	.135	.669	.009	0	9779.00	495.00	65.00
18	.014	.002	.169	.123	.683	.010	0	9907.51	481.23	66.02
	.012	.009	.164	.124	.683	.009	0	9754.09	491.73	74.95
	.014	.013	.160	.135	.668	.009	0	9779.00	401.00	60.00
19	.014	.002	.169	.123	.683	.010	0	9907.51	191.31	66.02
	.012	.009	.164	.124	.683	.009	0	9754.09	211.02	74.95
	.014	.013	.160	.135	.669	.009	0	9779.00	200.00	60.00
20	.016	.002	.188	.024	.759	.011	0	8353.79	123.20	60.01
	.012	.009	.167	.063	.741	.009	0	8879.36	159.20	60.01
	.015	.014	.171	.077	.713	.010	0	8826.00	159.00	60.00
21	.016	.002	.188	.024	.759	.011	0	8353.79	450.72	60.01
	.012	.009	.167	.063	.741	.009	0	8879.36	449.27	60.00
	.015	.014	.171	.077	.713	.010	0	8826.00	376.00	60.00
22	0	0	0	1.00	0	0	0	7136.43	325.21	95.72
	0	0	0	1.00	0	0	0	7035.18	328.36	100.45
23	0	0	0	1.00	0	0	0	7136.43	441.98	95.52
	0	0	0	1.00	0	0	0	7035.18	445.77	99.95
	0	0	0	1.00	0	0	0	7063.00	480.00	100.00
24	.040	.006	.479	.062	.386	.028	0	7418.01	845.90	47.48
	.029	.022	.410	.153	.364	.023	0	7891.28	760.12	49.97
	.035	.031	.398	.180	.332	.023	0	7924.00	761.00	50.00
25	0	0	.221	.235	0	.531	.013	21585.34	3266.50	23.49
	0	0	.207	.269	0	.512	.012	22298.94	3176.58	22.91
	0	0	.207	.270	0	.511	.012	22364.00	3184.00	15.00
26	0	0	.221	.235	0	.531	.013	21585.34	1042.89	21.14
	0	0	.207	.269	0	.512	.012	22298.94	1279.95	20.62
	0	0	.207	.270	0	.511	.012	22364.00	1432.00	15.00
27	0	0	.221	.235	0	.531	.013	21585.34	325.21	20.51
	0	0	.207	.269	0	.512	.012	22298.94	319.56	20.00
	0	0	.207	.270	0	.511	.012	22364.00	446.00	15.00
28	0	0	.221	.235	0	.531	.013	21585.34	249.92	20.41
	0	0	.207	.269	0	.512	.012	22298.94	231.09	19.90
	0	0	.207	.270	0	.511	.012	22364.00	355.00	15.00
29	.950	0	0	0	0	.050	0	2771.11	735.48	95.53
	.953	0	0	0	0	.047	0	2718.91	724.72	99.95

Table 2-8 continued

	Westinghouse Conceptual Design	Our Results-1	Our Results-2
System Simulation Method		Thermodynamic	Distributed
Natural Gas Comp. Vol %			
-CH4	90	95.3	95
-C2H6	5	0	0
-N2	5	4.7	5
-Pressure psia	100	100	98.5
Reformer Tube Type	Regenerative	Regenerative	Once-through
-Approach Diff. Temp. °F	25	25	
-Conversion of Methane	0.925	0.935	0.924
-Reforming Gas Inlet Temp. °F	800	798	856
-Reforming Gas Outlet Temp. °F	1100	1100	1230
-Reforming Gas Inlet Pressure psia	100	102	98
-Reforming Gas Outlet Pressure psia	75	75	76
-Combustion Gas Inlet Temp. °F	3184	3176	3267
-Combustion Gas Outlet Temp. °F	1432	1280	1043
High Temp. Shift Converter			
-Approach Diff. Temp. °F	-25	-25	
-Conversion of CO	0.51	0.51	0.38
-Inlet Temp. °F	720	722	793
-Outlet Temp. °F	840	851	888
-Inlet Pressure psia	75	75	76
-Outlet Pressure psia	70	75	72
Low Temp. Shift Converter			
-Approach Diff. Temp. °F	-25	-25	
-Conversion of CO	0.776	0.85	0.37
-Inlet Temp. °F	397	442	412
-Outlet Temp. °F	495	554	557
-Inlet Pressure psia	65	75	72
-Outlet Pressure psia	63	75	66
Fuel Cell Stack			
-Design Current Density ma/cm^2	325	325	325
-Design (Calculate) Cell Voltage volts/cell	0.683	0.616	0.665
-Operating Temperature (Average) °F	376	376	375
-Operating Pressure psia	50	50	50
-Effective Cell Area cm^2	1080	1080	1080
-Anode Inlet Temperature °F	376	449	451
-Anode Outlet Temperature °F	376	375	362
-Cathode Inlet Temperature °F	3[illegible]	368	350
-Cathode Outlet Temperature °F	376	375	393

Table 2-9 Comparison of simulations of Westinghouse PAFC system

[illegible] the product gas is recycled through the heat exchanger [illegible] some energy (heat). This design will save 10-15% of the [illegible] in reforming (Ref. 17)

combustion gas at 835°K. This condition lacks 1/3 to 1/4 the heat duty (see the output for this simulation in Appendix 7). One way to amend this problem is to recover some heat from the product gas by adding a heat exchanger between the evaporating water and product gas.

Considering the complex interactions of temperature and composition at each location, the agreement between the CSU simulations and Westinghouse conceptual design is very good.

•regenerative reformer: the product gas is recycled through the most inner tube to recover some energy (heat). This design will save 10-15% of the heat needed in reforming (Ref. 13)

2.4 Process Synthesis with Heat Exchanger Network

The CSU PAFC system developed originally can be cost improved by considering the energy conservation. Any heat recovered and reused in the process not only reduces the amount of fuel consumed but also reduces the amount of heat rejected to the cooling system. One way to solve this kind of problem is to find the optimal heat exchanger network. This task consists of finding a feasible sequence of heat exchangers in which pairs of streams are matched, such that the network is optimized as the total cost is minimized.

A new combined algorithmic-heuristic approach has been developed. This three-phase algorithm can generate, with great ease and considerable speed, a near optimal exchanger network. The description of this new algorithm and a comparison with other approaches is presented in Appendix 3. This approach was used to improve the heat exchanger network in the CSU original PAFC system shown in Figure 2-1. Figure 2-40 shows the network with the corresponding temperatures. Here the cooling media (steam without phase change) in the fuel cell stack is to be cooled from 433°K to 413°K by evaporating the pressurized steam (steam no. 25) and the outside loop cooling water. The outlet cooling water can be used in domestic applicitions. Figure 2-41 shows the improved heat exchanger network for the same operating conditions. The cost comparison is shown in Table 2-10, where the assumptions for the heat exchanger cost calculations are the same as in the sample problems described in Appendix 3 Table 2. There is 10% cost improvement for the new design over the old one. A greater reduction in cost could be expected if the inlet temperatures of the reformer, shift converters,

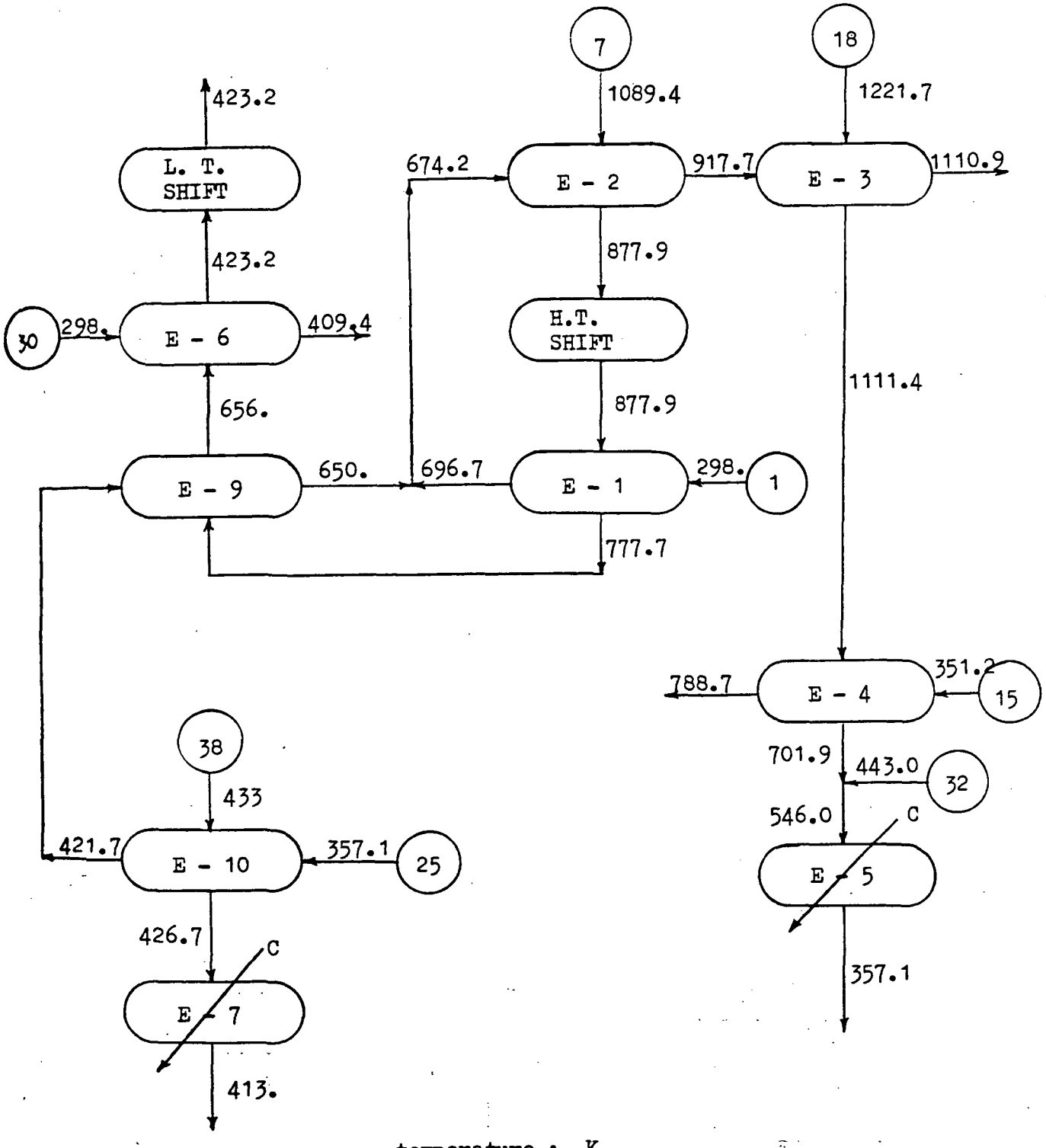

temperature : K

Figure 2-40 Heat exchanger network of original PAFC system

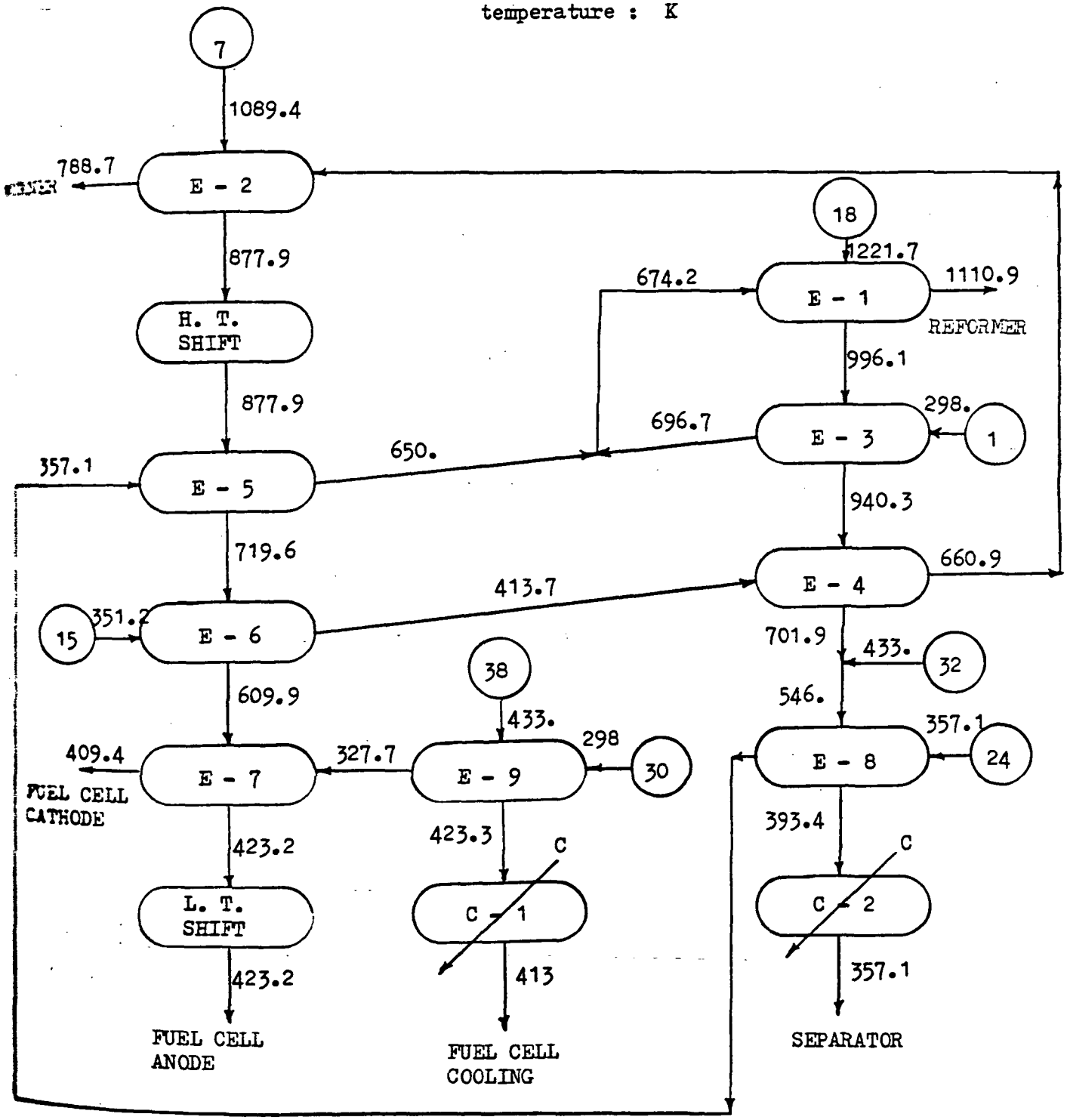

Figure 2-41 Optimal heat exchanger network of PAFC system

Cost of	Original network (Figure 2-40)	Optimal network (Figure 2-41)
E - 1	83.	251.
E - 2	164.8	149.5
E - 3	175.1	66.4
E - 4	529.6	209.1
E - 5	1216.3 (cooler)	112.6
E - 6	176.7	92.
E - 7	132.	191.2
E - 8		507.1
E - 9	972.8	115.6
E - 10	2071.7 (cooler)	
C - 1		2779.5
C - 2		411.5
Total	5522.1	4885.6

Table 2-10 Cost comparison of heat exchanger network

and mixer were not fixed.

The results presented depend upon the assumptions made in cost estimation and heat capacity calculations. However, this approach provides an optimal scheme for energy conservation.

CHAPTER 3

SIMULATION OF TRANSIENT STATE WITH LOAD CHANGE

In normal operation, the plant control system will act to maintain the electric power output at a level required to meet the plant load demands. The cathode air and anode fuel gas flow rates will be maintained at prescribed levels corresponding to the current demand level. The cooling air flow will be adjusted to maintain a constant fuel cell temperature. The fuel cell pressure level will be adjusted to match the compressor characteristics.

The daily electrical energy consumption either at a commercial or residential site is varying. Load change is an important and frequent operation in the power plant. Since the PAFC system can be subjected to sudden load changes and load ramping, an understanding of the effects of these transient conditions on the PAFC system's performance is essential for the optimal design and control of the system. For the PAFC system, the controlled variable is the level of output AC power required, and the manipulated variables are the input fuel and air quantities. In addition to the orderly analyses, evaluation of the performance under catastorphic conditions can provide a means of designing emergency shutdown systems, and thus prevent disasters in PAFC plant. Basically, the problem is a "what would happen if" situation that must be analyzed, preferably, before the plant is built.

Therefore, the process dynamics involve the modeling of the processing system in order to optimize investment and operating costs, achieve automatic control, and provide for startup, shutdown and emergency procedures.

3.1 Modeling Procedures of the Transient Response of the PAFC System

The steps to model the transient response of the PAFC system are described as follows:

(1) Set up the mathematical model for each major fuel cell system component.

(2) Estimate the design dimensions for each major fuel cell system component.

(3) Simulate the distributed system performance at steady state as the initial conditions for the next step.

(4) Calculate the transient state system responses.

The results of steps (2) and (3) have been shown and discussed in Chapter 2. The following chapters will concentrate on steps (1) and (4).

3.2 General Procedures for Transient State Simulation of Major Components

For computer simulation of the dynamic system, a mathematical model must first be developed which defines the input-output relationships of a process as a function of time. Usually these mathematical relationships are in the form of simultaneous differential equations. These differential equations are determined either empirically, from the operating system or a similar operating system, or analytically, from the physical laws governing the dynamics of the system. The computer simulation described in this work was derived from a combination of these two techniques.

A system of simultaneous partial differential equations was derived and subsequently solved from the physical and chemical laws, such as the law of conservation of mass, energy, and momentum, and the defining equations governing the PAFC system.

In solving these types of problems, the first step is problem definition. Once the problem has been defined, the next step for solving it is usually the application of conservation equations. These apply to mass, energy and momentum balances. Generally, this procedure is applied to steady-state or static problems. The general equations for mass, energy or momentum conservation for a system are given by:

$$\begin{matrix}\text{Flow} \\ \text{in}\end{matrix} - \begin{matrix}\text{Flow} \\ \text{out}\end{matrix} + \begin{matrix}\text{Reaction} \\ \text{product}\end{matrix} = \text{Accumulation} \qquad (3.1)$$

$$\begin{matrix}\text{Energy} \\ \text{in}\end{matrix} - \begin{matrix}\text{Energy} \\ \text{out}\end{matrix} + \begin{matrix}\text{Reaction} \\ \text{energy}\end{matrix} = \begin{matrix}\text{Accumulation} \\ \text{of energy}\end{matrix} \qquad (3.2)$$

Sum of forces acting = Change of momentum (3.3)

In Eq. (3.1), the flow and accumulation terms can represent the amount of a particular component, or all (i.e., total) components of the system. In Eq. (3.3), the change of momentum represents the mass multiplied by its velocity. Eq. (3.3) is applicable to a specific direction-i.e., it is a vector equation.

The general procedures for transient state simulation of major components are as follows:

(1) Set up the mathematical model for the transient condition.

(2) Formulate explicit differential-difference working equations* from the mathematical model.

(3) Delete time varying terms to obtain steady state solutions as the initial conditions.

(4) At t=0, perturb the controlled variables with a desired change.

(5) Solve these equations with a numerical integration routine for each time step.

(6) Increase time by one time step, if steady state is reached plot the results; otherwise go to (5).

*Differential-difference equation

By substituting the distance varying terms with backward or forward differences and keeping the equation in explicit form, the equations thus obtained form a set of initial value ordinary differential equations which can be solved by standard integration methods.

3.3 Computer Solutions for Differential Equations

The most powerful tool for solving the differential equations for modeling process-dynamics problems is probably the digital computer. Digital computers eliminate many of the disadvantages of their analog/hybrid counterparts. for example:

(1) Initial setup time is less.

(2) Once a digital program is developed that adequately simulates a certain phenomenon, we can retrieve the program and simulate the phenomenon under different conditions at a later time with less difficulty.

(3) Reproducibility of the results is much greater with the digital computer.

(4) The digital computer can handle very small numbers and very large numbers.

Problems arise in solving systems involing differential equations when numerical integration for digital simulation is used. All of the numerical integration methods that will be described require that a problem have known values of the dependent variables at some time, θ, that is usually set equal to zero. We then predict the values of the dependent variables that satisfy our differential equation at successive time intervals via one of several numerical techniques.

Most generalized numerical-integration subroutines are set up to solve equations of the following type (written for n first-order equations):

$$\frac{dy1}{d\theta} = f1\ (\theta, y1, y2, \ldots, yn)$$
$$\frac{dy2}{d\theta} = f2\ (\theta, y1, y2, \ldots, yn)$$
$$\vdots$$
$$\frac{dyn}{d\theta} = fn\ (\theta, y1, y2, \ldots, yn) \qquad (3.4)$$

(1) Euler method. We can calculate the point y at time $(\theta+h)$ by Taylor series for Equation (3.4) as:

$$y\ (\theta_0+h) = y\ (\theta_0) + h\frac{dy\ (\theta\ )}{d\theta} + \frac{h^2}{2}\frac{d^2y\ (\theta\ )}{d\theta^2} + \ldots \qquad (3.5)$$

where h is the step size.

In using this equation, the value of $y(\theta_0)$ is given by the initial condition and $y'(\theta_0)$ is evaluated from $f\ (\theta_0\ ,\ y_0\ )$, given by the differential equation, $dy/d\theta = f(\theta_0, y)$. It will of course be necessary to use this method iteratively, advancing the solution to $\theta = \theta_0 + 2h$ after $y\ (\theta_0 + h)$ has been found, then to $\theta = \theta_0 + 3h$, etc.

Adopting a subscript notation for the successive y-values and representing the error by the order relation, we may write the algorithm for the Euler method as:

$$yn+1 = yn + hy'n + O(h^2) \qquad (3.6)$$

(2) Fourth-order Runge-Kutta method. The most common used set of values in fourth-order Runge-Kutta method is summarized in Table 3.1.

(3) Runge-Kutta-Merson method. For integration purposes, procedures with automatic step-size control are recommended. The Runge-Kutta-Merson routine is summarized in Table 3.2. The error of integration can be (after one step) estimated from the relation for e.

Provided E is the maximum permissible error, the step size is halved, if E<e, and doubled, if e<E/32.

Table 3.1 Fourth-Order Runge-Kutta Routine

$$y_{n+1} = y_n + \frac{1}{6}(k_1 + 2k_2 + 2k_3 + k_4) + O(h^5)$$

$$k_1 = hf(\theta_n, y_n)$$

$$k_2 = hf(\theta_n + \tfrac{1}{2}h, y_n + \tfrac{1}{2}k_1)$$

$$k_3 = hf(\theta_n + \tfrac{1}{2}h, y_n + \tfrac{1}{2}k_2)$$

$$k_4 = hf(\theta_n + h, y_n + k_3)$$

Table 3.2 The Runge-Kutta-Merson Routine

$$y_{n+1} = y_n + \frac{1}{2}(k_1 + 4k_4 + k_5) + O(h^5)$$

$$k_1 = \frac{h}{3}f(\theta_n, y_n)$$

$$k_2 = \frac{h}{3}f(\theta_n + \frac{h}{3}, y_n + k_1)$$

$$k_3 = \frac{h}{3}f(\theta_n + \frac{h}{3}, y_n + \frac{k_1}{2} + \frac{k_2}{2})$$

$$k_4 = \frac{h}{3}f(\theta_n + \frac{h}{2}, y_n + \frac{3k_1}{8} + \frac{9k_3}{8})$$

$$k_5 = \frac{h}{3}f(\theta_n + h, y_n + \frac{3}{2}k_1 - \frac{9}{2}k_3 + 6k_4)$$

$$5e = k_1 - \frac{9}{2}k_3 + 4k_4 - \frac{k5}{2}$$

these equations

this chapter is shown in Figure

CHAPTER 4

DYNAMIC SIMULATION OF THE FUEL PROCESSING SUBSYSTEM

The fuel processing subsystem, discussed in Section 2.1 for design under steady state conditions, was analyzed dynamically for simulation of the transient response due to changing loads. This chapter describes the component and subsystem dynamic analyses.

The subsystem considered here is basically from the Westinghouse conceptual design (Figure 1-4). In the analysis, More attention was placed on the process components. Therefore, the auxiliary components were assumed to be at steady state conditions and were neglected in the simulation of the transient state response. Figure 4-1 shows this simplified subsystem.

A convenient method for analyzing the dynamic characteristics of dynamic in a component or system is to develop a computer program for the mathematical model and solve it. The objective here is to set up a system of simultaneous differential-difference equations, and use the numerical integration methods discussed in previous chapter to solve these equations. The general flowchart of the executive program used in this chapter is shown in Figure 4-2.

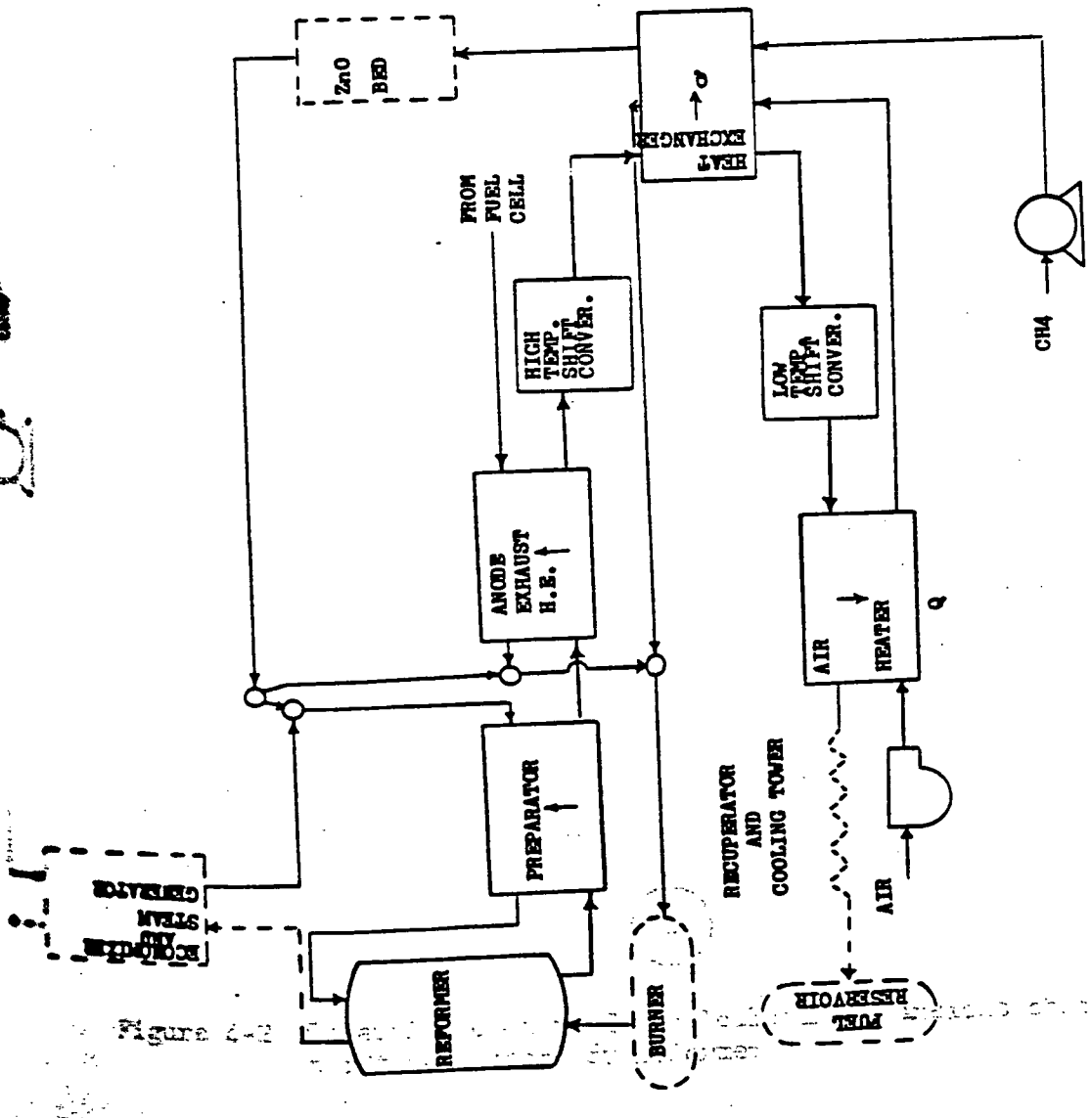

Figure 4-1 Fuel processing subsystem considered in transient study (components drawn with dashed lines were not considered)

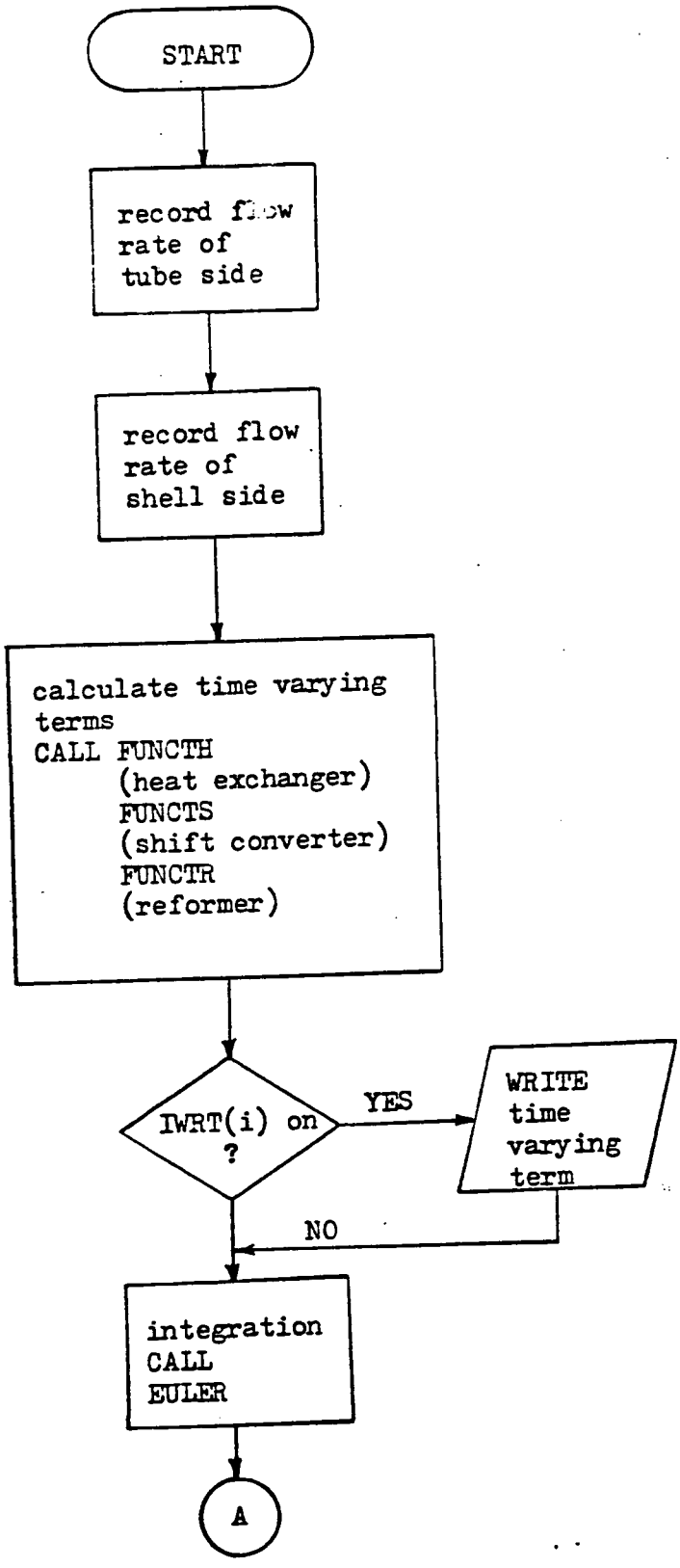

Figure 4-2 General flowchart for calculating transient change in heat exchanger, shift converter, or reformer

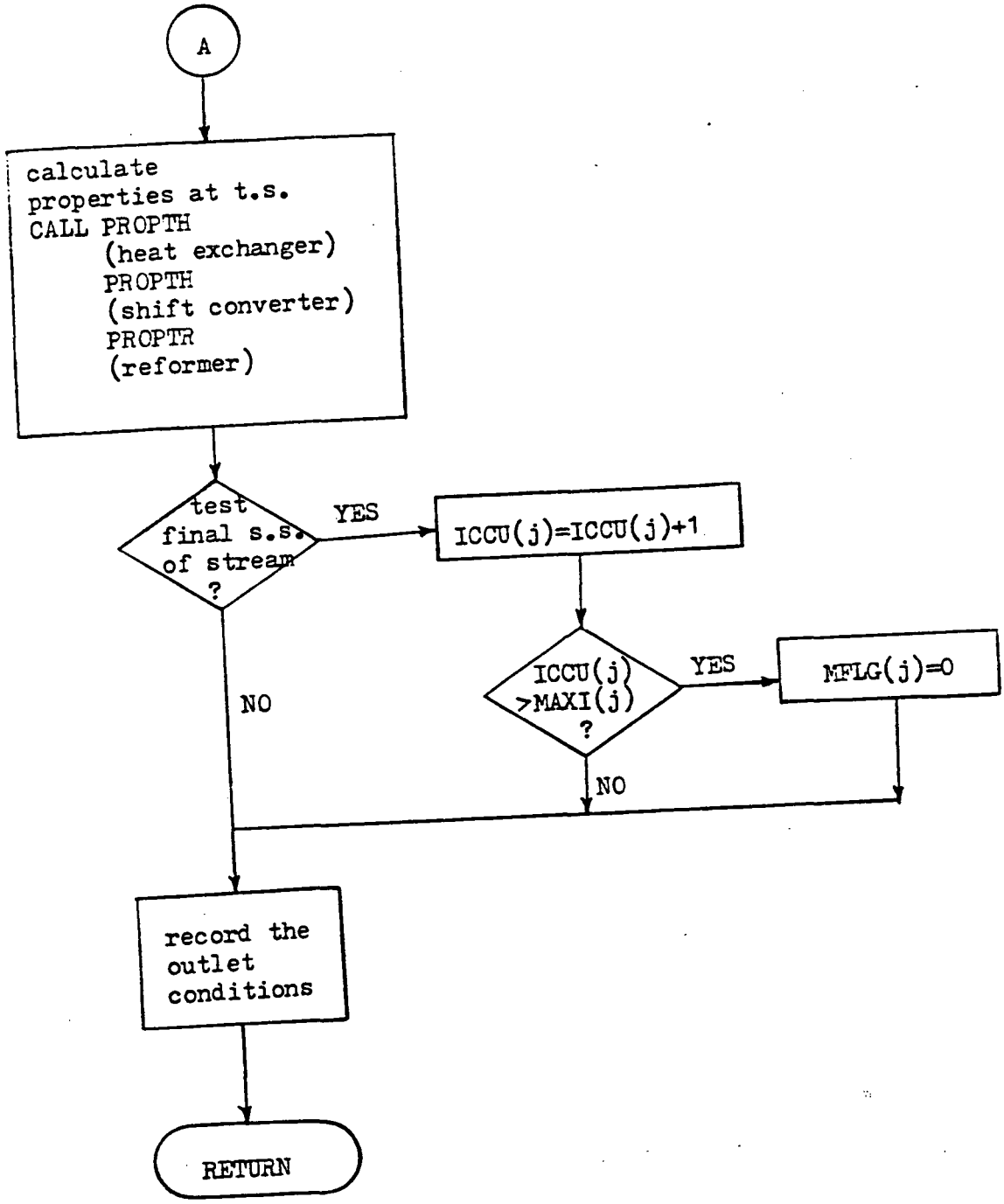

Figure 4-2 continued

4.1 Heat Exchangers

The heat exchangers in the PAFC system are simulated as counter current double-pipe heat exchangers as described in Chapter 2. The unsteady-state operation is considered with the dependent temperature variables as functions of the independent variables, time and distance. Since there is more than one independent variable, the relationship between temperature, time, and distance can be stated as a partial differential equation.

4.1.1 Mathematical Model

The heat balance equations on the tube-side and shell-side can be written as follows:

rate of heat accumulation = heat flow in - heat flow out + heat transfered

tube-side:

$$\lambda \rho_i (di)^2 \, Cp \, \partial t/\partial \theta = -\rho_i \, vi \lambda \, di^2 \, Cp \, \partial t/\partial Z + 4 \, hi \lambda \, di \, (Tw-t) \qquad (4\text{-}1\text{-}1)$$

shell-side:

$$\rho_o \, Ao \, Cpo \, \partial T/\partial \theta = -\rho_o \, Ao \, Cpo \, vo \, \partial T/\partial Z - ho \, do \, (T-Tw) \qquad (4\text{-}1\text{-}2)$$

where the variables are the same as those used in the distributed model (for steady state conditions).

The equation for the temperature of the tube-wall separating the shell and tube sections is

tube-wall:

$$\rho_w (do^2 - di^2) Cpw \, dTw/d\theta = ho \, do \, (T-Tw) - hi \, di \, (Tw-t) \qquad (4\text{-}1\text{-}3)$$

where the initial conditions are the steady state solutions

Boundary conditions

$$\frac{dt\ inlet}{d\theta} = 0$$

$$\frac{dT\ inlet}{d\theta} = 0 \qquad (4\text{-}1\text{-}4)$$

In Equations (4-1-1) and (4-1-2) the inside and the outside composite coefficients include the thermal resistance of the tube-wall. If we add half of this resistance to both the inside and the outside heat transfer coefficients, we can calculate the composite coefficients which are given by: (Ref. 21)

$$hi = \left[1/hi' + R + di\ (do-di)\ /\ kw\ (do+di)\right]^{-1} \qquad (4\text{-}1\text{-}5)$$

$$ho = \left[1/ho' + R + do\ (do-di)\ /\ kw\ (do+di)\right]^{-1} \qquad (4\text{-}1\text{-}6)$$

where hi' : inside tube heat transfer coefficient, J/m²-s-K

ho' : outside tube heat transfer coefficient, J/m²-s-K

R : fouling factor, m²-s-K/J

kw : thermal conductivity of tubewall, J/m-s-K

The fouling factor R was given the value 0.000176 m²-s-K/J.

Differential Difference Equations

Since the objective was to reduce the mathematical model to a set of simultaneous ordinary differential equations (i.e. only one independent variable, time), the equations were "finite differenced" to a set of differential-difference equations. The heat exchanger was divided into M sections with each section on the tube-side corresponding to a section on the shell side; a typical section j appears in Figure 2-2 . Fluid on the shell-side flows from section j+1 to section j,

while on the tube-side, it flows from section j to section j+1. The final set of differential-difference equations for the heat exchanger are

tube-side:

section 1:

$$\frac{dt_1}{d\theta} = 0$$

sections j=2 to j=M:

$$\frac{dt_j}{d\theta} = A_{j-1}\,(Tw_{j-1}-t_{j-1}) - vi_{j-1}\,(t_j-t_{j-1})/DZ$$

$$A_j = \frac{4 \cdot hi_j}{\rho i_j\, di\, Cp_j} \qquad (4\text{-}1\text{-}7)$$

tube-wall:

sections j=1 to j=M:

$$\frac{dTw_j}{d\theta} = B_j\,(T_j-Tw_j) - C_j\,(Tw_j-t_j)$$

$$B_j = \frac{4\, ho_j\, do}{\rho w Cpw(do^2-di2)}, \qquad C_j = \frac{4\, hi_j\, di}{\rho w Cpw(do^2-di^2)} \qquad (4\text{-}1\text{-}8)$$

shell-side:

sections j=1 to j=M-1:

$$\frac{dT_j}{d\theta} = -vo_j\,\left(\frac{T_{j+1}-T_j}{DZ}\right) - D_j\,(T_j-Tw_j)$$

$$D_j = \frac{4\, ho_j\, do}{\rho o_j Cpo_j(ds^2-do2)} \qquad (4\text{-}1\text{-}9)$$

where ds: shell inside diameter

section M:

$$\frac{dT_M}{d\theta} = 0$$

The resulting equations are then solved by one of the numerical-integration methods discussed in Chapter 3.

4.1.2 Example and Results

A computer program was written to simulate the dynamic characteristic of the heat exchanger. The program, which uses the Euler method with 0.018 sec. time intervals, was run on an IBM/370 to simulate the response of a step change (50°K) in the shell-side input temperature. Table 4-1 shows the input data and the results are given in Figure 4-3 and 4-4. The time scale in Figure 4-3 is 100 times of that in 4-4, which shows a more detailed change at the shell-side.

As expected, the rate of the steadily increasing temperature at tube-side was much slower than that at the tube-wall and shell-side. The final outlet temperature at the shell-side increased by 33°K and was 66% of the inlet step change. Finally, although this is a nonlinear system, the response of the shell-side is similar to a first-order response and the tube-side and tube-wall are similar to second-order response with a damping factor greater than 1.

Variable name	Dimension	Initial value	Unit	Definition
WSX	4	0.63	g-mole/s	Flow rate of H_2O in tubeside
	6	49.1	g-mole/s	Flow rate of N_2 in tubeside
	7	130.7	g-mole/s	Flow rate of O_2 in tubeside
PX		1.36	atm	Pressure of tubeside
TCO		300	K	Temperature of tubeside inlet
XE		1.83	m	Length of heat exchanger
D1		0.045	m	Inside diameter of tube
D2		0.0508	m	Outside diameter of tube
D3		0.0732	m	Inside diameter of shell
XT		55		Number of tubes
M		6		Number of finite-difference sections
RHW		8027.17	kg/m	Density of wall
CPW		0.502416	kJ/kg-K	Heat capacity of wall
THW		20.76882	J/m-s-K	Thermal conductivity of wall
WSC	1	1.49	g-mole/s	Flow rate of CH_4 in shellside
	2	1.37	g-mole/s	Flow rate of CO in shellside
	3	16.92	g-mole/s	Flow rate of CO_2 in shellside
	4	14.28	g-mole/s	Flow rate of H2O in shellside
	5	70.77	g-mole/s	Flow rate of H_2 in shellside
	6	0.96	g-mole/s	Flow rate of N_2 in shellside
PB		4.26	atm	Pressure of shellside
THZ		531	K	Temperature of shellside inlet

Table 4-1 Input data of dynamic simulation of heat exchanger

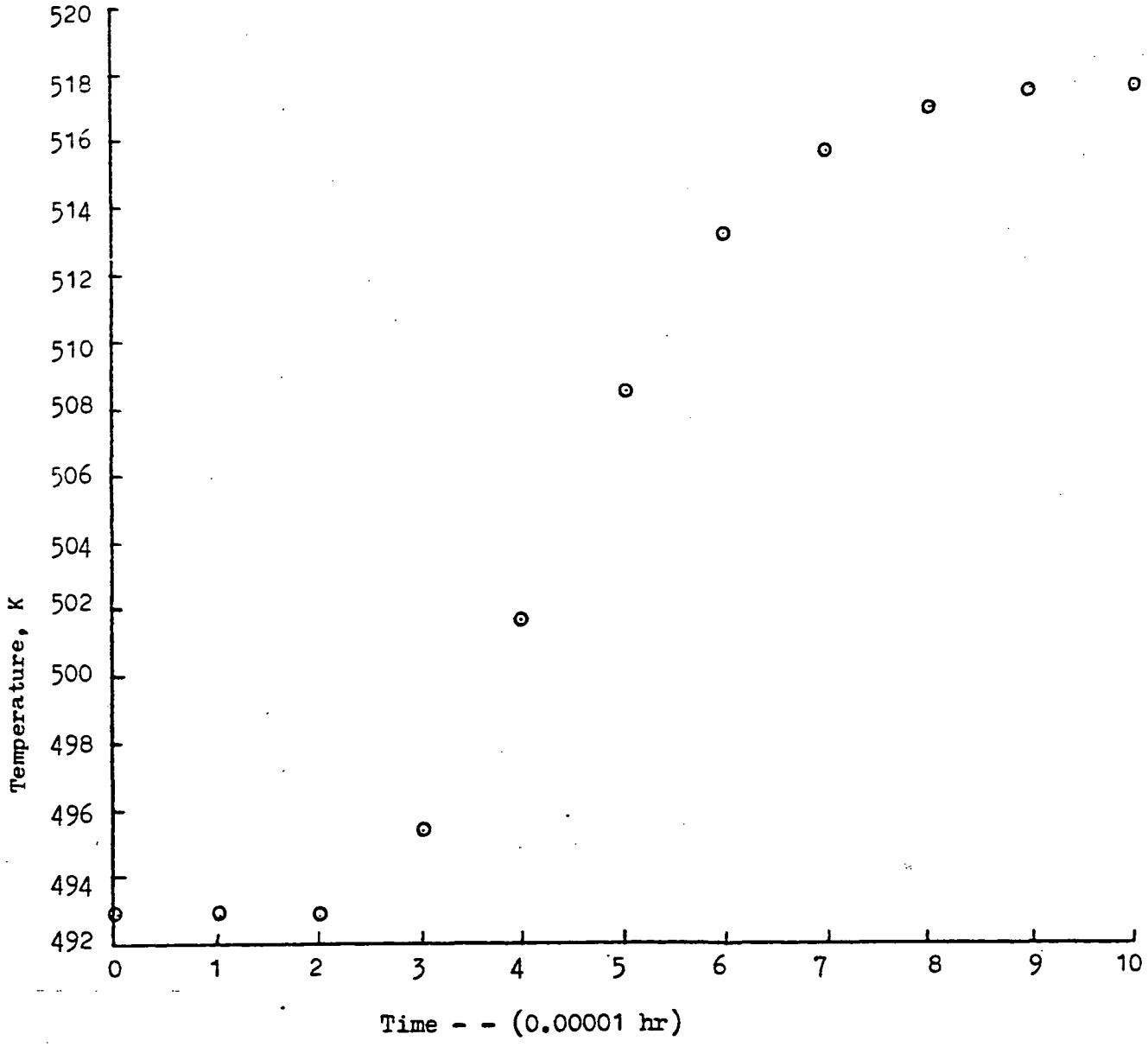

Figure 4-3 Shellside temperature change with time

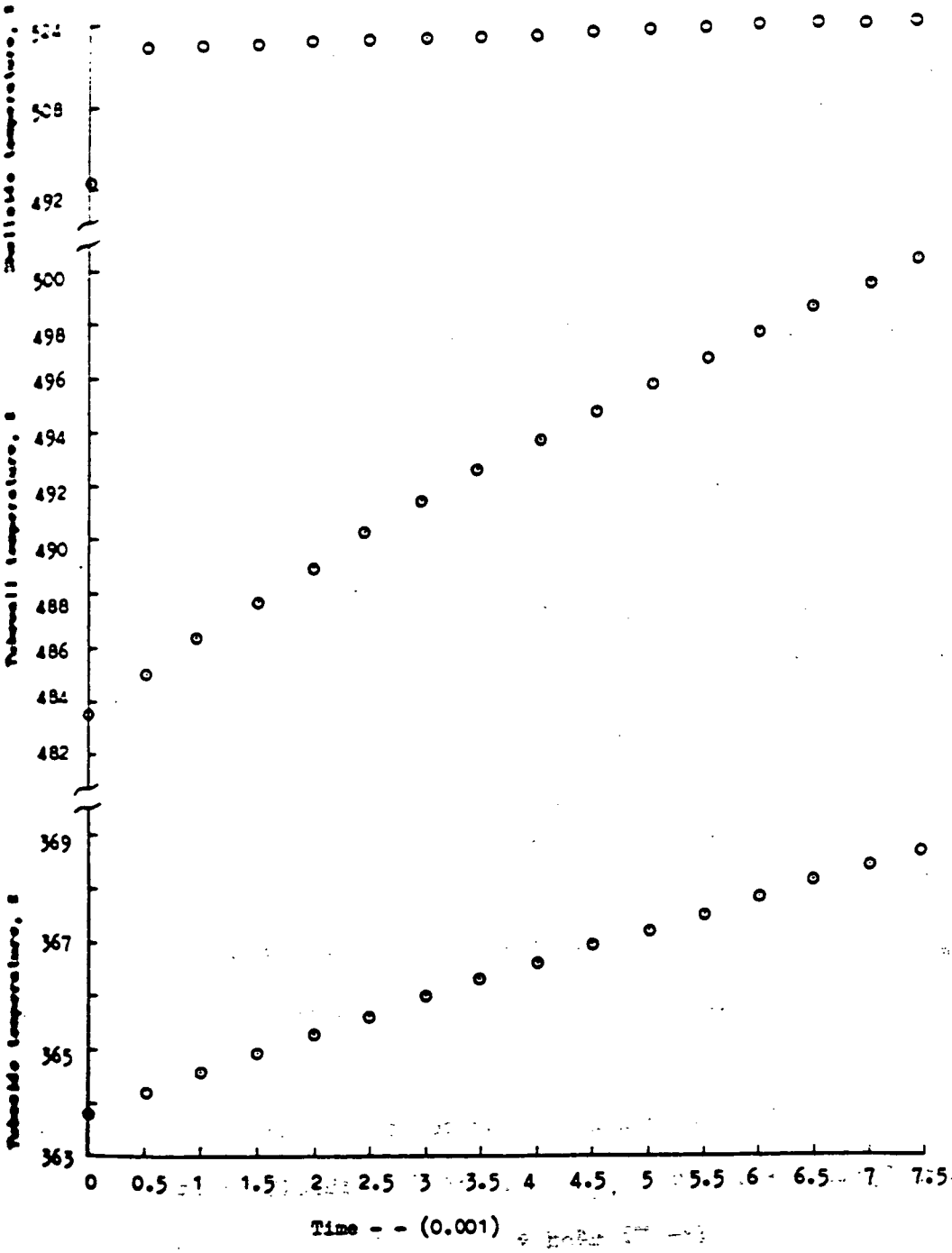

Figure 4-4 Temperatures change at transient state with shell side step change

4.2 Shift Converters

The shift converters discussed in Section 2.1.2 is remodeled here for dynamic analysis. The reactor, which was treated as a fix-bed reactor, has no provison for removing the heat of reaction, such as a jacket, so it operates with an adiabatic process. The heat generated by the reaction, therefore, heats up the gas as it flows through the reactor. The gas then exists at a higher temperature than the inlet feed temperature. All the assumptions described in Section 2.1.2 are also applicable here.

4.2.1 Mathematical Model

The dynamic modeling of the shift converters must take into account the energy balances of reacting gas and catalyst, and the material balances of reacting gas.

Similar to the distributed model at steady state, the mass balance is

$$\partial c/\partial\theta = -v\ \partial c/\partial Z - ra'\epsilon_B/\epsilon \qquad (4\text{-}2\text{-}1)$$

and the terms are the same as those in the steady state model.

The two energy balance equations are

reacting fluid: $Cp\ \rho\ \partial t/\partial\theta = -Cp\ \rho\ v\ \partial t/\partial Z + (-\Delta H_2)\ (ra'\ \epsilon_B/\epsilon) + hcAc\ (Tp-t)$ (4-2-2)

catalyst: $Cpc\ \epsilon_B\ \partial Tp/\partial\theta = hcAc\ (t-Tp)$ (4-2-3)

where hc: particle-fluid heat transfer coefficient, $J/m^2\text{-}s\text{-}K$

Ac: specific surface area of packing, m^2/m^2

Cpc: heat capacity of catalyst, J/kg-K

Tp: temperature of catalyst,K

The initial conditions are the distributed model's steady state solutions, where the catalyst temperature is assumed to be the same as the fluid temperature, and the boundary conditions are

$$\frac{dt\ inlet}{d\theta} = 0 \qquad (4\text{-}2\text{-}4)$$

$$\frac{dc\ inlet}{d\theta} = 0 \qquad (4\text{-}2\text{-}5)$$

The only parameter which has not been discussed is hc, the particle-fluid heat transfer coefficient. From Ref. 32 hc can be calculated by

$$\varepsilon\, jh = 0.395/Re^{0.36} \qquad 30 \leq Re \leq 10^5 \qquad (4\text{-}2\text{-}6)$$

$$\varepsilon\, jh = 0.725/Re^{0.36} \qquad 2 \leq Re \leq 30 \qquad (4\text{-}2\text{-}7)$$

where jh: Colburn analogy factor of heat transfer, and

$$jh = h\, Pr^{2/3} / v\, \rho\, Cp \qquad (4\text{-}2\text{-}8)$$

h: heat transfer coefficient, J/m²-s-K

v: velocity of fluid, m/s

ρ: molar density of fluid, g-mole/m³

Cp: molar heat capacity, J/g-mole-K

Pr: Prandtl number

Re: Reynold number

ε: void fraction

Differential-Difference Equations

The distance varying terms were changed to finite-difference form

(back-difference). The final set of differential-difference equations for the reacting fluid are:

Section 1:

$$\frac{dc_1}{d\theta} = 0 \qquad \frac{dt}{d\theta} = 0 \tag{4-2-9}$$

sections j=2 to j=M:

$$\frac{dcj}{d\theta} = -v_{j-1}\left(\frac{cj-cj-1}{DZ}\right) - ra'_{j-1}\,\epsilon_B/\epsilon \tag{4-2-10}$$

$$\frac{dtj}{d\theta} = -v_{j-1}\left(\frac{tj-tj-1}{DZ}\right) + \frac{(-\Delta Hj-1)ra'j-1\,\epsilon_B}{Cpj-1\,\rho j-1} + \frac{hcj}{Cpj\,\rho j\epsilon}Ac(Tpj-tj) \tag{4-2-11}$$

catalyst:

sections j=1 to j=M::

$$\frac{dTpj}{d\theta} = \frac{hcj\,Ac}{Cpc\,\epsilon_B}\,(tj - Tpj) \tag{4-2-12}$$

These simultaneous differential-difference equations, (4-2-9) through (4-2-12), were solved to obtain the temperature and concentrations of the reacting fluid under transient conditions.

4.2.2 Example and Results

The computer program, which utilizes the Euler method with a 0.00072 sec. time interval, was run on an IBM/370 computer to simulate the transient responses of the high temperature shift converter. Table 4-2 shows the example's input data and the results are shown in Figure 4-5.

Input data of dynamic simulation of high temperature shift converter.

Figure 4-5 shows that the outlet temperature did not change but the

Variable name	Dimension	Initial value	Unit	Definition
[illegible]	1	1.52	g-mole/s	Inlet flow rate of CH_4
	2	10.93	g-mole/s	Inlet flow rate of CO
	3	7.53	g-mole/s	Inlet flow rate of CO_2
	4	23.95	g-mole/s	Inlet flow rate of H_2O
	5	62.91	g-mole/s	Inlet flow rate of H_2
	6	1.05	g-mole/s	Inlet flow rate of N_2
[illegible]		1.5	atm	Inlet pressure
[illegible]		696.2	K	Inlet temperature
[illegible]		1.8288	m	Height of high temperature shift converter
[illegible]		0.09144	m	Diameter of high temperature shift converter
[illegible]		92		Number of tubes
[illegible]		6		Number of finite difference sections
[illegible]		964.57	m^2/m^3	Specific surface area of packing
[illegible]		0.879	kJ/kg-K	Heat capacity of catalyst
[illegible]		1281.5	kg catalyst/m^3 bed	Density of packing
[illegible]		0.469		Void fraction
[illegible]		0.00305	m	Diameter of catalyst

Table 4-2 Input data of dynamic simulation of high temperature shift converter

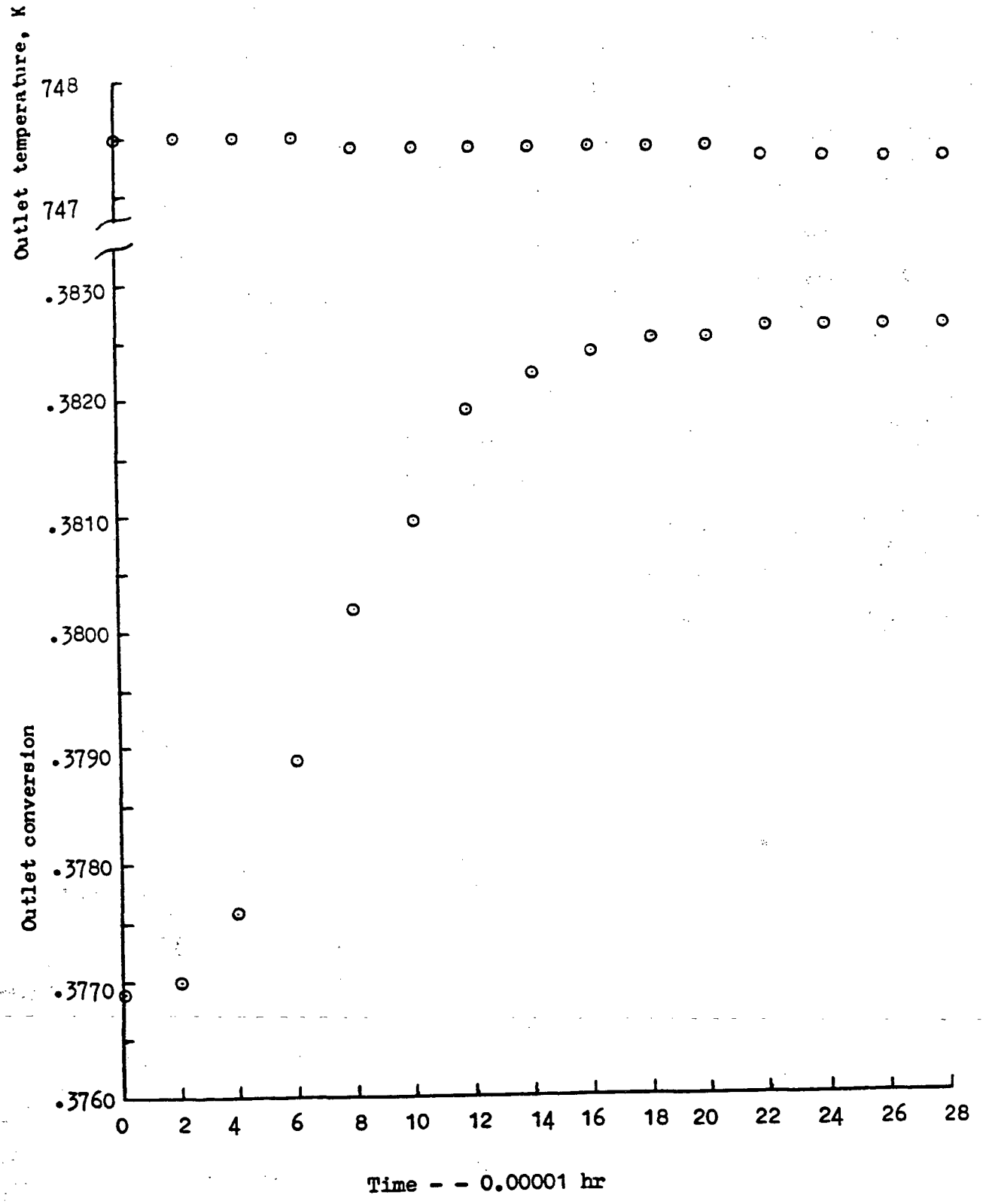

Figure 4-5 Outlet conditions of high temperature shift converter at transient state with step change

conversion rate is increased. The reason why this situation occurs can be observed from Equation 4-2-2, where the time varying temperature depends on three terms which are the material transport, the reaction, and the heat transfer terms. The reaction term is directly proportional to temperature (exothermic reaction) while the other two terms are inversely proportional. The temperature increase at the inlet is balanced inside the reactor. Actually, most of the increased heat energy is used to increase the temperature of the catalyst in this example.

Because the rate expression in shift converter is an expotential function of temperature, the accumulation term is very sensitive to the temperature and the stable time interval is small. The small time interval results in a larger trunction error and a longer running time for the computation. A method for improving this situation is discussed at the end of this chapter.

4.3 Reformer

The combustion gas heated steam reformer was discussed in Section 2.1.3 where it was modeled as a heat exchanging fixed-bed reactor. Equations were derived to determine the temperature and concentration gradient as a function of location in the reformer only. In order to eliminate time as an additional independent variable, steady-state operation was assumed. The more general case of unsteady-state operation is discussed here, with the the dependent temperature and concentration variables as functions of the independent variables, time and distance. The reformer is shown in Figure 2-6. Because there is more than one independent variable, the relationship between temperature, flow rate of the components, time, and distance can be stated as a partial differential equation. However, since the objective is to reduce the mathematical model to a set of simultaneous differential-difference equations (i.e., only one independent variable, time), the system will be "finite differenced" with respect to the location.

4.3.1 Mathematical Model

A detailed mathematical model for studying the dynamic response of the reformer was developed. All of the assumptions stated in Section 2.1.3 are applicable here.

Let [illegible] molar density [illegible]

Mass Balance

The material balance or design equation begins with the generalized continuity equation for a cylinder,

$$\frac{\partial}{\partial r}\left(rDr\frac{\partial c}{\partial r}\right) + r\frac{\partial}{\partial Z}\left(-uc + DL\frac{\partial c}{\partial Z}\right) - ra'\epsilon_B r = r\frac{\partial}{\partial \theta}C \qquad (4\text{-}3\text{-}1)$$

where c = methane molar concentration, g-mole/m³

u = superficial velocity, m/hr

Dr = radial diffusivity, m²/hr

D_L = axial diffusivity, m²/hr

ra' = methane reaction rate per unit mass of catalyst, g-mole/hr-kg catalyst, $ra' = -r_{CH4}$

ϵ_B = catalyst bed density, kg catalyst/m³reactor

r = radial dimension, m

Z = axial dimension (height), m

θ = time, hr.

If Dr and D_L are not sensitive to r or Z, then

$$Dr\frac{\partial}{\partial r}\left(r\frac{\partial c}{\partial r}\right) + r\frac{\partial}{\partial Z}(-uc) + rDL\frac{\partial^2 c}{\partial Z^2} - ra'\epsilon_B r = r\frac{\partial c}{\partial \theta} \qquad (4\text{-}3\text{-}2)$$

For a plug flow condition, dispersion is assumed to be negligible, thus, $D_L = Dr = 0$, and

$$\frac{\partial(-uc)}{\partial Z} - ra'\epsilon_B = \frac{\partial c}{\partial \theta} \qquad (4\text{-}3\text{-}3)$$

Let Ye be the mole-fraction of methane in the reactor and the molar density of bulk gas, then

$$C = \rho\ Ye$$

and

$$\frac{\partial(-uc)}{\partial Z} = \frac{-\partial(FYe)}{\partial Z}\frac{4}{\pi(di)^2} \qquad (4\text{-}3\text{-}4)$$

where F = molar flow rate inside the reactor, g-mole/hr

di = inside diameter, m

Equation (4-3-3) is replaced by

$$\frac{-\partial FYe}{\partial Z} - ra'\,e_B\frac{\pi(di)^2}{4} = \frac{\partial}{\partial\theta}(\rho\,Ye)\frac{\pi(di)^2}{4} \qquad (4\text{-}3\text{-}5)$$

The conversion, x1, can be replaced by the mole-fraction of methane:

$$Ye = \frac{F_1(1-x_1)}{Fo+2x_1F_1} \quad ; \quad x_1 = \frac{F_1-Fo\ Ye}{F_1+2F_1\ Ye} \qquad (4\text{-}3\text{-}6)$$

where Fo = initial total molar flow rate inside reactor, g-mole/hr

F_1 = initial methane flow rate inside reactor, g-mole/hr

The equations for the molar flow rate and density as a function of conversion are given by:

$$F = Fo + 2x_1\ F_1 \qquad (4\text{-}3\text{-}7)$$

$$\rho = \frac{P}{Rt}\left(\frac{F}{Fo}\right) \qquad (4\text{-}3\text{-}8)$$

where P = pressure, atm

R = gas constant

t = tube-side temperature, K

Energy Balance

Four energy balances are required for the reformer: one for the reformer gases (tube-side), one for the tube-wall, one for the combustion gases (shell-side), and one for the catalyst. The reformer gas balance includes its own sensible heat change, reaction enthalpies, heat transfer from the hotter tube-wall, heat transfer to the catalyst particles, and the accumulation term, which are as follows:

$$-\frac{\partial FCpt}{\partial Z} + \Sigma F(-\Delta H)\frac{\partial x}{\partial Z} + hi\,\pi\,di(Tw-t) + hcAc\frac{\pi di^2}{4}(Tp-t)$$

$$= \frac{\pi(di)^2}{4} Cp \frac{\partial(\rho t)}{\partial \theta} \qquad (4\text{-}3\text{-}9)$$

where Cp = heat capacity on the tube-side, J/g-mole-K

t = tube-side temperature, K

Ac = external surface area of particle per volume of catalyst bed, m^2/m^3

Tw = tube-wall temperature, K

Tp = catalyst temperature, K

hi = inside heat-transfer coefficient, J/hr-m-K

hc = particle-fluid heat transfer coefficient, J/hr-m-K

ΔH = heat of reaction, J/g-mole

In the heat of reaction term, the component molar flow rate, F, is for that component corresponding to the conversion x. Therefore, for the reactions at hand

$$\Sigma F(-\Delta H)\frac{\partial x}{\partial Z} = F_1(-\Delta H_1)\frac{\partial x_1}{\partial Z} + (F_3+x_1F_1)(-\Delta H_2)\frac{\partial x_2}{\partial Z} \qquad (4\text{-}3\text{-}10)$$

where ΔH_1 = the demethanation reaction enthalpy, J/g-mole CH_4

ΔH_2 = the water shift enthalpy, J/g-mole CO

The enthalpies, ΔH , are evaluated at the average reformer temperature. Negative values indicate an exothermic reaction.

Shell-side and tube-wall equations for the energy balance are as follows:

$$\rho_o \, Ao \, Cpo \, \frac{\partial T}{\partial \theta} = -\rho_o \, vo \, Ao \, Cpo \, \frac{\partial T}{\partial Z} - ho \lambda do(T-Tw) \qquad (4-3-11)$$

$$\rho_w(do^2-di^2) \, Cpw \, \frac{\partial Tw}{\partial \theta} = 4 \, ho \, do(T-Tw) - 4 \, hi \, di(Tw-t) \qquad (4-3-12)$$

where ρo = Fluid density at shell-side, g-mole/m^3

Ao = shell-side flow area, m^2

Cpo = heat capacity on shell-side, J/g-mole-K

T = temperature of shell-side, K

Vo = shell-side velocity, m/hr

ho = outside heat-transfer coefficient, J/hr-m^2-K

Tw = tube-wall temperature, K

do = outside diameter, m

ρw = density of tube-wall, kg/m^3

Cpw = heat capacity of tube-wall, J/kg-K

The energy balance equation for the catalyst is

$$Cpc \, \epsilon_B \, \frac{\partial Tp}{\partial \theta} = hc \, Ac(t-Tp) \qquad (4-3-13)$$

where Cpc = heat capacity of caralyst; J/kg-K

The initial conditions for these equations were taken as the steady state solutions and the boundary conditions were the new inlet variables.

Solving the Mathematical Models

Expanding Eq. (4-3-5) and Eq. (4-3-9) to obtain:

$$\frac{\pi di^2}{4}\left(\rho\frac{\partial Ye}{\partial \theta}+Ye\frac{\partial \rho}{\partial \theta}\right)=-\frac{\partial FYe}{\partial Z}-ra'e_B\frac{\pi di^2}{4} \qquad (4\text{-}3\text{-}14)$$

$$\frac{\pi di^2}{4}Cp\left(\rho\frac{\partial t}{\partial \theta}+t\frac{\partial \rho}{\partial \theta}\right)=-\frac{\partial FCpt}{\partial Z}+\sum F(-\Delta H)\frac{\partial x}{\partial Z}+hi\pi di(Tw-t)$$

$$+hc\,Ac\frac{\pi di^2}{4}(Tp-t) \qquad (4\text{-}3\text{-}15)$$

Expanding $\partial\rho/\partial\theta$ by using Eq. (4-3-6) and (4-3-8) and the following identity:

$$\frac{\partial \rho}{\partial \theta}=\left(\frac{\partial \rho}{\partial x_1}\right)\left(\frac{\partial x_1}{\partial Ye}\right)\left(\frac{\partial Ye}{\partial \theta}\right)$$

making the necessary substitutions into this identity, we will obtain:

$$\frac{\partial \rho}{\partial x_1}=\frac{2P\,F_1}{RtFo} \qquad (4\text{-}3\text{-}16)$$

$$\frac{\partial x_1}{\partial Ye}=\frac{-(F_1+2F_1\,Ye)\,Fo-(F_1-Ye\,Fo)\cdot 2\cdot F_1}{(F_1+2F_1\,Ye)^2} \qquad (4\text{-}3\text{-}17)$$

$$\frac{\partial \rho}{\partial \theta}=\frac{2\,P\,F_1}{R\,t\,Fo}\left(\frac{-(F_1+2F_1\,Ye)\cdot Fo-(F_1-Ye\,Fo)\cdot 2\cdot F_1}{(F_1+2F_1\,Ye)^2}\right)\frac{\partial Ye}{\partial \theta} \qquad (4\text{-}3\text{-}18)$$

In order to find solutions for the variables in the example for a tubular reactor, numerical data for all the variables at time θ is needed. In using the finite difference technique, the reactor is considered to have M sections (see Figure 2-7) and values for the variables at $(\theta + \Delta\theta)$ are obtained. The final set of differential-difference equations are as follows:

tube-side:

sections j=1 to j=M, define

$$Aj = \frac{2\ Pj\ F_1}{R\ tj\ Fo}\left(\frac{-(F_1+2F_1\ Yej)\cdot Fo - (F_1-Yej\ Fo)\cdot 2\cdot F_1}{(F_1+2F_1\ Yej)^2}\right)$$

$$Cj = D\ (\rho_j + Yej\ Aj)$$

$$\rho j = \frac{Pj}{Rtj}\left(\frac{Fo+2x_{1j}\ F_1}{Fo}\right)$$

$$Fj = Fo + F_1\ 2\ x_{1j}$$

$$Gj = D\ Cpj\ \rho j$$

$$D = \frac{\pi di^2 \epsilon}{4} \qquad (4\text{-}3\text{-}19)$$

section 1:

$$\frac{dt_1}{d\theta} = 0, \qquad \frac{d\ Ye1}{d\ \theta} = 0, \qquad \frac{d\ \rho_1}{d\ \theta} = 0 \qquad (4\text{-}3\text{-}20)$$

sections j=2 to j=M::

$$\frac{d\ Yej}{d\ \theta} = \frac{-(Fj\ Yej - F_{j-1}\ Y_{ej-1})}{DZ\ Cj} - \frac{ra'_{j-1}\ e_B\ D}{Cj\ \epsilon} \qquad (4\text{-}3\text{-}21)$$

$$\frac{d\rho_j}{d\ \theta} = Aj\left(\frac{d\ Yej}{d\ \theta}\right) \qquad (4\text{-}3\text{-}22)$$

define

$$Ej = tj \left(\frac{\partial \rho_j}{\partial \theta}\right) D\ Cpj \qquad (4\text{-}3\text{-}23)$$

$$\frac{dtj}{d\theta} = \frac{1}{Gj}\left[-\left(\frac{Cpj\ Fj\ tj - Cpj-1\ Fj-1\ tj-1}{DZ}\right) + (F_1\ (-\Delta H_{1j-1})\ \frac{x_{1j} - x_{1j-1}}{DZ} + (F_3 + x_{1j-1}\ F_1)(-\Delta H_{2j-1})\ \frac{x_{2j}-x_{2j-1}}{DZ}) + hcj\ Ac\ \frac{D}{\epsilon}(Tpj-tj) + \dot{m}ij-1(\pi\, di)\ (Twj-1-tj-1) - Ej\right] \qquad (4\text{-}3\text{-}24)$$

shell-side:

sections j=1 to j=M-1:

$$\frac{dTj}{d\theta} = \frac{-voj\ (T_{i+1} - Tj)}{DZ} - Hj\ (Tj - Twj)$$

where

$$Hj = \frac{\pi\ hoj\ do}{\rho oj\ Ao\ Cpoj} \qquad (4\text{-}3\text{-}25)$$

section M:

$$\frac{dTw}{d\theta} = 0 \qquad (4\text{-}3\text{-}26)$$

tube-wall:

sections j=1 to j=M:

$$\frac{dTwj}{d\theta} = Oj\ (Tj - Twj) - Qj\ (Twj - tj)$$

$$Oj = \frac{4\ hoj\ do}{\rho w\ Cpw\ (do^2-di^2)}$$

$$Qj = \frac{4\ hij\ di}{\rho w\ Cpw\ (do^2-di^2)} \qquad (4\text{-}3\text{-}27)$$

catalyst:

sections j=1 to j=M:

$$\frac{dTpj}{d\theta} = \frac{hcj\ Ac}{Cpc\ e_3}\ (t_j - Tpj) \qquad (4\text{-}3\text{-}28)$$

4.3.2 Example and Results

The corresponding computer program, which use the Euler method with a 0.0036 sec. time interval, was run on IBM/370 computer to simulate the dynamic response of the reformer. The initial disturbance was a 100 °K step increase in the inlet combustion gas temperature. Tables 4-3 and 4-4 present the input data and the output of the transient response, respectively.

Note that the outlet temperature on the combustion gas side increased by 16 °K while inlet temperature increase was 100 °K , and the outlet temperature of the reforming gas did not change much. Actually, the reforming gas outlet temperature would gradually increase with time. The increased energy is partly going into heating the wall (then reforming gas and catalyst) and partly simply "wasted" with stream flow. Here the competition between heat transfer and flow rate can been seen. A more complex condition in the reforming gas, occurs when the reaction rate is the third competitor (for an endothermal reaction) and more than one direction for heat transfer is allowed.

Again, the small value for the time interval is a problem, which required much computation time. In the following chapter, methods for improving this condition are discussed.

Variable name	Dimension	Initial value	Unit	Definition
FMSN	1	0.0375	g-mole/s	Input CH_4 flow rate
SMRA		3		Steam to carbon ratio
PX		1.5	atm	Inlet CH_4 pressure
TCO		811.1	K	Inlet CH_4 temperature
ZH		1.524	m	Height of reformer
D1		0.105	m	Outside diameter of regenerative tube
D2		0.1315	m	Inside diameter of reforming tube
D3		0.1414	m	Outside diameter of reforming tube
KO		10400		Rate constant of demethanation reaction
EA		83736	J/mole	Activity energy of demethanation reaction
RHOB		1281.48	kg/m3	Density of packing in reformer
EPS		0.469		Void fraction in reformer
S		0.229	m	Width of combustion gas square duct
DP		0.005	m	Diameter of catalyst
N		23		Number of finite difference sections
RHW		8027.17	kg/m3	Density of wall
CPW		0.6113	kJ/kg-K	Heat capacity of wall
SAREA		669.29	m^2/m^3	Specific surface area of catalyst
CPC		1.026	kJ/kg-K	Heat capacity of catalyst
DNSG	3	0.042	g-mole/s	Inlet CO2 flow rate in combustion gas
	4	0.036	g-mole/s	Inlet H_2O flow rate in combustion gas
	6	0.109	g-mole/s	Inlet N_2 flow rate in combustion gas
PB		1.5	atm	Inlet combustion gas pressure
THZ		1811.1	K	Inlet combustion gas temperature

Table 4-3 Input data for dynamic simulation of reformer

Time—hr.	Outlet temperature of reforming gas K	Outlet temperature of combustion gas, K	Last section wall temperature K	Last section catalyst temperature K
0.00000	0.95195D 03	0.10348D 04	0.99917D 03	0.95195D 03
0.50000D-04	0.95195D 03	0.10348D 04	0.99919D 03	0.95195D 03
0.10000D-03	0.95195D 03	0.10348D 04	0.99922D 03	0.95195D 03
0.15000D-03	0.95195D 03	0.10348D 04	0.99924D 03	0.95195D 03
0.20000D-03	0.95195D 03	0.10348D 04	0.99926D 03	0.95195D 03
0.25000D-03	0.95196D 03	0.10348D 04	0.99928D 03	0.95195D 03
0.30000D-03	0.95196D 03	0.10348D 04	0.99930D 03	0.95195D 03
0.35000D-03	0.95196D 03	0.10348D 04	0.99932D 03	0.95195D 03
0.40000D-03	0.95196D 03	0.10348D 04	0.99934D 03	0.95195D 03
0.45000D-03	0.95197D 03	0.10348D 04	0.99937D 03	0.95195D 03
0.50000D-03	0.95197D 03	0.10348D 04	0.99939D 03	0.95195D 03
0.55000D-03	0.95197D 03	0.10348D 04	0.99941D 03	0.95195D 03
0.60000D-03	0.95197D 03	0.10349D 04	0.99943D 03	0.95195D 03
0.65000D-03	0.95198D 03	0.10350D 04	0.99945D 03	0.95195D 03
0.70000D-03	0.95198D 03	0.10353D 04	0.99947D 03	0.95195D 03
0.75000D-03	0.95198D 03	0.10358D 04	0.99949D 03	0.95195D 03
0.80000D-03	0.95199D 03	0.10366D 04	0.99951D 03	0.95195D 03
0.85000D-03	0.95199D 03	0.10375D 04	0.99953D 03	0.95196D 03
0.90000D-03	0.95199D 03	0.10388D 04	0.99956D 03	0.95196D 03
0.95000D-03	0.95200D 03	0.10402D 04	0.99958D 03	0.95196D 03
0.10000D-02	0.95200D 03	0.10417D 04	0.99960D 03	0.95196D 03
0.10500D-02	0.95200D 03	0.10433D 04	0.99962D 03	0.95196D 03
0.11000D-02	0.95201D 03	0.10448D 04	0.99964D 03	0.95196D 03
0.11500D-02	0.95201D 03	0.10462D 04	0.99966D 03	0.95196D 03
0.12000D-02	0.95201D 03	0.10474D 04	0.99968D 03	0.95197D 03
0.12500D-02	0.95202D 03	0.10485D 04	0.99970D 03	0.95197D 03
0.13000D-02	0.95202D 03	0.10494D 04	0.99972D 03	0.95197D 03
0.13500D-02	0.95203D 03	0.10501D 04	0.99974D 03	0.95197D 03
0.14000D-02	0.95203D 03	0.10506D 04	0.99976D 03	0.95197D 03
0.14500D-02	0.95203D 03	0.10510D 04	0.99978D 03	0.95198D 03
0.15000D-02	0.95204D 03	0.10513D 04	0.99980D 03	0.95198D 03
0.15500D-02	0.95204D 03	0.10516D 04	0.99982D 03	0.95198D 03
0.16000D-02	0.95204D 03	0.10517D 04	0.99984D 03	0.95198D 03
0.16500D-02	0.95205D 03	0.10518D 04	0.99986D 03	0.95198D 03
0.17000D-02	0.95205D 03	0.10519D 04	0.99988D 03	0.95199D 03
0.17500D-02	0.95206D 03	0.10519D 04	0.99990D 03	0.95199D 03
0.18000D-02	0.95206D 03	0.10520D 04	0.99992D 03	0.95199D 03
0.18500D-02	0.95207D 03	0.10520D 04	0.99994D 03	0.95199D 03
0.19000D-02	0.95207D 03	0.10520D 04	0.99996D 03	0.95200D 03
0.19500D-02	0.95207D 03	0.10520D 04	0.99998D 03	0.95200D 03
0.20000D-02	0.95208D 03	0.10520D 04	0.10000D 04	0.95200D 03

Table 4-4 Output of the dynamic simulation of the reformer

4.4 Discussion

The objective of this chapter was to examine and develop a computer simulation for the dynamic characteristics of components in the fuel process subsystem. The main program and subroutines for each component will be modified to be a group of subroutines in the final simulation of whole system, and some of the duplicated subroutines will be omitted.

The examples illustrated in this chapter were not concerned with the flow rates which were assumed to be constant. However this does affect the transient responses due to transpotation lag in the pipe. This factor is considered in the next chapter.

The selection of an appropriate time interval in solving difference equations is a problem in digital simulation. Large values for time intervals will "blow-out" the computation. As the calculated value approaches infinity. However, smaller time interval values require more computation time to iterate, and increasing truncation error occurs in the computation. One possible solution to this problem may be the Runge-Kutta-Merson integration method (Section 3-4), which automatically selects the proper time interval. However, this method does not work well with a reaction term that is expontential with temperature change. An alternate method, which is discussed in the following paragraph, places the attention on the mathematical model.

For the heat exchanger, it can be observed from Equation 4-1-8 that the DZ/v term (the time needed to travel on section) determines the time

interval (H). The change in temperature of the previous section will be greater if H>DZ/v. Therefore, DZ/v is the maximum H value, especially when the transport rate is larger than heat transfer rate, which is usually the case. It is not the same condition in the catalytic reactor, where the maximum H is determined by the reaction rate which is much faster than the other two. If we add one more assumption to the simulation, such that no temperature difference exists between the reacting gas and the catalyst, then Cp in the accumulation term (see Equation 4-3-9) is the composite heat capacity of gas and catalyst, which is much larger than that of the gas only. Subsequently, this assumption will decrease the amplification, and thus increase the stable time interval. In the example for transient simulation of the reformer, this additional assumption increases the time interval from 0.0036 sec. to 0.05 sec. The simulation of the whole system discussed in Chapter 6, includes this assumption.

CHAPTER 5

DYNAMIC MODELING OF THE FUEL CELL STACK SUBSYSTEM

As stated in Chapter 2, within the fuel cell stack, hydrogen and oxygen react to continuously produce DC electricity, waste heat, and steam.

Generally, the operation of the PAFC system during a load change is to control the voltage level to obtain the required power level. A change in the voltage level will affect the current density on the cell plates. The relationship between the current density, voltage, and power is obtained from Ohm's law and the current-voltage characteristics stated in Chapter 2. One typical result is shown in Figure 2-27 for fixed operating conditions.

When the current density is changed, the inlet flow rates should also be changed to meet the requirements. Therefore, the variables that can be manipulated for control of the fuel cell stack subsystem are the input flow rates of fuel (hydrogen) and oxident (oxygen or air).

In addition to the assumptions made for calculating the steady state conditions in the stack, there are several other assumptions made for system simulation during the load change period:

1. The temperature and composition of both of the reservoirs (fuel and

air) outlets (see Figure 5-1) do not change. However, the flow rates are changed in proportion to the DC change. Also, the inlet temperature of the process air does not change.

2. The pressure in both reservoirs is slightly above the maximum (full load) operating pressure.

3. When changing the fuel cell operating temperature and pressure, a line of constant phosphoric acid concentration is to be followed. Figure 5-2 shows the total pressure of phosphoric acid solutions as a function of temperature. This criteria produces a significant increase in the estimated cell life at 25% of the rated power (Ref.27).

4. The utilization ratios of both fuel and process air are the same. In addition, the stoichiometric factor for the cooling air is hold constant.

5. Because the reaction rate (including the reacting gas diffusion and ion migration) is faster than the heat transfer rate and the component flow rate, the accumulation of components resulting from the reaction is neglected.

Page Intentionally Left Blank

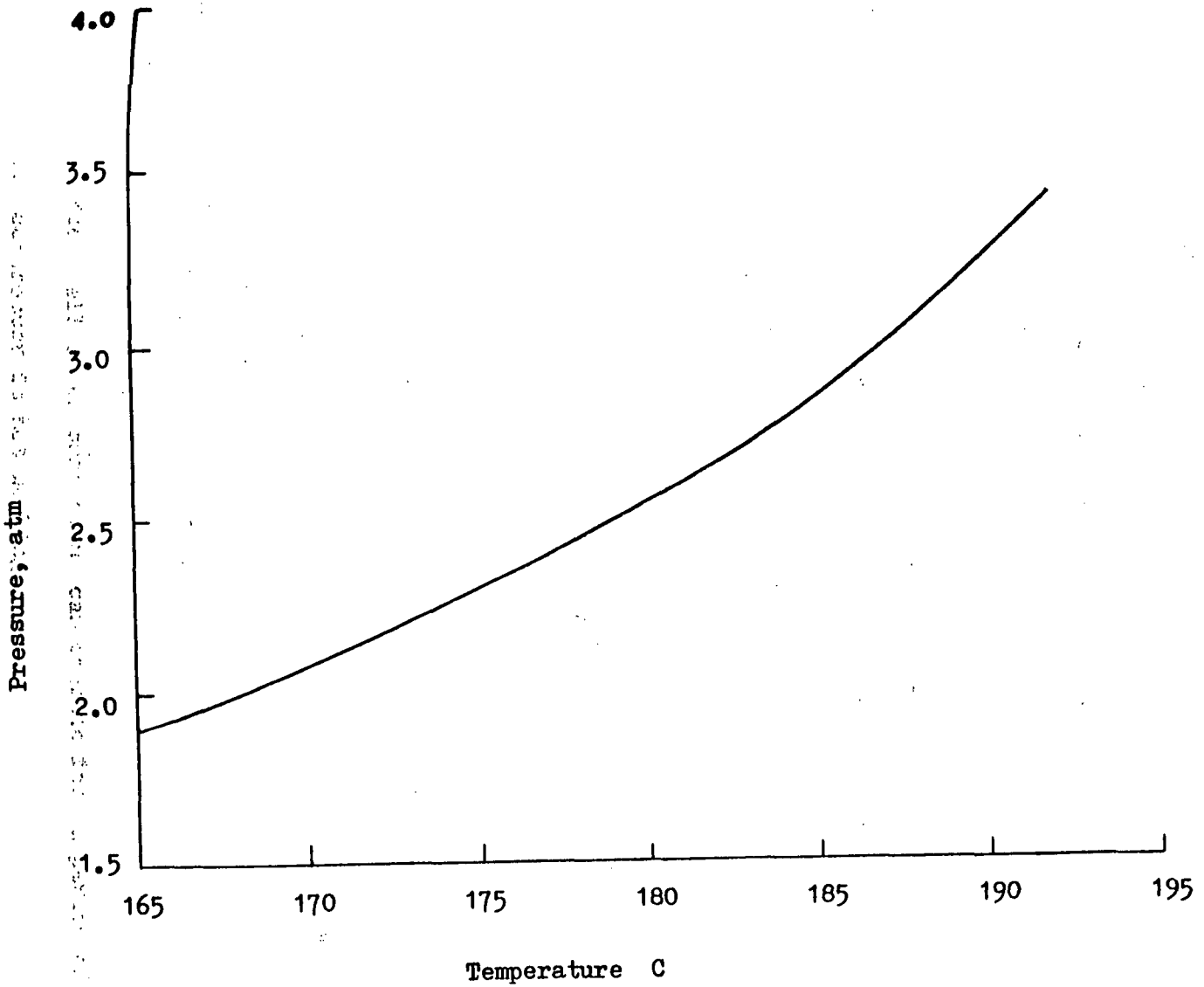

Figure 5-2 Equilibrium H_3PO_4 concentration - 94 wt. %

5.1 Design of The Subsystem for Load Change

A preliminary process flow diagram, for control of the load change, is shown in Figure 5-1 . The basic control steps for a load change in this subsystem are as follows:

1. The flow control valves (FCV-1 and FCV-2) regulate the flow of fuel and process air in direct proportion to the DC current.
2. The cooling air flow control valve (FCV-3) regulates the cooling air flow rate in proportion to the flow rate of the process air.
3. The governor control valve (RPM) regulates the speed of the air compressor (air flow rate is proportional to the speed). At steady state conditions the inlet air flow rate is the same as the process air flow rate required in the stack; however, the air flow rate depends on the pressure level of the reservoir in transient conditions.
4. The pressure levels of the fuel and process air are regulated by the pressure control valves (PCV-1 and PCV-2 respectively), while the cooling air pressure level is the same as that of the air reservoir and is complemented by the circulator through speed or pitch control.

The advantages of placing the two reservoirs before the fuel cell stack are as follows:

1. The flow rates can be rapidly changed because the independence of fuel processing subsystem.
2. The fuel cell stack subsystem can operate for a period of time when the air compressor is not working.

5.2 Mathematical Model

The mathematical model for evaluating the transient temperature distribution in the stack is similar to the model used to simulate the steady state temperature distribution. Additional accumulation terms are used in the transient model to represent the unsteady state situation. According to assumption (5), there is no accumulation of components caused by the reaction. The model for the current density distribution, which interprets the mass balance and was discussed in Section 2.2.2, is applicable for calculation under transient conditions, however, the inlet flow rates and the temperature at each grid section are functions of time.

Considering one strip of the PAFC stack (see Figure 2-17), we can write the energy balance for the plates in the form of differential-difference equations.

(1) Engergy balance in the stack

(a) cooling plate

section 1:

$$\frac{t'Ky}{\Delta y^2}T(1,2) - \left(\frac{t'Ky}{\Delta y^2} + \frac{2Kx}{\Delta x_1}\right)T(1,1) + \frac{2Kx}{\Delta x_1}T(2,1) - \frac{mc(1)Cc(1)}{Pc}\frac{(Tc(1)-Tco)}{\Delta y} = \rho c\ cc\ t'\frac{dT(1,1)}{d\theta} \qquad (5\text{-}2\text{-}1)$$

sections 2 to M-1:

$$-\frac{t'Ky}{\Delta y^2}T(1,j+1) - \left(\frac{2t'Ky}{\Delta y^2} + \frac{2Kx}{\Delta x_1}\right)T(1,j) + \frac{t'Ky}{\Delta y^2}T(1,j-1) + \frac{2Kx}{\Delta x_1}T(2,j) - \frac{mc(j)Cc(j)}{Pc\ \Delta y}(Tc(j)-Tc(j-1)) = \rho c\ cc\ t'\frac{dT(1,j)}{d\theta} \qquad (5\text{-}2\text{-}2)$$

section M:

$$\frac{t'Ky}{\Delta y^2} T(1,M-1) - \left(\frac{t'Ky}{\Delta y^2} + \frac{2Kx}{\Delta x_1}\right) T(1,M) + \frac{2Kx}{\Delta x_1} T(2,M)$$

$$- \frac{mc(M)Cc(M)}{Pc\,\Delta y} (Tc(M)-Tc(M-1)) = \rho c\ cc\ t' \frac{dT(1,M)}{d\theta} \qquad (5\text{-}2\text{-}3)$$

(b) cell plate No. 1

section 1:

$$\frac{Kyt}{\Delta y^2} T(2,2) - \left(\frac{Kyt}{\Delta y^2} + \frac{Kx}{\Delta x_1} + \frac{Kx}{\Delta x_2}\right) T(2,1) + \frac{Kx}{\Delta x_1} T(1,1)$$

$$+ \frac{Kx}{\Delta x_2} T(3,1) - \frac{mp(1,1)Cp(1,1)}{Pp\ \ -y} (Tp(1,1)-Tpo) + \left[V^*(1)-V(1)\right] I(1,1)$$

$$= \rho p\ cp\ t \frac{dT(2,1)}{d\theta} \qquad (5\text{-}2\text{-}4)$$

sections 2 to M-1:

$$\frac{Kyt}{\Delta y^2} T(2,j+1) - \left(\frac{2Kyt}{\Delta y^2} + \frac{Kx}{\Delta x_1} + \frac{Kx}{\Delta x_2}\right) T(2,j) + \frac{Kyt}{\Delta y^2} T(2,j-1) + \frac{Kx}{\Delta x_1} T(1,j)$$

$$+ \frac{Kx}{\Delta x_2} T(3,j) - \frac{mp(1,j)Cp(1,j)}{Pp\ \Delta y} (Tp(1,j)-Tp(1,j-1)) + \left[(V^*(1)-V(1))\right] I(1,j)$$

$$= \rho_p cp\ t \frac{dT(3,M)}{d\theta} \qquad (5\text{-}2\text{-}5)$$

section M:

$$\frac{Kyt}{\Delta y^2} T(2,M-1) - \left(\frac{Kyt}{\Delta y} + \frac{Kx}{\Delta x_1} + \frac{Kx}{\Delta x_2}\right) T(2,M) + \frac{Kx}{\Delta x_1} T(1,M) + \frac{Kx}{\Delta x_2} T(3,M)$$

$$- \frac{mp(2,M)Cp(2,M)}{Pp\ \Delta y} (Tp(1,M)-Tp(1,M-1)) + \left[(V^*(1)-V(1))\right] I(1,M)$$

$$= \rho_p cp \frac{dT(2,M)}{d\theta} \qquad (5\text{-}2\text{-}6)$$

(c) cell plate No. 2

section 1:

$$\frac{Kyt}{\Delta y^2} T(3,2) - \left(\frac{Kyt}{\Delta y^2} + \frac{2Kx}{\Delta x_2}\right) T(3,1) + \frac{Kx}{\Delta x_2} T(4,1)$$
$$- \frac{mp(3,1)Cp(3,1)}{Pp\ \Delta\ y} (Tp(2,1)-Tpo) + \left[(V^*(2)-V(2))\right] I(2,1)$$
$$= \rho_p cp\ t \frac{dT(3,1)}{d\theta} \qquad (5\text{-}2\text{-}7)$$

sections 2 to M-1:

$$\frac{Kyt}{\Delta y_2} T(3,j+1) - \left(\frac{2Kyt}{\Delta y} + \frac{2Kx}{\Delta x_2}\right) T(3,j) + \frac{Kyt}{\Delta y_2} T(3,j-1) + \frac{Kx}{\Delta x_2} T(2,j)$$
$$+ \frac{Kx}{\Delta x_2} T(4,j) - \frac{mp(3,j)Cp(3,j)}{Pp\ \Delta\ y} (Tp(2,j)-Tp(2,j-1)) + \left[(V^*(2)-V(2))\right] I(2,j)$$
$$= \rho_p cp\ t \frac{dT(3,j)}{d\theta} \qquad (5\text{-}2\text{-}8)$$

section M:

$$\frac{Kyt}{\Delta y^2} T(3,M-1) - \left(\frac{Kyt}{\Delta y} + \frac{2Kx}{\Delta x_2}\right) T(3,M) + \frac{Kx}{\Delta x_2} T(2,M) + \frac{Kx}{\Delta x_2} T(4,M)$$
$$- \frac{mp(3,M)Cp(3,M)}{Pp\ \Delta\ y} (Tp(2,M)-Tp(2,M-1)) + \left[(V^*(2)-V(2))\right] I(2,M)$$
$$= \rho_p\ cp\ t \frac{dT(3,M)}{d\theta} \qquad (5\text{-}2\text{-}9)$$

(d) cell plate No. 3 (symmetry plate)

section 1:

$$\frac{Kyt}{\Delta y^2} T(4,2) - \left(\frac{Kyt}{\Delta y^2} + \frac{2Kx}{\Delta x_2}\right) T(4,1) + \frac{2Kx}{\Delta x_2} T(3,1)$$
$$- \frac{mp(4,1)Cp(4,1)}{Pp\ \Delta\ y} (Tp(3,1)-Tpo) + \left[(V^*(3)-V(3))\right] I(3,1)$$
$$= \rho_p\ cp\ t \frac{dT(4,1)}{d\theta} \qquad (5\text{-}2\text{-}10)$$

sections 2 to M-1:

$$\frac{Kyt}{\Delta y^2} T(4,j+1) - \left(\frac{2Kyt}{\Delta y^2} + \frac{2Kx}{\Delta x_2}\right) T(4,j) + \frac{Kyt}{\Delta y} T(4,j-1) + \frac{2Kx}{\Delta x_2} T(3,j)$$

$$- \frac{mp(3,j)Cp(3,j)}{Pp\,\Delta y} (Tp(3,j)-Tp(3,j-1)) + \left[(V^*(3)-V(3))\right] I(3,j)$$

$$= \rho_p cp\ t \frac{dT(4,j)}{d\theta} \qquad (5\text{-}2\text{-}11)$$

section M:

$$\frac{Kyt}{\Delta y^2} T(4,M-1) - \left(\frac{Kyt}{\Delta y^2} + \frac{2Kx}{\Delta x_2}\right) T(4,M) + \frac{2Kx}{\Delta x_2} T(3,M)$$

$$- \frac{mp(3,M)\ Cp(3,M)}{Pp\ \Delta y} (Tp(3,M)-Tp(3,M-1)) + \left[(V^*(3)-V(3))\right] I(3,j)$$

$$= \rho_p cp\ t \frac{dT(4,M)}{d\theta} \qquad (5\text{-}2\text{-}12)$$

Initial Conditions : T(x,y,0)=Ti(x,y) -- steady state distribution

where

Cc(j) : molar heat capacity of cooling air in element (i,j), J/g-mole-K

Cp(i,j) : molar heat capacity of process air in element (i,j), J/g-mole-K

I(i,j) : current density of element (i,j), A/cm²

kx : thermal conductivity along stack direction, J/hr-m-K

ky : thermal conductivity in flow direction, J/hr-m-K

M : number of elements along air flow direction

$\dot{m}c(j)$: molar flow rate of cooling air in element (i,j), g-mole/hr-channel

$\dot{m}p(i,j)$: molar flow rate of process air in element (i,j), g-mole/hr-channel

Pc : pitch of cooling channel, m

Pp : pitch of process air channel, m

t : thickness of cell plate including matrix, bipolar plate,

and electrodes, m

t' : thickness of cooling plate, m

T(i,j) : temperature of cell plate, K

i = 1 cooling plate

i = 2 cell plate No. 1

i = 3 cell plate No. 2

i = 4 cell plate No. 3

j : sections defined along air flow direction

Tc0 : inlet temperature of cooling air, K

Tc(j) : temperature of cooling air, K

Tp0 : inlet temperature of process air, K

Tp(i,j) : temperature of process air, K

i = 1 plate No. 1

i = 2 plate No. 2

i = 3 plate No. 3

V(i) : operating voltage of cell plate i, V

V*(i) : ideal voltage of plate i under operating conditions, V

x1 : t/2 + t'/2, m

x2 : t, m

y : finite difference distance along air flow direction, m

ρp : density of cell plate, kg/m³

ρc : density of cooling plate, kg/m³

θ : time, hr

cc : specific heat of cooling plate, J/kg-K Transform method, and the

cp : specific heat of cell plate, J/kg-K with the properly chosen time

intervals (detailed discussion is in Appendix 4).

(2) Convective heat transfer (energy balance) in the channels (both process and cooling air)

$$\rho A_o C \, \partial T/\partial \theta = hs(T_w - T) - \dot{m} C \, \partial T/\partial x$$

B.C. $x = 0 \quad T = T_{j-1} \; (\theta)$

I.C. $\theta = 0 \quad T = T'$

where

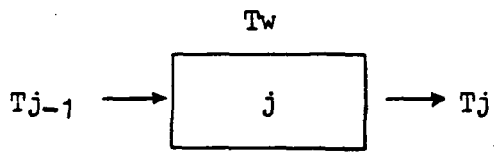

h : heat transfer coefficient, J/m²-hr-K

s : perimeter of the channel, m

m : molar flow rate per channel, g-mole/hr

c : molar heat capacity, J/g-mole-K

Tw : temperature of cell plate, K

T : temperature of air, K

x : distance from the edge, m

ρ : molar density, g-mole/m³

Ao : cross area per channel, m²

θ : time, hr

' : steady state solutions

The equations were solved by the Laplace Transform method, and the solutions were changed to difference form with the properly chosen time intervals (detailed discussion is in Appendix 4).

for process air

$\theta = H$ $\quad T_j(H) = T_{j-1}(0) \exp\left(\frac{-A\Delta x}{B}\right) + Tw_j\left(1-\exp\left(\frac{-A\Delta x}{B}\right)\right)$

$\theta = 2H$ $\quad T_j(2H) = T_{j-1}(H) \exp\left(\frac{-A\Delta x}{B}\right) + Tw_j\left(1-\exp\left(\frac{-A\Delta x}{B}\right)\right)$

.
.
.
.
etc.

for cooling air

$\theta = H$ $\quad T_j(H) = T_{j-1}(H) \exp\left(\frac{-A\Delta x}{B}\right) + Tw_j\left(1-\exp\left(\frac{-A\Delta x}{B}\right)\right)$

$\theta = 2H$ $\quad T_j(2H) = T_{j-1}(2H) \exp\left(\frac{-A\Delta x}{B}\right) + Tw_j\left(1-\exp\left(\frac{-A\Delta x}{B}\right)\right)$

.
.
.
.
etc.

where $\quad A = \frac{hs}{\rho AC}$

$B = \frac{\dot{m}}{\rho A}$

$Tw_j = (Tw(\theta) + Tw(\theta+H))/2$

5.3 Computer Program

The procedure for the simulation of the transient respones of the current density and temperature distributions on the cell plates, when the system load decreases, are as follows:

1. Obtain the steady state solutions.
2. From time=0, decrease the load at a fixed ramping rate until the required load ratio (the minumum ratio is 25%) is reached.
3. Calculate the corresponding operating pressure to keep the phosphoric acid (electrolyte) concentration constant (see Figure 5-2).
4. Estimate the mean current density and operating voltage at the new operating conditions to fulfill the new load. Two typical figures (Figure 2-27 and Figure 5-4) show the relationships between the power, current density, and operating voltage.
5. Calculate the flow rates of the fuel, the process air, and the cooling air at each position from the new mean current density.
6. Estimate the current density distribution from the new flow rates and pressures.
7. Calculate the new temperature distribution on the cell plate.
8. Calculate the new temperatures of the gases at each position.
9. Stop the procedure when the final (new) steady state is reached. Otherwise, increase the time by a time interval and go back to step 2.

This procedure was developed into a Fortran computer program. The final set of differential-difference equations described in previous section was solved by one of the integration methods discussed in Section 3.4. In Figure 5-3, a simplified flowchart of the computer

OLTAGE-CURRENT DENSITY CHARACTERISTIC CHART

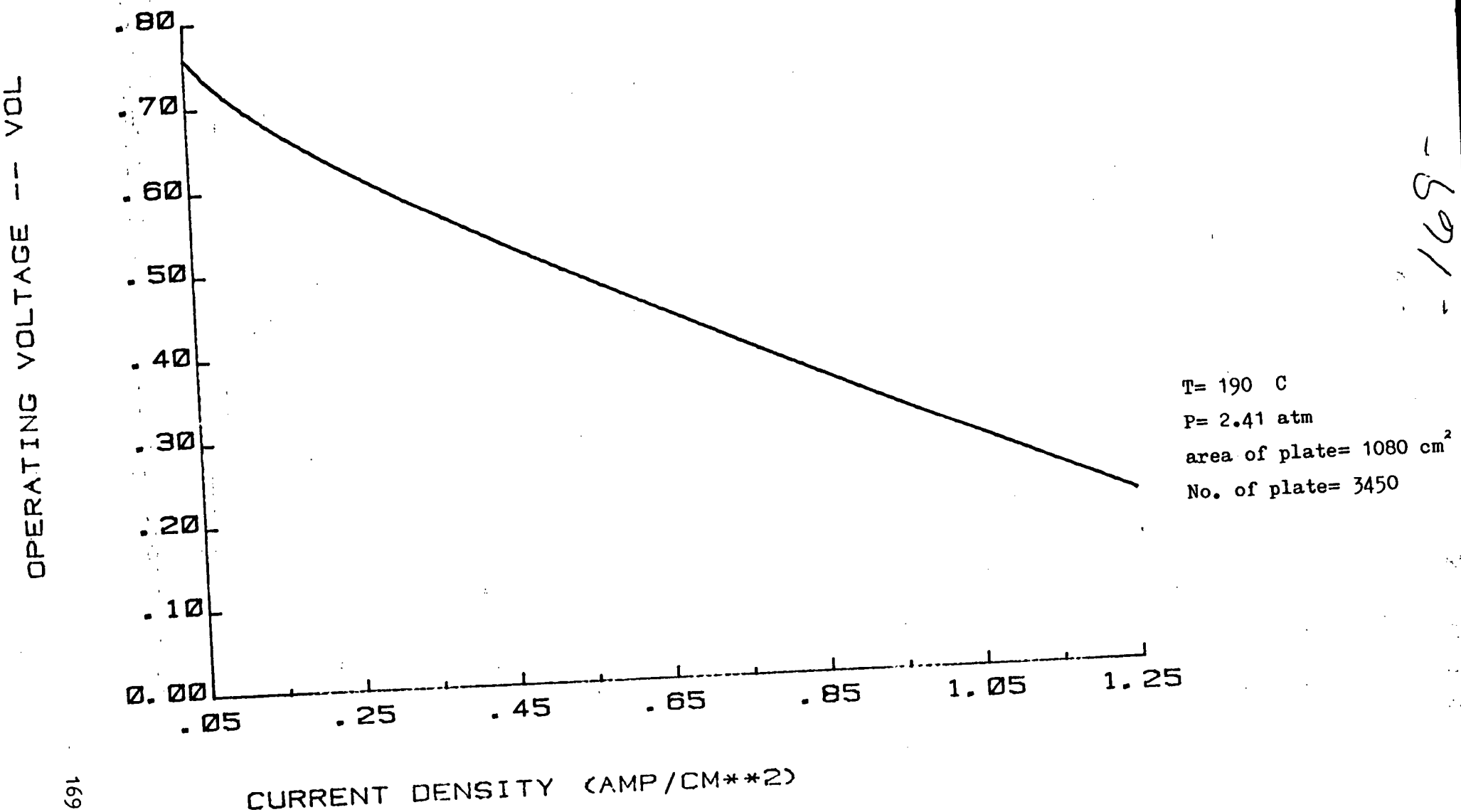

169

Figure 5-4

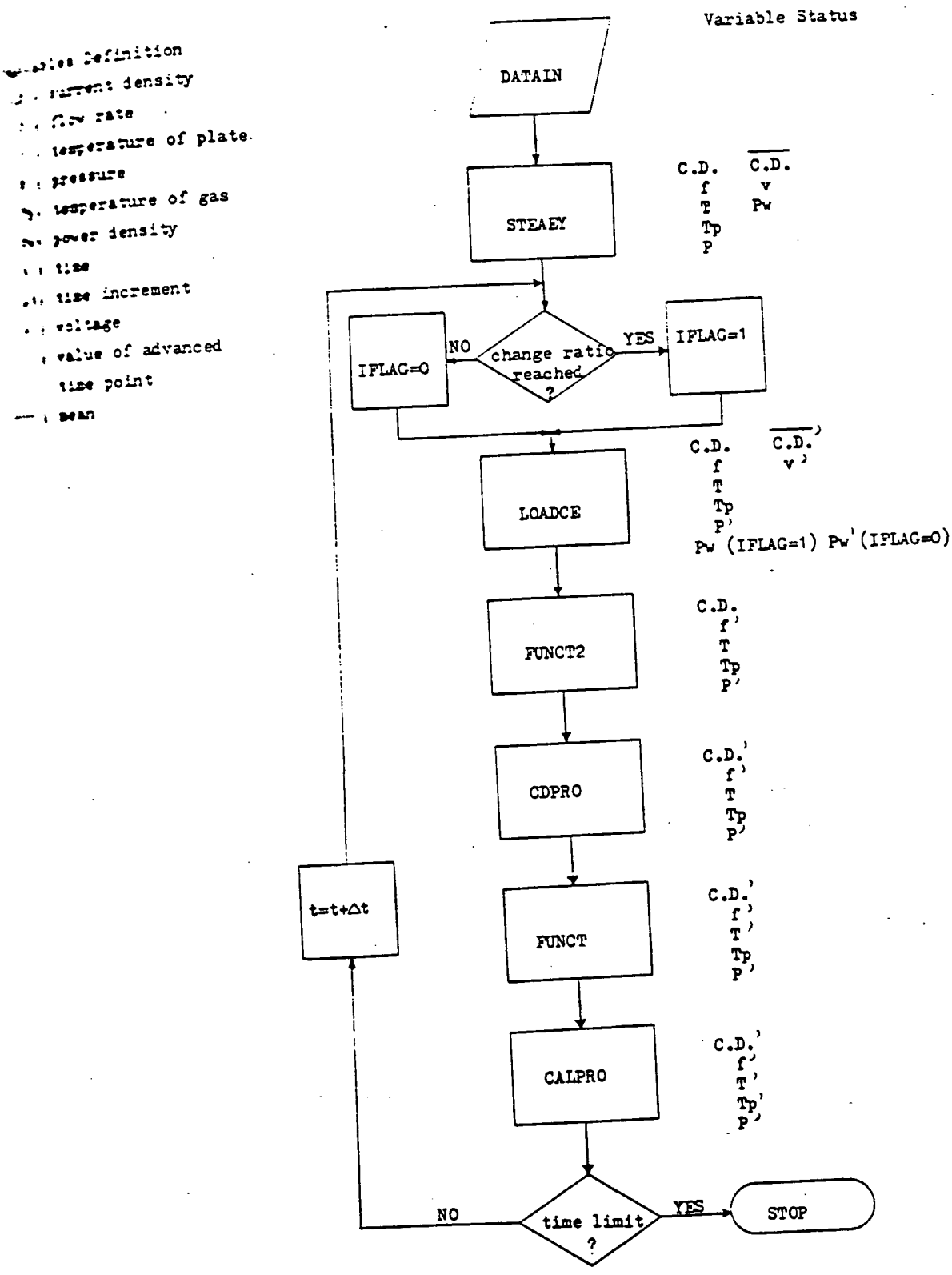

Figure 5-3 Simplified flow chart of PAFC stack dynamic program

program, where the status of various variables (current density, flow rate, temperature of plate and gases, pressure, voltage, and power output) at different times (θ and $\theta+\Delta\theta$) is shown. Figure 5-3 also expresses the function of each calling subroutine.

5.4 Results and Discussion

The program, which uses the Euler method (Section 3.4) with a time interval of 0.108 seconds, was run on an IBM 370 computer and the results are shown in Figures 5-5 through 5-16. Using a 12.5% per second ramping rate, the load decrease (from full to 50%) can almost be treated like a step change. Table 5-1 lists the input data in SI units. The cooling configuration is a "straight" type (see Section 2.2.3.3) and the inlet flow temperature is close to the average operating temperature.

Figures 5-5 through 5-10 show the numeric distributions of the temperature and current density in each finite-difference cell on the symmetric plate (plate no. 3) at the initial steady state, the transient state (10.152 sec.), and the final steady state (280 sec.). The plots of the temperature distribution for the three cases are shown in Figure 5-11 and 5-12. Finally the mean values of the temperature, voltage, and current density at special points were plotted vs time, with a small time scale and a large time scale. The results are shown in Figures 5-13 through 5-16. From the results of the small time scale plot, the changes in the early transient state, which decide the stable ramping rate and dead time for control, can be seen. The plots with the larger scale provide information concerning the transient time period, the system response between the two steady state periods, and the final steady state conditions.

As expected, the temperature responds slower than the current density which is dependent upon the inlet flow rates. The damping

217.1	215.9	214.4	212.2	209.2	204.4
211.8	210.6	209.2	207.2	204.4	200.0
202.4	201.4	200.2	198.5	196.2	192.7
190.8	190.1	189.2	187.9	186.1	183.5
179.3	178.8	178.1	177.2	176.0	174.3
170.8	170.5	170.0	169.4	168.6	167.5

Fuel →

$\bar{T}$=192.1 C

Air

Figure 5-5 Steady state temperature distribution

.3857	.3797	.3723	.3619	.3465	.3218
.3908	.3843	.3762	.3647	.3482	.3220
.3721	.3662	.3588	.3487	.3344	.3129
.3378	.3332	.3275	.3199	.3094	.2943
.3004	.2972	.2931	.2879	.2809	.2710
.2753	.2730	.2701	.2663	.2615	.2547

Fuel →

$\overline{C.D.}$= .3250 A /cm^2

V= .58299 volt

Air

Figure 5-6 Steady state current density distribution

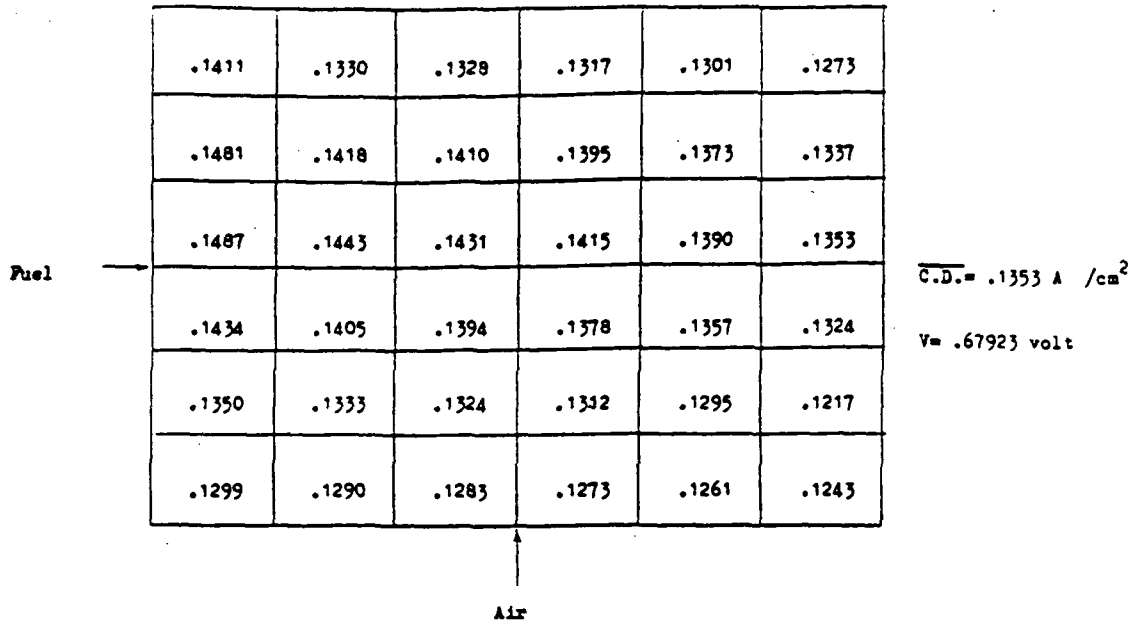

Figure 5-7 Transient state current density distribution (10.152 sec.)

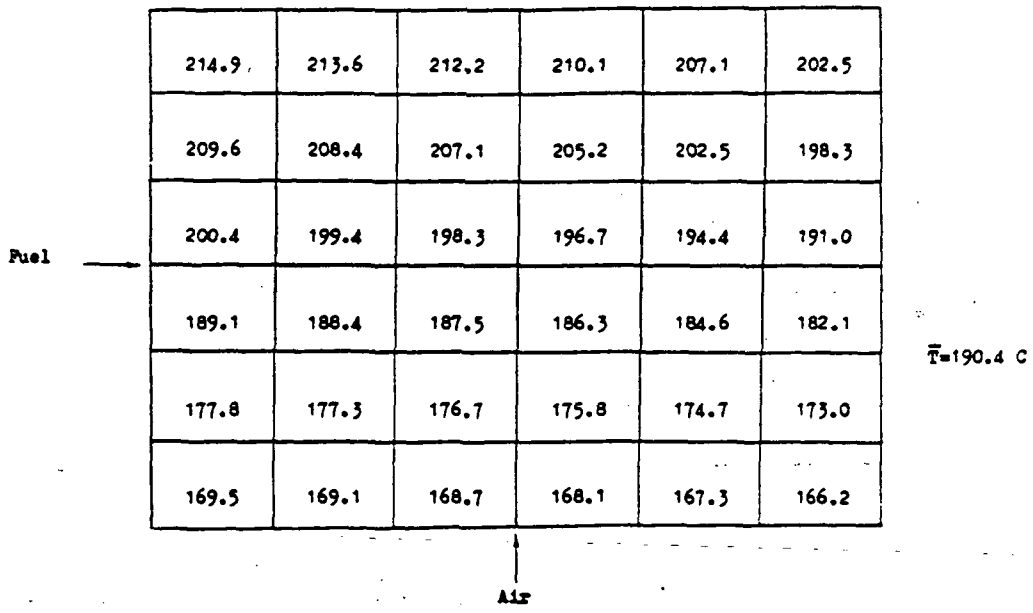

Figure 5-8 Transient state temperature distribution (10.152 sec.)

202.9	201.1	200.3	199.0	197.2	194.5
200.5	198.9	198.1	196.9	195.2	192.6
195.9	194.6	193.8	192.7	191.2	188.8
189.7	188.7	188.0	187.0	185.7	183.7
183.0	182.2	181.6	180.8	179.7	178.0
177.5	176.9	176.5	175.8	174.9	173.5

Fuel →

$\bar{T}$=188.8 C

↑ Air

Figure 5-9 Final steady state temperature distribution (280 sec.)

.1226	.1141	.1147	.1143	.1137	.1127
.1357	.1290	.1288	.1281	.1269	.1251
.1440	.1389	.1383	.1373	.1358	.1334
.1474	.1438	.1430	.1418	.1402	.1376
.1475	.1451	.1443	.1431	.1415	.1390
.1488	.1473	.1464	.1453	.1437	.1414

Fuel →

$\overline{C.D.}$ = .1356 A/cm^2

V= .67446 volt

↑ Air

Figure 5-10 Final steady state current density distribution (280 sec.)

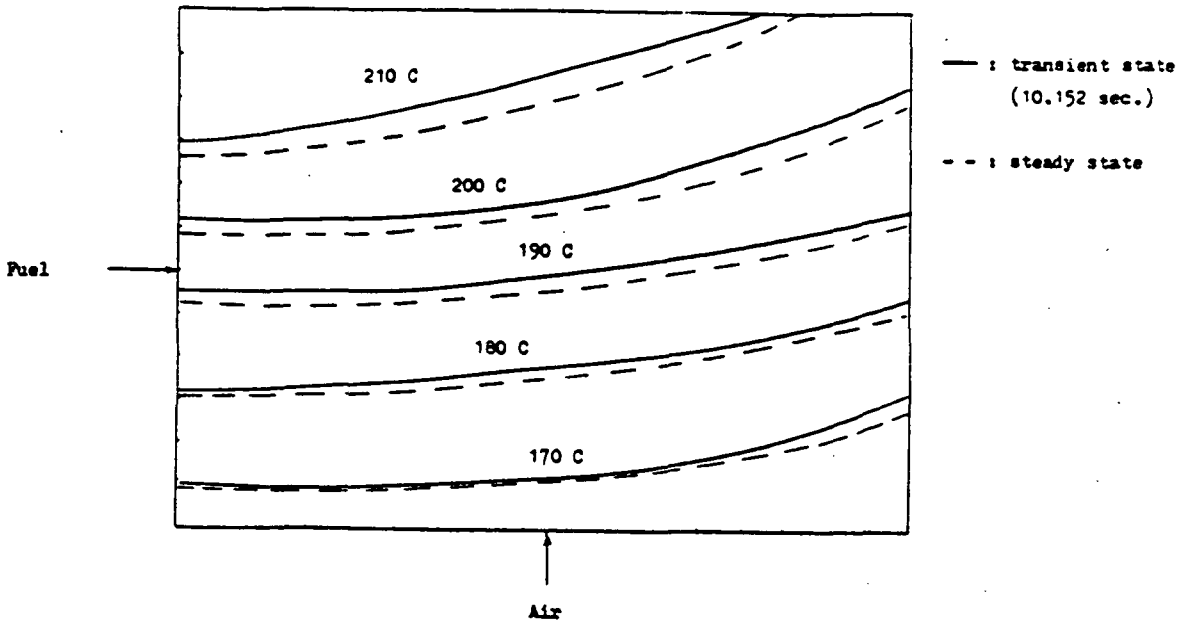

Figure 5-11 Temperature distribution change at transient state

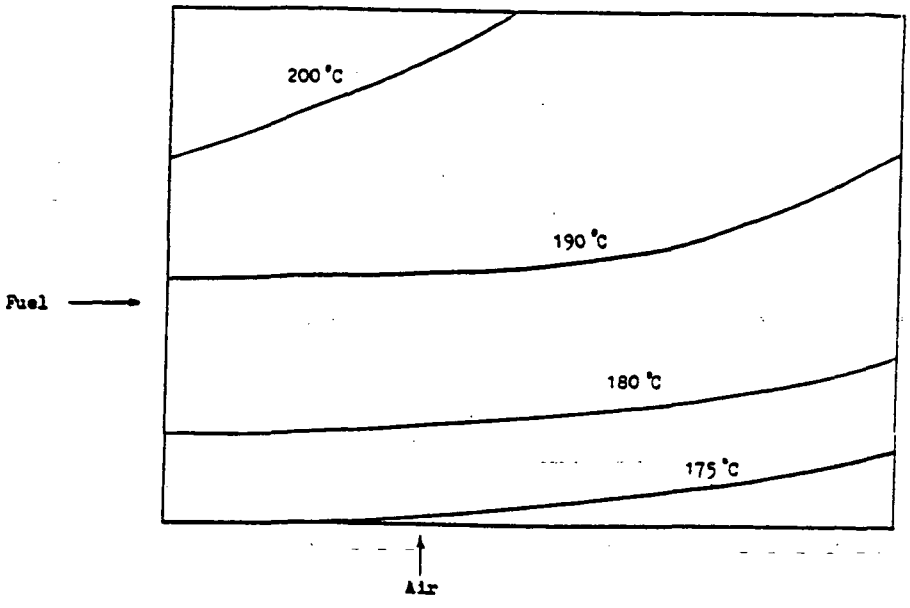

Figure 5-12 Temperature distribution at final steady state (280 sec.)

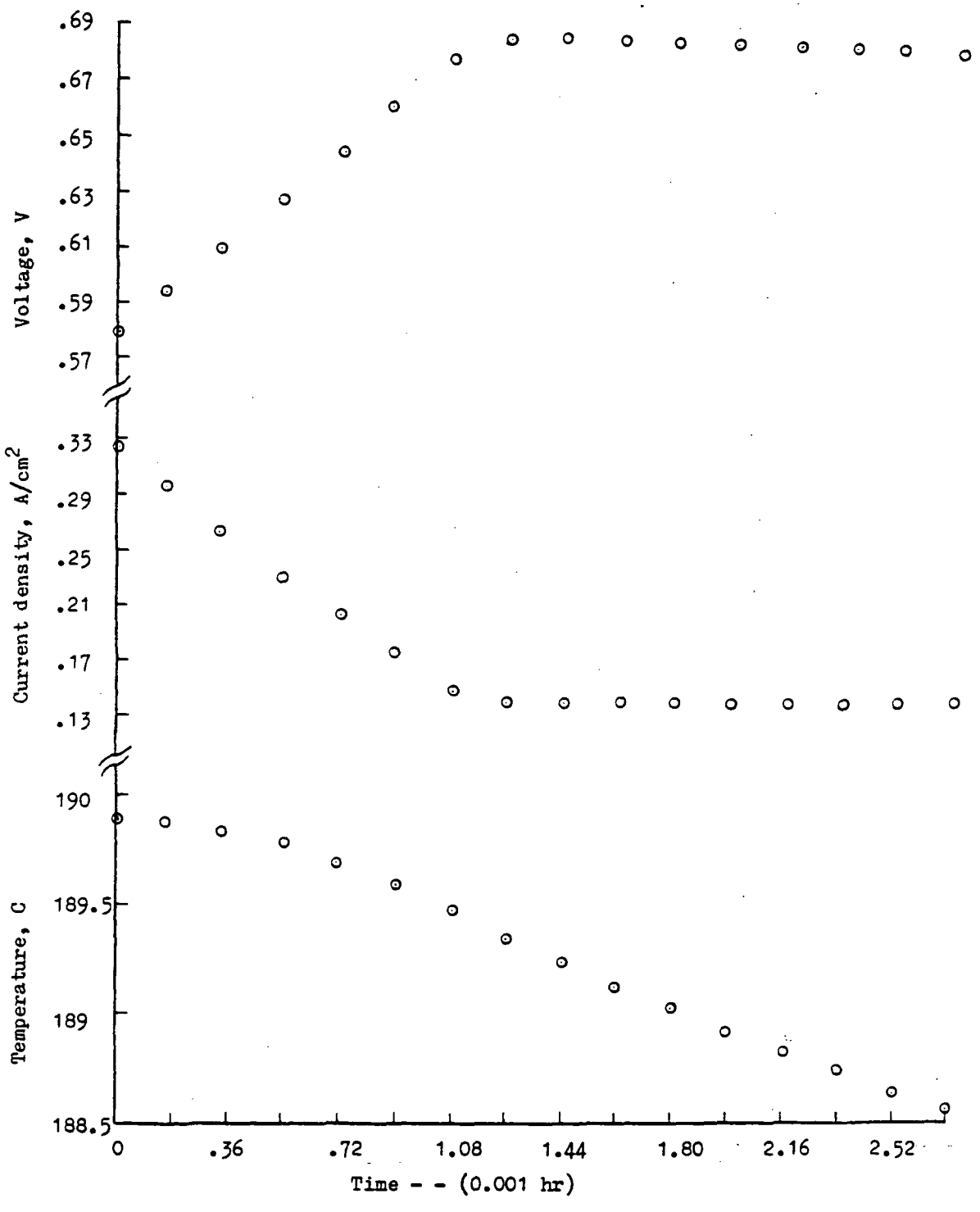

Figure 5-13 Mean temperature, current density, and voltage at transient state (small time scale)

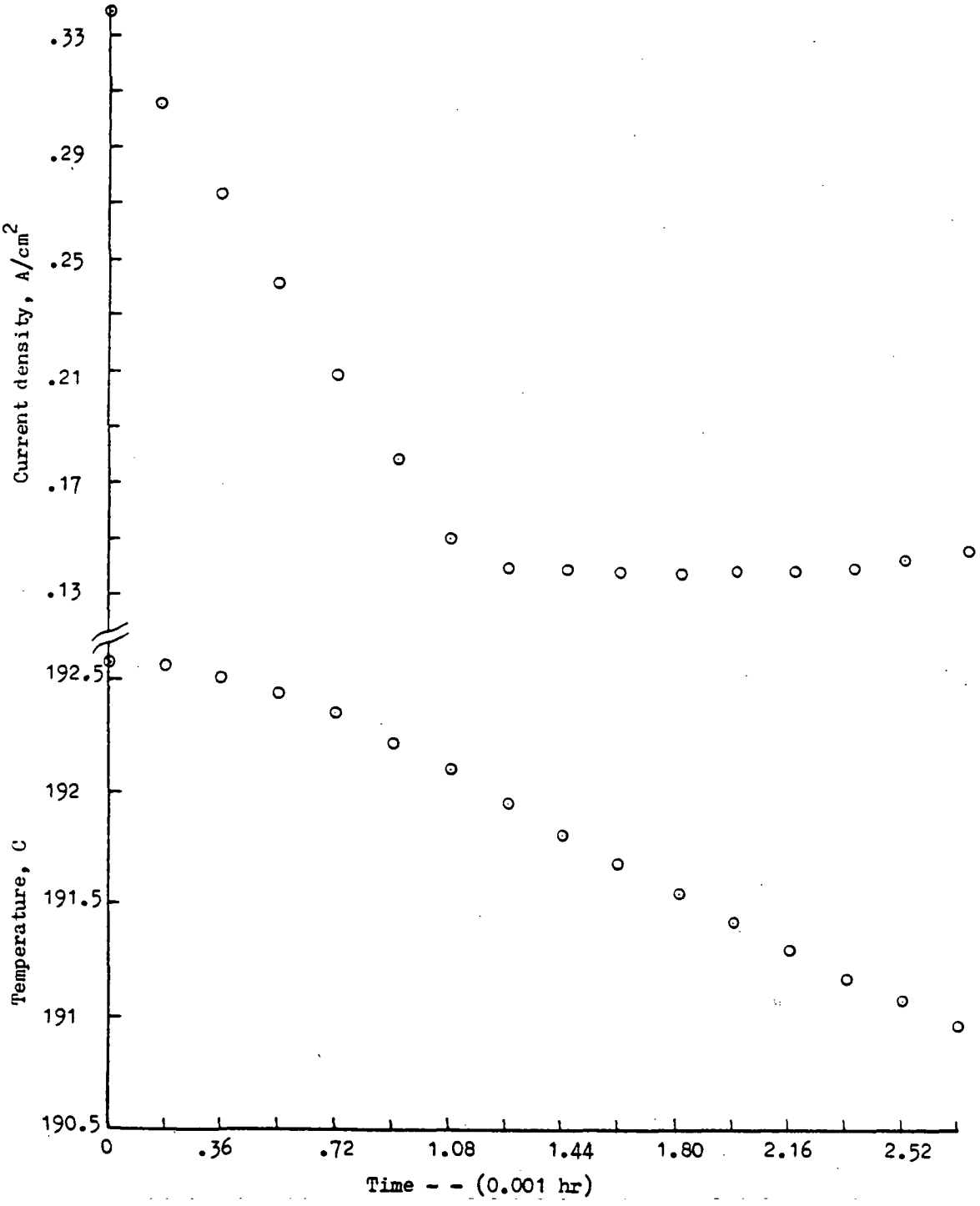

Figure 5-14 Middle point responses at transient state (small time scale)

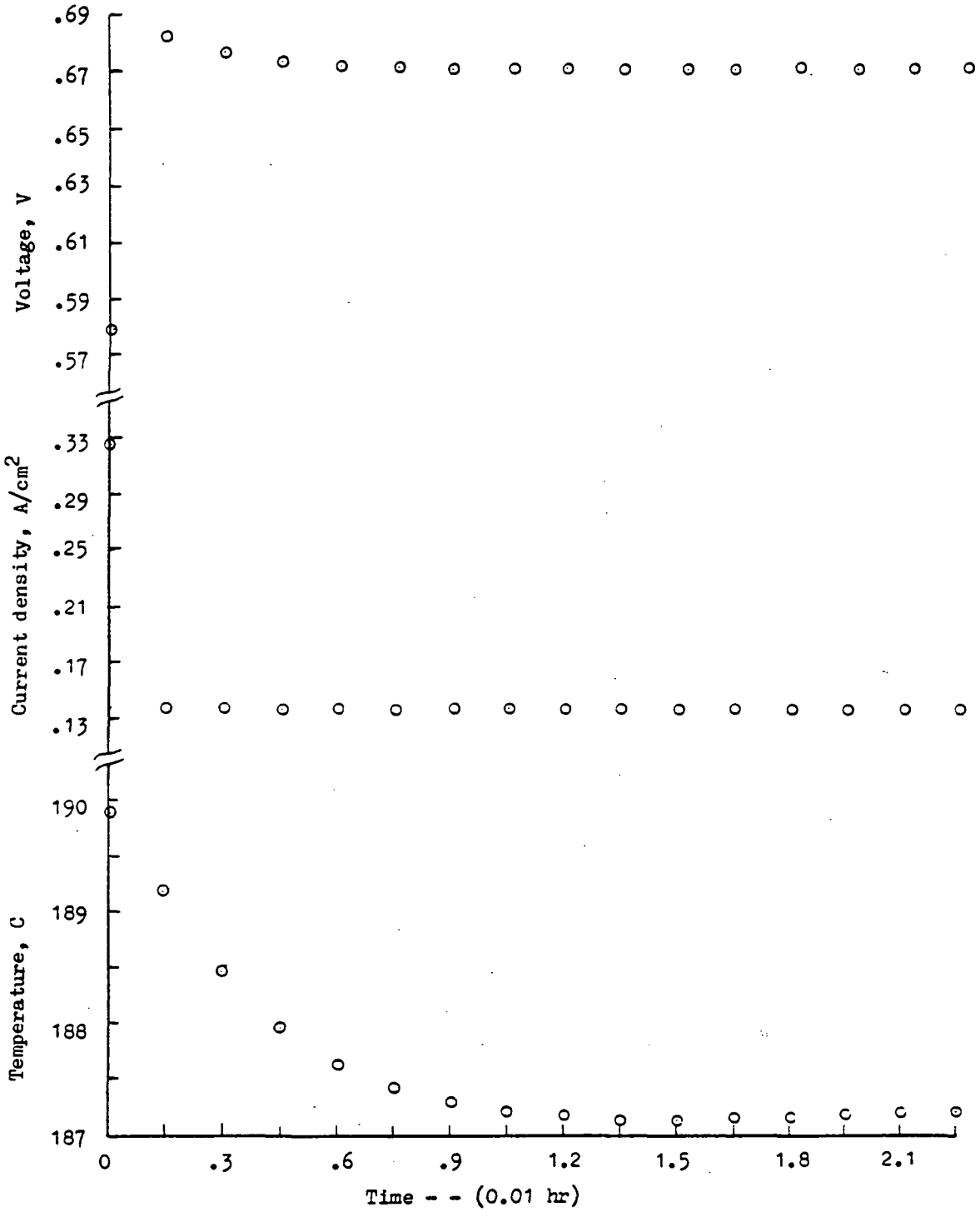

Figure 5-15 Mean temperature, current density, and voltage at transient state (large time scale)

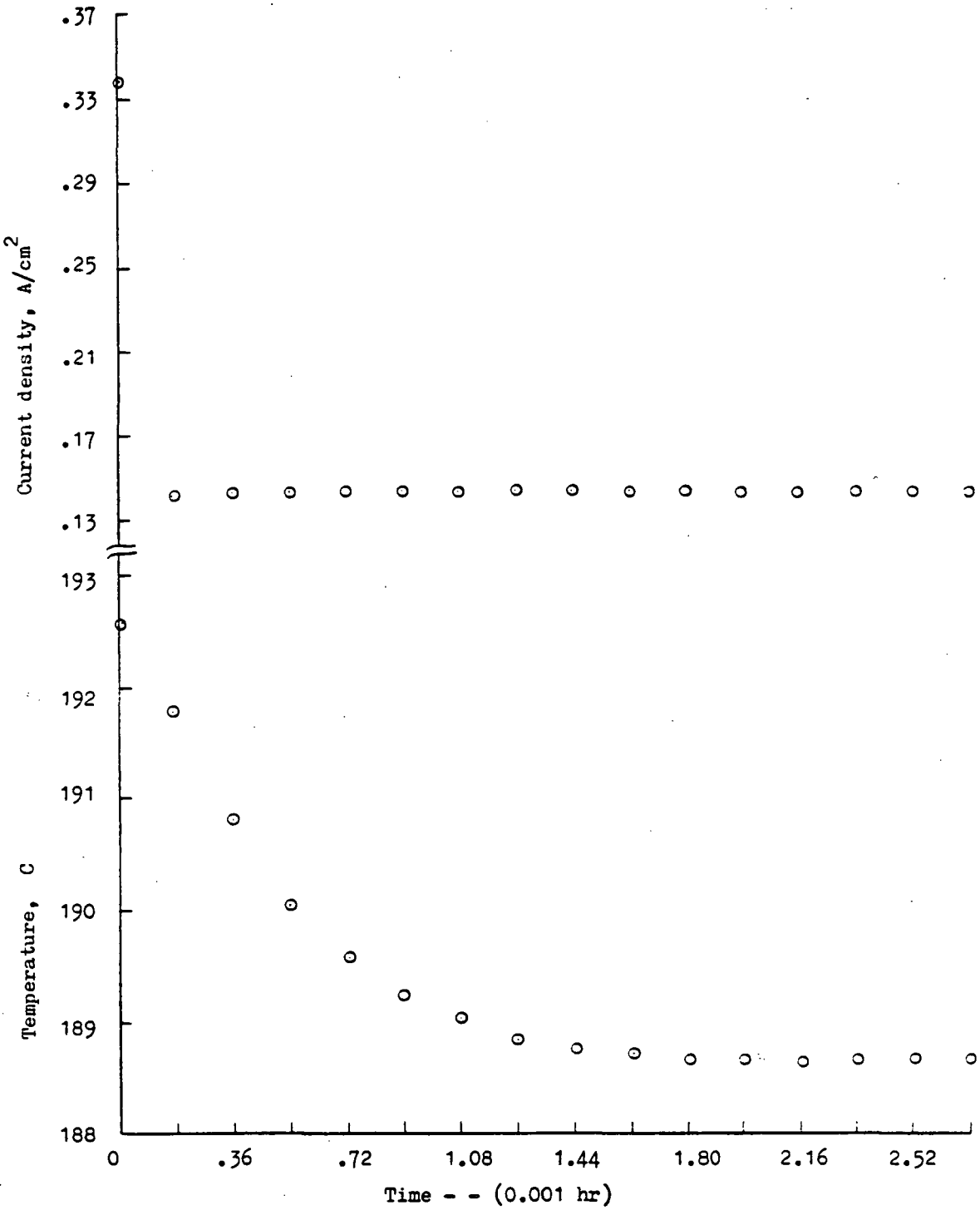

Figure 5-16 Middle point responses at transient state (large scale)

C-3.

Variable name	Dimension	Initial value	Unit	Definition
XN		0.41	m	Length of cell plate in x-direction
YN		0.28	m	Length of cell plate in y-direction
XDNSO		3250	A/cm^2	Designed current density
UTA		0.5		Utilization of O_2 in stack
UTH		0.75		Utilization of H_2 in stack
POPC		3.4	atm	Pressure of cooling air
POP		3.4	atm	Operating pressure in stack
TKA		443	K	Inlet temperature of process air
WFD		0.001016	m	Depth of fuel channel
WFW		0.003048	m	Width of fuel channel
NCC		30		Number of cooling channels
WE		0.001016	m	Thickness of cell (electrode and matrix)
TKF		450	K	Inlet temperature of fuel
T		0.003302	m	Thickness of cell plate
NK		5		Number of plates between two cell plates
WAD		0.001016	m	Depth of process air channel
WAW		0.003048	m	Width of process air channel
NP		23		Number of cell plates
NCA		80		Number of process air channels
NF		55		Number of fuel channels
T1		0.008891	m	Thickness of cooling plate
NX		6		Finite difference number in x-direction
NY		6		Finite difference number in y-direction
ER		0.01		Criteria for convergence
CLCA		0.0052	kg/m^2	Catalyst loading on cathode side
CLAN		0.0034	kg/m^2	Catalyst loading on anode side
CU		0.15		Utilization of catalyst
SA		50000	m^2/kg	Surface area of catalyst
SRO		0.000044	$-m^2$	Cell resistance at 450 K

Table 5-1 Input data for simulation of dynamic PAFC stack

Variable name	Dimension	Initial value	Unit	Definition
ALFA		0.5		Transfer coefficient
DKC		240000	A/atm	Constant to calculate limiting current density
R		8.314	J/g-mole-K	Gas constant
Z		2	g-equivalent	Number of Faraday equivalents transferred
FCONST		96500	C/g-equivalent	Faraday constant
NC		36		Ratio of cooling air to air consumed in stack
KX		2.5961	J/m-s-K	Effective thermal conductivity in stacking direction
KY		51.92205	J/m-s-K	Effective thermal conductivity on the cell plate
TKC		403.3	K	Inlet cooling air temperature
WCW		0.00559	m	Width of cooling channel
WCD		0.00559	m	Depth of cooling channel
Y1H2		0.76		Mole fraction of H_2 in anode inlet
Y1C02		0.24		Mole fraction of CO_2 in anode inlet
Y202		0.208		Mole fraction of O_2 in cathode inlet
Y2N2		0.782		Mole fraction of N_2 in cathode inlet
Y2H20		0.01		Mole fraction of H_20 in cathode inlet
RHOP		2611.01	kg/m^3	Density of cell plate
RHOC		2162.49	kg/m^3	Density of cooling plate
CCP		1.0467	kJ/kg-K	Heat capacity of cell plate
CCC		0.841547	kJ/kg-K	Heat capacity of cooling plate

Table 5-1 continued

ratios of all of the presented variables are small, less than 1% for the mean voltage and less than 0.1% for the others (see Figure 5-15 and 5-16).

It is not necessarily true to say that the final steady state is reached at 280 seconds. Actually at that time the calculated temperature of the stack is still fluctuating. This fluctuation is caused in part by the damping characteristics of the system and in part by the computation errors. From Figure 5-15, the final steady state may be considered to be reached at 43 seconds when the mean temperature reaches a steady value.

CHAPTER 6

TRANSIENT RESPONSE OF THE PAFC SYSTEM IN LOAD CHANGING PERIODS

The objective of this chapter is to combine all of the programs developed in the previous chapters to determine the performance of the power plant and its components in the following transient conditions: sudden and gradual change from full power load to partial load, from standby to partial load, and from the shutdown to standby condition.

The final computer program was then used to simulate the performance of a 7.5 megawatt power plant (Figure 1-4) subjected to a power reduction linearly ramping from full load to partial load. The results obtained include: the temperature, pressure, and flow rate of the components at various locations in the system; the transient temperature and current density distributions in the fuel-cell stack; the dead time for major components considered in the simulation; and the amount of heat and electric energy output.

6.1 Assumptions

For simplicity, several assumptions were made to simulate the load change responses. The five assumptions made for the fuel cell stack subsystem in Chapter 5, are also applicable to the simulation of the whole system. In addition, the following assumptions were also made for the transient state study.

1. There are voltage and power constraints, resulting from the fact that the platinum and carbon components can corrode at cell potentials above 0.8 volts. This maximum allowable voltage determines the minimum load at which the system can operate. 25% of the fuel load has been chosen as the minimum load.
2. The loads linearly decrease or increase with time.
3. The conversion rate of methane in the reformer is fixed, as well as the carbon dioxide to carbon monoxide ratio. Therefore, the amount of input methane is proporitional to the amount of hydrogen needed in the stack. The temperature level will be monitored to determine the flow rate of methane into the burner.
4. The inlet air which flows through the air blower, is proportional to the inlet fuel at the burner with the excess ratio fixed.
5. The steam to carbon ratio is fixed and transient changes in the economizer and steam generator are not considered, therefore the inlet steam is proportional to inlet methane. The transport lag of water pumping and steam generating is neglected.
6. The recuperator, ZnO bed, and cooling power are not considered in this transient study.
7. Transport lag is not considered in the piping which combines

components.

6.2 Program Description

A computer program for simulating the transient behavior of the PAFC power plant was developed. The steady state conditions for the system presented in Chapter 2 were used for the initial conditions in the transient state calculation. Efficient, i.e. numerically stable and adequately accurate computer models with relatively short computation times, were utilized for the individual components and were described in Chapters 4 and 5. Finally, by means of the "on-off" flags, which controls computations between components, simulation of real-time computation can be done on a batch-type computer.

This Fortran program, which includes 45 subroutines and 20 functions (descriptions of these subroutines and functions are in Appendix 8), was used to simulate the system's transient responses, with the required power load being decreased from full load to partial load.

Although no experimental data was available, this simulation provides information concerning the optimal design, operation requirements, and control procedure within the load changing period.

The main (executive) program calls three subroutines which are DATAIN, STMAIN, and STTRAN for reading input data, calculating initial steady state performances, and simulating transient state responses, respectively. The flow chart of main program is shown in Figure 6-1.

The steady state solution was discussed in Chapter 2. The

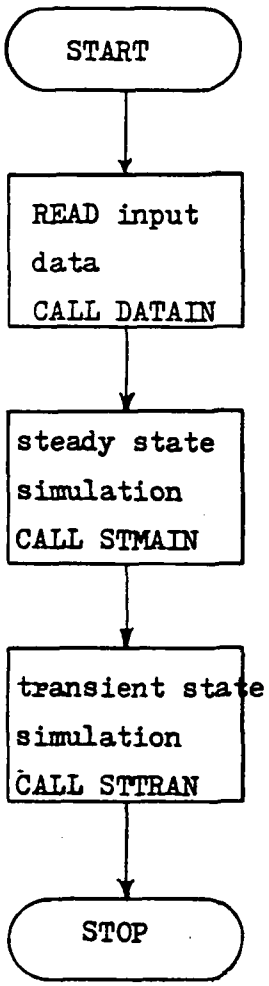

Figure 6-1 Flow chart of Main program

following section will concentrate on the transient responses.

To decrease the computation time, several assumptions have been made. They are

1. neglet the temperature difference between the stream and the catalyst in the reactors. This was discussed in Section 4.4;
2. decrease the finite-difference section. There are two advantages resulting from this modification: first, fewer equations must be solved; second, because the maximum stable time interval is decided by the time needed to travel one section (except in the reactors). A decrease in section number leads to an increase in the maximum stable time, and then an increase in the time interval. However, this procedure will also lose some accuracy in the final results;
3. increase the time interval in each component to its maximum stable value: If there are two streams in a component (like the tube-side and shell-side streams), the greatest common divisor (GCD) of the two maximum values is chosen to be the fixed time interval. Thus, the system time interval is estimated from the GCD of these components' time interval;
4. neglect the transport lag in the pipes connecting components and in the auxiliary components.

"PAGE MISSING FROM AVAILABLE VERSION"

6.3.1 Simulation of the Real-time Procedure

To simulate the real-time computation on a "batch" computer, the program uses controlled clock time and "on-off" flags in the computer coding. There are four flags which will be discussed as follows:

(1). IFLAG: flag to indicate the load changing period, 0 indicates outlet power under ramping, whereas a 1 indicates that the required load has been reached.

(2). IFLG: flag for the registering of one of the components so that the component may be evaluated for its transient response. Where a 0 means no registered reaction of the component and a 1 indicates registration. There are two situations for "0" being assigned to a component, they are the initial steady state and the final steady state.

(3). NFLG: NFLG is used when the calculation will be "operated" at some system processing time. Because the time intervals for calculation of the components are multiples of system's time intervals, at some specific system time, some components may not be calculated even if the IFLG of these components are on.

(4). MFLG: flag is used to indicate the condition of the outlet(s) in a component. There are three possible values, 2 for initial steady state, 1 for transient state, and 0 for the final steady state. By means of these "on-off" flags, the calculations among these components (subroutines) can be controlled, and the results printed at specific transient times to present the components and system conditions.

When the system time=0, all MFLGs are equal to 2, IFLGs are equal to 0 except for the IFLGs of Heat Exchanger-2, Air Heater, and Fuel cell

stack (see Figure 4-1), NFLGs are equal to 0, and IFLAG is 0 also. The MFLGs will be changed to 1 if the corresponding outlet's temperature is greater (or less) than the initial steady state value determined by CRT2. CRT2 may be some specific value of a temperature criteria or some percentage criteria. The MFLGs will be changed to 0 if a change of the corresponding outlet temperature is smaller than Y·CRT1, where Y is the outlet temperature and CRT1 is another convergence criteria. This situation will last for some period of time (5 seconds in the example). Then a new IFLGs' value will be assigned according to the previous component's MFLGs. In addition, the NFLGs' value will depend upon the corresponding IFLG and component's time interval.

6.3.2 Transport Lag Consideration

Because this is a gas system, the transport lag of streams in pipes, reactors, and channels cause a "time delay". A typical example would be one pipe (finite-difference) section (in the heat exchanger for instance) transporting gas from one location to another. An input flow rate change will not immediately transport to the exit. This situation can be characterized by specifying the inlet stream as I and the outlet stream as J. The flow rate in J will be "delayed" from the flow rate in stream I by the time to travel down the section length l. Such a dead time can be simulated on a computer by a "time delay" procedure. This can be constructed in several ways, the most direct of which would be the "bucket brigade" approach, a self-explanatory term (Ref. 31).

The operating principle of this approach is to allocate NTN spaces to the delay channel, where NTN=time delay/(IDH x SDT) where IDH is a

multiple of the system time interval (SDT) for a specific component. Instead of feeding the input signal (flow rate for instance) in at the front end, and moving the values in each space one position toward the exit end, and finally reading the value in the last space as the exit value ("bucket brigade"), the technique does not move the values but the pointer for the readin and readout moves from space to space.

Each difference section is treated the same way. For simplicity, the mean flow velocity is used to estimate the transport time (time delay) of one section, then the NTN for every section is the same. However, there may be two different values of NTN for one component, one is of the tube-side gas, and the other is the shell-side gas.

6.3.3 Determination of Final Steady State

Determination of the final steady state is a problem because of the fluctuation of the calculated values. However, there are several criteria to use,

(1). calculate the final steady state performance using the required input data, then when transient responses reach 99.5% or more of these values, the solutions are considered final steady state solutions.

(2). decide by the temperature damping ratio - if the ratio is less than 0.1%, e.g., the final s.s. is assumed to be reached.

(3). decide by the temperature change between the continuous time period - if the change is less then 0.05°K, say, and lasts for a period of time (e.g. 5 seconds), it is assumed be the final steady state.

For simplicity in the computer programming, the last criterion was selected for this simulation.

6.3.4 Flowchart of the Program

The flowchart of the executive program is given in Figure 6-2, which shows how the "on-off" flags function and how the program executes the computations for the transient period.

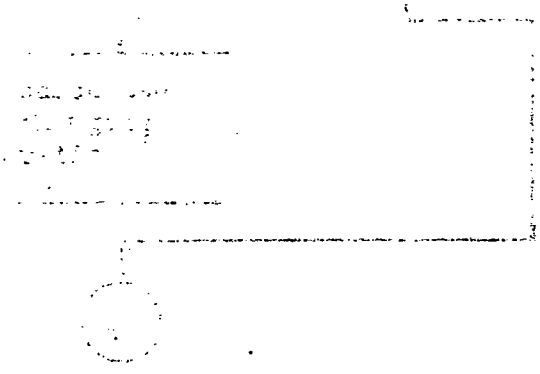

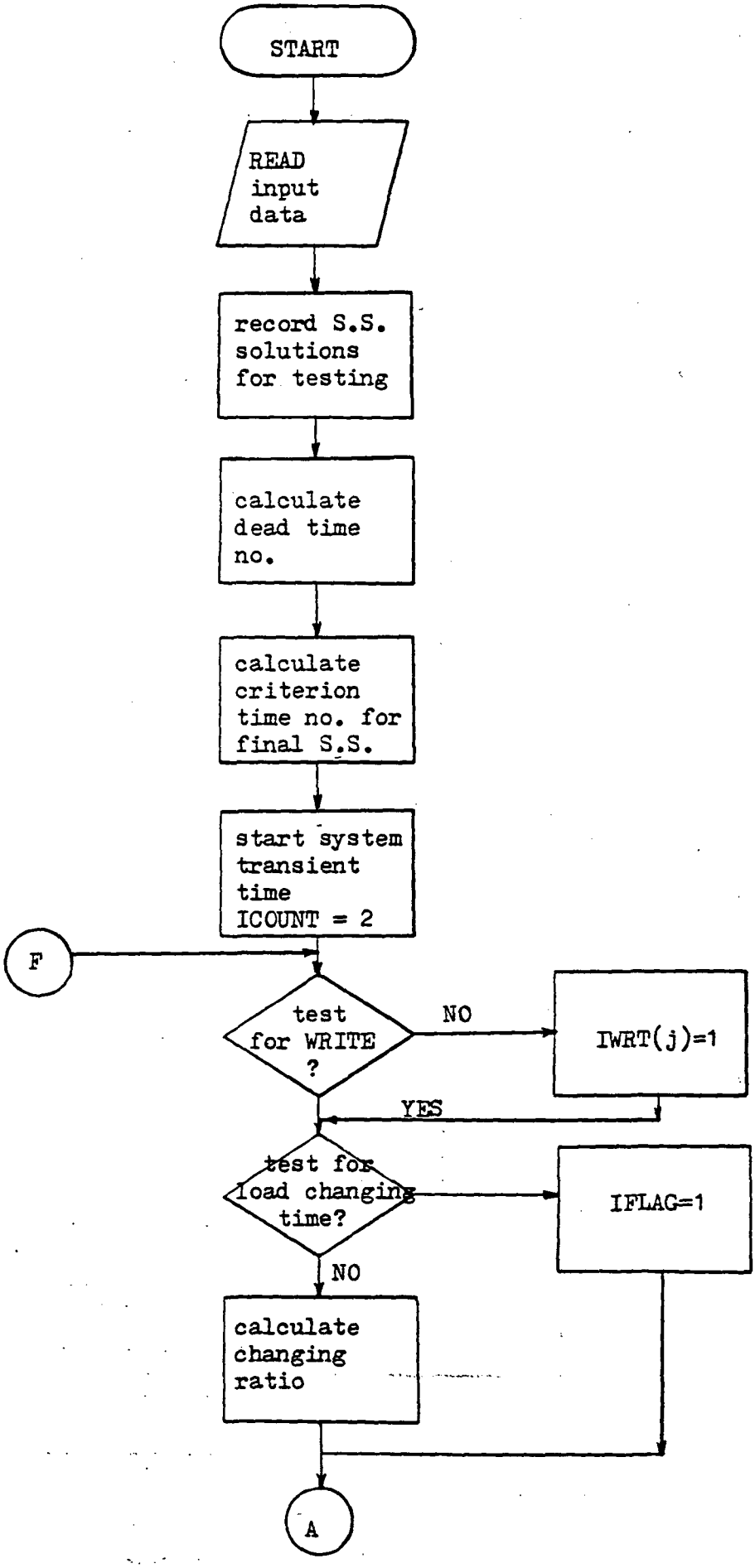

Figure 6-2 Flow chart of PAFC system transient state simulation

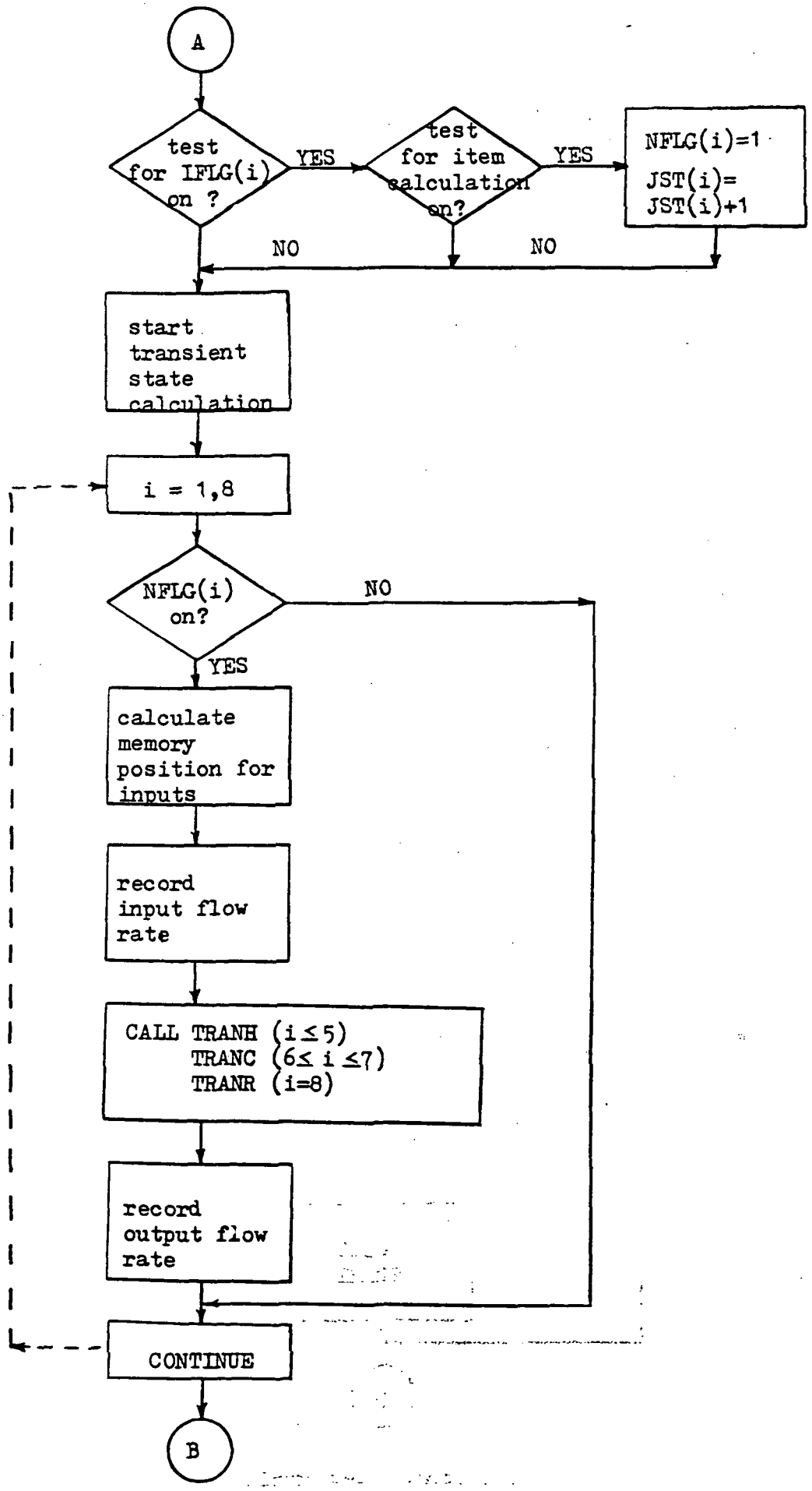

Figure 6-2 continued

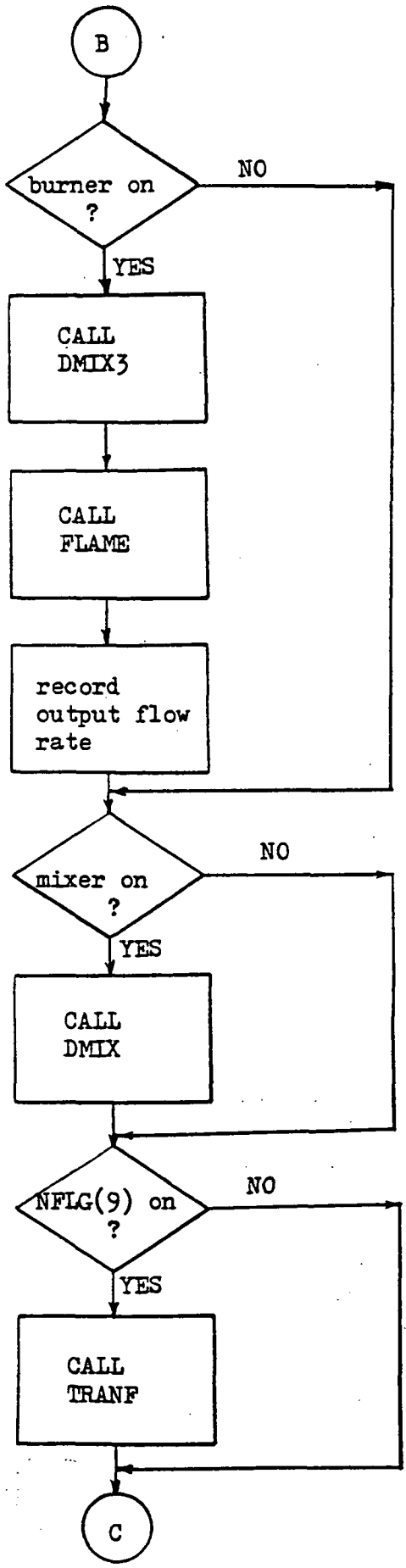

Figure 6-2 continued

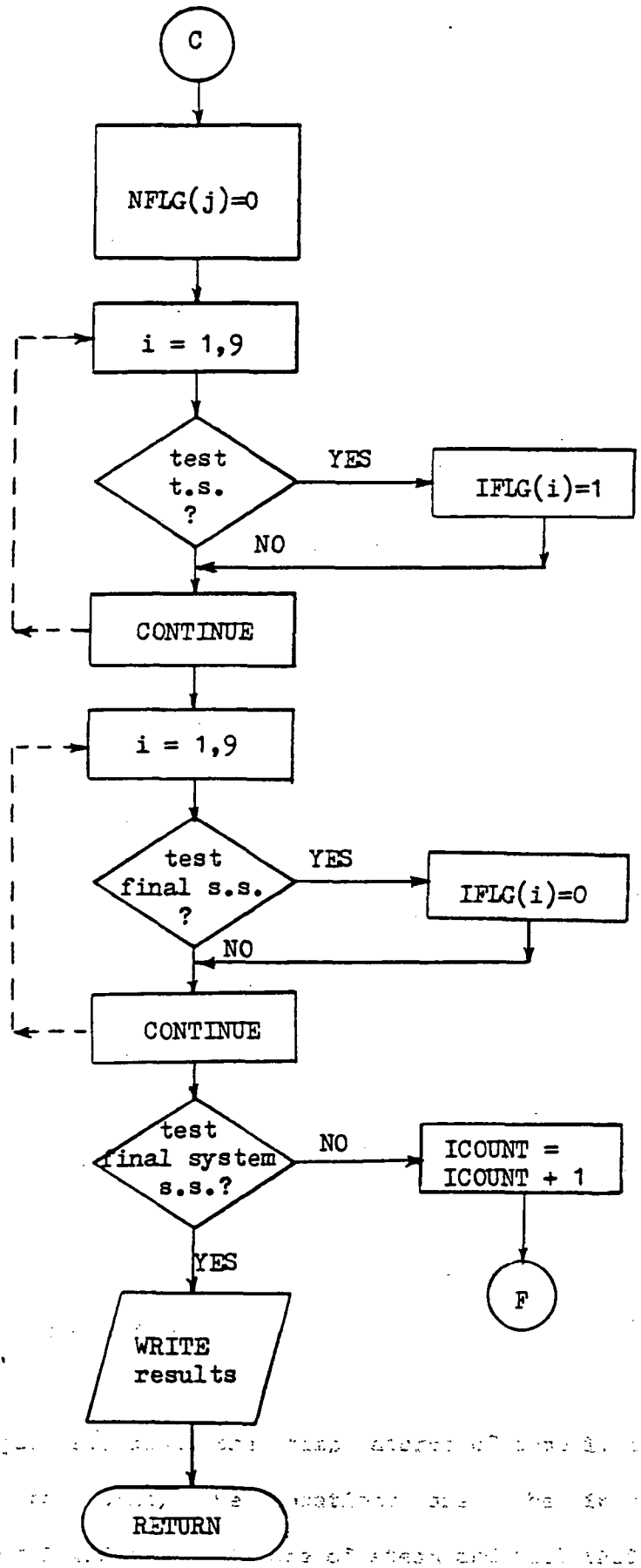

Figure 6-2 continued

6.4 Example and Results

The example discussed in this section involes the simulation of the PAFC system response for an output power decrease from full load to 90% load. The assumed ramping rate is 5% per second for this power decreasing operation. Appendices 6 and 7 provide the definitions and values of the input data for the steady state and transient state analyses, respectively. Some of the input data used here for the steady state simulation differs from that of the previous simulation in Chapter 2. The values are listed in Appendix 6.2. All of the input data is in SI or SI acceptable units.

This sample example was run on the NASA-LeRC IBM/370 computer. It required 115.39 minutes of CPU time to reach the final steady state which occured at a system time of 14.38 minutes. The criteria used for determining the final steady state was discussed in Section 6.3.3.

The results include the operating conditions in each finite-difference grid (in the fuel cell) or section (in other components) at specific transient times, and initial and final steady state solutions. Portions of the solutions for the transient time and both of the steady state periods are in Appendix 9. Some of the results will be discussed here.

Figure 6.3 shows the temperatures of some important locations with respect to time, the locations are: the input fuel after heat exchanger-1 (A8); the mixture of steam and fuel (A10); the reacting gas

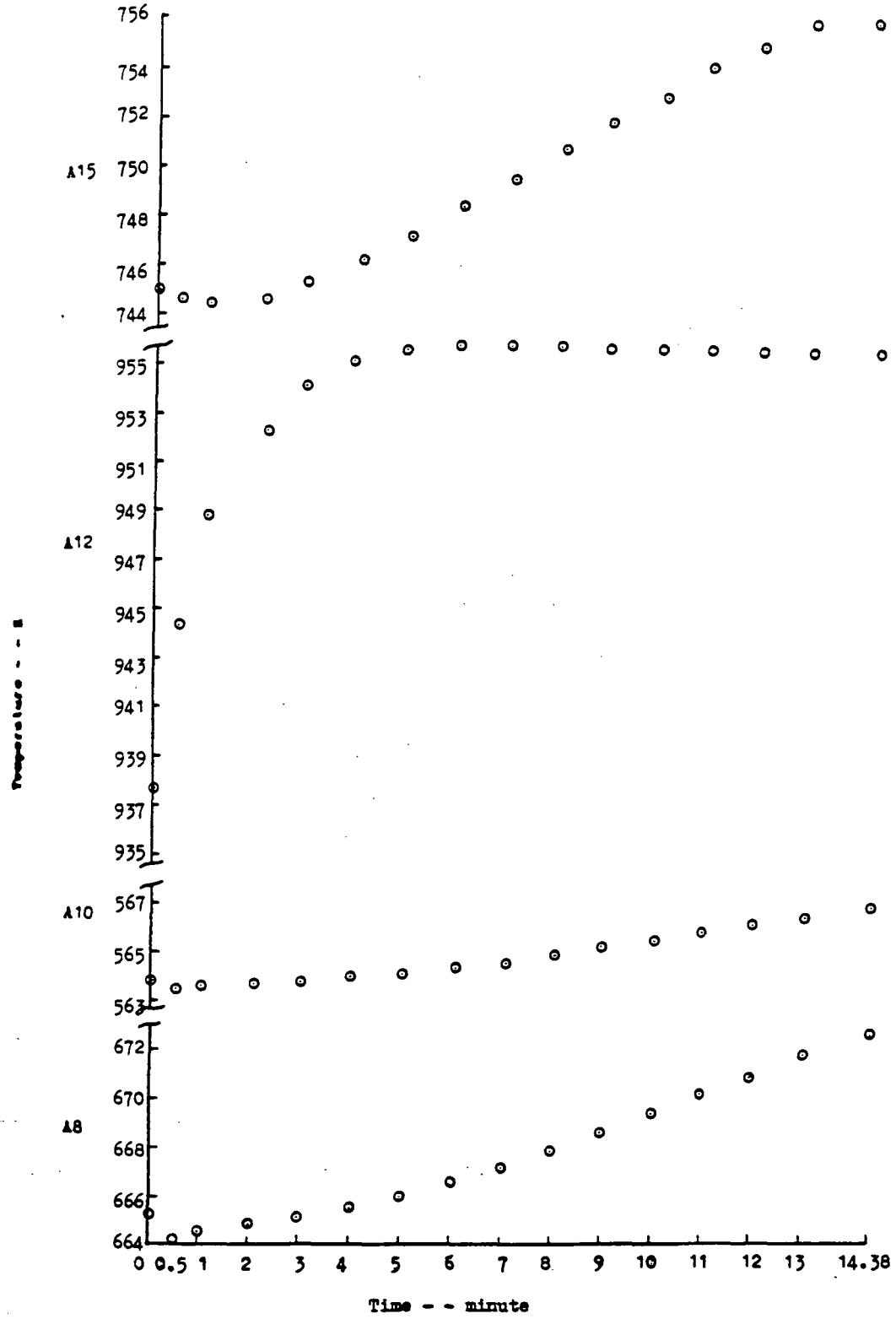

Figure 6-3 Location temperature changes with time
(Number refer to Figure 1-4)

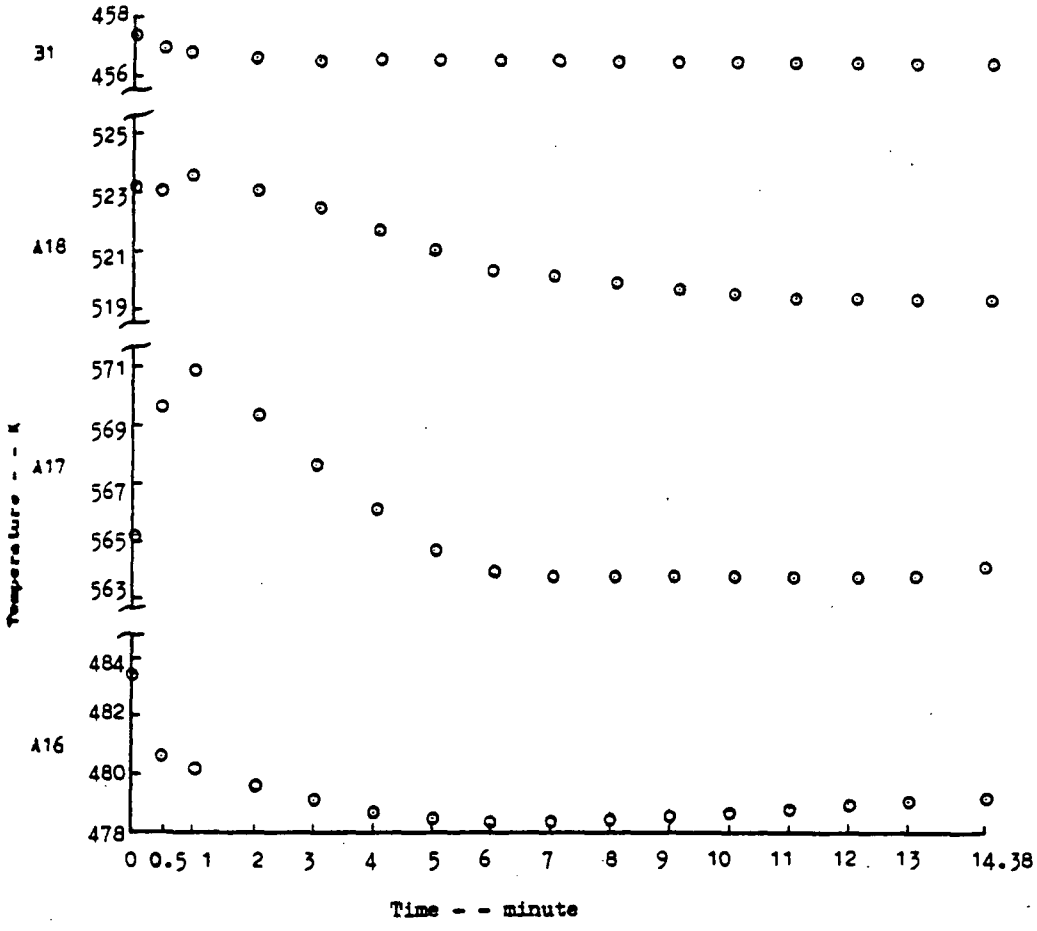

Figure 6-3 continued

outlet of reformer (A12); the outlet of the high temperature shift converter (A15); the shell-side outlet of the heat exchanger (A16); the outlet of the low temperature shift converter (A17); the shell-side outlet of the air heater; and finally, the anode outlet (B1). The nomenclature for the streams refers to Figure 1-4. Note that most of the stream temperatures fluctuate somewhat before the first minute. Because there are several process loops in the system, the temperature at any location is affected by other changes in the system. This is specially true for the initial changes which result from adjustments in the flow rates at four inputs: air for combustion and the fuel cell stack, and fuel for the reformer and the fuel cell stack.

Table 6-1 shows the operating conditions of the fuel cell stack in a transient period, the conditions include the operating voltage, mean current density, average temperature in the stack, anode side outlet temperature, operating pressure, and output power. Because a fixed anode inlet composition was assumed (Section 5.1), the fuel cell stack subsystem is independent from other components in the calculations. Therefore, the time needed for the fuel cell stack to reach the final steady is much faster than that of the whole system, actually, the fuel processing subsystem. The time period is 3.3 minutes compared to 14.38 minutes for whole system. In Table 6-1, it is evident that the current density and operating voltage are changing dramatically in the first 2 seconds when the manipulations (of input flow rates) occur, whereas no significant change in temperature appears after that time. Table 6-2 also lists the change of voltage and current density in the first two seconds. Note that the linear change in these two sets of data has

Time s	Operating voltage volt	Mean C.D. A/cm^2
0	0.667	0.325
0.324	0.669	0.319
0.540	0.671	0.316
0.756	0.673	0.312
1.08	0.676	0.305
1.296	0.678	0.301
1.512	0.680	0.296
1.836	0.683	0.290
2.052	0.685	0.287

Table 6-2 Operating voltage and mean current density of PAFC stack changing with time - small time scale

resulted from the linear manipulation of the inlet flow rates. In conclusion, the current density is initially affected by the concentrations (flow rates) of fuel and air during the adjustment period, and then by the temperature distribution in the stack. The resulting current density distribution also affects the temperature distribution at the same time.

It is difficult to see both of the distribution changes in Table 6-1. The temperature and current density at each finite-difference section of the middle strip in the symmetric plate (see Figure 2-17) are given in Table 6-3 and 6-4, respectively. Both of the changes at the outlet sections are greater than those of the inlet sections, they are 2.49 to 0.76 °K for the temperature and 0.0443 to 0.0306 A/cm² for the current density.

Appendix 10 provides a listing of the initial and final steady state solutions for the current density and the temperature distributions.

The assumption that the same concentrations of hydrogen occurs after the reformer and shift converters is not accurate (see the listing of the initial and final steady state performances). However there is only a 1.69% ((0.5928-0.5829)/0.5829) difference after the reformer and a 2.35% difference ((0.7000-0.6839)/0.6839) after the shift converters. The same conversion assumption is essential to calculate the inlet fuel flow rate for the first step. However, this does not greatly affect the anode inlet composition, because the cooling tower before the reservoir

Finite-difference section along air flow direction

Time - - sec. T-K	1	2	3	4	5	6
0	180.43	186.65	193.24	197.57	202.46	204.06
20	179.89	185.98	192.54	196.90	201.68	203.25
40	179.68	185.68	192.16	196.50	201.2	202.74
60	179.65	185.58	191.98	196.30	200.94	202.44
80	179.64	185.54	191.90	196.18	200.76	202.24
100	179.64	185.52	191.83	196.07	200.62	202.08
120	179.65	185.5	191.79	196.0	200.51	201.94
140	179.66	185.49	191.75	195.93	200.41	201.83
198	179.67	185.48	191.67	195.78	200.41	201.57

Table 6-3 Temperatures of the middle portions of the PAFC stack symmetric plate (see Figure 2-16) changing with time

Time - sec.	c.d.- A/cm^2	Finite-difference section along air flow direction					
		1	2	3	4	5	6
	0	.3074	.3204	.3357	.3397	.3431	.3311
	0.324	.3034	.316	.3307	.3343	.3372	.3252
	0.756	.2963	.3082	.3223	.3258	.3285	.3165
	1.08	.2903	.3018	.3153	.3184	.3210	.3096
	1.296	.2866	.2976	.3108	.3136	.3160	.3047
	1.512	.2829	.2936	.3063	.3090	.3112	.2998
	1.836	.2773	.2875	.2997	.3020	.3038	.2925
	2.052	.2749	.2849	.2969	.2990	.3006	.2893
	4.104	.2755	.2855	.2973	.2992	.3004	.2884
	60.48	.2763	.2856	.2970	.2990	.3000	.2881
	198	.2768	.2865	.2972	.2985	.2990	.2868

Table 6-4 Current densities of the middle portions of the PAFC stack symmetric plate (see Figure 2-16) changing with time

can provide some adjustment.

Although there is some CPU time spent in the iteration of the steady state solution, there is still too much CPU time spent in obtaining the transient solution. Other than running this program on a more powerful "supercomputer" (like CRAY-1), it is necessary to improve the computation time by adding some simplifying assumptions which will be discussed in the following chapter.

This program can be modified to simulate the startup and shutdown responses of PAFC system, but the procedures for these operations should be standardized beforehand.

CHAPTER 7

CONCLUSION

7.1 Summary

1. The fuel cell is an attractive option for electrical energy generation due to its high efficiency and lack of disturbance to the environment. Because of its flexibility in size and operating characteristics, the fuel cell can also be placed on-site at the point of end use. In this location, the fuel cell not only povides electricity but thermal energy as well.

2. Phosphoric acid fuel cells (PAFC) are the most advanced of all of the fuel cell technologies. Pilot plants up to 4.8-MW have been successfully operated.

3. The PAFC system has three subsystems, which are the fuel processor, the fuel cell stack, and the power conditioner. The fuel processor converts a hydrocarbon fuel to a hydrogen-rich gas that is fed to the fuel cell stack to produce DC power. The power conditioner transforms the DC power to AC power compatible with user's requirements.

4. The accuracy of digital simulation depends upon the mathematical models, parameter estimation, and numerical methods used.

5. There are two modeling methods used in this simulation, one is the lumped model and the other is the distributed model. The former uses

the thermodynamic balances to set up algebraic equations, whereas the latter use kinetic and thermodynamic expressions to form simultaneous ordinary-differential equations. The finite-difference method is used to solve the differential equations.

6. In distributed modeling, the reformer is treated as a combustion-gas heated heat-exchanger type catalytic reactor; the shift converters are treated as adiabatic catalytic reactors; and counter-current double pipe heat exchangers are used to model the heat exchangers in the PAFC system.

7. The steady state simulation of the reformer will be limited by the uncertainties of the rate expression and estimation of the heat transfer coefficient.

8. The regenerative type reformer recycles the product gas to save 10 to 15% of the energy in the combustion gas, which can be used to evaporate the water for reforming. In addition, this can be accomplished by means of an external heater using product gas to evaporate part of the required water.

9. The performance of the PAFC is controlled primarily by the rate of oxygen reduction on the platinum.

10. For the design of fuel cell systems, modeling is needed to obtain the local current generation as a function of position, flow rates, temperatures, feed concentrations, voltages, etc. Non-uniform current generation results in non-uniform heat generation in the cell. More heat should be removed at the locations of highest current density and thus highest heat generation . This gives rise to various possibilities

for devising better cooling schemes for optimum performance. Among the proposed cooling schemes in the cooling plate, the branched channel can obtain the best cooling effect but suffers from structural deflection and complication, however, the varying-width scheme can provide good uniformities of both current density and temperature and has a simple structure.

11. In the analysis of the fuel cell stack, both the concentration gradient and cooling scheme determine the uniformity of performance of the cell plate. High utilization of hydrogen or oxygen will increase the concentration gradient.

12. The models for steady state performance in the reformer, fuel cell stack, and the whole PAFC system agree very well with the experimental results.

13. The developed steady state model can be used in the design of the components and system of the PAFC. The model is also used for further simulation of the transient state.

14. A combined algorithmic-heuristic approach was developed to synthesize the heat-exchanger network in PAFC system. There was a 10% cost improvement from this synthesis.

15. Load change occurs in the operation of the power plant in both residential and commerial applications. Some transient operation methods and assumptions were developed in order to simulate the PAFC system response under transient conditions.

16. The dynamic study of each component was the first step in the

simulation of PAFC system's transient response. The distributed model was used to estimate the response of each component.

17. Usually, the stable time interval is a problem in a digital dynamic study. A small value will require a large amount of computation time and a larger truncation error will result, and the larger time interval values will lose information in the initial time interval and may result in a divergent solution.

18. The maximum value of the time interval in one component depends on the time required to travel one finite-difference section in a non-reacting component, or the sensitivity of the reaction rate to the temperature in the reactor.

19. Neglecting the kinetic considerations in the PAFC dynamic study results in no accumulation of components in each section and also in the equilibrium calculations in the transient state computation. Because the time constant of reaction rate process is less than that of the material transport and much less than that of the heat exchange, this assumption is acceptable.

20. The length of the computation times prevents the use of a real-time computer in the simulation of PAFC system's trnasient responses. By means of the "on-off" flags and a process controlled clock the real-time computation procedure was simulated on a batch-type computer.

21. Although no experimental data is available to test the transient state simulation of the components and system, the accurate steady state simulation, and the smooth transient responses, indicate reasonable dynamic results.

22. The computer program developed is useful for establishing the controller settings, to design a procedure for power ramping, and to study the transient responses.

7.2 DISCUSSION AND RECOMMANDATIONS

1. One way to decrease the computation time in the reactors is to assume no accumulation of components in the finite-difference section. This assumption was used in the simulation of the fuel cell stack in the transient study. There are two advantages resulting from this assumption: one is the simplification of the differential equations by deleting the concentration terms, and the other is the increased time interval. If the transport lag in the reactors is neglected, further increases of time interval are possible. A comparison was made with these simplified conditions in the reformer, which assumes a fixed wall temperature profile. The operation definitions, assumptions, and stable time intervals are shown in Figure 7-1, where Model I was used in Chapter 4, Model II was used in Chapter 6, and Model III was proposed here with previously discussed assumption(s). Model III-A, taken from Chapter 5, also includes the assumption of no accumulating components, in addition, Model III-B also assumes no transport lag in the reformer. It is evident that the stable time interval is dramatically increased 500 times by using Model III-B instead of Model I, or even in comparison with Model II (40 times). A futher reduction of computation time results from fewer variables in Model III. However, the results of Mode III-B lose the information for the design of the operation procedure (ramping rate) and controllers. If we treat the PAFC stack as a reactor, Model III-B can save a large amount of computation time.

2. Because of the iterative trial-and-error procedures in the steady state calculation, the accuracy of the final solutions depends on the convergence criteria. Loose criteria may result in an unstable

Descriptions	Model I	Model II	Model III	
			A	B
Additional Assumptions (all assumptions in Section 2.1.3 are available)		1. no temperature difference between stream and catalyst	1. no temperature difference between stream and catalyst 2. no accumulation of components in the finite-difference section 3. A: transport lag of each section is equal to one time interval B: no transport lag, time interval is greater than transport time through the reformer	
Time Interval	0.0072 sec.	0.09 sec.	0.18 sec.	3.6 sec.
Variables	1.mole fraction of CH_4 2.reforming gas density 3.reforming gas temp. 4.catalyst temp.	1.mole fraction of CH_4 2.reforming gas density 3.reforming gas temp.	1.reforming gas temp.	1.reforming gas temp.

General Descriptions: height of reformer: 40 ft

temperature profile of wall: $1300+17x-0.2x^2$, °F; x: height,ft

inlet temperature of reforming gas: 687°F

finite-difference sections number: 21

S.S. outlet conversion: 82%

kinetic expression: $10400 \cdot e^{-(20000/T)} \cdot P_{CH_4}$

where T in °R

initial condition: input flow rate decrease to 50% of original, rate: 50% per 0.18 sec.

Figure 7-1 Description of different models to compare the stable time interval

calculation (divergence) in the transient state calculation which uses the steady state solution as the initial conditions. The convergence error may accumulate with the initial manipulation changes and result in a divergent solution. A preliminary step can be taken to "stabilize" the steady state solution. The dynamic program with the steady state solutions is run, without any initial changes, until the difference between the calculated steady state solutions and the "stabilized" solutions is reduced, which means that the accumulation terms approach zero. This require some extra computation time, however, it is important to start from the "real" steady state conditions (the initial conditions).

3. Non-uniform temperature distribution in the stack results from non-uniform current density distribution. The non-uniform concentration profiles cause these non-uniformities. Use of Zee plate or hexagonal plate stated in Section 2.2.2 is one solution. The combinition of new cell plate configurations, effective cooling shemes, and suitable coolant is a goal for future research.

4. In order to reach a balance between accuracy and computation time, this system's dynamic model neglects some small changes which can be considered in future work. The steady and fixed transport lag in each component can be reconsidered as a function of position and time, the transport lags in pipes and auxiliaries can be estimated and added to the simulation. A more important consideration is that the conversions in reformer and shift converters should not be fixed. All of the calculation can be based on this data which will be updated with the most recent values.

5. Good models can also be used to explore behavior where only limited experimental data are available. For example, atmospheric pressure data can be used to model fuel cell performance at elevated pressures.

6. Digital simulation is a powerful tool for the design of the process plant, and it may be expected that the day will come when engineers will substitute pilot plant establishment with simulation on digital computers.

7. Although PAFC power plant operation is not as critical as that of a nuclear power plant, it is necessary to establish a simulator which can be used for the design of safety features. A number of "what if" questions (sometimes problems) can be answered with this type of simulator. The program developed here is really the first step in the development of a PAFC power plant simulator.

8. Other future research could be on (1) the estimation of wall heat transfer coefficients in a catalytic reactor, (2) the kinetic expression of the demethanation reaction, (3) a new algorithm with decomposition procedure for the heat exchanger network, (4) the reliable prediction of the current-voltage relationship.

REFERENCE

1. NEMA standard, Publ. No. CV 1-1968, National Electrical Mfgs. Assoc., New York, 1968

2. Benjamin, T.G., H.C. Elias, and L.G. Marianowski," Handbook of Fuel Cell Performance ," Institute of Gas Technology, DOE contract EC-77-C-03-1545, Chicago, Ill, May, 1980

3. Fickett, A.P., "Fuel-Cell Power Plants," Scientific American, p.70-76, Dec., 1978

4. Kordesch, K.V., "25 Years of Fuel Cell Development,(1951-1976)" J. Electrochem. Soc., Vol. 125, No. 3, 77c-91c, March, 1978

5. Tunnah, B.G. and B. Appelbaum, "Use of Fuel Cells in Refining," Hydrocarbon Processing, Vol. 57, No. 9, p. 119-122, July, 1978

6. Maru, H.C., C. Chi, D. Patel, and D. Burns, "Heat Transfer in Phosphoric Acid Fuel Cell Stacks," proceeding of the 13th intersociety energy conversion engineering conference, Vol. 1, p. 723-731, San Diego, August, 1978

7. Baukal, W., "Solid Oxide Electrolytes with Time Dependent Conductivity," From Electrocatalysis to Fuel Cells, University of Washington Press, Seattle, p. 247-254, 1972

8. "Advanced Fuel Cell Ready for a Tryout," Chemical Engineering, Vol. 90, p. 35-36, June, 1983

9. Bockris, J. O'M. and S. Srinivasan, " Fuel Cell: Their Electrochemistry ," McGraw-Hill, New York, 1969

10. Hoover, D.Q., " Cell and Stack Design Alternatives ," First Qtly. Rept. of Westinghouse Corp. to NASA, Lewis, Contract No. ET-78-C-03-2031, Jan. 1979

11. Hoover, D.Q., " Cell module and Fuel Conditioner Development ," Final Report of Westinghouse Corp. to NASA, Lewis, Contract No. DEN 3-161, Feb. 1982

12. Le, M.T., "A 7.5 MW Phosphoric Acid Fuel Cell System Concept with a Natural Gas Fueled Nonintegrated Fuel Processing Subsystem," DRM: 129, Westinghouse Electric Corporation, March 23, 1982

13. Murray, A.P., " BOLTAR Update-Methane Reformer Kinetic ," Rept. of Westinghouse Corp. to NASA, Lewis, D.O.E. Contract No. DEN 3-161, Aug. 27, 1981

14. Baker, B.S., D. Gidaspow and D. Wasan, "Thermal Phenomena in Fuel Cells and Batteries," in Tobias, C.W. (ed.), Advances in Electrochemistry and Electrochemical Engineering , Vol. 8, p. 63, Wiley, New York, N.Y., 1971

15. Gidaspow, D. and B.S. Baker, "Heat Transfer in a Fuel Cell Battery," A.I.C.H.E. Journal, Vol. 11, No. 5, p. 825, 1965

16. Alkasab, K.A., A.F. Presler, and C.Y. LU, " Thermodynamic and performance Model for Phosphoric Acid Fuel-Cell System," Proceedings of Sixth IASTED International Symposium on ENERGY '83, San Francisco, May 16-18, 1983

17. Pierce, B.L., "PAFC Power Plant Power Control Mode Trade Study," DRM: 95, Westinghouse Electric Corporation, Dec. 14, 1981

18. Rohsenow, W.M. and J.P. Hartnett, " Heat Transfer Handbook ," McGraw Hill, New York, 1973

19. Eckert, E.R.G. and R.M. Drake, " Heat and Mass Transfer ," Second Edition, McGraw Hill, New York, 1973

20. Kays, W.M. and A.L. London, " Compact Heat Exchangers ," McGraw-Hill, New York, 1958

21. Guy, J.L., "Modeling Heat-Transfer Systems," Chemical Engineering, Vol.89, No. 9 , p. 93-96, May 3, 1982

22. Perry, J.H. (ed.), " Chemical Engineers' Handbook ," 4th ed., McGraw-Hill Book Company, New York, 1981

23. Eley, D.D., H. Pines, and P.B. Weisz (eds.)," Advances in Catalysis ," Vol. 28, Academic Press, New York, 1979

24. Murray, A.P. and T.S. Snyder, " REPENT-Methane Reformer Kinetic Computer Model ," Rept. of Westinghouse Corp. to NASA, Lewis, D.O.E. contract No. DE-AC03-78ET11300, Feb. 5, 1980

25. Hyman, M.H., "Simulate Methane Reformer Reactions," Hydrocarbon Processing, Vol. 47, No. 7, p. 131-137, July 1968

26. Allen, D.W., E.R. Gerhard, and M.R. Likins, Jr., "Kinetics of the Methane-Steam Reaction," Ind. Eng. Chem., Process Des. Dev., Vol. 14, No. 3, p. 256-259, 1975

27. Pierce, B.L., "PAFC Power Plant Power Control Mode Trade Study," Westinghouse Report, DRM: 095, Dec. 1981

28. Chao, R.E., R.A. Caban, and M.M. Irizarry," Wall Heat Transfer to Chemical Reactors," Can. Chem. Eng., Vol. 51, p.67, 1973

29. Beek, J., "Design of Packed Catalytic Reactors," Adv. Chem. Eng., Vol. 3, p. 303, 1962

30. Thoenes, D., Jr., and H. Kramers, "Mass Transfer from Spheres in Various Regular Packing to a Flowing Fluid," Chem. Eng. Sci., Vol. 8, p. 271. 1958

31. Franks, R.G.E.," Modeling and Simulation in Chemical Engineering ," John Wiley & Sons, New York, p. 366, 1971

32. Aerov, M.E., and O.M. Todes, "Hydraulic and Thermal Basis of the Operation of Packed and Fluidized Bed Equipment," Chemija, Leningrad, 1968

APPENDIX

Appendix 1

Minimum Steam to Carbon Ratio

A possibility exists that during reforming elemental carbon may form and deposit on the catalyst bed. Primary control is by proper selection of a suitable steam/carbon ratio.

Many reactions are possible in this system. A few, including the more likely are as follow (Ref. A-1-1):

$$CH_4 = C + 2H_2 \qquad \text{(A-1-1)}$$

$$C + H_2O = CO + H_2 \qquad \text{(A-1-2)}$$

$$CH_4 + H_2O = CO + 3H_2 \qquad \text{(A-1-3)}$$

$$CO + H_2O = CO_2 + H_2 \qquad \text{(A-1-4)}$$

$$2CO = C + CO_2 \qquad \text{(A-1-5)}$$

$$CO_2 = CO + 1/2\ O_2 \qquad \text{(A-1-6)}$$

$$H_2O = H_2 + 1/2\ O_2 \qquad \text{(A-1-7)}$$

$$2CH_4 = C_2H_6 + H_2 \qquad \text{(A-1-8)}$$

Consideration of the values of these equilibrium constants indicates that, at normal reformer operating temperature, reactions (A-1-6), (A-1-7), and (A-1-8) can proceed only to negligible extents, and hence that O_2 and C_2H_6 cannot be appreciably present at equilibrium. If no carbon is to appear in the equilibrium mixture represented by these three reactions, it is necessary to add sufficient steam so that the activity ratio $a^2_{H_2}/a_{CH_4}$ may be equal to or greater than K1, the equilibrium constant of reaction (A-1-1), and that the activity ratio $(a_{CO})(a_{H_2})/a_{H_2O}$ be equal to or less than K2, the equilibrium constant of reaction (A-1-2). If the first ratio is greater than K1,

then carbon added to such a system can react with hydrogen and form methane until the ratio is reduced to K1. If the second ratio is less than K2, then carbon added to such a system can react with steam until the ratio is elevated to K2.

When the ratio of steam to methane in the feed is sufficiently high so that carbon cannot be present at equilibrium, the equilibrium composition may be calculated by considering only reactions (A-1-3) and (A-1-4), which involve all the significant reactants in the absence of carbon. In order to determine the minimum steam ratio required for freedom from carbon, a constrained minimization problem was set up:

min. $x(3)$

subject to:

$$1.\ \frac{(3x(1)+x(2))^2\,P}{(1-x(1))(1+x(3)+2x(1))} > K1$$

$$2.\ \frac{(3x(1)+x(2))(x(1)-x(2))\,P}{(x(3)-x(1)-x(2))(1+x(3)+2x(1))} < K2$$

$$3.\ \frac{(x(1)-x(2))(3x(1)+x(2))^3\,P^2}{(1-x(1))(x(3)-x(1)-x(2))(1+x(3)+2x(1))^2} = K3$$

$$4.\ \frac{x(2)(3x(1)+x(2))}{(x(1)-x(2))(x(3)-x(1)-x(2))} = K4$$

$$5.\ \frac{x(2)(1+x(3)+2x(1))}{(x(1)-x(2))^2\,P} > K5$$

$$6.\ x(2)-x(1) < 0$$

where $x(1)$: moles CH_4 converted by reaction (A-1-3)

$x(2)$: moles CO converted by reaction (A-1-4)

$x(3)$: steam to carbon ratio

K1, K2,..., K5: equilibrium constant of reaction (A-1-1),

..., (A-1-5)

So at equilibrium (assume initial CH is 1 mole),

moles CH_4: 1 - x(1)

H_2O: x(3) - x(2) - x(1)

CO: x(1) - x(2)

CO_2: x(2)

H_2: 3x(1) + x(2)

Total moles: x(3) + 1 + 2x(1)

This minimization problem was solved by COMPUTE computer program (Ref. A-1-2). The COMPUTE code solves the constrained optimization problems using mixed penalty funtion* together with Hooke and Jeeves pattern search method for extremization.

Each equilibrium constant was calculated utilizing a correlation of the form

$$\ln K = \frac{a}{T^3} + \frac{b}{T^2} + \frac{c}{T} + d. \qquad \text{(A-1-9)}$$

This correlation is found to be a very good fit over the range 800-2000

*: By mixed penalty functions, we mean if the first l constraints are inequalities and constraints (l+1) to m are equalities, our problem becomes: minimize $\phi = fo(x) - K \sum_{i=1}^{l} \ln(gi(x)) + 1/K \sum_{i=l+1}^{m} (gi(x))^2$. The function $\phi(x,K)$ is then minimized for a sequence of monotonically decreasing K > 0.

T_c (°C) / P (atm)	450	500	550	600	650	700	750	800
1	0.94	1.18	1.35	1.38	1.28	1.15	1.05	1.01
2	0.75	0.97	1.15	1.26	1.25	1.16	1.07	1.01
3	0.66	0.85	1.03	1.16	1.19	1.15	1.07	1.01
4	0.60	0.78	0.96	1.09	1.14	1.12	1.06	1.00
5	0.56	0.73	0.90	1.03	1.10	1.10	1.05	0.99

Table A-1-2 Minimum steam/carbon ratio at different temperatures and pressures

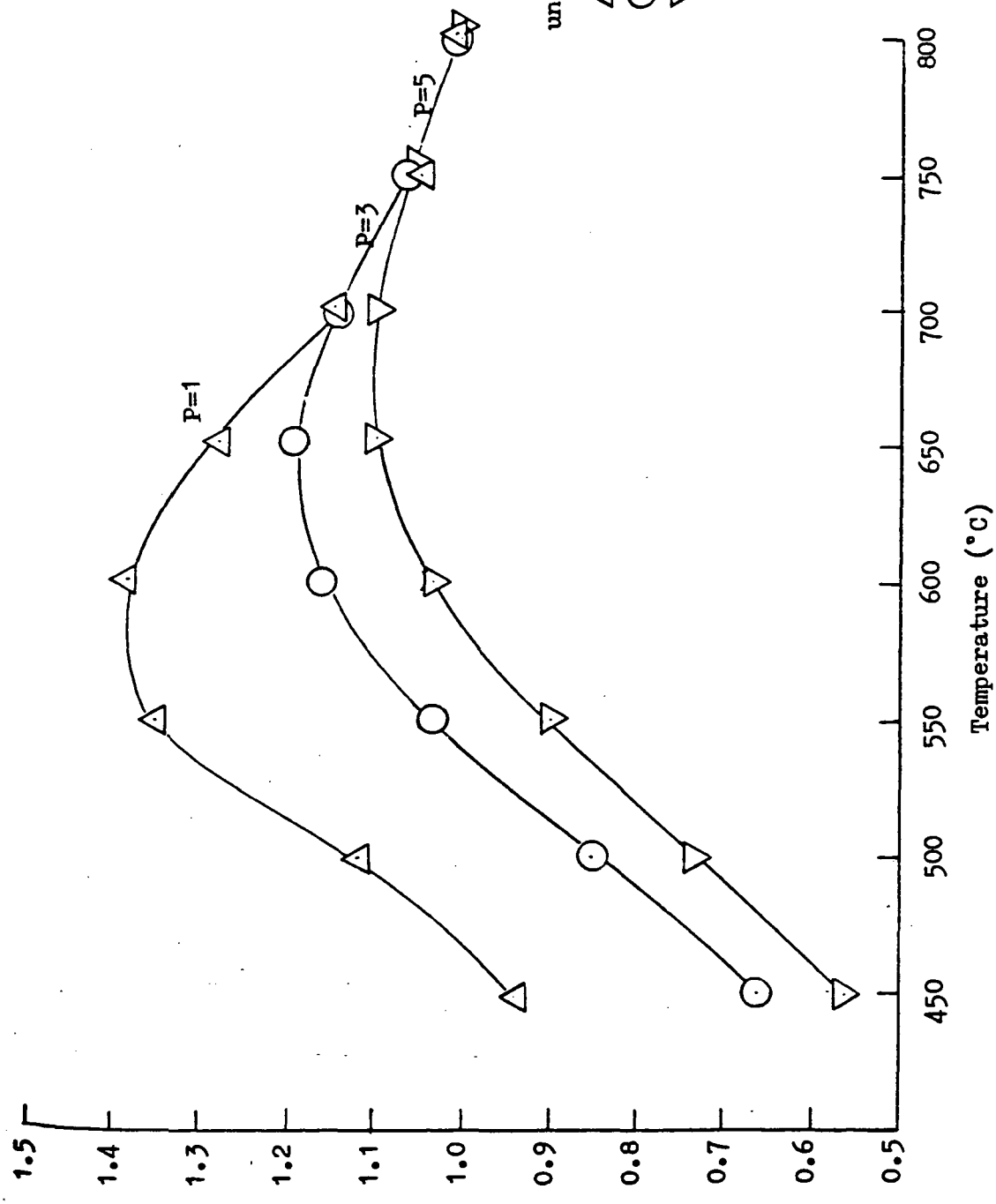

Figure A-1-1 Minimum S/C ratio at different temperatures and pressures

Reference

A-1-1: Hougen, O.A. and K. Watson," Chemical Process Principles Part two - Thermodynamics, " John Wiley & Sons, Inc., New York, 1947, p. 731-736

A-1-2: Lu, C.Y., " Global Optimization in Engineering Design Problems, " Master thesis, University of Cincinnati, June 1980

A-1-3: Smith, J.M., and H.C. Van Ness, " Introduction to Chemical Engineering Thermodynamics, " 3d ed., McGraw-Hill Book Company, New York, 1975

Appendix 2

External and Internal Effectiveness Factors in Reformer and Shift Converters

Consider the fixed bed of catalyst particles shown in Figure A-2-1. In general the easiest parameters to measure in such a reactor are inlet and outlet conditions and perhaps a temperature profile.

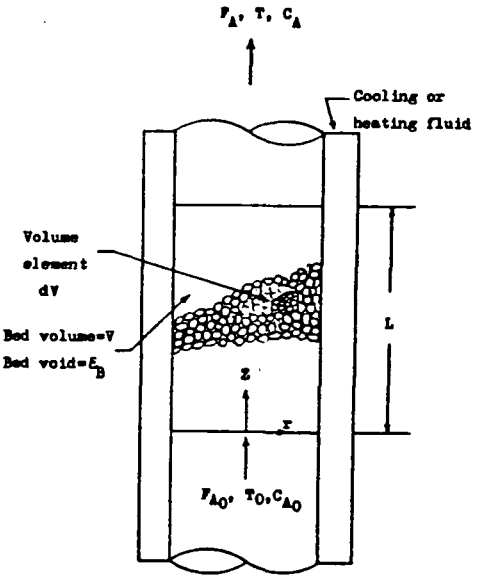

Figure A-2-1 Fixed bed reactor

The surface reaction rate expression explicitly contains concentration and temperature terms which must be evaluated at the surface. These conditions may be very different from the measurable conditions.

If we let the observed (sometimes termed "global") reaction rate of component A in a fixed bed reactor, r_A, be a function of the measurable quantities,

$$r_A = r_{obs} = r_{global} = a\, Rs(C_{AO}, C_{BO}, \ldots, T_O)\, E\tau \qquad \text{(A-2-1)}$$

where a = active catalyst surface area/unit volume of reactor bed (sq.ft. catalyst/ cu.ft. bed)

R = heterogeneous (surface) reaction rate, (#moles A/(hr)(sq.ft. active catalyst))

E = internal "effectiveness" factor

τ = external "effectiveness" factor

CAo, CBo,..., To = bed avg. comp. and temp.

The internal effectiveness factor, E, accounts for the differences between concentration and temperature at the external surface of a catalyst particle (CAs, Ts) and on the inside of the catalyst pores (CA , T).

The external effectiveness factor, τ , accounts for the differences between conditions at catalyst surface (C_{As}, Ts) and the bulk gas (CAo, To).

Internal Effectiveness Factor

An examination of Figure A-2-2 shows that the concentration of reactant A is at maximum at the pore mouth and then decreases down the length of the pore. Thus, the surface reaction rate must vary toward the center of the catalyst particle. We need to evaluate the difference between the actual reaction rate in the pore and the rate when the pore mouth concentration prevailed throughout the pore.

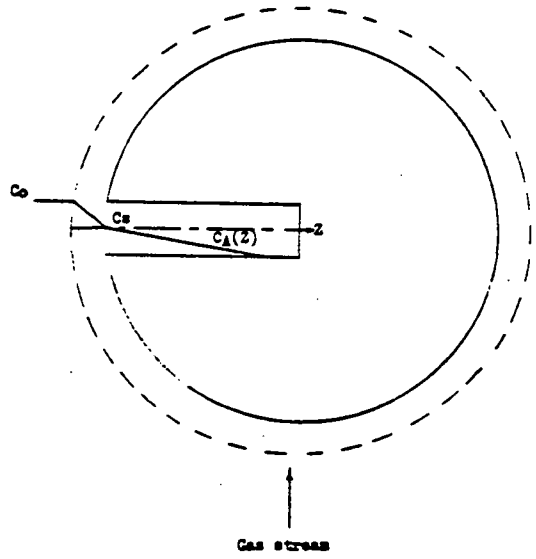

Figure A-2-2 Model of a catalyst bead with a micropore

This difference is evaluated in terms of the internal "effectiveness factor" which is the ratio of the rate of the process occuring in the pore to the chemical reaction rate which would occur if the inner pore surface was totally exposed to the pore mouth concentration.

Thus,

$$E = \frac{\text{Rate of process occurring in the pore}}{\text{Rate of surface reaction @ gas phase conds.}}$$

External Effectiveness Factor

No matter how active a catalyst particle is, it can be effective only if the reactants can reach the catalytic surface. The transfer of reactant from the bulk fluid to the outer surface of the catalyst

particle requires a driving force, the concentration difference. The concentration of reactant is smaller at the surface than in the bulk fluid. Hence the observed rate, the global rate, is less than the intrinsic rate evaluated at the concentration of reactant in the bulk fluid. The same reasoning suggests that there will be a temperature difference between bulk fluid and catalyst surface. External effectiveness factor is to evaluate these differences. Thus

$$\eta = \frac{\text{heterogeneous surface reaction rate @ surface conditions}}{\text{heterogeneous surface reaction rate @ bulk gas conditions}}$$

Effectiveness Factors of Catalysts Used in the Reformer and Shift Converters

There are several different kinds of of catalysts used in the reformer and shift converters. For instance, in the reformer, there are four kinds of catalyst for experimental or industrial use: Girdler's G-56B (Ref. 9 and 10), I.C.I. 57-1 (Ref. 11 and 12), Catalyst 100, and Halder Topsφe's RKNA/S (Ref. 11). In this study, only one kind of catalyst for each kind of reactor is examined, which are Girdler's G-56B for reformer, 93% Fe_2O_3 and 7% Cr_2O_3 (Ref. 13 and 14) for high temperature shift converter, and Girdler's G-66B (Ref. 15) for low temperature shift converter.

The definitions of variables and algorithm used in the calculations of both internal and external effectiveness factors are in Table A-2-1 and A-2-2, respectively. The data of catalysts, reactions, and the reacting gases are listed in Table A-2-3. Some catalyst data is estimated from similar kind of catalyst.

The final results are listed in Table A-2-4. The G-56B catalyst shows small internal effectiveness factor, which means the concentration of methane and the temperature of the reforming gas are much lower down the pore than at the pore mouth. Therefore, the calculation of global reaction rate of demethanation reaction in the reformer should consider this difference if G-56B is used as the catalyst. The assumption, which neglects the internal effectiveness in calculating the reaction rate, is generally correct in the simulation of shift converter. Usually when the differences between the conditions at catalyst surface (C_{As}, T_s) and

Variable	Description	Unit
DP	size (diameter) of catalyst	ft
APR	average pore radius	Å
PP	catalyst porosity	
II	shape of catalyst	
IM	model used in cal. effective diffusivity	
RMA	aver. radius in macro region (IM=2)	Å
RMI	aver. radius in micro region (IM=2)	Å
EPA	void fraction in macro region (IM=2)	
EPI	void fraction in micro region (IM=2)	
NA	stoi. number of reactant (IM=1)	
NB	stoi. number of product (IM=1)	
TOR	tortuosity factor (IM=1)	
DAE	effective diffusivity (IM=3)	ft^2/hr
RID	internal dia. of reactor	ft
BWE	bed weight	lb
BD	bed density	lb/ft^3
BTH	bed length	ft
EPS	bed porsity or for sphere (Ref. 1 & 2)	
TOP	operating temperature	R
P	operating pressure	ATM
X	conversion	
FL(i)	average flow rate of gas i i=1:CH_4, 2:CO, 3:CO_2, 4:H_2O, 5:H_2, 6:N_2, 7:O_2	lb-mole/hr
DLC	thermal conductivity of catalyst	BTU/hr-ft-R
FACTR	factor for cal. effective diff. (option)	
ACT	activation energy	BTU/lb-mole
N	order of reaction	

Table A-2-1 Definitions of variables for calculating effectiveness factors

(1) Check radial temperature gradient; (Ref. 5)

(2) Check axial dispersion effect; (Ref. 5)

(3) Check differential reactor approach;

(4) Calculate superficial mass flow rate of bulk gas (GO);

(5) Calculate Reynold Number (RE); (Ref. 6)

(6) Calculate Chilton and Colburn JD factor (JD); (Ref. 3)

$$JD = 1.82 * RE^{**}(-0.51) \quad RE < 350.$$
$$JD = 0.99 * RE^{**}(-0.41) \quad RE > 350.$$

(7) Calculate Schmidt Number (SC); (Ref. 4, 6, and 7)

(8) Calculate mass transfer coefficient (KG);

(9) Calculate (or input) observed reaction rate (ROBS);

(10) Calculate characteristic length (AC);

(11) Calculate Damkohler Number (DA);

(12) Calculate (or input) effective thermal conductivity (DLA); (Ref. 4 and 6)

(13) Calculate Prandtl Number (PR); (Ref. 6)

(14) Calculate factor BATA;

(15) Calculate Weisz Number (Arrhenius Group) (RO);

(16) Use Newton's method to estimate external effectiveness factor;

(17) Calculate surface conc. (CAS);

(18) Calculate surface temp. (TS);

(19) Check the conc. and temp. differences are significant or not; (Ref. 5)

Table A-2-2 Algorithm to calculate internal and external effectiveness factors

(20) Calculate internal effective diffusivity (DAE); (Ref. 4)
(21) Calculate Damkohler Group II (PHI);
(22) Calculate heat generation function (BAT); (Ref. 5)
(23) Calculate max. internal temp. difference;
(24) Check plots in (Ref. 8) to estimate internal effectiveness factor or check PHI (1./ABS(N-RO*BAT)) (Ref. 5) to see internal effectiveness factor is significant or not (5% interval)

Table A-2-2 continued

DATA

Catalyst	G-56B	93% Fe_2O_3 7%Cr_2O_3	G-66B
Reaction	steam reforming	water shift (high)	(low)
DP	0.015625	0.001837	0.00177
APR	305.	32.5	175.
PP	0.407	0.623	0.56
II	2	1	1
IM	2	3	1
RMA	993.		
RMI	33.2		
EPA	0.328		
EPI	0.0792		
NA			-1
NB			1
TOR			4.
DAE		0.02286	
RID	0.0677	0.002133	1.41
BWE	0.02866	0.001433	668.
BD	80.	85.52	76.78
BTH	0.1025	0.0469	5.58
EPS	0.467	0.39	0.51
TOP	1640.	1177.5	888.
P	1.	1.	1.5
ROBS		6.52482	
X	0.054		0.78
FL(1)	0.02145	0.	0.234
(2)	0.0003968	0.0004966	0.37
(3)	0.001708	0.0004192	2.626
(4)	0.0653	0.000854	2.29
(5)	0.001984	0.00038	13.27
(6)	0.	0.	0.
(7)	0.	0.	0.
DLC	1.	0.5	7.
FACTR	0.07		
ACT	36000.	43200.	22860.
N	1	1	1

Table A-2-3 Input data of examined catalysts

	G-56B	93% Fe_2O_3 7% Cr_2O_3	G-66B
CAS/CAO	0.99	0.998	0.9999
TAS/TAO	0.99	1.000	1.000
External Effectiveness Factor	0.8872	1.01	0.9999
Max. Internal Temp. Diff.	-27.8	0.87	0.042
Internal Effectiveness Factor	0.3	1.00	1.00

Table A-2-4 Results of examined catalysts

the bulk gas (C_{Ao}, To) are small, then the external effectiveness factor is close to 1.

Reference

A-2-1: Lapidus, L. and N. R. Amundson (eds)," Chemical Reactor Theory - A Review, " Prentice-Hall, Engliwood Cliffs, N. J., 1977

A-2-2: Roblee, L. H. S., R. M. Baird and J. W. Tierney, "Radial Porosity Variations in Packed Beds," A.I.C.H.E. J., vol. 4, No. 4, p.460-464, Dec. 1958

A-2-3: Perry, J. H. (ed.)," Chemical Engineers' Handbook, " 4th ed., McGraw-Hill Book Company, New York, 1963

A-2-4: Smith, J. M., " Chemical Engineering Kinetics, " 3rd ed., McGraw-Hill Book Company, New York, 1981

A-2-5: Satterfield, C. N.," Heterogeneous Catalysis in Practice, " McGraw-Hill Book Company, New York, 1980

A-2-6: Reid, R. C. and T. K. Sherwood," The Properties of Gases and Liquids, " McGraw-Hill Book Company, New York, 1958

A-2-7: Gilliland, E. R.,"Diffusion Coefficients in Gaseou System," Ind. Eng. Chem., vol. 26, p. 681, 1934

A-2-8: Weisz, P. B. and J. C. Hicks, Chem. Eng. Sci., vol. 17, p 265 (1962)

A-2-9: Allen, D. W., E. R. Gerhard and M. R. Linkins, Jr. "Kinetics of the Methane-Steam Reaction" Ind. Eng. Chem., Process Des. Dev., vol. 14, No. 3, 1975

A-2-10: Brown, L. F., H. W. Haynes and W. H. Manogue, "The Prediction of Diffusion Rates in Porous Materials at Different Pressures" J. of Catalysis, vol. 14, p. 220-225, 1969

A-2-11: Thomas, C.L.," Catalytic Process and Proven Catalysts ," Academic Press, New York, 1970

A-2-12: (I.C.I.) Catalyst Handbook, Wolfe Scientific Books, London, 1970, Springer-Verlag, New York

A-2-13: Eley, D. D., H. Pines and P. B. Weisz (eds.), " Advances in

Catalysis, " vol. 28, p. 265, Academic Press, New York, 1979

A-2-14: Podolski, W. F., and Y. G. Kim,"Modeling the Water-Gas Shift Reaction," Ind. Eng. Chem., Process Des. Dev., vol.13, No. 4, p. 415-420, 1974

A-2-15: Baldi, G, S, Goto, C.-K. Chow, and J. M. Smith," Catalytic Oxidation of Formic Acid in Water. Intraparticle Diffusion in Liquid-Filled Pores," Ind. Eng. Chem., Process Des. Dev., vol. 13, No. 4, p. 448, 1974

[illegible] problem include [illegible] based on [illegible] (for example, B&B enumeration, Ref. A-3-12), and [illegible] methods which often involve some established optimization principles (for example, Branch-and-Bound in Ref. A-3-6;

Appendix 3

Heat Exchanger Network

A combined algorithmic-heuristic approach to the systematic synthesis of heat exchangers, heaters, and coolers is proposed. This three-phases algorithm may generate, with great ease and considerable rapidity, a near optimal exchanger network. All the sample problems ranging in size from 4 to 10 streams were examined.

Results compare favorably with the presently available techniques and allow to handle realistically large problems.

Introduction

The area of energy conservation that has been receiving increased attention is the improved process heat recovery. Any heat recovered and reused in the process not only reduces the amount of fuel consumed but also lowers the amount of heat rejected to the cooling system.

Essentially, the synthesis task consists of finding a feasible sequence of heat exchangers in which pairs of streams are matched, such that the network is optimal as the total cost is minimum.

The general techniques that have been developed recently for solving this problem include the heuristic approach which is based on the use of rules of thumb (for example, H/H combination in Ref. A-3-12), and algorithmic methods which often involve some established optimization principles (for example, Branch-and Bound in Ref. A-3-6;

illustrate the method. The results are compared with the present synthesis methods. Also, more detail considerations of different structures are examined and some recommendations are also given.

Although this proposed method does not favor all the problems, less computation time and relatively easier algorithm still give us good understanding in this kind of problems.

Further extensions of the present approach along with decomposition for the synthesis of heat exchanger network are recommended.

Problem Statement

The synthesis problem to be considered has been defined by Masso and Rudd (Ref. A-3-9). In brief, there are M hot streams Shi(i=1,2,...,M) to be cooled and N cold streams Scj(j=1, 2,...,N) to be heated. Associated with each stream are its known input temperature Ti, output temperature Tti, and heat capacity flow rate Wi. There are also available auxiliary steam heater and water coolers Suk(k=1,2,...,p) called utilities. The problem is to create a minimum cost network of exchangers, heaters and/or coolers so that the desired output temperature of each process stream is reached. Heat transfer area of an exchanger of this type is expressed by

A = Q*log(d2/d1)/(UF*(d2-d1))

where d1=Tho-Tci, d2=Thi-Tco.

In general, the investment cost for the ith exchanger, heater, and cooler, denoted by Cei, Chi, and Cci, respectively, can be correlated to their corresponding heat transfer area Aei, Ahi, and Aci by the

empirical expressions Cei=a*Aei**b, Chi=a*Ahi**b, and Cci=a*Aci**b. The total cost of investment and utility of the network to be minimized can be expressed as

$$J=d*\left(\sum_{ei} a*Aei**b+\sum_{hi} a*Ahi**b+\sum_{ci} a*Aci**b\right)+\sum_{k}\sum_{l} uk*Sukl \qquad \text{(A-3-1)}$$

For convenience, the following simplifying assumptions, which have been used in most previous studies of synthesis of heat exchanger networks, are included: the use of countercurrent shell and tube exchangers with minimum allowable approach temperature (MAAT), no phase changes of process streams, and equal values of the effective heat transfer coefficients for all exchangers. The illustrative examples in this paper are all taken from the literature, and their specifications of process streams and design data are summarized in Table 1 and 2.

Algorithm

phase I:

(1) Calculate the upperbound of heat duty on the level of energy recovery.

(2) Calculate the minimum heating capacity in the heater.

(3) Select Tct*=Max(Tcti) and Th*=Max(Thj) corresponding to cold stream i and hot stream (include heater) j, respectively.

(4) Consider a exchanger or heater deciding the Th* of which Tct* and Th* are the cold outlet and hot inlet temperature respectively.

(5) Use an appropriate heuristic (maximal heat recovery or minimal exchanger area for example) to determine the quantity of heat transferred in this exchanger, while for heater the minimum heating capacity is considered.

	4SP1	All other problems
Steam:		
Pressure (lb/in.^{2}abs)	962.5	450.0
Latent heat (Btu/lb)	656.6	767.5
Temperature (°F)	540	456
Cooling water:		
Temperature	100 °F	
Heat capacity	1.0 Btu/lb°F	
Maximum water output temperature	180°F	
Minimum allowable approach temperatures:		
Heat exchanger	20 °F	
Steam heater	25 °F	
Water cooler	20 °F	
Overall heat transfer coefficients:		
Heat exchanger	150 Btu/hr ft^2 °F	
Steam heater	200 Btu/hr ft^2 °F	
Water cooler	150 Btu/hr ft^2 °F	
Equipment down time	380 hr/yr for 4SP1 and 6SP1	
	260 hr/yr for all other problems	
Network cost parameters	a = 350 b = 0.6	
Annual rate of return	δ = 0.1	
Cooling water cost	5 x 10^{-5} \$/lb	
Steam cost	1 x 10^{-3} \$/lb	

Table 2 Design Data

(6) Calculate the new conditions for the exchanged system and delete the fulfilled stream.

(7) Repeat steps (3) to (6) until no further matches can be made.

(8) Heat any remaining Tci to Tcti using heaters, and cool any Thi to Thti with coolers.

The above procedure will generate only one process, but it is nearly always close to the optimum.

Phase II

(1) Calculate the lower bound of units by the following rule (Ref. A-3-3)

"The minimum number of units is nearly always one less than the number of streams required in the problem".

(2) Eliminate the unnecessary heaters when the minimum capacity of heater criterion is violated.

(3) Eliminate the unnecessary exchangers by evolutionary rules (Ref. A-3-7 and A-3-8).

(4) Go back to phase I and recalculate the new structure and compare to the original one. If improved result is obtained go to Phase III; otherwise, keep the original structure and go to Phase III.

Phase II can be omitted when the criterion (stated in (2)) is not violated. It also can skip steps (1) and (3).

Phase III

(1) Count the number, NC, of "critical" exchangers (which means that the approach temperature is equal to MAAT).

(2) If NC=0, the optimal solution has been obtained;

if NC=1, Golden-ratio search method is used to find optimal MAAT and the results;

if NC>1, Pattern search method is used to find optimal MAAT and the results.

Results and Comparison

The sample problems listed in Table 1 are solved using this algorithm by IBM/370. These results have been compared with other approaches and summarized in Table 3.

Discussion and Recommendation

Phase III will improve a lot in Problem 4SP1. The Golden-ratio search method is discussed in Ref. A-3-10, and the results are summarized in Table 4. However, in other problems the improvement will not be apparent (see Table 5). Whether the optimal MAAT will be larger or smaller than 20 °F is dependent on the temperature differences in the "critical" exchanger and properties of streams. In conclusion, 20 °F is a good approach of MAAT and Phase III can be omitted for saving computation time.

Cost of	4SP1	4SP2	5SP1	6SP1	7SP1	7SP2	10SP1
Masso and Rudd			38762		34376	28328	
Lee et al	13688a	72400 (acyclic)	38762a	37331			
McCalliard and Westerberg	13688a		38762a	35780			
Pho and Lapidus	13688a		38762	35659	32152a	28518b	44160
Rathore and Powers	13590						
Ponton and Donaldson	13590	23716d	45199	35407	40625		44673
Kelahan and Gaddy	10634		38762	35048			
Nishida et al.	13590	20353c	38713c	35010			43984
Linnhoff and Flower	13590	21644ad 19557ac	38777a	35010	35735a	27960a	43949a
This work	10586e	21921df 19512c	38762	35010	30414f	29325	44389h 44675i

a: the cost is corrected for the different design data used here
b: not feasible
c: splitting
d: cyclic
e: MAAT 1.39 F
f: MAAT 24.47 F
g: MAAT 40 F
h: max. heat recovery
i: min. exchanger area

Table A-3-3 Comparison with Previous Studies

MAAT (F)	Cost of Problem 4SP1
20	13590
15.5	12746
9.6	11695
5.9	11099
3.7	10781
1.4	10586

Table A-3-4 Search for Optimal MAAT of Problem 4SP1

MAAT (F)	Cost of Problem 7SP1
20	30850
22	30754
25	30654
27	30597
30	30534
35	30453
40	30414

Table A-3-5 Search for Optimal MAAT of Problem 7SP1

"Cyclic" structure is better than "acyclic" structure espically in the problems where the number of hot streams is quite different from the number of cold streams. Some algorithmic methods (Ref. A-3-6 and A-3-11) can only obtain acyclic solution and should not be considered in solving this kind of problems. The most apparent example is 4SP2, the result is a three-fold decrease in annual cost.

"Splitting" structure was discussed by Linnhoff and Flower (Ref. A-3-8) and will not be repeated here. Two different answers of 4SP2 using splitting structure are listed in Table 3. Our solution uses usual optimal technique to obtain optimal splitting ratio and is referred to that of Linnhoff and Flower's. Although this procedure is not included in our algorithm in which splitting structure can not be created, it is worthy to note the difference for this special problem. Besides, in order to ensure that its temperature difference at the hot end does not, in turn, violate MAAT, the heat capacity flow rate chosen for the bypass must not be chosen below a certain threshold value.

Maximal heat recovery or minimal exchanger area approach for calculating the duty of heat exchanger in which Qci is larger than Qhj is considered in this work (in Phase I). Though it does not make much difference in Problem 10SP1 (see Table 3 the last two results), it is a good consideration to obtain a better solution. Some constraints and criteria are mentioned for choosing these different approaches in our algorithm.

This proposed algorithm does not guarantee the "best" solutions

(neither do the other approaches), but the less computation time, relatively easier algorithm, and almost optimal solution still make it attractive to go further.

Decomposition method is recommended to combine with this proposed algorithm and hopefully will give a better result. An element duty Q is chosen by the greatest common divisor of overall duty (Qhi or Qci), then we substitute each cold or hot stream by a number of equivalent pseudo-streams with each one labelled by a duty Q. These pseudo-streams are then solved by the procedures described in this paper. A large number of pseudo-streams, which exists in the revised problem, will result in longer computation time.

Reference

A-3-1: Cena, V., C. Mustacchi, and F. Natali,"Synthesis of Heat Exchanger Networks: A Non-Iterative Approach," Chem. Eng. Sci., vol. 32, p. 1227, 1977

A-3-2: Gottfried, B. S., and J. Weisman, Introduction to Optimization Theory, " Prentice Hall, New Jersey

A-3-3: Hohmann, E. C., and F. J. Lockart,"Optimum Heat Exchanger Network Synthesis," Paper No. 22a, A.I.C.H.E. National Meeting, Atlantic City, N. J., 1976

A-3-4: Hwa, C. S.,"Mathematical Formulation and Optimization of Heat Exchanger Networks Using Separable Programming," A.I.C.H.E.-Intern. Chem. Eng. Symp. Series, No. 4, p. 101, 1965

A-3-5: Kelahan, R. C., and J. L. Gaddy,"Synthesis of Heat Exchanger Networks by Mixed Integer Optimization," Paper No. 22c, A.I.C.H.E. National Meeting, Atlantic City, N. J.

A-3-6: Lee, K. F., A. H. Masso, and D. F. Rudd,"Branch and Bound Synthesis of Integrated Process Design," Ind. Eng. Chem. Fundamentals, vol. 9, p. 48, 1970

A-3-7: Nishida, N., Y. A. Liu, and L. Lapidus,"Studies in Process Design and Synthesis: III A Simple and Practical Approach to the Optimal Synthesis of Heat Exchanger Networks," A.I.C.H.E. J., vol. 23, p. 77, 1977

A-3-8: Linnhoff, B. and J. R. Flower,"Synthesis of Heat Exchanger Networks: I Systematic Generation of Energy Optimal Network," A.I.C.H.E. J., vol. 24, p. 633, 1978

A-3-9: Masso, A. H., and D. F. Rudd,"The Synthesis of System Design: Heuristic Structuring," A.I.C.H.E. J., vol. 15, p. 10, 1969

A-3-10: McGalliard, R. L., and A. W. Westerberg,"Structrual Sensitive Analysis in Design Synthesis," Chem. Eng. J., vol. 4, p. 127, 1972

A-3-11: Pho, T. K., and Leon Lapidus,"Topics in Computer-Aided Design II: Synthesis of Optimal Heat Exchanger Network by Tree Searching Algorithms," A.I.C.H.E. J., vol. 19, p. 1182, 1973

A-3-12: Ponton, J. W., and R. A. B. Donaldson,"A Fast Method for the Synthesis of Optimal Heat Exchanger Networks," Chem. Eng. Sci., vol. 29, p. 2375, 1974

A-3-13: Rathore, R. N. S., and G. J. Powers,"A Forward Branching Scheme for the Synthesis of Energy Recovery System," Ind. Eng. Chem. Process Design Develop., vol. 14, p. 175, 1975

Appendix 4

Use Laplace Transform Method to Solve Transient Convective Heat Transfer in the Channels

In the mathematical function of the transient convective heat transfer along the channels in the fuel cell stack, only one grid is considered, is

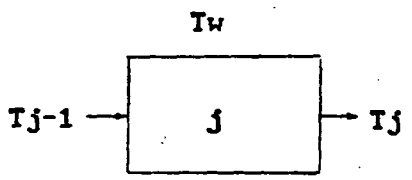

$$\rho AoC \frac{T}{\theta} = hs\ (Tw(\theta) - T) - \dot{m}C \frac{T}{x} \qquad (A\text{-}4\text{-}1)$$

where $T = T(x,\theta)$

B.C. $x = 0 \quad T = Tj \quad (\theta)$

I.C. $\theta = 0 \quad T = T'$

where ρ : molar density

Ao: cross area per channel

θ : time

' : previous value

then $$\frac{\partial T}{\partial \theta} = \frac{hs}{AoC}(Tw(\theta)-T) - \frac{\dot{m}C}{A_oC}\frac{\partial T}{\partial x} \qquad (A\text{-}4\text{-}2)$$

Let $\frac{hs}{AoC} = A$, $\frac{\dot{m}C}{AoC} = B$, and $E = x/B$

then $$\frac{\partial T}{\partial \theta} = A\ (Tw(\theta) - T) - B\frac{\partial T}{\partial x} \qquad (A\text{-}4\text{-}3)$$

Taking Laplace Transforms, we have, if $\tilde{T}(x,s) = \mathcal{L}\{T(x,t)\}$,

$$S\tilde{T} - T(x,o) = A \cdot Tw(s) - A\tilde{T} - B\frac{d\tilde{T}}{dx} \qquad (A\text{-}4\text{-}4)$$

$$\frac{d\tilde{T}}{dx} + \frac{A+S}{B}\tilde{T} = \frac{A-Tw(S)}{B} + \frac{T'}{B} \qquad (A\text{-}4\text{-}5)$$

$$\tilde{T} = (A \cdot Tw(s) + T') \frac{1}{A+S} + C1 \exp\left(-\frac{A+S}{B} x\right) \qquad (A\text{-}4\text{-}6)$$

at $x = 0 \quad T = T_{j-1}(s)$

then $C1 = T_{j-1}(s) - (A\,Tw(s) + T')\left(\frac{1}{A+S}\right)$

$$\tilde{T} = \underset{(I)}{\frac{Tw(s)\cdot A}{A+S}} + \underset{(II)}{\frac{T'}{A+S}} + \underset{(III)}{T_{j-1}(s)} \exp\left(-\frac{A+S}{B} x\right) - \underset{(IV)}{\frac{Tw(s)\cdot A}{A+S}} \exp\left(-\frac{A+S}{B} x\right)$$

$$- \underset{(V)}{\frac{T'}{A+S}} \exp\left(-\frac{A+S}{B} x\right) \qquad (A\text{-}4\text{-}7)$$

The inverse Laplace transform of

$$(I) = \int_0^\theta A \exp(-Au)\, Tw(\theta-u)\, du \quad \text{by convolution property}$$

$$(II) = T' \exp(-A\theta)$$

$(III) = \exp(-A\,Ex)\, T_{j-}(\theta - E)\, U(\theta - E)$ by

second shifting property

where $U(\theta - E)$ is the Heaviside unit step function

$$U(\theta - E) = \begin{cases} 1 & \text{when } \theta > E \\ 0 & \text{when } \theta < E \end{cases}$$

$$(IV) = -A \exp(-AEx) \int_0^\theta \exp(-A(u-E))\, U(u-E)\, Tw(\theta-u)\, du$$

$$= \begin{cases} -A \int_0^\theta \exp(-Au)\, Tw(\theta-u)\, du & \theta > E \\ 0 & \theta < E \end{cases}$$

$$(V) = -T' \exp(-AEx) \exp(-A(\theta-E))\, U(\theta-E)$$

$$= -T' \exp(-A\theta)\, U(\theta-E)$$

at $x = \Delta x$

let $D = \Delta x/B$

$$Tj = \begin{cases} Tj' \exp(-A\theta) + A \int_0^\theta \exp(-Au)\, Tw(\theta-u)\, du \\ \qquad \text{if } \theta < D \end{cases} \qquad (A\text{-}4\text{-}8)$$

$$\left| \exp(-ADx)\, Tj \quad (\theta - D) + A \int_0^D \exp(-Au)\, Tw(\theta - u)\, du \right.$$

$$\text{if } \theta > D$$

if we use trapezoidal formula (2 points for 0 being small) to approximate the integration, then

$$Tj \approx \begin{cases} Tj' \exp(-A\theta) + 1/2(A\theta)\,(Tw(\theta) + Tw(0) \exp(-A\theta) \\ \qquad \text{for } \theta < D \\ Tj_{-1}\,(\theta - D) \exp(-D) + 1/2(D)\,(Tw(\theta) + \exp(-D) \\ Tw(\theta - D)) \qquad \text{for } \theta > D \end{cases} \tag{A-4-9}$$

if we let $H\ (=\Delta\theta) \approx D$ but larger than D,

then at $\theta = H$ $Tj(H) \approx Tj_{-1}(0) \exp(-D) + 1/2(D)$

$$(Tw(H) + Tw(0) \exp(-D))$$

$\theta = 2H$ $Tj(2H) \approx Tj_{-1}(H) \exp(-D) + 1/2(D)$

$$(Tw(2H) + Tw(H) \exp(-D)$$

$\theta = 3H$ $Tj(3H) \approx Tj_{-1}(2H) \exp(-D) + 1/2(-D)$

$$(Tw(3H) + Tw(2H) \exp(-D))$$

. . .

. . .

. . .

. . .

etc.

for $j=1$ Tj_{-1} is constant and equal to inlet temperature.

The problem is that B is quite different between process air and cooling air, therefore H can not be estimated. That is

$$B = \frac{\dot{m}}{\rho A o} \quad \text{and} \quad (D)_{\text{cooling}} \approx \frac{1}{48.6} (D)_{\text{process}}, \tag{A-4-11}$$

so if we estimate H from D process then H >> D cooling.

Therefore, for cooling air,

at $\theta=H$ $\quad Tj(H) \quad Tj\ (H)\exp(-D) + 1/2(D)\,Tw(H)(1+\exp(-D))$

$\theta=2H$ $\quad Tj(2H) \quad Tj\ (2H)\exp(-D)+1/2(D)\,Tw(2H)(1+\exp(-D))$

.

.

.

.

etc.

But, if D is close to or larger than 1, which happens in the process air channel when we consider larger grid (Δx is larger), then 2 points trapezoidal formula approximation does not work.

Reconsider the mathematical model and take Tw as a constant (can be the average of the time period), then Laplace transform of Tw term is $\frac{Tw}{S}$ and

$$T = \underset{(I)}{\frac{Tw \cdot A}{(S)(A+S)}} - \underset{(II)}{\frac{T'}{A+S}} - \underset{(III)}{T_{j-1}(s)\exp\left(-\frac{A+S}{B}x\right)}$$

$$- \underset{(IV)}{\frac{Tw \cdot A}{(S)(A+S)}\exp\left(-\frac{A+S}{B}x\right)} - \underset{(V)}{\frac{T'}{A+S}\exp\left(-\frac{A+S}{B}x\right)} \qquad (A\text{-}4\text{-}12)$$

The inverse Laplace transforms are the same except (I) and (IV) are (Tw (1-exp(-Aθ)) and (Tw (exp(-Aθ) -exp (-AE))) U (θ- E), respectively. Then the final solutions are

$$Tj = \begin{cases} Tj' \exp(-A\theta)+Twj(1-\exp(-A\theta)) & \text{if } \theta < D \\ Tj_{-1}\ (\theta - D)\exp(-AD)+Twj(1-\exp(-AD)) & \text{if } \theta > D \end{cases} \qquad (A\text{-}4\text{-}13)$$

After going through the same treatments as before, the solutions are as follows;

for process air:

$\theta=H \quad T_j(H) = T_{j-1}(0)\exp(-AD)+T_{wj}(1-\exp(-AD))$

$\theta=2H \quad T_j(2H) = T_{j-1}(H)\exp(-AD)+T_{wj}(1-\exp(-AD))$

.

.

.

.

etc.

where $T_{wj} = (T_w(\theta)+T_w(\theta+H))/2$.

for cooling air:

$\theta=H \quad T_j(H) = T_{j}(H)\exp(-AD)+T_{wj}(1-\exp(-AD))$

$\theta=2H \quad T_j(2H) = T_{j}(2H)\exp(-AD)+T_{wj}(1-\exp(-AD))$

.

.

.

.

etc.

Appendix 5

Input Data for Simulation of CSU PAFC System Steady State Performance

Variable name	Dimension	Initial value	Unit	Definition
TOPFC		443	°K	Operating temperature in fuel cell
UT		0.8		Utilization of H2 in stack
CD		600	mA/cm^2	Designed current density
DNSM	1	1216.	g-mole/hr	Input mole flow rate of CH_4
	2	0	g-mole/hr	Input mole flow rate of O_2
	3	1.36	g-mole/hr	Input mole flow rate of CO
	4	21.8	g-mole/hr	Input mole flow rate of CO_2
	5	166.	g-mole/hr	Input mole flow rate of H_2
	6	0	g-mole/hr	Input mole flow rate of H_2O
	7	0	g-mole/hr	Input mole flow rate of N_2
TAT		298	°K	Ambient temperature
PAT		1	atm	Ambient pressure
SMRA		3.0		Steam to carbon ratio
POPR		5.0	atm	Operating pressure of reformer
IFUEL		1		=1 Input fuel is methane =2 Input fuel is methanol =3 Input fuel is naphtha
ERR		0.01		Criterion of convergence in system trial and error procedure
IP		2		=1 adiabatic operation in shift converters =2 isothermal operation in shift converters
I		7		Number of components in whole system
EXT		100		Extra percentage of needed air in burner
EXA		100		Extra per centage of air in fuel cell stack
ZH		2.438	m	Height of reformer

Variable name	Dimension	Initial value	Unit	Definition
DX1		0	m	Outside diameter of regenerative tube
DX2		0.0457	m	Inside diameter of reforming tube
DX3		0.0509	m	Outside diameter of reforming tube
KO		10400		Rate constant of demethanation reaction
EA		83736	J/mol	Activity energy of demethanation reaction
RHOB		1281.477	Kg/m^3	Density of packing in reformer
EPS		0.487		Void fraction in reformer
S		0.0762	m	Width of cimbustion gas square duct
DP		0.001	m	Diameter of catalyst in reformer
DZZ		0.0762	m	Height of finite-difference section
CN		1.3	$m^2-°K$	Q x A/C min in heat exchanger
U		56.78263	$J/m^2-s-°K$	Overall heat transfer coefficient in heat exchanger
HA	7	0.2	m^2	Transfer area in E-7
	10	0.2	m^2	Transfer area in E-10
NPH		2		Number of tube passes
NRH		5		Number of tube rows
BASPC		0.3048	m	Buffle space
ODTH		0.019	m	O.D. of tube
PITCH		0.0254	m	Pitch of heat exchanger
CLH		0.00634	m	Clearance in heat exchanger
IDSH		0.254	m	I.D. of shell
IDTH		0.0142	m	I.D. of tube
FLOAR		0.00016	m^2	Flow area in heat exchanger
SURFC		0.0136	m^2	Surface area per line
CLENH		0.61	m	Length of tube

variable name	Dimension	Initial value	Unit	Definition
SITSZ		0.5		Ratio of total inside tube cross-sectional area per pass to header cross-sectional area per pass
DTH		0.7		Fraction of ΔT over inlet gas film in heat exchanger
DPD	1	0.36	m	Diameter of shift converters
AHRN	1	0.66		Void fraction in shift converters
APPD	1	6.41	m^2	Total surface area of packing
CLEPD	1	1.8	m	Length of shift converters
NTPD	1			Number of tubes in shift converters
NTAF		140		Number of fuel flow channels in stack
FULE		0.433	m	Length of fuel channel
WIDAF		0.00297	m	Width of square fuel channel
NPFU		3365		Number of cell plates
NTAA		40		Number of process air flow channels
AIRL		0.3048	m	Length of air channel
WIDAA		0.00157	m	Width of square process air channel
SRO		0.000044	Ω-m^2	Cell resistance at 450 °K
SA		40000	m^2/Kg	Surface area of catalyst
CU		0.15		Utilization of catalyst
CL		0.0075	Kg/m^2	Catalyst loading
ALFA		0.50		Transfer coefficient
SN		2	g-equivalent	Number of Faraday equivalents transferred
FCONST		96500	C/g-equivalent	Faraday constant
DKC		240000	A/atm	Constant to calculate limiting current density

Appendix 6

A6.1 Input Data for Simulation of Westinghouse PAFC System S.S. Performance

Variable name	Dimension	Initial value	Unit	Definition
XN		0.35433	m	Length of cell plate in x-direction
YN		0.3048	m	Length of cell plate in y-direction
XINSO		3250	A/m^2	Designed current density
UTA		0.5		Utilization of O2 in stack
UTH		0.8		Utilization of H2 in stack
POPC		3.4	atm	Pressure of cooling air
POP		3.4	atm	Operating pressure in stack
TKA		450	K	Inlet temperature of process air
WFD		0.001016	m	Depth of fuel channel
WFW		0.003048	m	Width of fuel channel
NCC		36		Number of cooling channels
WE		0.001016	m	Thickness of cell(electrode and matrix)
T		0.003302	m	Thickness of cell plate
NK		5		Number of plates between two cooling plates
WAD		0.001016	m	Depth of process air channel
WAW		0.003048	m	Width of process air channel
NP		32400		Number of cell plates
NCA		80		Number of process air channels
NF		55		Number of fuel channels
T1		0.008891	m	Thickness of cooling plate
NX		6		Finite difference number in x-direction
NY		6		Finite difference number in y-direction
ER		0.005		Criteria for convergence
CLCA		0.0075	kg/m^2	Catalyst loading on cathode side
CLAN		0.0034	kg/m^2	Catalyst loading on anode side
CU		0.35		Utilization of catalyst
SA		50000	m^2/kg	Surface area of catalyst
SRO		0.000044	$\Omega\text{-}m^2$	Cell resistance at 450 K
ALFA		0.55		Transfer coefficient
DKC		240000	A/atm	Constant to calculate limiting current density

Variable name	Dimension	Initial value	Unit	Definition
R		8.314	J/(g-mol)(K)	Gas constant
Z		2	g-equivalent	Number of Faraday equivalents transferred
FCONST		96500	C/g-equivalent	Faraday constant
NC		29		Ratio of cooling air to air consumed in stack
KX		1.730735	J/m.s.K	Effective thermal conductivity in stacking direction
KY		51.92205	J/m.s.K	Effective thermal conductivity on the cell plate
TKC		403.3	K	Inlet cooling air temperature
NTREED		3		=0 Straight or varying width cooling configuration =3 Branched cooling configuration
WTRE	1	0.1524	m	First section length of branched cooling configuration
	2	0.1016	m	Second section length of branched cooling configuration
	3	0.0508	m	Third section length of branched cooling configuration
WCW	1	0.00508	m	First width of branched or varying width cooling configuration
	2	0.00254	m	Second width of branched or varying width cooling configuration
	3	0.00127	m	Third width of branched or varying width cooling configuration
WCD		0.00508	m	Depth of cooling channel
NVARY		0		=0 Straight or branched cooling configuration =1 Varying width cooling configuration
IVA	1	0		First width section number
	2	0		Second width section number
	3	0		Third width section number
Y2O2		0.208		Mole fraction of O2 in cathode inlet

Variable name	Dimension	Initial value	Unit	Definition
Y2N2		0.782		Mole fraction of N_2 in cathode inlet
Y2H2O		0.01		Mole fraction of H_2O in cathode inlet
RHOP		2611.01	kg/m^3	Density of cell plate
RHOC		2162.49	kg/m^3	Density of cooling plate
CCP		1.0467	kJ/(kg.K)	Heat capacity of cell plate
CCC		0.841547	kJ/(kg.K)	Heat capacity of cooling plate
SAREA	1	964.5670	m^2/m^3	Specific surface area of packing in high temperature shift converter
	2	2411.417	m^2/m^3	Specific surface area of packing in low temperature shift converter
CPC	1	0.879228	kJ/(kg.K)	Heat capacity of catalyst in high temperature shift converter
	2	0.753624	kJ/(kg.K)	Heat capacity of catalyst in low temperature shift cinverter
RHOB	1	1281.501	kg catalyst/m^3 bed	Density of packing in high temperature shift converter
	2	1229.920	kg catalyst/m^3 bed	Density of packing in low temperature shift converter
DP	1	0.003048	m	Diameter of catalyst in high temperature shift converter
	2	0.001219	m	Diameter of catalyst in low temperature shift converter
EPS		0.469		Void fraction in shift converters
ZHS	1	1.8288	m	Height of high temperature shift converter
	2	0.6096	m	Height of low temperature shift converter
D1S	1	0.09144	m	Diameter of high temperature shift converter
	2	0.0762	m	Diameter of low temperature shift converter
NTS	1	92		Number of tubes in high temperature shift converter
	2	92		Number of tubes in low temperature shift converter

Variable name	Dimension	Initial value	Unit	Definition
MS	1	6		Number of finite difference sections in high temperature shift converter
	2	6		Number of finite difference sections in low temperature shift converter
ZH	1	1.8288	m	Length of air heater
	2	4.2672	m	Length of anode exhaust heat exchanger
	3	2.7432	m	Length of preparator
	4	5.7912	m	Length of heat exchanger-1
	5	5.7912	m	Length of heat exchanger-2
D1	1	0.0452628	m	Inside diameter of tube in air heater
	2	0.0452628	m	Inside diameter of tube in anode exhaust heat exchanger
	3	0.0452628	m	Inside diameter of tube in preparator
	4	0.0198729	m	Inside diameter of tube in heat exchanger-1
	5	0.0198729	m	Inside diameter of tube in heat exchanger-2
D2	1	0.0508101	m	Outside diameter of tube in air heater
	2	0.0508101	m	Outside diameter of tube in anode exhaust heat exchanger
	3	0.0508101	m	outside diameter of tube in preparator
	4	0.0253898	m	Outside diameter of tube in heat exchanger-1
	5	0.0253898	m	Outside diameter of tube in heat exchanger-2
D3	1	0.073152	m	Inside diameter of shell in air heater
	2	0.073152	m	Inside diameter of shell in anode exhaust heat exchanger
	3	0.073152	m	Inside diameter of shell in preparator
	4	0.0370332	m	Inside diameter of shell in heat exchanger-1
	5	0.0370332	m	Inside diameter of shell in heat exchanger-2

Variable name	Dimension	Initial value	Unit	Definition
NT	1	55		Number of tubes in air heater
	2	220		Number of tubes in anode exhaust heat exchanger
	3	177		Number of tubes in preparator
	4	178		Number of tubes in heat exchanger-1
	5	402		Number of tubes in heat exchanger-2
MH	1	6		Number of finite difference sections in air heater
	2	6		Number of finite-difference sections in anode exhaust heater
	3	6		Number of finite-difference sections in preparator
	4	6		Number of finite-difference sections in heat exchanger-1
	5	6		Number of finite-difference sections in heat exchanger-2
RHW		8027.17	kg/m^3	Density of wall in heat exchangers
CPW		0.502416	kJ/(kg.K)	Heat capacity in heat exchangers
THW		20.76882	J/m.s.K	Thermal conductivity in heat exchangers
ZHR		12.192	m	Height of reformer
D1R		0	m	Outside diameter of regenerative tube
D2R		0.12701	m	Inside diameter of reforming tube
D3R		0.149992	m	Outside diameter of reforming tube
KO		10400		Rate constant of demethanation reaction
EA		83736	J/mol	Activity energy of demethanation reaction
RHOR		1281.477	kg/m^3	Density of packing in reformer
EPSR		0.45		Void fraction in reformer
S		0.2286	m	Width of combustion gas square duct
DPR		0.004572	m	Diameter of catalyst in reformer
MR		21		Number of finite-difference sections in reformer
RHWR		8027.1725	kg/m^3	Density of wall in reformer

Variable name	Dimension	Initial value	Unit	Definition
CPWR		0.6112728	kJ/(kg.K)	Heat capacity of wall in reformer
SAREAR		669.29133	m^2/m^3	Specific surface area of catalyst in reformer
CPCR		1.025766	kJ/(kg.K)	Heat capacity of catalyst in reformer
IRATE		0		=0 First order reaction kinetic of demethanation reaction =1 Westinghouse kinetic model of demethanation reaction
NTR		35		Number of tubes in reformer
CTAN	1	0.95		Mole fraction of CH_4 in input fuel
	2	0		Mole fraction of CO in input fuel
	3	0		Mole fraction of CO_2 in input fuel
	4	0		Mole fraction of H_2O in input fuel
	5	0		Mole fraction of H_2 in input fuel
	6	0.05		Mole fraction of N_2 in input fuel
	7	0		Mole fraction of O_2 in input fuel
TAT		300	K	Ambient temperature
PAT		1	atm	Ambient pressure
SMRA		2.5		Steam to carbon ratio
IFUEL		1		=1 Input fuel is methane =2 Input fuel is methanol =3 Input fuel is naphtha
IP		1		=1 Adiabatic operation =2 Isothermal operation
I		7		Number of components in whole system
EXT		10		Extra percentage of needed air in burner
ERR		0.0025		Criterion of convergence in system trial and error procedure
U		56.78359	$J/(m^2.s.K)$	Overall heat transfer coefficient of recuperator
HA		371.04	m^2	Transfer area of recuperator
RREF		0.971		Divider fraction of input fuel
PFI		3.4	atm	Initial input fuel pressure

Variable name	Dimension	Initial value	Unit	Definition
PFO		6.7	atm	Designed input fuel pressure
TDRUM		394.4	K	Temperature of steam drum
PDRUM		2.04	atm	Pressure of steam drum
OPTC		324	K	Operating temperature in the direct contact condenser
OPPC		4.082	atm	Operating pressure in the direct contact condenser
DUTYM		0.062		Extra heat duty in steam generating super heater
PDESIG		1.36	atm	Designed pressure of air used in burner
TOPRS		464	K	Temperature of anode side gas reservoir
RATO		1.8		Multiple factor of Beek corelation in calculating wall heat transfer coefficient in reformer
PDST		0.02		Pressure drop ratio of steam through steam generating super heater
PDR		0.1		Pressure drop ratio of combustion gas through reformer
PDS		0.03		Pressure drop ratio of combustion gas through steam generating super heater
PDE		0.005		Pressure drop ratio of water through economizer
PDB		0.1		Pressure drop ratio of combustion gas through burner
PDFU		0.05		Pressure drop ratio of anode side fuel in fuel cell stack
PDZN		0.03		Pressure drop ratio of input fuel through ZnO bed
EFBLO		0.75		Efficiency of air blower
EFCOM		0.6		Efficiency of fuel compressor
EFPUMP		0.7		Efficiency of water pump
X		0.92417		Initial guess of conversion in reformer
DTM2		86.11		Initial guess of CO2 to CO ratio in the anode side inlet

Variable name	Dimension	Initial value	Unit	Definition
DTM1		0.68724		Initial guess of CO2 to CO ratio after reformer
TAI3		806.16	K	Initial guess of 13th stream temperature
PAI3		5.159	atm	Initial guess of 13th stream pressure
TA3		374.58	K	Initial guess of 3rd stream temperature
PA3		1.3587	atm	Initial guess of 3rd stream pressure

A6.2 Different Data Used in Chapter 6

Variable name	Dimension	Data used in Chapter 6	Unit
MS	1	4	
	2	4	
ZH	1	2.286	m
D1	1	0.0762	m
D2	1	0.08535	m
D3	1	0.10973	m
MH	1	4	
	2	4	
	3	4	
	4	4	
	5	4	
X		0.923	
DTM2		270.	
DTM1		0.6886	
TA13		805.8	K
PA13		5.17	atm
PA3		1.3599	atm

Appendix 7

Input Data for Simulating Transient State Responses

Variable name	Dimension	Initial value	Unit	Definition
CRT		5×10^{-7}		Criterion for testing reach of final steady state
SDT		3.6×10^{-2}	s	Standard (system) time interval
MT		9		Number of major components considered in transient simulation
				component (i)
				i=1 : air heater
				i=2 : anode exhaust heat exchanger
				i=3 : preparator
				i=4 : heat exchanger-1 (CH_4 side)
				i=5 : heat exchanger-2 (air side)
				i=6 : high temperature shift converter
				i=7 : low temperature shift converter
				i=8 : reformer
				i=9 : fuel cell stack
IDH	9	4,5,4,5,2, 4,1,1,3		Multiple of system time interval in component (i)
IFLG	9	9 x 0		Flag for register of component (i)
NFLG	9	9 x 0		Flag for operation of component (i)
MFLG	15	15 x 2		Flag for condition of gas stream outlets:
				2: initial steady state
				1: transient state
				0: final steady state
				gas stream:
				j=1 tubeside of i=1
				j-2 shellside of i=1
				j=3 tubeside of i=2
				j=4 shellside of i=2
				j=5 tubeside of i=3
				j=6 shellside of i=3

Variable name	Dimension	Initial value	Unit	Definition
				j=7 tubeside of i=4 j=8 shellside of i=4 j=9 tubeside of i=5 j=10 shellside of i=5 j=11 reacting gas of i=6 j=12 reacting gas of i=7 j=13 reforming gas of i=8 j=14 combustion gas of i=8 j=15 anode gas of i=9
NTN	15	1,1,5,3,3, 2,5,3,1,8, 1,1,3,1,1		Multiple of system time interval for calculating hold-up of gas stream(j)
JST	9	9 x 1		Counted number of calculations in component (i)
ITIME	9	9 x 0		Counted system time number of component (i) when previous calculation performed
ICCU	15	15 x 0		Lasting time number counted for testing final steady state
CRT2		0.01	K	Criterion for testing transient state occurance
NCR		139		Number of system time intervals for testing final steady state

Appendix 8

Definitions of Subroutines and Functions

SUBROUTINE	DESCRIPTION
BURN	calculation of mass balance in burner
CALPRO	calculations of the new temperature of process air and cooling air after one time interval at transient state in fuel cell stack
CDPRO	calculation of current density distribution at transient state
CMASS	calculation of mass fractions of gas stream
CMOLE	calculation of mole fractions of gas stream
COMP	calculations of power needed and outlet temperature in compressor
COND	estimation of heat duty in condenser
CONV	Wegsten method used for algebraic convergence
CUPRO	calculation of steady state current density distribution on cell plate
DATACB	calculations of fuel input rate, process and cooling air input rate, and coefficients at different cooling configurations
DATAIN	input data reading and change of units
DIVID	calculations of material and energy balances in divider
DMIX	calculations of material and energy balances in mixer
DMIX3	calculations of material and energy balances in 3 streams' mixer
EULER	Euler method used to solve ordinary differential equations
EXHEJ	estimation of the outlet temperature in tube side with input heat duty
EXHEK	estimation of the outlet temperature in shell side with input heat duty
EXHER	estimation of the energy balance in heat exchanger

SUBROUTINE	DESCRIPTION
FLAME	calculation of the maximum flame temperature in burner
FUNCT	calculations of time rate of change for plate temperature in fuel cell stack
FUNCTH	calculations of the time rate of change for temperatures of tube side, shell side, and tube wall in heat exchanger
FUNCTR	calculations of the time rate of change for molar fraction of CH_4, temperature of reforming gas, density of reforming gas, and temperature of combustion gas, wall, and catalyst in reformer
FUNCTS	calculations of the time rate of change for molar fraction of CO and temperatures of reactant and catalyst in shift converter
FUNCT2	calculations of the new flow rates of fuel, process air, and cooling air after one time interval at transient state in fuel cell stack
GAUSS	Gauss-Seidel iteration used to solve simultaneous linear equations
HEPD	calculation of pressure drop in heat exchanger
LOADCE	calculations of operation conditions and flow rates of fuel and air at transient state
PROPTH	calculations of the properties and coefficients of stream in heat exchanger after new temperature and flow rate obtained
PROPTR	calculations of the properties and coefficients of stream in reformer after new temperature and flow rate obtained

SUBROUTINE	DESCRIPTION
PROPTS	calculations of the properties and coefficients of stream in shift converter after new temperature and flow rate obtained
PUMP	calculations of power and outlet temperature in water pump
PVI	estimations of the current density and voltage from input power at given conditions
SNAE	Newton-Raphson iteration used to solve equilibrium compositions in reformer with given equilubrium constants
SORT	sorting of the largest input data
STEADF	calculations of steady state current density and temperature distributions on cell plates in fuel cell stack
STEADH	calculations of steady state solutions (include temperature) in heat exchanger
STEADR	calculations of steady state solutions (include conversion, temperatures, and pressures) in reformer
STEADS	calculations of steady state solutions (include conversion, temperatures) in shift converter
STMAIN	calculations of the steady state solutions of PAFC system - the procedure control subroutine
STTRAN	simulation of the transient responses in PAFC system with load change - the procedure control subroutine
TRANC	execution of the simulation of heat exchanger at transient state
TRANF	execution of the simulation of fuel cell stack at transient state

SUBROUTINE	DESCRIPTION
TRANH	execution of the simulation of heat exchanger at transient state
TRANR	execution of the simulation of reformer at transient state
VI	calculation of relationship between voltage and current density in fuel cell stack

FUNCTION	DESCRIPTION
DH1	calculation of heat of demethanation reaction - CO2 is product
DH2	calculation of heat of water shift reaction
F	calculation of total flow rate with conversion x in reformer
HC	calculation of heat transfer coefficient between gas stream and catalyst
HI	calculation of heat transfer coefficient in tube side
HIR	calculation of tube side heat transfer coefficient in reformer
HO	calculation of heat transfer coefficient in annular shell side
HOR	estimation of heat transfer coefficient of annular shell side in reformer
HTCP	calculation of heat capacity of gas mixture
K1	calculation of equilibrium constant of demethanation reaction - CO_2 is product
K2	calculation of equilibrium constant of water shift reaction
K3	calculation of equilibrium constant of demethanation reaction - CO is product
RAGE	calculation of reaction rate in low temperature shift converter
RATE	calculation of reaction rate in high temperature shift converter
RUNGE	fourth-order Runge-Kutta method used to solve ordinary differential equations
RUNGM	Runge-Kutta-Merson method used to solve ordinary differential equations
THC	calculation of thermal conductivity of gas mixture
UI	calculation of total heat transfer coefficient in reformer

FUNCTION	DESCRIPTION
VIS	calculation of viscosity of gas mixture
X2	estimation equilibrium conversion of water shift reaction in reformer

Appendix 9

Printout of PAFC System Transient Responses

A 9.1 Initial Steady State Solutions

A 9.2 Transient Responses at Specific Time
(1 sec.,4.5 min., 9.0 min., and 13.5 min.)

A 9.3 Final Steady State Solutions (14.38 min.)

```
 THE STEAM/METHANE RATIO IN THE REFORMER IS    2.50

THE REFORMER IS OPERATING UNDER THESE CONDITIONS:
INLET PRESSURE:    6.66ATM
OUTLET PRESSURE:   5.18ATM
INLET TEMP.: 732.59 K
OUTLET TEMP.: 937.66 K

THE HIGH TEMP. SHIFT IS OPERATING UNDER THESE CONDITIONS :
INLET PRESSURE :    5.17 ATM
OUTLET PRESSURE:    4.89 ATM
INLET TEMP.: 692.59 K
OUTLET TEMP.: 744.90 K

THE LOW TEMP. SHIFT IS OPERATING UNDER THESE CONDITIONS:
INLET PRESSURE:     4.89 ATM
OUTLET PRESSURE:    4.52 ATM
INLET TEMP.: 483.54 K
OUTLET TEMP.: 565.24 K

THE FUEL CELL IS OPERATING UNDER THESE CONDITIONS
THE ANODE SIDE INLET TEMPERATURE: 464.00 K
               OUTLET TEMPERATURE:  457.43 K


THE POWER OF METHANE COMPRESSOR:  0.49689D 02KW,
THE POWER OF PUMP :            0.60316D 00KW
THE POWER OF AIR BLOWER :  0.62859D 02KW


 AIR HEATER      ANODE E. H.   PREPARATOR      HEAT EXCH.      REFORMER     HI T. SH. CON.   LOW T. SH. CON.
THE TOTAL NUMBER OF TUBES
          80             220            177             580             35               92               92

THE LENGTH OF TUBE -- FT
 0.75000D 01    0.14000D 02    0.90000D 01     0.19000D 02    0.40000D 02     0.60000D 01      0.20000D 01

THE I. D. OF TUBE -- FT
 0.25000D 00    0.14850D 00    0.14850D 00     0.65200D-01    0.41670D 00     0.30000D 00      0.25000D 00

THE O. D. OF TUBE -- FT
 0.28000D 00    0.16670D 00    0.16670D 00     0.83300D-01    0.49210D 00

THE I. D. OF SHELL -- FT
 0.36000D 00    0.24000D 00    0.24000D 00     0.12150D 00    0.75000D 00



THE FRACTION OF CO IN THE ANODE INLET IS0.00007


*** THE STEAM GENERATING SUPER HEATER DUTY IS  0.70049D 10 J
    BUT SHORT OF HEAT  0.22443D 10J (MINIMUM)


*** THE ECONOMIZER DUTY IS  0.57473D 09 J
    BUT SHORT OF HEAT  0.10129D 09 J (MINIMUM)
```

A STREAM	CH4	CO	CO2	H2O	H2	N2	O2	RATE(G/SEC.)	TEMP.(K)	PRE.(ATM)
1	.0000	.0000	.0000	0.0100	.0000	.7820	.2080	1765.16	300.00	1.00
2	.0000	.0000	.0000	0.0100	.0000	.7820	.2080	1765.16	300.00	1.36
3	.0000	.0000	.0000	0.0100	.0000	.7820	.2080	1765.16	375.34	1.36
4	.0000	.0000	.0000	0.0100	.0000	.7820	.2080	1765.16	671.07	1.35
5	.9500	.0000	.0000	0.0000	.0000	.0500	.0000	359.00	300.00	3.40
6	.9500	.0000	.0000	0.0000	.0000	.0500	.0000	359.00	356.34	6.70
7	.9500	.0000	.0000	0.0000	.0000	.0500	.0000	359.00	665.34	6.70
8	.9500	.0000	.0000	0.0000	.0000	.0500	.0000	359.00	665.34	6.50
9	.9500	.0000	.0000	0.0000	.0000	.0500	.0000	10.40	665.34	6.50
10	.2815	.0000	.0000	0.7037	.0000	.0148	.0000	1246.35	563.80	6.66
11	.2815	.0000	.0000	0.7037	.0000	.0148	.0000	1246.35	732.59	6.66
12	.0142	.1011	.0699	0.2222	.5829	.0097	.0000	1246.35	937.66	5.18
13	.0142	.1011	.0699	0.2222	.5829	.0097	.0000	1246.35	805.35	5.17
14	.0142	.1011	.0699	0.2222	.5829	.0097	.0000	1246.35	692.59	5.17
15	.0142	.0623	.1087	0.1834	.6217	.0097	.0000	1246.35	744.90	4.89
16	.0142	.0623	.1087	0.1834	.6217	.0097	.0000	1246.35	483.54	4.89
17	.0142	.0001	.1709	0.1212	.6839	.0097	.0000	1246.35	565.24	4.52
18	.0142	.0001	.1709	0.1212	.6839	.0097	.0000	1246.35	523.17	4.52
19	.0142	.0001	.1709	0.1212	.6839	.0097	.0000	1246.35	361.67	4.52
20	.0158	.0001	.1898	0.0243	.7592	.0108	.0000	1053.85	324.00	4.08
21	.0158	.0001	.1898	0.0243	.7592	.0108	.0000	1053.85	506.11	4.08
22	.0000	.0000	.0000	1.0000	.0000	.0000	.0000	897.75	436.87	6.63
23	.0000	.0000	.0000	1.0000	.0000	.0000	.0000	897.75	501.66	6.50
24	.0403	.0002	.4836	0.0619	.3864	.0276	.0000	935.96	734.30	3.23
25	.0000	.0000	.2215	0.2365	.0000	.5295	.0125	2711.52	2066.71	1.61
26	.0000	.0000	.2215	0.2365	.0000	.5295	.0125	2711.52	833.60	1.44
27	.0000	.0000	.2215	0.2365	.0000	.5295	.0125	2711.52	436.87	1.40
28	.0000	.0000	.2215	0.2365	.0000	.5295	.0125	2711.52	394.40	1.39
29	.9500	.0000	.0000	0.0000	.0000	.0500	.0000	348.60	665.34	6.50

B STREAM	CH4	CO	CO2	H2O	H2	N2	O2	RATE(G/SEC.)	TEMP.(K)	PRE.(ATM)
1	.0403	.0002	.4836	0.0619	.3864	.0276	.0000	935.96	457.43	3.23
2	.0158	.0001	.1898	0.0243	.7592	.0108	.0000	1053.85	464.00	3.40

C STREAM	CH4	CO	CO2	H2O	H2	N2	O2	RATE(G/SEC.)	TEMP.(K)	PRE.(ATM)
1	.0000	.0000	.0000	1.0000	.0000	.0000	.0000	897.75	394.40	6.63
23	.0000	.0000	.0000	1.0000	.0000	.0000	.0000	897.75	394.40	2.04

C-4

A.9.2 Transient Responses at Specific Time

```
SYSTEM TIME:  0.10080D 01 SEC.
PW=  0.20575D 00  W/CM**2 V=0.672VOLT C.D.=.3064A/CM**2
TOP=  0.46349D 03 K POP=3.400 ATM
N2=  0.24996D 06 G-MOLE/HR  O2=  0.19997D 06 G-MOLE/HR
SYSTEM TIME NUMBER    28
IFLG = 1 0 0 1 1 0 0 1 INFLG = 1 0 0 0 1 0 0 1 0
IJ= 1 F(1-12)
     0.00000 -0.14223D 04  0.38385D 03  0.45748D 03  0.21736D 01  0.11918D 01
 0.64281D 00       0.00000 -0.60392D 01  0.41810D 01  0.33992D 01  0.26863D 01


TIME=  0.10080D 01    SEC.
    *** AIR HEATER ***
TUBESIDE TEMP.   SHELL TEMP.    TUBEWALL TEMP.  INCR.
    F                F                F

       80.000        481.721          406.661     1
      127.478        507.988          436.069     2
      172.730        533.219          464.359     3
      215.669        557.432          491.535     4
IJ= 5 F(1-12)
     0.00000 -0.18739D 04  0.38932D 04 -0.31466D 04  0.16130D 02  0.66768D 01
 0.10383D 02       0.00000  0.27667D 02 -0.50895D 01  0.71758D 01  0.22543D 00


TIME=  0.10080D 01    SEC.
    *** HEAT EXCHANGER -2 ***
```

TUBESIDE TEMP. F	SHELL TEMP. F	TUBEWALL TEMP. F	INCR.
215.650	414.267	349.726	1
416.958	586.767	533.006	2
593.831	741.442	695.609	3
747.830	880.815	840.868	4

TIME= 0.10080D 01 SEC.

*** REFORMER ***

REFORMER GAS TEMP DEG. R	COMB. GAS TEMP DEG. R	WALL TEMP DEG. R	CATALYST TEMP DEG. R	PRESSURE ATM	IN. HEAT XFER COEF BTU/HR*F*FT*FT	OUT. HEAT XFER COEF BTU/HR*F*FT*FT	INC
1318.666	1500.482	1332.335	1318.666	6.658	97.414	6.705	1
1137.377	1518.791	1165.935	1137.377	6.601	98.784	6.770	2
1153.999	1557.493	1184.128	1153.999	6.550	101.062	6.906	3
1168.967	1599.065	1200.999	1168.967	6.496	103.474	7.051	4
1182.789	1644.083	1217.057	1182.789	6.442	106.052	7.206	5
1196.038	1693.169	1232.876	1196.038	6.386	108.825	7.375	6
1209.248	1746.991	1249.000	1209.248	6.328	111.826	7.559	7
1222.863	1806.276	1265.893	1222.863	6.268	115.085	7.760	8
1237.236	1871.839	1283.941	1237.236	6.207	118.634	7.981	9
1252.652	1944.608	1303.482	1252.652	6.143	122.505	8.224	10
1269.373	2025.660	1324.844	1269.373	6.077	126.732	8.494	11
1287.674	2116.257	1348.383	1287.674	6.009	131.349	8.794	12
1307.883	2217.887	1374.536	1307.883	5.937	136.391	9.128	13
1330.430	2332.312	1403.861	1330.430	5.862	141.889	9.502	14
1355.906	2461.621	1437.107	1355.906	5.783	147.870	9.924	15
1385.167	2608.287	1475.327	1385.167	5.700	154.355	10.401	16
1419.522	2775.226	1520.053	1419.522	5.611	161.362	10.944	17
1461.087	2965.844	1573.644	1461.087	5.516	168.914	11.564	18
1513.547	3184.033	1639.968	1513.547	5.414	177.067	12.276	19
1583.949	3434.050	1726.002	1583.949	5.302	185.976	13.097	20
1687.796	3720.065	1846.336	1687.796	5.178	196.038	14.046	21

MFLG = 1 1 2 2 2 2 2 2 1 2 2 2 2 2 2

TEMPERATURE OF STREAMS -- K

0.30000D 03	0.30000D 03	0.37537D 03	0.67102D 03	0.30000D 03	0.35634D 03	0.66534D 03
0.66534D 03	0.66534D 03	0.56380D 03	0.73259D 03	0.93766D 03	0.80535D 03	0.69259D 03
0.74490D 03	0.48354D 03	0.56524D 03	0.52318D 03	0.36167D 03	0.32400D 03	0.50611D 03
0.43687D 03	0.50166D 03	0.73430D 03	0.20677D 04	0.83360D 03	0.43687D 03	0.39440D 03 0.66534D 03 0.45743D 03

IJ= 4 F(1-12)

0.00000	-0.35429D 04	0.66209D 03	-0.94257D 02	0.73838D 02	-0.17711D 01
-0.55094D 00	0.00000	0.14013D 03	-0.67002D 01	0.10251D 01	0.91595D 00

TIME= 0.10800D 01 SEC.

*** HEAT EXCHANGER -1 ***

TUBESIDE TEMP. F	SHELL TEMP. F	TUBEWALL TEMP. F	INCR.
181.419	401.564	336.739	1
400.759	573.793	518.510	2
581.521	732.044	682.967	3
737.602	880.815	834.271	4

```
 TIME=  0.10800D 01 SEC.
      *** FUEL CELL STACK ***
 THE VOLTAGE IS      0.66842D 00

  .3326 .3271 .3202 .3108 .2977 .2783
  .3471 .3407 .3325 .3215 .3062 .2833
  .3370 .3308 .3230 .3126 .2984 .2778
  .3355 .3294 .3217 .3116 .2978 .2780
  .3144 .3093 .3030 .2948 .2837 .2683
  .2904 .2866 .2818 .2757 .2676 .2564
 THE VOLTAGE IS      0.67865D 00

  .3279 .3225 .3156 .3063 .2933 .2741
  .3424 .3360 .3278 .3168 .3015 .2789
  .3384 .3319 .3236 .3127 .2978 .2761
  .3352 .3288 .3207 .3102 .2958 .2753
  .3175 .3121 .3053 .2964 .2846 .2680
  .3008 .2964 .2909 .2839 .2746 .2616
 THE VOLTAGE IS      0.68173D 00

  .3264 .3211 .3142 .3050 .2920 .2729
  .3411 .3347 .3265 .3155 .3002 .2777
  .3389 .3323 .3239 .3128 .2976 .2757
  .3353 .3288 .3206 .3099 .2954 .2746
  .3188 .3132 .3063 .2972 .2851 .2681
  .3043 .2997 .2940 .2866 .2769 .2633
 FUEL CELL STACK F(1-24)
  0.52252D 03  0.29159D 03  0.23271D 03  0.38052D 03  0.21520D 03  0.21792D 03
 -0.11351D 03 -0.10641D 03 -0.11547D 03 -0.11868D 03 -0.12454D 03 -0.12711D 03
 -0.11568D 03 -0.11112D 03 -0.11729D 03 -0.12267D 03 -0.12583D 03 -0.12794D 03
 -0.11104D 03 -0.10904D 03 -0.11454D 03 -0.11987D 03 -0.12297D 03 -0.12494D 03

 PLATE 2
  200.85 199.62 198.08 196.03 193.19 189.04
  199.68 198.46 196.92 194.87 192.05 187.95
  193.48 192.37 190.98 189.15 186.64 183.01
  189.82 188.81 187.54 185.88 183.61 180.37
  182.21 181.39 180.37 179.04 177.24 174.68
  173.92 173.32 172.58 171.61 170.31 168.48
 ***  COOLING OR PROCESS AIR TEMPERATURE
  200.86 199.63 198.08 196.03 193.19 189.04
  199.68 198.46 196.92 194.87 192.06 187.95
  193.48 192.37 190.98 189.15 186.64 183.01
  189.82 188.81 187.55 185.88 183.62 180.37
  182.21 181.39 180.37 179.04 177.24 174.68
  173.92 173.32 172.58 171.62 170.32 168.48

 PLATE 3
  206.43 205.10 203.42 201.20 198.12 193.61
  204.91 203.58 201.92 199.71 196.66 192.21
  199.52 198.30 196.76 194.74 191.96 187.95
  195.00 193.89 192.51 190.69 188.21 184.65
  187.64 186.73 185.60 184.12 182.13 179.29
  180.46 179.78 178.92 177.81 176.31 174.20
 ***  COOLING OR PROCESS AIR TEMPERATURE
  206.43 205.10 203.43 201.20 198.12 193.62
```

```
 204.91 203.59 201.92 199.71 196.66 192.21
 199.52 198.30 196.76 194.74 191.96 187.95
 195.00 193.89 192.51 190.69 188.21 184.65
 187.64 186.73 185.60 184.13 182.13 179.29
 180.46 179.78 178.92 177.81 176.31 174.20

PLATE 4
 208.27 206.90 205.19 202.90 199.75 195.12
 206.66 205.30 203.59 201.32 198.19 193.63
 201.50 200.24 198.66 196.57 193.71 189.57
 196.73 195.59 194.17 192.29 189.74 186.08
 189.46 188.52 187.35 185.83 183.76 180.83
 182.61 181.90 181.00 179.84 178.28 176.07
XXX  COOLING OR PROCESS AIR TEMPERATURE
 208.27 206.90 205.19 202.90 199.75 195.12
 206.66 205.30 203.59 201.32 198.20 193.63
 201.50 200.24 198.66 196.57 193.71 189.57
 196.73 195.59 194.17 192.29 189.74 186.08
 189.46 188.52 187.36 185.83 183.76 180.83
 182.61 181.90 181.00 179.84 178.28 176.07
THE AVERAGE TEMPERATURE IS  0.46348D 03 K
THE OUTLET TEMPERATURE OF ANODE SIDE IS  0.45742D 03K
```

```
SYSTEM TIME NUMBER  7504
IFLG = 1 1 1 1 1 1 1 1 ONFLG = 1 0 1 0 1 1 1 1 0
IJ= 1 F(1-12)
     0.00000 -0.64013D 01 -0.11393D 02 -0.15807D 02 -0.81274D 02 -0.97409D 02
-0.12151D 03       0.00000 -0.43694D 02 -0.40041D 02 -0.40884D 02 -0.48508D 02


TIME=  0.27014D 03    SEC.
    *** AIR HEATER ***
TUBESIDE TEMP.  SHELL TEMP.   TUBEWALL TEMP.  INCR.
     F                F               F

       80.000        478.416         404.943      1
      127.647        505.762         436.087      2
      173.178        532.210         466.341      3
      216.700        557.681         495.748      4
IJ= 3 F(1-12)
     0.00000  0.66480D 02  0.10861D 03  0.13791D 03  0.15062D 03  0.14778D 03
 0.11747D 03       0.00000  0.16060D 03  0.18977D 03  0.19522D 03  0.16484D 03


TIME=  0.27014D 03    SEC.
    *** PREPARATOR ***
TUBESIDE TEMP.  SHELL TEMP.   TUBEWALL TEMP.  INCR.
     F                F               F

      555.073        998.399         888.172      1
      665.615       1086.852         982.024      2
      771.481       1173.970        1074.573      3
      873.012       1259.261        1165.492      4
IJ= 5 F(1-12)
     0.00000 -0.77720D 02 -0.10589D 03 -0.34488D 02 -0.59697D 02 -0.75041D 02
-0.29071D 02       0.00000 -0.55081D 02 -0.94511D 02 -0.59980D 02  0.56775D 02


TIME=  0.27014D 03    SEC.
    *** HEAT EXCHANGER -2 ***
TUBESIDE TEMP.  SHELL TEMP.   TUBEWALL TEMP.  INCR.
     F                F               F

      216.701        402.451         343.613      1
      408.795        574.506         523.702      2
      585.381        734.607         689.975      3
      742.987        883.727         841.323      4

TIME=  0.27014D 03    SEC.
    *** HIGH TEMPERATURE SHIFT CONVERTER ***

CONVERSION     TEMPERATURE    PRESSURE     INCRIMENT
  OF CO         OF FLUID      OF FLUID
                    F            ATM

     0.0000         784.460       5.170          1
     0.3906         881.789       5.085          2
     0.3820         882.302       4.990          3
```

```
    0.3851          883.731         4.894           4
IJ= 6 F(1-8)        0.00000 -0.21013D-03  0.19987D-03 -0.11655D-03       0.00000  0.13535D 03  0.90647D 01  0.11617D 03

TIME=  0.27014D 03    SEC.
    *** LOW  TEMPERATURE SHIFT CONVERTER ***

CONVERSION     TEMPERATURE    PRESSURE     INCRIMENT
  OF CO         OF FLUID      OF FLUID
                   F            ATM

    0.0000          401.430         4.894           1
    0.2294          443.901         4.780           2
    0.5695          499.600         4.656           3
    0.9656          557.680         4.520           4
IJ= 7 F(1-8)        0.00000  0.13928D-03  0.16530D-03  0.23900D-03       0.00000 -0.64580D 02 -0.11665D 03 -0.15534D 03

TIME=  0.27014D 03    SEC.
    *** REFORMER ***
    REFORMER    COMB. GAS       WALL      CATALYST    PRESSURE      IN. HEAT XFER      OUT. HEAT XFER      INC
   GAS TEMP        TEMP         TEMP        TEMP                       COEF               COEF
     DEG. R       DEG. R       DEG. R      DEG. R         ATM      BTU/HR*F*FT*FT      BTU/HR*F*FT*FT

    1333.006     1467.147     1339.030    1333.006        6.658          92.185             6.539          1
    1084.801     1481.701     1129.576    1084.801        6.296          92.789             6.590          2
    1142.777     1521.939     1179.116    1142.777        6.486          97.000             6.730          3
    1170.861     1561.738     1199.166    1170.861        6.507          99.960             6.867          4
    1180.488     1604.468     1213.457    1180.488        6.429         102.258             7.014          5
    1194.786     1651.272     1229.469    1194.786        6.379         104.969             7.173          6
    1207.474     1702.600     1245.175    1207.474        6.318         107.827             7.347          7
    1221.199     1759.234     1261.892    1221.199        6.259         110.950             7.538          8
    1235.497     1821.950     1279.709    1235.497        6.198         114.336             7.748          9
    1250.978     1891.668     1299.065    1250.978        6.135         118.026             7.979         10
    1267.774     1969.442     1320.259    1267.774        6.069         122.044             8.236         11
    1286.233     2056.518     1343.677    1286.233        6.002         126.423             8.523         12
    1306.685     2154.360     1369.773    1306.685        5.931         131.192             8.842         13
    1329.611     2264.708     1399.145    1329.611        5.858         136.377             9.202         14
    1355.664     2389.621     1432.604    1355.664        5.782         142.001             9.607         15
    1385.813     2531.538     1471.300    1385.813        5.702         148.084            10.065         16
    1421.561     2693.327     1516.940    1421.561        5.619         154.641            10.588         17
    1465.394     2878.315     1572.194    1465.394        5.533         161.704            11.186         18
    1521.758     3090.260     1641.567    1521.758        5.443         169.349            11.873         19
    1599.509     3333.146     1733.523    1599.509        5.354         177.769            12.665         20
    1719.261     3610.531     1866.787    1719.261        5.274         187.455            13.577         21
MFLG = 0 1 0 1 1 1 0 1 1 0 0 1 0 0 0
TEMPERATURE OF STREAMS -- K
 0.30000D 03  0.30000D 03  0.37594D 03  0.66833D 03  0.30000D 03  0.35634D 03  0.66566D 03
 0.66566D 03  0.66566D 03  0.56393D 03  0.74056D 03  0.95515D 03  0.81022D 03  0.69137D 03
 0.74652D 03  0.47857D 03  0.56538D 03  0.52134D 03  0.36167D 03  0.32400D 03  0.50611D 03
 0.43687D 03  0.50166D 03  0.73398D 03  0.20059D 04  0.81508D 03  0.43687D 03  0.39440D 03  0.66566D 03  0.45643D 03
IJ= 4 F(1-12)
     0.00000  0.30688D 02  0.40321D 02  0.51081D 02  0.26017D 02  0.40612D 02
 0.85619D 02      0.00000  0.22041D 02  0.36818D 02  0.48037D 02  0.83278D 02


TIME=  0.27018D 03    SEC.
    *** HEAT EXCHANGER -1 ***
TUBESIDE TEMP.  SHELL TEMP.   TUBEWALL TEMP.  INCR.
```

```
     F                  F                  F

       181.419            399.121            339.888      1
       401.749            572.076            521.377      2
       581.455            731.717            686.178      3
       738.193            883.731            839.407      4
IJ= 2 I(1-12)
      0.00000   0.43279D 02   0.65046D 02   0.91378D 02   0.75902D 02   0.94111D 02
 0.11308D 03       0.00000   0.61014D 02   0.78292D 02   0.10837D 03   0.15946D 03


TIME=  0.27029D 03    SEC.
    *** ANODE EXHAUST HEAT EXCHANGER ***
TUBESIDE TEMP.   SHELL TEMP.    TUBEWALL TEMP.   INCR.
     F                  F                  F

       361.566            784.463            707.836      1
       607.337            884.382            835.533      2
       759.899            950.888            916.907      3
       861.161            998.399            972.426      4
```

```
SYSTEM TIME NUMBER 15568
IFLG = 1 1 1 1 0 1 1 0 ONFLG = 1 1 1 0 0 1 1 0 0
IJ= 1 F(1-12)
     0.00000 -0.44738D 01 -0.80261D 01 -0.10812D 02 -0.17748D 02 -0.13314D 02
-0.78107D 01       0.00000 -0.30490D 02 -0.28322D 02 -0.26469D 02 -0.24591D 02


TIME=  0.56045D 03    SEC.
    *** AIR HEATER ***
TUBESIDE TEMP.   SHELL TEMP.    TUBEWALL TEMP.  INCR.
     F                F                F

       80.000         475.309          401.537     1
      127.147         502.703          432.745     2
      172.256         529.201          462.855     3
      215.392         554.800          491.853     4
IJ= 2 F(1-12)
     0.00000  0.40870D 02  0.61626D 02  0.71379D 02  0.61244D 02  0.67620D 02
 0.59289D 02       0.00000  0.57518D 02  0.74068D 02  0.78904D 02  0.69134D 02


TIME=  0.56045D 03    SEC.
    *** ANODE EXHAUST HEAT EXCHANGER ***
TUBESIDE TEMP.   SHELL TEMP.    TUBEWALL TEMP.  INCR.
     F                F                F

       361.566         790.126          712.783     1
       610.850         891.223          842.073     2
       765.309         958.318          924.910     3
       868.118        1005.152          981.672     4
IJ= 3 F(1-12)
     0.00000  0.40700D 02  0.43041D 02  0.40257D 02  0.40599D 02  0.30099D 02
 0.15452D 02       0.00000  0.55402D 02  0.48810D 02  0.33940D 02  0.12826D 02


TIME=  0.56045D 03    SEC.
    *** PREPARATOR ***
TUBESIDE TEMP.   SHELL TEMP.    TUBEWALL TEMP.  INCR.
     F                F                F

       557.335        1005.154          896.354     1
       669.876        1092.687          990.556     2
       777.198        1177.737         1082.081     3
       879.334        1259.915         1170.367     4

TIME=  0.56045D 03    SEC.
    *** HIGH TEMPERATURE SHIFT CONVERTER ***

CONVERSION     TEMPERATURE    PRESSURE     INCRIMENT
  OF CO         OF FLUID      OF FLUID
                    F            ATM
```

```
    0.0000          790.123         5.170           1
    0.4064          891.381         5.085           2
    0.3542          881.991         4.990           3
    0.3995          893.467         4.894           4
IJ= 6 F(1-8)      0.00000 -0.11277D-03  0.21273D-03 -0.13855D-03       0.00000  0.10271D 03 -0.14275D 02  0.11364D 03

TIME=  0.56045D 03    SEC.
    *** LOW  TEMPERATURE SHIFT CONVERTER ***

CONVERSION     TEMPERATURE    PRESSURE     INCRIMENT
  OF CO         OF FLUID      OF FLUID
                    F           ATM

    0.0000          401.819         4.894           1
    0.2314          443.905         4.780           2
    0.5711          498.573         4.656           3
    0.9608          554.800         4.520           4
IJ= 7 F(1-8)      0.00000 -0.14975D-04 -0.54483D-04 -0.21020D-04       0.00000  0.99748D 01  0.88681D 01 -0.68676D 00
NFLG = 0 1 0 1 0 1 0 1 0 0 0 0 0 0 0 0
TEMPERATURE OF STREAMS -- K
 0.30000D 03  0.30000D 03  0.37522D 03  0.66820D 03  0.30000D 03  0.35634D 03  0.66880D 03
 0.66880D 03  0.66880D 03  0.56519D 03  0.74407D 03  0.95551D 03  0.81397D 03  0.69451D 03
 0.75193D 03  0.47879D 03  0.56378D 03  0.51962D 03  0.36167D 03  0.32400D 03  0.50611D 03
 0.43687D 03  0.50166D 03  0.73784D 03  0.20059D 04  0.81311D 03  0.43687D 03  0.39440D 03  0.66880D 03  0.45643D 03
IJ= 4 F(1-12)
     0.00000  0.30341D 02  0.54308D 02  0.80287D 02  0.28503D 02  0.59246D 02
 0.66240D 02      0.00000  0.21831D 02  0.45988D 02  0.72345D 02  0.10674D 03


TIME=  0.56052D 03    SEC.
    *** HEAT EXCHANGER -1 ***
TUBESIDE TEMP.  SHELL TEMP.    TUBEWALL TEMP.  INCR.
    F               F               F

      181.419         401.329         341.602     1
      404.133         576.028         524.759     2
      585.372         737.810         691.302     3
      743.844         893.467         847.686     4
```

```
SYSTEM TIME NUMBER 22512
IFLG = 0 0 0 1 0 0 1 0 0NFLG = 0 0 0 0 0 0 1 0 0

TIME=  0.81043D 03    SEC.
    *** LOW  TEMPERATURE SHIFT CONVERTER ***

CONVERSION     TEMPERATURE    PRESSURE     INCRIMENT
  OF CO         OF FLUID      OF FLUID
                   F            ATM

    0.0000         402.443        4.894          1
    0.2340         444.661        4.780          2
    0.5765         499.344        4.656          3
    0.9650         555.000        4.520          4
IJ= 7 F(1-8)       0.00000 -0.67612D-04 -0.39217D-04 -0.37773D-04       0.00000  0.13309D 02  0.18111D 02  0.13848D 02
MFLG = 0 0 0 0 0 0 0 1 0 0 0 0 0 0 0
TEMPERATURE OF STREAMS -- K
 0.30000D 03  0.30000D 03  0.37506D 03  0.66820D 03  0.30000D 03  0.35634D 03  0.67186D 03
 0.67186D 03  0.67186D 03  0.56641D 03  0.74426D 03  0.95551D 03  0.81416D 03  0.69619D 03
 0.75544D 03  0.47914D 03  0.56389D 03  0.51936D 03  0.36167D 03  0.32400D 03  0.50611D 03
 0.43687D 03  0.50166D 03  0.73969D 03  0.20059D 04  0.81311D 03  0.43687D 03  0.39440D 03  0.67186D 03  0.45643D 03
IJ= 4 F(1-12)
     0.00000  0.31192D 02  0.53898D 02  0.68663D 02  0.27814D 02  0.45960D 02
 0.48929D 02      0.00000  0.22409D 02  0.45932D 02  0.64250D 02  0.64712D 02


TIME=  0.81054D 03    SEC.
    *** HEAT EXCHANGER -1 ***
TUBESIDE TEMP.   SHELL TEMP.    TUBEWALL TEMP.   INCR.
    F                F               F

      181.419        403.362         343.166      1
      406.307        579.701         528.038      2
      589.241        743.037         696.304      3
      749.343        899.784         854.446      4
```

A 9.3 Final Steady State

```
*** THE SYSTEM STEADY STATE HAS BEEN REACHED ***
  TIME =    865.08 SEC.
THE REFORMER IS OPERATING UNDER THESE CONDITIONS:
INLET PRESSURE:    6.66ATM
OUTLET PRESSURE:    5.18ATM
INLET TEMP.: 744.26 K
OUTLET TEMP.: 955.51 K

THE HIGH TEMP. SHIFT IS OPERATING UNDER THESE CONDITIONS :
INLET PRESSURE :    5.17 ATM
OUTLET PRESSURE:    4.89 ATM
INLET TEMP.: 696.19 K
OUTLET TEMP.: 755.44 K

THE LOW TEMP. SHIFT IS OPERATING UNDER THESE CONDITIONS:
INLET PRESSURE:    4.89 ATM
OUTLET PRESSURE:    4.52 ATM
INLET TEMP.: 479.20 K
OUTLET TEMP.: 564.05 K

THE FUEL CELL IS OPERATING UNDER THESE CONDITIONS
THE DC POWER OUTLET IS 6.8310 DC-MW
THE OPERATING VOLTAGE IS 0.6807 V
THE CURRENT DENSITY IS 0.2868 A/CM**2
THE AVERAGE OPERATING TEMPERATURE IS  462.22 K
THE OPERATING PRESSURE IS   3.305 ATM
THE ANODE SIDE INLET TEMPERATURE: 464.00 K
               OUTLET TEMPERATURE:  456.43 K



THE FRACTION OF CO IN THE ANODE INLET IS 0.0001
```

----- A STREAM -----

STREAM	CH4	CO	CO2	H2O	H2	N2	O2	RATE(G/SEC.)	TEMP.(K)	PRE.(ATM)
1	.0000	.0000	.0000	0.0100	.0000	.7820	.2080	1695.49	300.00	1.00
2	.0000	.0000	.0000	0.0100	.0000	.7820	.2080	1695.49	300.00	1.36
3	.0000	.0000	.0000	0.0100	.0000	.7820	.2080	1695.49	375.06	1.36
4	.0000	.0000	.0000	0.0100	.0000	.7820	.2080	1695.49	668.20	1.35
5	.9500	.0000	.0000	0.0000	.0000	.0500	.0000	316.79	300.00	3.40
6	.9500	.0000	.0000	0.0000	.0000	.0500	.0000	316.79	356.34	6.70
7	.9500	.0000	.0000	0.0000	.0000	.0500	.0000	316.79	672.37	6.70
8	.9500	.0000	.0000	0.0000	.0000	.0500	.0000	316.79	672.37	6.50
9	.9500	.0000	.0000	0.0000	.0000	.0500	.0000	9.17	672.37	6.50
10	.2815	.0000	.0000	0.7037	.0000	.0148	.0000	1099.83	566.62	6.67
11	.2815	.0000	.0000	0.7037	.0000	.0148	.0000	1099.83	744.26	6.66
12	.0071	.1094	.0662	0.2149	.5928	.0096	.0000	1099.83	955.51	5.18
13	.0071	.1094	.0662	0.2149	.5928	.0096	.0000	1099.83	814.16	5.17
14	.0071	.1094	.0662	0.2149	.5928	.0096	.0000	1099.83	696.19	5.17
15	.0071	.0646	.1110	0.1701	.6376	.0096	.0000	1099.83	755.44	4.89
16	.0070	.0664	.1092	0.1718	.6360	.0096	.0000	1099.83	479.20	4.89
17	.0070	.0022	.1734	0.1076	.7001	.0096	.0000	1099.83	564.05	4.52
18	.0070	.0025	.1731	0.1079	.6999	.0096	.0000	1099.83	519.36	4.52
19	.0142	.0001	.1709	0.1212	.6839	.0097	.0000	1246.35	361.67	4.52
20	.0158	.0001	.1898	0.0243	.7592	.0108	.0000	1053.85	324.00	4.08
21	.0158	.0001	.1898	0.0243	.7592	.0108	.0000	1053.85	506.11	4.08
22	.0000	.0000	.0000	1.0000	.0000	.0000	.0000	897.75	436.87	6.63
23	.0000	.0000	.0000	1.0000	.0000	.0000	.0000	792.21	501.66	6.50
24	.0403	.0002	.4835	0.0619	.3866	.0276	.0000	825.96	739.69	3.23
25	.0000	.0000	.2092	0.2240	.0000	.5435	.0233	2530.63	2005.92	1.58
26	.0000	.0000	.2092	0.2240	.0000	.5435	.0233	2530.63	813.11	1.44
27	.0000	.0000	.2092	0.2240	.0000	.5435	.0233	2530.63	436.87	1.40
28	.0000	.0000	.2092	0.2240	.0000	.5435	.0233	2530.63	394.40	1.39
29	.9500	.0000	.0000	0.0000	.0000	.0500	.0000	307.62	672.37	6.50

----- B STREAM -----

STREAM	CH4	CO	CO2	H2O	H2	N2	O2	RATE(G/SEC.)	TEMP.(K)	PRE.(ATM)
1	.0403	.0002	.4835	0.0619	.3866	.0276	.0000	825.96	456.43	3.14
2	.0158	.0001	.1898	0.0243	.7592	.0108	.0000	929.97	464.00	3.30

Appendix 10

Printout of PAFC Stack Current Density and Temperature Distributions at Transient State

A 10.1 Initial Steady State

A 10.2 Transient Distribution at 96.77 sec.

A 10.3 Final Steady State (197.64 sec.)

A 10.1 Initial Steady State

```
THE VOLTAGE IS      0.65842D 00

 .3567 .3506 .3429 .3324 .3177 .2956
 .3721 .3649 .3559 .3436 .3265 .3006
 .3606 .3537 .3450 .3335 .3177 .2946
 .3583 .3515 .3430 .3318 .3165 .2944
 .3347 .3291 .3222 .3131 .3009 .2838
 .3081 .3039 .2987 .2920 .2831 .2708
THE VOLTAGE IS      0.66925D 00

 .3517 .3457 .3380 .3276 .3130 .2912
 .3672 .3600 .3509 .3386 .3215 .2959
 .3623 .3550 .3458 .3337 .3170 .2927
 .3580 .3509 .3420 .3303 .3143 .2914
 .3381 .3321 .3246 .3149 .3018 .2834
 .3192 .3144 .3084 .3007 .2904 .2762
THE VOLTAGE IS      0.67264D 00

 .3499 .3439 .3363 .3259 .3114 .2897
 .3655 .3583 .3492 .3370 .3198 .2943
 .3625 .3551 .3458 .3335 .3166 .2920
 .3579 .3507 .3416 .3298 .3136 .2905
 .3392 .3331 .3254 .3154 .3021 .2833
 .3226 .3176 .3114 .3034 .2926 .2777
       AIR COOLING



THE AVERAGE TEMPERATURE OF COOLING PLATE AND        3 CELL PLATES(C)
  0.16975D 03  0.18622D 03  0.19151D 03  0.19327D 03


THE AVERAGE TEMP. ALONG AIR FLOW DIR. OF COOLING    PLATE AND 3 CELL PLATES(C)
 151.99 163.68 171.32 171.48 180.17 179.86
 171.72 179.17 186.02 189.29 195.00 196.15
 177.92 184.26 190.84 194.88 199.84 201.33
 179.96 185.97 192.45 196.72 201.46 203.04


CELL PLATE  1 TEMPERATURE RATIO
   1.032  1.029  1.026  1.021  1.015  1.006
   1.029  1.027  1.023  1.019  1.013  1.004
   1.016  1.013  1.010  1.006  1.001  0.993
   1.008  1.006  1.003  0.999  0.994  0.987
   0.991  0.990  0.987  0.984  0.980  0 975
```

A 10.2 Transient Distribution at 96.77 sec.

```
TIME=  0.96768D 02 SEC.
     *** FUEL CELL STACK ***
THE VOLTAGE IS      0.67485D 00


.3075 .3027 .2966 .2883 .2765 .2589
.3227 .3169 .3095 .2996 .2855 .2643
.3160 .3103 .3031 .2935 .2802 .2605
.3156 .3099 .3028 .2933 .2802 .2610
.2930 .2933 .2872 .2793 .2686 .2533
.2776 .2739 .2692 .2631 .2550 .2436
THE VOLTAGE IS      0.68316D 00


.3040 .2993 .2932 .2849 .2733 .2559
.3191 .3134 .3060 .2960 .2820 .2610
.3175 .3116 .3040 .2940 .2800 .2594
.3158 .3099 .3024 .2925 .2789 .2591
.3012 .2961 .2897 .2812 .2698 .2535
.2874 .2831 .2778 .2709 .2617 .2485
THE VOLTAGE IS      0.68591D 00


.3025 .2978 .2917 .2835 .2720 .2547
.3177 .3119 .3045 .2946 .2807 .2598
.3176 .3116 .3039 .2937 .2796 .2588
.3155 .3096 .3020 .2921 .2783 .2583
.3021 .2968 .2903 .2817 .2700 .2533
.2902 .2859 .2803 .2732 .2635 .2498
FUEL CELL STACK F(1-24)
 0.66470D 00 -0.88062D 00 -0.46111D 01 -0.76501D 01 -0.13523D 02 -0.15187D 02
 0.46630D 00 -0.28747D 01 -0.87937D 01 -0.14416D 02 -0.21505D 02 -0.25935D 02
 0.24907D 00 -0.38467D 01 -0.10621D 02 -0.17086D 02 -0.24748D 02 -0.30047D 02
 0.16792D 00 -0.45850D 01 -0.11705D 02 -0.18458D 02 -0.26354D 02 -0.31950D 02


PLATE 2
 199.68 198.50 197.01 195.02 192.28 188.27
 198.64 197.46 195.97 193.99 191.27 187.29
 192.83 191.76 190.41 188.62 186.17 182.62
 189.19 188.21 186.98 185.35 183.13 179.94
 181.93 181.13 180.13 178.81 177.02 174.47
 174.00 173.40 172.65 171.68 170.35 168.48
***  COOLING OR PROCESS AIR TEMPERATURE
 199.68 198.50 197.01 195.02 192.28 188.27
 198.64 197.46 195.97 193.99 191.27 187.29
 192.83 191.76 190.41 188.62 186.17 182.62
 189.19 188.21 186.98 185.35 183.13 179.94
 181.93 181.13 180.13 178.81 177.02 174.47
 174.00 173.40 172.65 171.68 170.35 168.48

PLATE 3
 204.53 203.26 201.66 199.53 196.58 192.27
 203.14 201.88 200.28 198.17 195.25 190.98
 198.08 196.91 195.44 193.49 190.82 186.94
 193.69 192.63 191.30 189.54 187.14 183.68
 186.70 185.82 184.72 183.27 181.32 178.52
 179.88 179.20 178.35 177.24 175.74 173.61
***  COOLING OR PROCESS AIR TEMPERATURE
```

```
 204.53 203.26 201.66 199.53 196.58 192.27
 203.14 201.88 200.28 198.17 195.25 190.93
 193.08 196.91 195.44 193.49 190.82 186.94
 193.69 192.63 191.30 189.54 187.14 183.63
 186.70 185.82 184.72 183.27 181.32 178.52
 179.88 179.20 178.35 177.24 175.74 173.61

PLATE 4
 206.13 204.83 203.19 201.02 198.00 193.59
 204.65 203.36 201.73 199.57 196.58 192.22
 199.81 198.61 197.09 195.09 192.34 188.35
 195.20 194.11 192.74 190.94 188.48 184.93
 188.30 187.39 186.26 184.77 182.76 179.83
 181.81 181.10 180.22 179.07 177.51 175.29
XXX  COOLING OR PROCESS AIR TEMPERATURE
 206.13 204.83 203.19 201.02 198.00 193.59
 204.65 203.36 201.73 199.57 196.58 192.22
 199.81 198.61 197.09 195.09 192.34 188.35
 195.20 194.11 192.74 190.94 188.48 184.93
 188.30 187.39 186.26 184.77 182.76 179.83
 181.81 181.10 180.22 179.07 177.51 175.29
THE AVERAGE TEMPERATURE IS  0.46245D 03 K
THE OUTLET TEMPERATURE OF ANODE SIDE IS  0.45657D 03K
```

A 10.3 Final Steady State

```
TIME=  0.19764D 03 SEC.
    *** FUEL CELL STACK ***
THE VOLTAGE IS    0.67415D 00

.3064  .3018  .2957  .2876  .2761  .2589
.3216  .3160  .3088  .2990  .2853  .2644
.3155  .3099  .3028  .2933  .2802  .2607
.3156  .3100  .3029  .2935  .2804  .2613
.2985  .2938  .2878  .2799  .2692  .2538
.2784  .2747  .2700  .2639  .2557  .2442
THE VOLTAGE IS    0.68252D 00

.3027  .2981  .2921  .2841  .2727  .2557
.3179  .3123  .3050  .2953  .2816  .2610
.3168  .3110  .3035  .2936  .2799  .2595
.3156  .3098  .3024  .2926  .2791  .2593
.3016  .2966  .2901  .2817  .2703  .2538
.2881  .2839  .2786  .2717  .2623  .2490
THE VOLTAGE IS    0.68522D 00

.3013  .2967  .2908  .2828  .2715  .2546
.3165  .3109  .3037  .2940  .2803  .2598
.3169  .3110  .3035  .2935  .2796  .2590
.3155  .3096  .3021  .2922  .2786  .2587
.3026  .2974  .2908  .2822  .2706  .2538
.2911  .2867  .2812  .2740  .2643  .2504
FUEL CELL STACK F(1-24)
 0.46434D 00 -0.50433D 00 -0.25475D 01 -0.43240D 01 -0.77203D 01 -0.83380D 01
 0.12834D 01 -0.19383D 00 -0.30348D 01 -0.62640D 01 -0.10055D 02 -0.11905D 02
 0.97552D 00 -0.71174D 00 -0.38790D 01 -0.75796D 01 -0.11582D 02 -0.13813D 02
 0.14607D 01 -0.24362D 00 -0.34686D 01 -0.73087D 01 -0.11359D 02 -0.13704D 02

PLATE 2
 199.12 197.97 196.52 194.58 191.91 187.99
 198.14 196.99 195.54 193.61 190.95 187.05
 192.49 191.44 190.12 188.37 185.97 182.47
 188.99 188.03 186.82 185.21 183.02 179.85
 181.88 181.08 180.09 178.78 177.00 174.44
 174.02 173.43 172.68 171.71 170.38 168.49
```

```
***  COOLING OR PROCESS AIR TEMPERATURE
 199.12 197.97 196.52 194.58 191.91 187.99
 198.14 196.99 195.54 193.61 190.95 187.05
 192.49 191.44 190.12 188.37 185.97 182.47
 189.00 188.03 186.82 185.21 183.02 179.85
 181.88 181.08 180.09 178.78 177.00 174.44
 174.02 173.43 172.68 171.71 170.38 168.49

PLATE 3
 203.90 202.67 201.11 199.04 196.17 191.96
 202.60 201.37 199.82 197.75 194.90 190.72
 197.70 196.56 195.12 193.21 190.58 186.76
 193.48 192.43 191.12 189.39 187.02 183.58
 186.63 185.77 184.68 183.24 181.29 178.50
 179.90 179.23 178.38 177.27 175.77 173.63
***  COOLING OR PROCESS AIR TEMPERATURE
 203.90 202.67 201.11 199.04 196.17 191.96
 202.60 201.37 199.82 197.75 194.90 190.72
 197.70 196.56 195.12 193.21 190.58 186.76
 193.48 192.43 191.12 189.39 187.02 183.58
 186.63 185.77 184.68 183.24 181.29 178.50
 179.90 179.23 178.38 177.27 175.77 173.63

PLATE 4
 205.48 204.22 202.63 200.51 197.57 193.27
 204.09 202.83 201.24 199.13 196.22 191.95
 199.41 198.24 196.76 194.80 192.10 188.17
 194.98 193.91 192.56 190.78 188.35 184.83
 188.23 187.34 186.22 184.74 182.73 179.85
 181.84 181.14 180.26 179.10 177.54 175.31
***  COOLING OR PROCESS AIR TEMPERATURE
 205.48 204.22 202.63 200.51 197.57 193.27
 204.09 202.83 201.24 199.13 196.22 191.95
 199.41 198.24 196.76 194.80 192.10 188.17
 194.98 193.91 192.56 190.78 188.35 184.83
 188.23 187.34 186.22 184.74 182.73 179.85
 181.84 181.14 180.26 179.10 177.54 175.31
THE AVERAGE TEMPERATURE IS  0.46222D 03 K
THE OUTLET TEMPERATURE OF ANODE SIDE IS  0.45643D 03K
```